Regulation of autophagosome formation by the PX-domain proteins SNX18 and HS1BP3

Kristiane Søreng

Thesis for the degree of Philosophiae Doctor

Department of Molecular Medicine

Institute of Basic Medical Sciences

UNIVERSITY OF OSLO

2017

Series of dissertations submitted to the
Faculty of Medicine, University of Oslo

ISBN 978-82-8377-104-6

Cover: Hanne Baadsgaard Utigard.
Print production: Reprosentralen, University of Oslo.

TABLE OF CONTENTS

ACKNOWLEDGEMENTS

The work of this thesis was performed in the laboratory of Professor Anne Simonsen, at the Department of Molecular Medicine, Institute of Basic Medical Sciences at the University of Oslo from 2011 to 2017. The period included a 25 % teaching position that has provided me with the useful experience of being a PBL/LSB-teacher.

First I want to express my gratitude to my supervisor, Professor Anne Simonsen, for giving me the opportunity to be a part of this group. Thank you for all your help and valuable guidance and for always taking the time to answer questions and allowing me to develop as a researcher. Your enthusiasm, broad scientific knowledge and concern for your group have inspired me and given me a genuine interest for scientific research.

Thanks to Tore Jahnsen at the section of Biochemistry, for being my co-supervisor.

To the past and presents members of the group, you have all contributed to this work by sharing your knowledge and taking time to discuss both scientific and non-scientific matters, which I am very grateful for. Thanks to Christian Bindesbøll, my "office-mate", for our nice conversations. Special thanks to Alf Håkon Lystad for being a good friend, bearing with my ups and downs, and to Gunnveig Toft Bjørndal for your continuous encourage and support! Many thanks to Helene Knævelsrud for everything you taught me during my first years, for great teamwork and collaboration.

I would like to thank all co-authors for your collaboration, input and feedback. Thanks to Sven Carlsson for your contribution, help and scientific input on all three papers. Especially I want to thank Sharon Tooze and her lab members at the Francis Crick Institute, London, for giving me the opportunity to come and spend six very nice and exciting months in your autophagy lab.

To my dear family, thank you for your care and support during these years, and for your extremely valuable help in order for me to finish this thesis. A special thanks to Kristoffer, for your love, patience and for believing in me. I could not have done this without you. Finally, a big thanks to my two beautiful children, Helle and Eivind, for providing times of distractions filled with love and joy.

Oslo, May 2017

Kristiane Søreng

LIST OF PUBLICATIONS

I. Knaevelsrud, H.*, Soreng, K.*, Raiborg, C., Haberg, K., Rasmuson, F., Brech, A., Liestol, K., Rusten, T.E., Stenmark, H., Neufeld, T.P., Carlsson, S.R. & Simonsen, A. (2013), **Membrane remodeling by the PX-BAR protein SNX18 promotes autophagosome formation.** *Journal of Cell Biology,* 202, 331-49.

II. Holland, P.*, Knæveslrud, H.*, Søreng, K., Mathai, B.J., Lystad, A. H., Pankiv, S., Bjørndal, G. T., Schultz, S. W., Lobert, V. H., Chan, R. B., Zhou, B., Liestøl, K., Carlsson, S. R., Melia, T. J., Di Paolo, G. & Simonsen, A., (2016), **HS1BP3 negatively regulates autophagy by modulation of phosphatidic acid levels.** *Nature Communications,* 7, 13889.

III. Søreng, K., Munson, M. J., Lamb, C. A., Tooze, S., Carlsson, S. R. & Simonsen, A., **SNX18 regulates ATG9 trafficking from recycling endosomes by recruiting dynamin-2.** Manuscript in preparation

* Contributed equally

Related publications not included in this thesis:

Søreng, K., Neufeld, T., Simonsen, A., (2017), **Membrane trafficking in autophagy.** Review article, *IRCMB,* in press.

Søreng, K., Knævelsrud, H., Holland, P. & Simonsen, A. (2017), **HS1BP3 inhibits autophagy by regulation of PLD1,** Autophagic punctum, *Autophagy,* 1-2

ABBREVIATIONS

3MA	3-methyladenine
ALFY	Autophagy-linked FYVE protein
ALR	Autophagic lysosome reformation
AMP	Adenosine monophosphate
AMPK	AMP-activated protein kinase
AP	Adaptor protein
APP	Amyloid precursor protein
Arp	Actin related protein
ATG	Autophagy-related
BafA1	Bafilomycin A1
BAR	Bin/Amphiphysin/Rvs-homology
Cas	CRISPR-associated
CMA	Chaperone-mediated autophagy
CME	Clathrin-mediated endocytosis
CRISPR	Clustered Regularly Interspaced Short Palindromic Repeats
DFCP1	Double FYVE containing protein 1
DAG	Diacylglycerol
DAGK	Diacylglycerol kinase
ECM	Extracellular matrix
EEA1	Early endosome antigen 1
ER	Endoplasmic reticulum
ERES	ER-exit sites
ERGIC	ER-Golgi intermediate compartment
FIP200	Focal adhesion kinase interacting protein of 200 kDa
FIP5	RAB11 family interacting protein 5
FYCO1	FYVE and coiled-coil domain containing protein 1
FYVE	Fab1, YOTB, Vac1 and EEA1
GABARAP	Gamma-aminobutyric acid receptor-associated protein
GAP	GTPase-activating protein
GDP	Guanosin diphosphate

GEF	GFP/GTP exchange factor
GFP	Green fluorescent protein
GTP	Guanosin triphosphate
HDAC6	Histone deacetylase 6
HS1BP3	HCLS1-binding protein 3
INPP5E	Inositol polyphosphate-5-phosphatase E
KO	knock-out
LC	Low complexity
LC3	Microtubule associated protein 1 light chain 3
LIR	LC3 interacting region
LPAAT	Lysophosphatidic acid acyltransferase
mTORC	mechanistic target of rapamycin complex 1
MTMR3	Myotublarin related phosphatase 3
N-WASP	Wiskott-Aldrich syndrome like
PA	Phosphatidic acid
PAP	Phosphatidic acid phosphatase
PAS	Phagophore assembly site
PC	Phosphatidylcholine
PE	Phosphatidylethanolamine
PH	Plextrin homology
PI	Phosphoinositide
PtdIns	Phosphastidylinositol
PtdIns(3)P	Phosphatidylinositol-3-phosphate
PtdIns(3,4,5)P_3	Phosphatidylinositol-3,4,5-triphosphate
PtdIns(3,5)P_2	Phosphatidylinositol-3,5-bisphosphate
PtdIns(4)P	Phosphatidylinositol-4-phosphate
PtdIns(4,5)P_2	Phospahtidylinositol-4,5-bisphosphate
PtdIns(5)P	Phosphatidylinositol-5-phosphate
PIK3C3	Phosphatidylinositol-3-kinase class III
PLD1	Phospholipase D1
PX	Phox homology

SH3	Src homology 3
siRNA	Short interfering RNA
SNARE	Soluble *N*-ethylmaleimide-sensitive factor attachment protein receptor
SNX	Sorting nexin
SQSTM1	Sequestosome-1
TBC1D14	TBC1 domain family member 14
Tfn	Transferrin
TfR	Transferrin receptor
TGN	Trans-Golgi network
TRAPPIII	Trafficking protein particle complex III
ULK	Unk-51-like autophagy activating kinase
VAMP7	Vesicle associated membrane protein 7
WIPI	WD repeat protein interacting with phosphoinositides
WT	Wild type

INTRODUCTION

The endomembrane system and membrane trafficking

For cells to stay alive and healthy, they need to handle specific cellular processes such as nutrient uptake and metabolism, waste recycling and communication, both within the cell and between cells. In addition to the surrounding ered plasma membrane, eukaryotic cells contain smaller cytoplasmic compartments built up by lipid layers, called organelles. The different organelles allow compartmentalisation of cellular functions, which is important for the cell to perform all its necessary tasks to maintain a homeostatic environment. The organelles of the endomembrane system comprise the secretory, endocytic and degradative pathways, which are connected by dynamic interactions between different compartments, facilitated by vesicle trafficking between the organelles (Figure 1).

In general, the organelles making up the secretory pathway includes the endoplasmic reticulum (ER) where the protein synthesis and folding occur, ER-exit sites (ERES) which are regions of the ER from where the proteins are exported in transport vesicles, the ER-Golgi intermediate compartment (ERGIC) and the Golgi apparatus, consisting of stacks of flat membranes where the proteins are further modified before they are transported through the plasma membrane to the cell exterior (Farhan and Rabouille, 2010, Barlowe and Miller, 2013). Moreover, vesicles traffic between the TGN to endosomes containing proteins destined for the lysosomes, such as mannose-6-phosphate receptor (Griffiths et al., 1988). The endocytic pathway includes early and late endosomes, as well as recycling endosomes and other vesicles, containing extracellular substances and proteins destined for the interior of the cell. Endocytic vesicles are formed and pinched off at the plasma membrane (Doherty and McMahon, 2009) and later these vesicles fuse with the endosomes resulting in the release and proper sorting of their content. Substances that are destined to go back to the cell surface, such as nutrient-sensing receptors, are sorted into recycling endosomes from where vesicles containing the proteins form and traffic to the plasma membrane. Endocytic material destined for degradation pass through late endosomes before they end up in the degradative compartment of the endomembrane system, the lysosomes. Lysosomes have a low pH that is maintained by an H+-ATPase pumping protons into the lysosomal lumen. This low pH allows lysosomal enzymes to degrade the material that reaches this compartment. The resulting degradation products are released back to the cytosol to be reused by the cell to generate new products and energy (Saftig and Klumperman, 2009). The second lysosomal degradation pathway of the

endomembrane system is the process of macroautophagy (hereafter autophagy), which involves lysosomal degradation of cytoplasmic components. Autophagy is characterised by the formation of a double-membrane autophagosome that sequesters cytoplasmic material and delivers it to the lysosomes for degradation. This process will be discussed in more detail later.

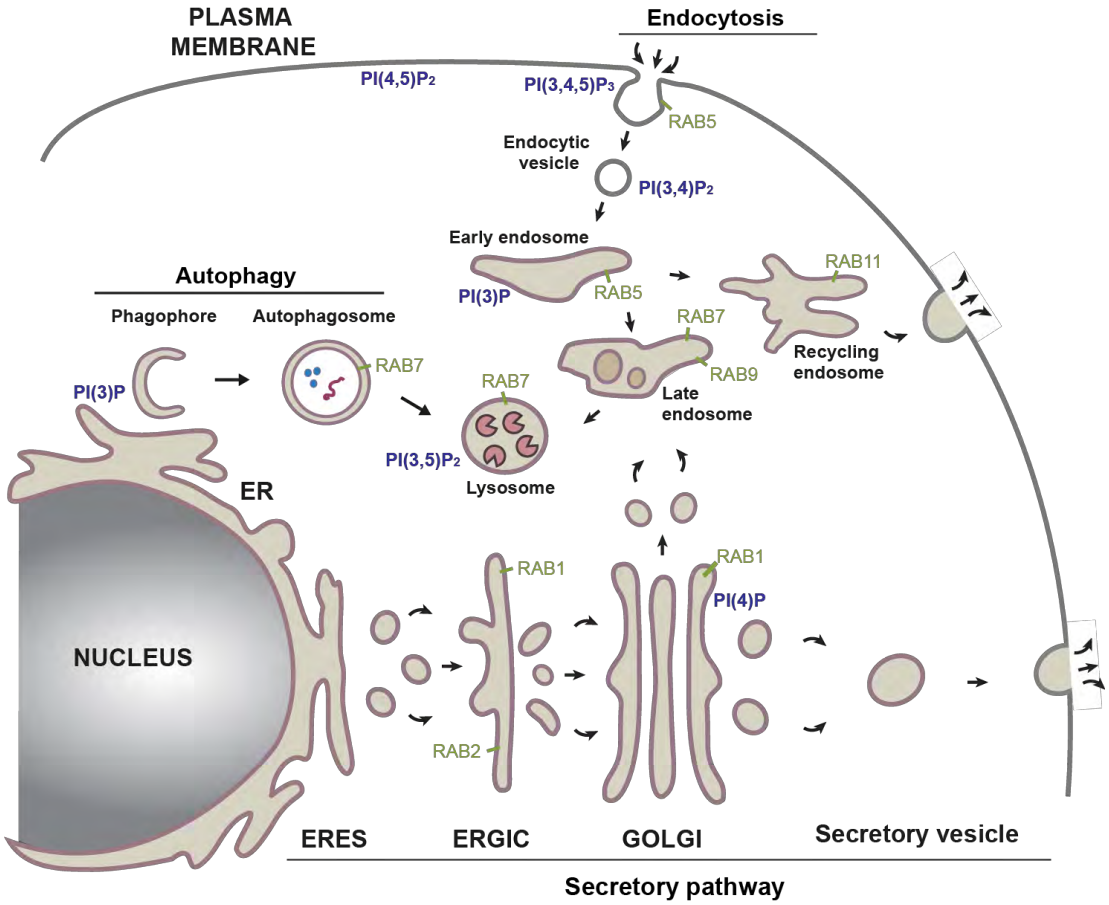

Figure 1: The endomembrane system. Proteins destined for the plasma membrane and extracellular matrix (ECM) are synthesised at the ER and transported along the secretory pathway in vesicles exiting from ERES, passing through ERGIC and the Golgi, before ending up in secretory vesicles fusing with the plasma membrane. Proteins are also transported in vesicles from the TGN to endosomes. Endocytosis is the uptake of proteins from the plasma membrane and ECM into endocytic vesicles that fuse with early and late endosomes before they reach the lysosomes. Substances transported back to the plasma membrane are sorted in recycling endosomes. The process of autophagy captures intracellular material and delivers it to the lysosomes for degradation. Different membranes contain specific RAB proteins and phosphoinositides, assigning membrane identity. Modified from (Søreng et al.) (in press).

Vesicle formation

Intracellular membrane trafficking is defined by the formation of a vesicle from a donor membrane, which buds off, traffics to and fuses with a target membrane to allow cargo transport between organelles (Rothman, 2002) (Figure 2). Vesicle traffic occurs between all the compartments of the endomembrane system. In order to form a vesicle from the donor compartment, cytosolic coat-proteins assemble onto the membrane, driving the modulation of the membrane resulting in a bud (Bonifacino and Lippincott-Schwartz, 2003, Kirchhausen, 2000). Several coat-proteins have been identified, including clathrin, COP-I and COP-II and the different coat-protein complexes promote vesicle formation from different membranes in the cells. Clathrin-coats are recruited to membranes through binding to adaptor proteins (AP), such as AP-1 and AP-2. AP-2 is involved in vesicle formation and clathrin-mediated endocytosis (CME) from the plasma membrane, whereas AP-1 mainly drives vesicle formation and transport from the trans-Golgi network (TGN) (Schmid, 1997). After assembly and formation of a clathrin-coated pit, dynamin is recruited to its neck to drive fission of the membrane to allow budding of the vesicle. Dynamin is a small GTPase and the energy needed for fission is obtained through hydrolysis of GTP to GDP (Hanna Damke, 1994, Cocucci et al., 2014).

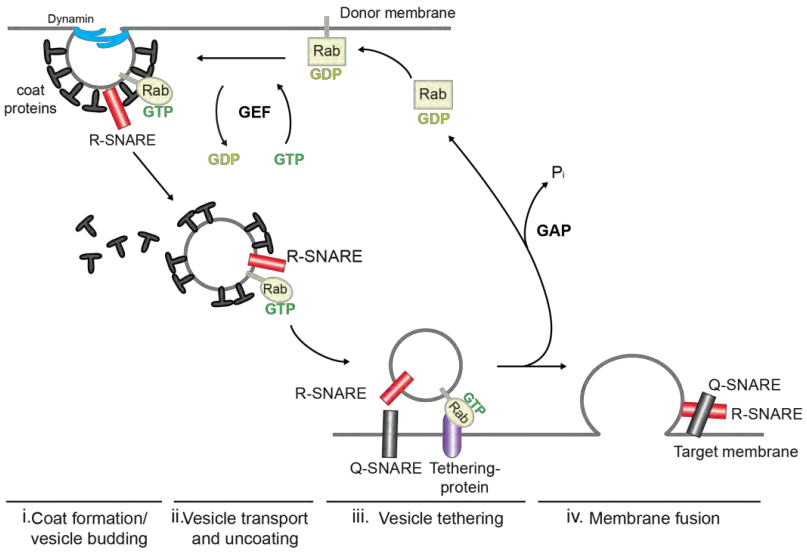

Figure 2: Vesicle formation. The assembly of coat-proteins drives formation of vesicle buds (**i**) which pinch off after recruitment of dynamin. During vesicle transport to the target membrane, the coat proteins are released (**ii**). Active GTP-bound RABs in the vesicle membrane bind to tethering proteins in the target membrane to allow docking (**iii**), before a SNARE complex is formed between SNARE proteins present in both membranes, driving membrane fusion (**iv**). The RAB protein is inactivated upon hydrolysis of the bound GTP by a GAP, resulting in dissociation of RAB. Re-activation of the RAB protein is mediated by a GEF, exchanging the bound GDP to GTP. Modified from (Søreng et al.) (in press).

Coat-proteins other than clathrin have also been found to drive vesicle formation from the plasma membrane, through other endocytic processes such as micropinocytosis and phagocytosis (Mayor et al., 2014). Additionally, vesicle formation and transport intra-Golgi, between the Golgi-to-ER and ER-to-ERGIC/Golgi was demonstrated to depend on the COP-I and COP-II coats, respectively (Letourneur et al., 1994, Barlowe et al., 1994). The vesicles are connected to cytoskeleton-associated motor proteins allowing transport of the vesicles along the cytoskeleton to their destination membrane (Kamal and Goldstein, 2000).

Membrane identity in the endomembrane system

Phosphoinositides

The different compartments of the endomembrane system are characterised by unique lipid compositions of their membranes, where in particular different phosphoinositides (PI) are important for recruitment of compartment-specific proteins. PIs are phospholipids that can be reversibly phosphorylated at position 3, 4 and 5 in the inositol ring of phosphatidylinositol (PtdIns), giving rise to seven different phosphoinositides found in eukaryotic cells (Shewan et al., 2011). They are generated through the action of PtdIns-kinases and phosphatases and the different PIs are concentrated on the cytosolic side of the subcellular compartments serving as determinants of membrane identity and as important players during intracellular signalling (Shewan et al., 2011). Some of the different PIs and their localisation are shown in Figure 1. The plasma membrane normally harbours PtdIns(4,5)P_2 and PtdIns(3,4,5)P_3. PtdIns(3)P is enriched on early endosomes whereas endocytic vesicles on their way from the plasma membrane to early endosomes contain PtdIns(3,4)P_2 and late endocytic membranes harbour PtdIns(3,5)P_2. The Golgi apparatus and Golgi-derived vesicles destined for the cell exterior are enriched in PtdIns(4)P (Di Paolo and De Camilli, 2006).

In addition to provide membrane identity to different compartments, PIs operate to recruit effector proteins to the membranes through binding to their head groups. Proteins that bind PIs are characterised by the presence of a PI-binding domain, such as WD-repeats, PH-, FYVE- or PX-domains. It has been shown that some of these PI-binding proteins are recruited to specific membranes through coincident binding, e.g. binding to an active RAB protein in addition to the PI. This is typical for FYVE-domain containing proteins, such as EEA1 and FYCO1, which bind PtdIns(3)P in addition to RAB5 or RAB7, respectively (Simonsen et al., 1998, Lawe et al., 2000, Pankiv et al., 2010).

RABs and SNAREs

RAB proteins and soluble *N*-ethylmaleimide-sensitive factor attachment protein receptors (SNAREs) are other groups of proteins involved in the targeting and recruitment of cytosolic proteins and vesicles to the correct target membranes.

RAB proteins comprise the largest family of small GTP-binding proteins (GTPases) localising to specific intracellular compartments where they shuttle between an active GTP-bound state and an inactive GDP-bound state, thus functioning as molecular switches coordinating vesicle trafficking (Lamb et al., 2016a). An overview of the localisation of some of the most common RAB proteins is shown in Figure 1. RAB protein activity is tightly controlled by GEFs (guanine nucleotide exchange factors) and GTPase-activating proteins (GAPs) (Takai et al., 2001, Stenmark, 2009). GEFs mediate the exchange of GDP to GTP, leading to activation of the RAB protein. Once active, RAB proteins can further bind to effector proteins, often tethering proteins in the target membrane helping to anchor the vesicles (Figure 2). To inactivate the RAB protein, GAPs catalyse GTP-hydrolysis of the bound GTP, resulting in displacement of the RAB protein from the membrane.

SNARE proteins are also required for proper fusion of a membrane vesicle to a target membrane. They all share a SNARE motif and are named Q-SNARES or R-SNARES depending on whether this motif contains a conserved glutamate (Q) or an arginine (R) (Ungermann and Langosch, 2005). During membrane fusion a trans-SNARE complex is formed, consisting of one R-SNARE located in the donor membrane and three Q-SNAREs located in the target membrane (Fasshauer et al., 1998). This interaction allows the two membranes to come in close proximity to one another, resulting in membrane fusion (Jahn et al., 2003).

Autophagy

Autophagy is an intracellular lysosomal degradation pathway important for eliminating cytoplasmic components such as long-lived proteins, organelles and pathogens in order to maintain cellular homeostasis. The pathway is important during cell division and development, and in general has a protective role in times of diseases and infections. Moreover, autophagy is upregulated under stressful periods such as starvation to provide cells with free amino acids, lipids and carbohydrates that can be reused by the cell. There are three types of autophagy described in eukaryotic cells: microautophagy, chaperone-mediated autophagy (CMA) and

macroautophagy (Boya et al., 2013). In this thesis we focus on macroautophagy, hereafter referred to as autophagy.

Autophagy occurs in all cells and is defined by a forming double-membrane structure called a phagophore or isolation membrane that expands and sequesters cytoplasmic components, before it closes to form an autophagosome (Figure 3). The autophagosomes mature by fusing with endosomes, creating structures called amphisomes that further fuse with lysosomes (Eskelinen, 2005). Alternatively, autophagosomes can also directly fuse with lysosomes, giving rise to autolysosomes. Due to the acidic environment and the presence of hydrolases in the lysosomes, the sequestered material is degraded (Boya et al., 2013). The degraded components are then released from the autolysosomes back into the cytosol to be reused by the cell. For a long time it was believed that autophagy occurs during starvation periods only, but it has become evident that autophagy also is upregulated to degrade specific cargo such as organelles, protein aggregates and invading pathogens (Klionsky et al., 2007).

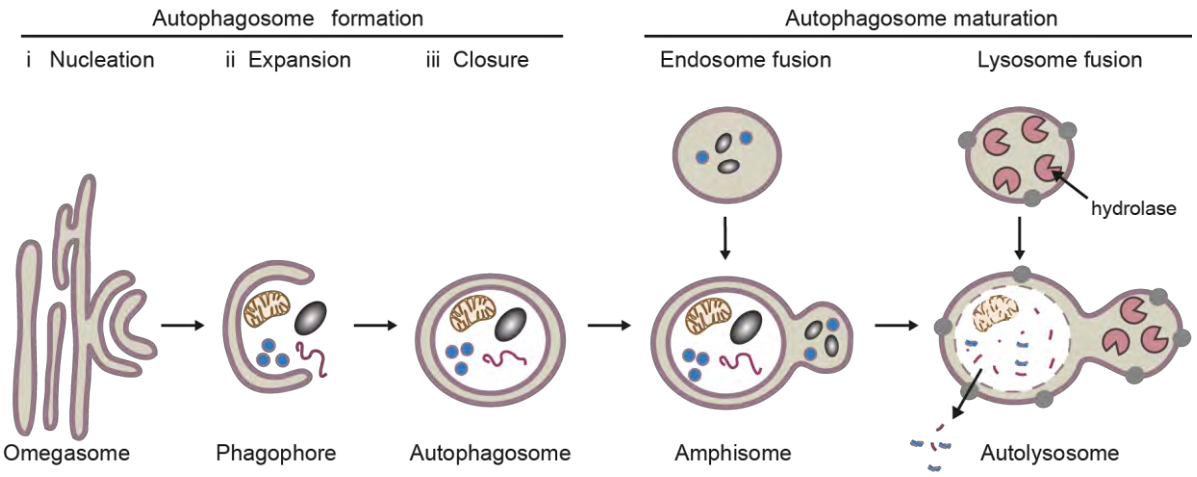

Figure 3: Autophagy. Autophagy starts by nucleation of a phagophore from omegasomes (**i**), which expands to sequester cytoplasmic material (**ii**), generating a double-membrane autophagosome (**iii**). Autophagosomes mature by fusing with endosomes (amphisomes) and lysosomes (autolysosomes) resulting in degradation of the sequestered material, which is released back into the cytoplasm to be reused. Modified from (Søreng et al.) (in press).

A*utophagy from a historical perspective*

The history of autophagic research dates back to 1955 with the discovery and identification of the lysosomes (de Duve et al., 1955). This was followed by a decade of morphological studies using electron microscopy in different tissues resulting in the

identification of membranes sequestering cytoplasmic material into autophagic vesicles that fuse with lysosomes (de Duve and Wattiaux, 1966, Arstila and Trump, 1968). Over the next decades, several functional studies of autophagy were done using biochemical approaches demonstrating that autophagy is induced by nutrient and amino acid starvation (Seglen et al., 1980, Mortimore et al., 1983) and identified autophagic inhibitors (Seglen and Gordon, 1982, Blommaart et al., 1997, Holen et al., 1992). In 1992, Ohsumi and co-workers showed that autophagy in yeast is similar to that observed in mammalian cells (Takeshige et al., 1992) and this paved the way for the revolutionary yeast screens that led to the identification of the first genes responsible for autophagy (Tsukada and Ohsumi, 1993) for which Ohsumi was awarded the Nobel Prize in 2016. Several screens were done in other labs and other yeast species, resulting in different names given to genes responsible for autophagy, before a unified gene and protein nomenclature was adopted, naming them Atg, for "*a*uto*p*ha*g*y-related" (Klionsky et al., 2003). In parallel, human ATG genes were cloned, demonstrating that most Atg-genes are highly conserved in mammals (Mizushima et al., 1998, Kabeya et al., 2000). From this point until today, research on autophagy has expanded dramatically, revealing the existence of more than 30 Atg proteins and the great importance of autophagy in health and disease (Klionsky, 2007).

Core autophagic machinery and regulation

Induction of autophagy is regulated by several ATG proteins, where some are part of multi-subunit complexes, which together compose the core autophagic machinery (Figure 4). They include the Atg1/unc-51-like kinase (ULK) complex, the Vps34/class III phosphatidylinositol 3-kinase complex (PIK3C3), the two ubiquitin-like conjugation systems that mediate conjugation of Atg12 to Atg5 and conjugation of Atg8/LC3 to phosphatidylethanolamine (PE) in the autophagic membrane and the multi-spanning transmembrane protein Atg9 (Kabeya et al., 2000, Nakatogawa et al., 2009, Mizushima et al., 2011).

The Atg1/ULK1 complex

The ULK-complex in mammalian cells consists of the kinase ULK1 (yeast Atg1) or ULK2, ATG13, FIP200 (FAK family kinase-interacting protein of 200 kDa) and ATG101 (Hara et al., 2008, Hosokawa et al., 2009b, Mercer et al., 2009, Chan et al., 2009) (Figure 4a).

ULK1 and ULK2 have been suggested to be functionally redundant during starvation induced autophagy, but this redundancy seems to be cell-type specific (Lee and Tournier, 2011).

The activity of the ULK complex is regulated by mechanistic target of rapamycin complex 1 (MTORC1), a major nutrient sensing regulator of autophagy in addition to being a regulator of cell growth and proliferation (Neufeld, 2010). When nutrients are available, mTORC1 is active and inhibits the ULK kinase complex by phosphorylating ULK1 and ATG13, resulting in the deactivation of the complex and inhibition of autophagy. Upon nutrient depletion however, mTORC1 becomes inactivated, leading to dephosphorylation and activation of the ULK complex (Ganley et al., 2009, Hosokawa et al., 2009a, Jung et al., 2009, Puente et al., 2016). Subsequently, the activated ULK complex phosphorylates its subunits ATG13 and FIP200 resulting in autophagy induction (Jung et al., 2010). ULK complex activity is also regulated by the cellular energy sensor, AMP-activated protein kinase (AMPK). When cellular energy levels drop, AMPK phosphorylates ULK1 to induce autophagy (Kim et al., 2011).

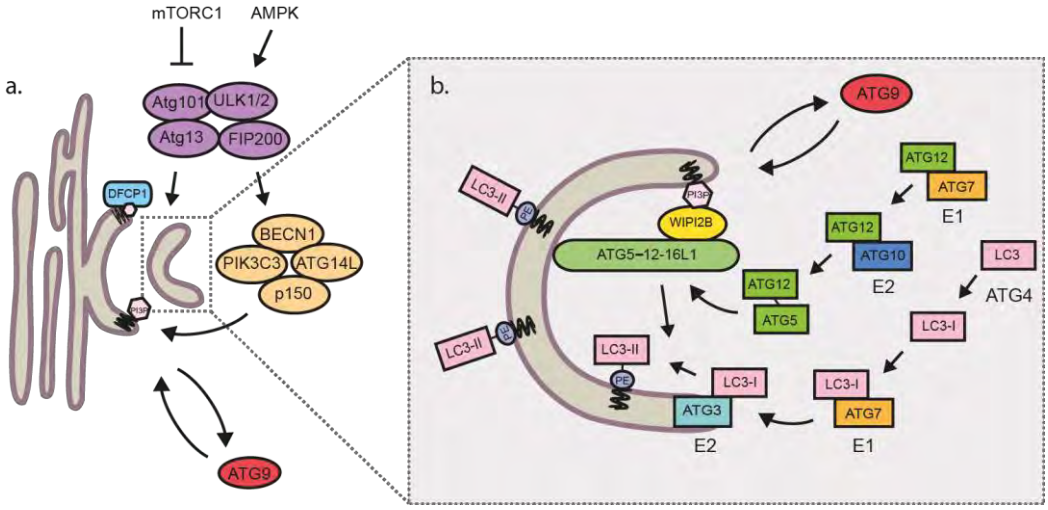

Figure 4: Core autophagic machinery. a. The ULK-complex (including ULK1/2, ATG101, ATG13 and FIP200) is regulated by the upstream nutrient and energy-sensing kinases mTORC1 and AMPK and induces autophagy by recruitment and activation of the PIK3C3-complex (consisting of PIK3C3, BECN1, ATG14L and p150). The resulting generation of PtdIns(3)P in the ER recruits other core autophagic proteins to the site of phagophore formation. Cycling of ATG9 to and from this site is crucial for autophagosome formation. **b.** Binding of WIPI2 to PtdIns(3)P in the phagophore recruits the Atg12–5-16L1-complex to the membrane for lipidation of LC3/GABARAP. ATG12 conjugation to ATG5 is mediated by ATG7 and ATG10, whereas LC3/GABARAP is processed by ATG4, ATG7 and ATG3 before it is conjugated to PE in the membrane facilitated by ATG12–5-16L1 complex. Modified from (Søreng et al.) (in press).

The PIK3C3/Vps34 complex

Another important complex of the autophagic core machinery is the class III Vps34/PIK3C3 complex consisting of PIK3C3 (Vps34 in yeast), its adaptor protein p150, ATG14L/Barkor and BECLIN1 (BECN1) and is activated by the ULK-complex (Russell et al., 2013, Park et al., 2016) (Figure 4a). PIK3C3 generates PtdInsI(3)P) from PtdIns, important to drive autophagy (Petiot et al., 2000). The kinase complex is recruited to the ER by a targeting sequence in ATG14L (Matsunaga et al., 2010), which results in production of PtdIns(3)P at cup-shaped structures in the ER, called omegasomes, from which phagophores seem to emerge (Axe et al., 2008, Hayashi-Nishino et al., 2009, Yla-Anttila et al., 2009). The importance of the PIK3C3/Vps34-complex in autophagy has been highlighted, as inhibition or mutation of the kinase blocks the pathway (Eskelinen et al., 2002, Blommaart et al., 1997, Juhász et al., 2008). Nonetheless, autophagy has also been reported to occur in the absence of PIK3C3/Vps34 and Beclin1, but the physiological importance of this non-canonical autophagy needs further investigation (Zhu et al., 2007, Scarlatti et al., 2008, Zhou et al., 2010). Furthermore, although the class III PIK3C3-complex is the main generator of PtdIns(3)P upon autophagy induction, there are evidence that also the class II PI3K kinase can generate PtdIns(3)P for autophagy in the absence of the class III complex (Devereaux et al., 2013)

Atg12 and Atg8 and their conjugation systems

The conjugation of the ubiquitin-like proteins ATG12 and Atg8/LC3 to ATG5 and PE, respectively, is well conserved between species and is important during formation of autophagosomes (Figure 4b).

There are several mammalian homologues of the yeast Atg8 protein and they are divided into two groups: the family of microtubule associated protein 1 light chain 3 (LC3) containing LC3A, LC3B and LC3C and the gamma-aminobutyric acid receptor-associated protein (GABARAP) family, including GABARAP, GABARAP-L1 and GABARAP-L2/GATE-16 (Shpilka et al., 2011). To become conjugated to PE, the Atg8-homologues are cleaved at the C-terminus by the cysteine protease ATG4, exposing a C-terminal glycine. This form of Atg8 homologues is cytosolic and is named Atg8/LC3-I (Kabeya et al., 2004). Atg8/LC3-I is further conjugated to PE in the membrane by ATG7 (E1) and ATG3 (E2), and

the conjugated version of Atg8/LC3 is called LC3-II (Fujita et al., 2008a, Geng and Klionsky, 2008, Tanida et al., 2004).

The E1- and E2-like enzymes ATG7 and ATG10 mediate conjugation of ATG12 to ATG5 and the resulting conjugate further forms a complex with ATG16L1. The ATG12–5-16L1 complex (E3-like) mediates the conjugation of Atg8-homologues to PE in the autophagic membrane (Fujita et al., 2008a, Geng and Klionsky, 2008, Tanida et al., 2004). Yeast Atg8 and its mammalian homologues are conjugated to both the inside and the outside of the phagophore membrane and therefore get sequestered in the closing autophagosome, leading to their degradation in the autolysosome (Kabeya et al., 2004). Fluorescently tagged LC3 is therefore widely used as a tool to follow autophagy.

The exact roles of the different mammalian Atg8 homologs in autophagy are not clear. LC3 has been suggested to mediate tethering and hemifusion of membranes and it was speculated that LC3 proteins were involved in the expansion of the phagophore membrane whereas GABARAP proteins played a role at a later step during autophagosome biogenesis (Weidberg et al., 2010, Nakatogawa et al., 2007). However, recent data indicate that GABARAP is crucial for formation of autophagosomes during periods of starvation while LC3 is important for selective types of autophagy (Engedal and Seglen, 2015, Haobam et al., 2014). Interestingly it was recently demonstrated that the Atg8-homologues are rather important for closing of the autophagosomes and for autophagosomes-lysosome fusion (Tsuboyama et al., 2016, Nguyen et al., 2016).

ATG9

ATG9 is so far the only conserved transmembrane protein among the core autophagic machinery and has been shown to play an important role during formation of autophagosomes (Reggiori and Tooze, 2012). It is a multi-spanning transmembrane protein, harbouring six transmembrane domains with both its N- and C-terminus facing the cytosol (Noda et al., 2000, Young et al., 2006). Upon induction of autophagy ATG9 is recruited to the site of phagophore formation and both yeast and mammalian cells depend on Atg9 to activate autophagy (Lang et al., 2000, Young et al., 2006).

Yeast Atg9 cycles between the Golgi and peripheral Atg9 reservoirs making a pool of Atg9 ready to shuttle between these compartments and the phagophore assembly site (PAS) during initiation of autophagy (Mari et al., 2010). It has been demonstrated that localisation of

Atg9 to the PAS is regulated by phosphorylation by the Atg1-complex (Papinski et al., 2014). Moreover, it was demonstrated that ATG9 is responsible for recruiting the TRAPPIII complex and the yeast RAB1 homologue, ypt1, which act as a tethering factor to recruit the Vps34-kinase complex to the site of autophagosome formation (Kakuta et al., 2012). Atg9-vesicles deriving from Golgi undergo fusion before they are incorporated into the outer phagophore membrane. Atg9 is recycled from the autophagosome upon fusion with the vacuoles (Yamamoto et al., 2012).

Under fed conditions, mammalian ATG9 cycles between the *trans*-Golgi network (TGN) and endosomes (Young et al., 2006) including recycling endosomes (Longatti et al., 2012, Lamb et al., 2016b, Imai et al., 2016). During starvation it traffics to omegasomes and the phagophore (Young et al., 2006, Popovic and Dikic, 2014, Orsi et al., 2012) and similar as in yeast, the ULK-complex regulates trafficking of ATG9 away from the TGN (Young et al., 2006, Chan et al., 2009). In contrast to yeast, mammalian ATG9 is not inserted into the phagophore and only transiently associates with the phagophore membrane (Orsi et al., 2012). It was recently proposed that as for yeast, maintaining a cycling pool of ATG9 between the Golgi apparatus, endosomes and a peripheral ATG9 compartment is necessary for autophagy initiation. ATG9 cycling important for autophagy has been demonstrated to require TRAPP-III (Shirahama-Noda et al., 2013). This is in line with recent findings showing that trafficking of ATG9 from recycling endosomes to the Golgi was found to depend on a complex consisting of the RAB-GAP TBC1D14 together with TRAPP-III (Lamb et al., 2016b).

Membrane input for autophagosome formation

It is widely believed that autophagosomes form from a pre-existing membrane source, where phagophore nucleation is followed by input from several membrane sources, allowing elongation and closure of the autophagosomes (Lamb et al., 2013, Abada and Elazar, 2014).

Phagophore nucleation

In yeast, phagophores nucleate at the PAS, a specific site located in close proximity to the vacuole and the ER (Suzuki and Ohsumi, 2010). Nucleation occurs when Atg1 is recruited to the PAS and further recruits the Vps34-complex to generate PtdIns(3)P, which stimulates autophagosome formation (Suzuki et al., 2013). In mammalian cells, however, autophagosomes can form at several sites, with the cup-shaped omegasomes and ER-mitochondria contact sites as the main sites of phagophore nucleation during starvation

induced autophagy (Axe et al., 2008, Hamasaki et al., 2013). Omegasomes are rich in PtdIns(3)P generated by the PIK3C3-complex and marked by the PtdIns(3)P-binding proteins DFCP1 (double-fyve containing protein 1) which is used as a marker for early autophagic structures (Axe et al., 2008, Hayashi-Nishino et al., 2009). The ER-mitochondria contact sites are lipid rafts containing regions in the ER that recruit members of the PIK3C3-complex to promote formation of the phagophore (Hamasaki et al., 2013, Garofalo et al., 2016). Similar to yeast, the ULK-complex is involved in recruiting the PIK3C3-complex to the ER for PtdIns(3)P production and phagophore nucleation (Burman and Ktistakis, 2010, Russell et al., 2013, Park et al., 2016).

Membranes sources contributing to forming autophagosomes

Expansion of the phagophore to form a complete autophagosome involves input from different membrane sources. Lipidation of LC3/GABARAP also contributes to membrane expansion and is thought to occur at the highly curved ends of the phagophore targeted by the E2-like enzyme ATG3 (Geng and Klionsky, 2008, Nath et al., 2014). The PtdIns(3)P-binding protein WIPI2 (WD-repeat protein interacting with phosphoinositides 2) binds to PtdIns(3)P in the phagophore and has been shown to be important for LC3 lipidation by recruiting the ATG12–5-16L1 complex to the membrane (Polson et al., 2010, Dooley et al., 2014).

Several compartments including the mitochondria, ER-Golgi intermediate compartment (ERGIC), the Golgi, plasma membrane and recycling endosomes have been found to provide the phagophore with lipids and proteins required for elongation and this seems to occur through vesicle transport or interaction through membrane contact sites (Figure 5).

Mitochondria

In addition to the already mentioned ER-mitochondria contact sites (Hamasaki et al., 2013), mitochondria have been suggested to provide expanding phagophores with membranes. This was demonstrated by the colocalisation of the autophagy proteins ATG5 and LC3 with the mitochondrial membrane upon starvation and that mitochondria form continuous LC3-positive structures (Hailey et al., 2010, Cook et al., 2014). Moreover, a mitochondrial membrane lipid was transferred onto autophagosomes during starvation, indicating that mitochondria supply membranes and lipids to the forming autophagosomes, possibly through the ER-mitochondria contact sites where autophagosomes are formed.

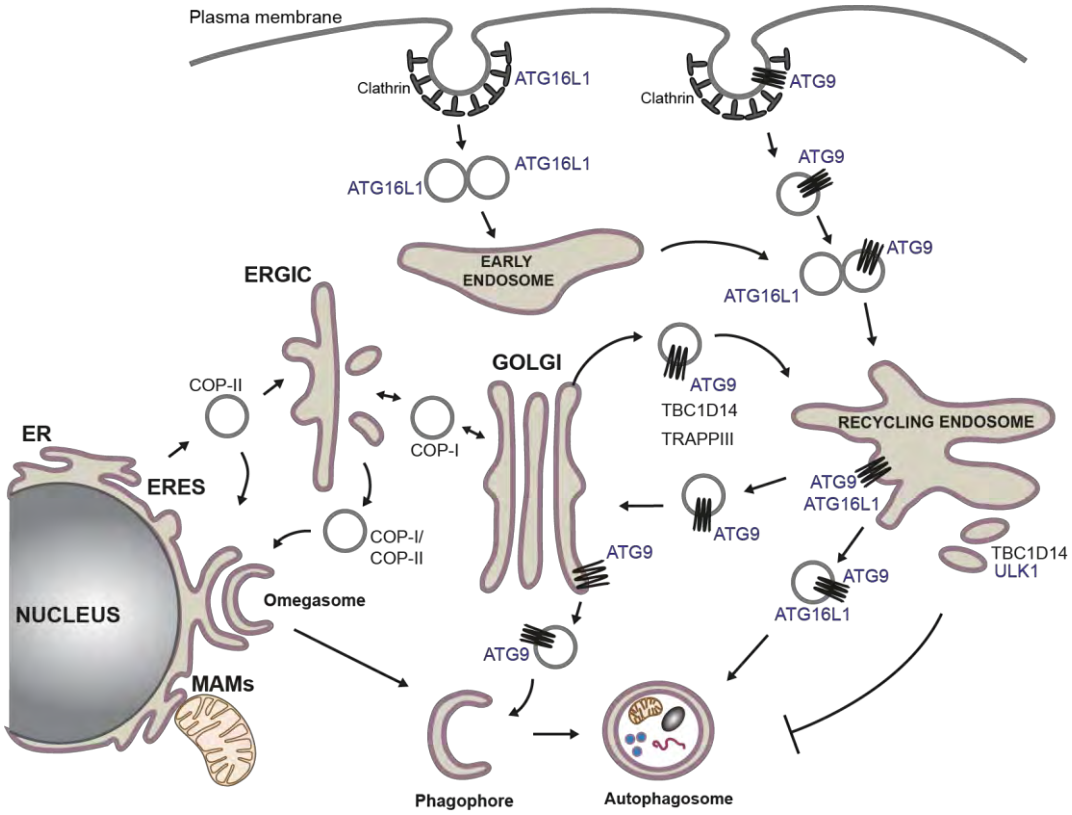

Figure 5: Membrane sources in autophagosome formation. Several organelles provide membrane input to the phagophore, including mitochondria and MAMs, ERES, ERGIC, the Golgi network, plasma membrane and recycling endosomes (ATG proteins are indicated in blue). LC3-lipidation can occur on both ERES and the ERGIC transported to the phagophore in COP-I/COP-II vesicles. COP-I trafficking from the Golgi is also important in autophagy. ATG9 cycles between the TGN and endosomes, including recycling endosomes, regulated by TRAPPIII-like complex including TBC1D14 and is redirected to the forming autophagosomes during starvation. Modified from (Søreng et al.) (in press).

The Golgi apparatus

The Golgi apparatus has also been proposed as a possible membrane source contributing to the forming autophagosomes as demonstrated by a block in autophagosome formation and autophagic degradation upon impaired vesicle traffic from the Golgi apparatus (Razi et al., 2009, van der Vaart et al., 2010). In line with this, AP-1 and clathrin mediated trafficking from the TGN was found to be important for LC3-associated vesicles budding from the TGN (Guo et al., 2012). Moreover, shuttling of ATG9 between the Golgi and endosomes was found to be important for autophagosome biogenesis upon starvation (Young et al., 2006).

ERGIC and ERES

Trafficking of proteins from the ER to the Golgi occurs from ER-exit sites (ERES) and COP-II vesicle formation from ERES was demonstrated to be important for autophagy (Zoppino et al., 2010, Graef et al., 2013). Furthermore, LC3 lipidation at membranes of the ER-Golgi intermediate compartment (ERGIC) indicates that also the ERGIC could be a source for membrane contribution to the autophagosomes. This was supported by the findings that starvation-induced LC3 spot formation was inhibited upon drug-mediated disruption of ERGIC (Ge et al., 2013).

Plasma membrane and Recycling endosomes

The plasma membrane has also been implicated in delivery of membranes to the forming autophagosomes. It was shown that ATG16L1 directly interacts with AP-2 and clathrin and is internalised into clathrin-coated vesicles (Moreau et al., 2011, Ravikumar et al., 2010). Depletion of either AP-2 or clathrin decreased the number of ATG16L1 positive precursor membranes and mature autophagosomes (Ravikumar et al., 2010). ATG16L1-containing vesicles undergo homotypic fusion to form autophagic precursor membranes important for autophagy (Puri et al., 2013). Also ATG9 traffics in endocytic vesicles from the plasma membrane on its way to the phagophore, although in different vesicles than ATG16L1 (Puri et al., 2013). In line with this, ATG9 was found to interact with the AP-2 complex and clathrin which mediates proper sorting of ATG9 to the autophagosomes in a TBC1D5-dependent manner (Popovic and Dikic, 2014). Loss of AP-2 or TBC1D5 resulted in missorting of ATG9 and reduced autophagy.

The vesicles deriving from the plasma membrane containing ATG9 and ATG16L1 were found to undergo heterotypic fusion and coalesce at recycling endosomes (Puri et al., 2013). Their further trafficking from recycling endosomes is important for autophagosome formation (Puri et al., 2013, Imai et al., 2016). It was recently shown that mutating the N-terminal AP-2 interacting motif of ATG9 resulted in accumulation of ATG9 in recycling endosomes and inhibition of autophagy (Imai et al., 2016). Moreover, ATG9 was found to accumulate on juxtanuclear recycling endosomes upon excess levels of the membrane lipid sphingomyelin, resulting in accumulation of unclosed autophagosomes (Corcelle-Termeau et al., 2016).

Both ULK1 and ATG9 have been found to colocalise with RAB11- and transferrin receptor (TfR)-positive recycling endosomes (Longatti et al., 2012). Furthermore, TBC1D14,

a RAB GAP that upon overexpression generates tubules from recycling endosomes, was identified as a negative regulator of autophagy (Longatti et al., 2012).

In this thesis we provide additional evidence for the contribution of recycling endosomes in autophagy showing that the PX-BAR domain protein Sorting nexin 18 (SNX18) promotes autophagy by generating tubules from recycling endosomes that are positive for ATG16L1 and GFP-LC3 (paper I). Depletion of SNX18 inhibits autophagy and results in accumulation of ATG9 on TfR-positive juxtanuclear recycling endosomes, a phenotype that can be rescued by SNX18-mediated recruitment of dynamin (paper III). Finally, we show that the PX domain containing protein HS1BP3 localises to ATG9- and ATG16L1-positive structures and negatively regulates autophagy by modulation of phosphatidic acid levels through regulation of phospholipase D1 activity at recycling endosomes (paper II).

Phospholipids and lipid modifying enzymes in autophagy

Phospholipids comprise a group of membrane lipids including phosphoinositides, phosphatidylethanolamine and phosphatidic acid, all shown to be important for autophagy.

Among the phosphoinositides having a role in autophagy, PtdIns(3)P generated by the Vps34/PIK3C3 kinase is best studied, with a crucial role in recruiting the core machinery during induction of autophagy (Simonsen and Tooze, 2009). The PtdIns(3)P level in the autophagic membrane is regulated by the PtdIns(3)P phosphatases, Jumpy, and myotublarin related phosphatase 3 (MTMR3) which dephosphorylate PtdIns(3)P and thus negatively regulate autophagy (Vergne et al., 2009, Taguchi-Atarashi et al., 2010). Dephosphorylation by Jumpy impaired recruitment of WIPI1 and other early autophagy proteins to the phagophore during autophagy (Vergne et al., 2009). Moreover, MTMR3 was found to negatively regulate autophagy initiation and overexpression of MTME3 resulted in smaller autophagosomes, suggesting that PtdIns(3)P is also important for determining autophagosome size (Taguchi-Atarashi et al., 2010). In addition to its role as a phosphatase, MTME3 was also recently demonstrated to bind to and suppress mTORC1 activity, thus suggesting a dual role for MTME3 in autophagy (Hao et al., 2016). Interestingly, PtdIns(5)P was found to act as an alternative for PtdIns(3)P during glucose starvation, to recruit DFCP1 and WIPI2 to the phagophore membrane and for mediating ATG12–5 conjugation (Vicinanza et al., 2015).

PtdIns(3)P can be converted into PtdIns(3,5)P_2 by the PtdIns(3)-5-kinase PIKfyve/FAB1 which has been found to be involved during maturation of the

autophagosomes (Rusten et al., 2007, Martin et al., 2013). The inositol polyphosphate-5-phosphatase E (INPP5E) was recently identified as a regulator of PtdIns(3,5)P_2 and autophagy (Hasegawa et al., 2016). It localises to the lysosomes where it dephosphorylates PtdIns(3,5)P_2 to PtdIns(3)P in the lysosomal membrane important for autophagosome-lysosome fusion .

Other phosphoinositides are also found to play a role during autophagosome formation. Among these is PtdIns(3,4,5)P_3, which is normally produced from PtdIns(4,5)P_2 at the plasma membrane and has been found to regulate mTOR activity thus affecting autophagy (Dall'Armi et al., 2013).

PE and PA are phospholipids involved in autophagy. Both lipids are synthesised in the mitochondrial membrane from where they are transferred to the ER through ER-mitochondria contact sites, allowing their further transport onto other organelles such as autophagosomes (Rowland and Voeltz, 2012). PE is a cone-shaped lipid providing structure to membranes due to its relatively large head group and narrow carbon chain. Insertion of PE into membranes induces local curvature stress (Marsh, 2007), facilitating formation of vesicular structures such as autophagosomes. As previously described, lipidation of the Atg8-protein family occurs by conjugation to PE during autophagy.

PA is also a cone-shaped lipid, containing a small charged head group that provides negative curvature to membranes (Kooijman et al., 2005). PA is involved in cell signalling (Wang et al., 2006) and has been implicated in autophagy by directly interacting with and activating mTOR (Fang et al., 2001). Moreover, it was proposed that PA can be generated in the autophagosomal membrane, as the PA-producing enzyme phospholipase D1, making PA from phosphatidylcholine (PC) (Lassègue et al., 1993), partially colocalised with LC3 and its inhibition resulted in decreased autophagy (Dall'Armi et al., 2010). Furthermore, PLD1 was also found to stimulate the autophagic degradation of α-synuclein aggregates associated with Alzheimer's and Parkinson's disease (Bae et al., 2014), further implicating PA in the autophagic process. In addition, PA can be generated from diacylglycerol (DAG) by the action of DAG-kinase (DAGK), and blocking the kinase was found to inhibit autophagy (Takita et al., 2011). In line with this, PA can also be converted to DAG through phosphatidic acid phosphatase (PAP), and increased levels of DAG induce autophagy (Shahnazari et al., 2010). Furthermore, PA can be generated from Lysophosphatidic acid (LPA) by LPA acyltransferases (LPAATs) (Leung, 2001). Although it has been demonstrated that LPAATs are necessary for mTOR signalling (Blaskovich et al., 2013), not much is known about

LPAATs in the autophagic process. However, in paper III we observed that drug-mediated inhibition of LPAATs inhibited autophagy.

Autophagic PI-binding proteins

The WIPI proteins belong to the PROPPIN family of WD40 repeat containing proteins and four different WIPI members exist in humans (WIPI1-4) (Proikas-Cezanne et al., 2015) and these proteins can interact with PtdIns(3)P and PtdIns(3,5)P2. WIPI1 and 2 are best characterized, both being recruited to PtdIns(3)P containing phagophores upon starvation (Gaugel et al., 2012, Proikas-Cezanne et al., 2004). WIPI2b was demonstrated to recruit the ATG12–5-16L1 complex to the phagophore for LC3-lipidation (Dooley et al., 2014).

Several FYVE domain-containing proteins, which all bind PtdIns(3)P, have been implicated in autophagy. As previously mentioned, DFCP1 binds to PtdIns(3)P at the omegasomes and is a marker for the very early stage of autophagosome formation, although its possible role in autophagy is unclear (Axe et al., 2008). Other FYVE domain proteins linked to autophagy are FYCO1 (FYVE and coiled-coil domain-containing 1) and ALFY (Autophagy-linked FYVE protein), involved in autophagosome maturation and selective autophagy, respectively (Pankiv et al., 2010, Olsvik et al., 2015, Simonsen et al., 2004, Filimonenko et al., 2010, Lystad et al., 2014)

PX-domain proteins are involved in many aspects of membrane trafficking (Seet and Hong, 2006) and 47 human PX-proteins have been identified. Although many of them have a binding preference for PtdIns(3)P, PX-proteins can also bind to other PIs (Teasdale and Collins, 2012). As previously mentioned, the PA-generating enzyme PLD1 is involved in autophagy, and contains a PX domain reported to bind to PtdIns(3,4,5)P_2 and PtdnsI(3)P as well as other PIs (Stahelin et al., 2004).

A big group of PX-domain proteins is the family of sorting nexins (SNX), consisting of more than 30 members. Some SNXs also contain a BAR (Bin/Amphiphysin/Rvs-homology)-domain that can both sense and induce membrane curvature (Itoh and De Camilli, 2006). An example of PX-BAR proteins is the SNX9 family, including SNX9, SNX18 and SNX33. The three family members share a similar domain sequence, all containing an N-terminal SH3-domain, followed by an unstructured LC-domain and a C-terminal PX-BAR region with a connecting Yoke domain on each side of the PX-BAR (Håberg et al., 2008, Pylypenko et al., 2007). SNX9 is a well characterised protein involved in clathrin-mediated endocytosis from

the plasma membrane (Lundmark and Carlsson, 2003, Soulet et al., 2005, Yarar et al., 2007). It has been found to interact with several components of the clathrin coat-machinery and recruits dynamin to mediate scission of vesicles from the plasma membrane during endocytosis (Lundmark and Carlsson, 2002, Lundmark and Carlsson, 2004, Shin et al., 2008, Yarar et al., 2007). Whereas AP-2 was identified as a binding partner of SNX9, its family member SNX18 was found to bind AP-1 and mediate transport between the Golgi network and endosomes (Håberg et al., 2008). Although SNX9 and SNX18 seem to bind to different adaptor proteins, it was still proposed that they may have redundant roles in clathrin-mediated endocytosis from the plasma membrane (Park et al., 2010). The third family member, SNX33, also binds dynamin and has been implicated in endocytic trafficking of amyloid precursor protein (APP) and prion proteins (Heiseke et al., 2008, Schöbel et al., 2008).

AIMS OF THE STUDY

The overall aim of this work has been to elucidate and characterise the roles of the phosphoinositide binding PX-domain containing proteins SNX18 and HS1BP3 in autophagy. The specific aims for each paper included in the thesis are described below:

Paper I: Membrane remodelling by the PX-BAR protein SNX18 promotes autophagosome formation.

To identify phosphoinositide-binding proteins involved in autophagy, we performed a high content imaging based siRNA screen searching for human PX-domain proteins in autophagy. We identified the PX-BAR protein SNX18 as a positive regulator of autophagy, and aimed to further investigate its localisation and specific role in the autophagic process, focusing on its membrane remodelling properties.

Paper II: HS1BP3 negatively regulates autophagy by modulation of phosphatidic acid levels.

The PX-domain containing protein HS1BP3 was identified as a negative regulator of autophagy in the screen performed in paper I. We therefore wanted to obtain a better understanding of its specific role in autophagy, focusing on its localisation and lipid binding properties, in order to unravel the involvement of different lipids in regulation of autophagy.

Paper III: SNX18 regulates ATG9 trafficking from recycling endosomes by recruitment of dynamin-2.

In paper I, we found that SNX18 promotes autophagy by generating tubules from recycling endosomes that provide membrane input to the forming autophagosome. As it has become evident that trafficking of the autophagic transmembrane protein ATG9 through recycling endosomes is important for autophagy we wanted to elucidate the role of SNX18 in ATG9 trafficking. Moreover, we asked whether the previously described binding of SNX18 to dynamin is important for its role in autophagy.

SUMMARY OF INCLUDED PAPERS

Paper I: Membrane remodelling by the PX-BAR protein SNX18 promotes autophagosome formation.

To investigate the role of PX-domain containing proteins in autophagy, we performed an imaging-based siRNA-screen in HEK cells stably expressing GFP-LC3, targeting all human PX-domain proteins. Formation of GFP-LC3 spots upon starvation was used as readout and we identified SNX18 as a positive regulator of autophagy, as knockdown of SNX18 strongly inhibited formation of GFP-LC3 spots and lipidation of GFP-LC3. Moreover siRNA-mediated SNX18 depletion impaired the autophagic flux as measured by long-lived protein degradation assay. On the contrary, overexpression of SNX18 in these cells resulted in increased LC3-lipidation and formation of GFP-LC3 spots, which was dependent on members of the core autophagic machinery, although SNX18 expression did not induce autophagic flux.

We further investigated the localisation of SNX18 and found it to localise in a juxtanuclear region positive for DFCP1, LC3 and ATG16L1. Depletion of SNX18 inhibited localisation of ATG16L1 to this area, but as it did not affect the number of DFCP1-spots, we concluded that SNX18 acts downstream of the PIK3C3-complex but upstream of ATG16L1 and GFP-LC3 lipidation.

SNX18 contains a C-terminal PX-BAR region that mediates membrane binding and tubulation (Håberg et al., 2008) and accordingly, we observed formation of membrane tubules positive for GFP-LC3 and ATG16L1 upon SNX18 overexpression. Moreover we found markers for recycling endosomes to be present both in the juxtanuclear region and in SNX18-induced tubules, suggesting that SNX18 generates tubules from recycling endosomes. By introducing mutations that prevent membrane binding of the PX-BAR domains, the membrane binding of SNX18 and the SNX18-induced formation of GFP-LC3 spots was disrupted. In addition, we found that the serine residue 233 of SNX18 is phosphorylated upon starvation in a time-dependent manner and that phosphorylation of S233 is important for the tubulation activity of SNX18 in autophagy.

We found SNX18 to both colocalise and co-fractionate with LC3, leading us to investigate a possible interaction between these proteins. Indeed, both LC3 and GABARAP proteins interact with SNX18 and we identified a WDDEW motif in the LC region of SNX18 to be essential for this interaction. Mutations of either one or both tryptophans in the

WDDEW motif abolished the interaction, as well as formation of GFP-LC3 spot and recruitment of GFP-LC3 to the SNX18-induced tubules.

Last, *in vivo* studies in of the drosophila homologue of SNX18, SH3PX1, revealed that formation of autophagic compartments marked by mCherry-Atg8a was inhibited in SH3PX1-depleted or mutated cells when compared to their neighbouring wild type cells. These findings show that the autophagic function of SNX18 is conserved.

Taken together, our results indicate that SNX18 recruits ATG16L1 and LC3 to membrane tubules generated from recycling endosomes that promote LC3 lipidation and provide membrane input to the growing phagophores.

Paper II: HS1BP3 negatively regulates autophagy by modulation of phosphatidic acid levels.

In our search for PX-domain containing proteins in autophagy we also identified a negative regulator of autophagy, the PX-protein HS1BP3. Depletion of HS1BP3 was found to increase LC3 spot formation and LC3 lipidation both under basal and starved conditions, and furthermore autophagic flux was increased in cells lacking HS1BP3 as measured by long-lived protein degradation assay and degradation of the autophagy cargo receptor SQSTM1/p62. *In vivo* analysis in GFP-LC3 zebrafish showed an increased number of GFP-LC3 in embryos lacking Hs1bp3, indicating a conserved role for HS1BP3 in regulation of autophagy in vivo.

HS1BP3 shows a diffuse localisation throughout the cytoplasm, but is enriched on structures positive for ATG9 and ATG16L1. Moreover, these structures also contained TfR, suggesting they are recycling endosome membranes. Live-cell imaging analysis demonstrated that these HS1BP3-positive structures fused with LC3-vesicles, suggesting that HS1BP3 regulates membrane transport from recycling endosomes to sites of autophagosome formation.

We found the N-terminal PX-domain of HS1BP3 to mainly bind to PA, although the full-length protein also binds to 3-phosphorylated PIs. Interestingly, lipidomics analysis of the total cellular lipid content revealed that depletion of HS1BP3 results in a 2-fold increase of PA-levels compared to control.

To further investigate the relationship between HS1BP3, PA and autophagy, cells depleted of HS1BP3 were treated with drugs that inhibit various PA-producing enzymes.

Interestingly, we observed that inhibition of PLD, the enzyme that generates PA from phosphatidylcholine (PC) blocked the increased autophagy seen upon HS1BP3-depletion. Moreover, the total PLD activity was increased in siHS1BP3-treated cells. Taken together, our findings indicate that HS1BP3 is a negative regulator of PLD activity and thus PA production.

We found PLD1, but not PLD2 to colocalise with HS1BP3 and ATG16L1 and interestingly, depletion of HS1BP3 increased the colocalisation of PLD1 and ATG16L1. Whereas overexpression of full length HS1BP3 or only the PX-domain reduced PLD1/ATG16L1 colocalisation, this was not the case upon overexpression of a HS1BP3 mutant lacking the PX-domain. Last, we showed that simultaneous knockdown of both HS1BP3 and PLD1 blocked the increased number of LC3-spots observed in cells depleted of only HS1BP3.

Taken together, our results indicate that membrane binding of HS1BP3 prevents access of PLD1 to ATG16L1-containing membranes, thereby regulating PLD1 activity and PA-levels on these structures. We propose that HS1BP3 though its binding to PA in AT16L1/ATG9 positive recycling endosome membranes provides a negative feedback mechanism, controlling PLD1 activity and its access to autophagic precursor membranes.

Paper III: SNX18 regulates ATG9 trafficking from recycling endosomes by recruitment of dynamin.

Our observations from paper I showing that SNX18 promotes autophagy by generating membrane tubules from recycling endosomes positive for ATG16L1 and thus regulates ATG16L1 traffic to the omegasomes led us to further investigate if SNX18 also is involved in trafficking of ATG9.

We generated a SNX18 knockout (KO) cell line using the CRISPR-Cas9 technology and found that autophagy was inhibited in these cells, similarly to cells treated with siRNA against SNX18. The number of GFP-LC3 spots formed upon starvation, as well as the autophagic flux as measured by degradation of long-lived proteins, was inhibited in the SNX18 KO cells compared to control cells. In addition, colocalisation of the early autophagy markers WIPI2 and ATG16L1 was decreased in cells lacking SNX18 compared to control cells, confirming our previous study showing a role for SNX18 in delivery of ATG16L1 to early autophagic structures.

It is becoming evident that ATG9 traffics through recycling endosomes on its way to the autophagosomes and that this trafficking is important for autophagy (Corcelle-Termeau et al., 2016, Imai et al., 2016, Lamb et al., 2016b, Puri et al., 2013). Since the tubules generated by SNX18 were positive for autophagic markers such as GFP-LC3 and ATG16L1, we asked if also ATG9 could be present, and indeed, we observed a clear localisation of ATG9 along the SNX18-induced tubules. In line with ATG9 trafficking through recycling endosomes in autophagy, we observed that ATG9 colocalised well with the recycling endosome-marker TfR, which was further increased upon starvation. Interestingly, ATG9 accumulated in a juxtanuclear region positive for TfR in the SNX18 KO cells, suggesting that SNX18 is required for trafficking of ATG9 away from this area.

SNX18 interacts with dynamin through its N-terminal SH3-domain (Håberg et al., 2008) and as dynamin is involved in vesicle scission, we were wondering if dynamin is recruited by SNX18 to mediate ATG9 traffic from recycling endosomes. In line with this hypothesis we found dynamin to localise to the SNX18-induced tubules. Furthermore, we generated a dynamin-binding mutant of SNX18 which no longer could co-immunoprecipitate with dynamin. Whereas overexpression of wild-type SNX18 could rescue the phenotype of ATG9 accumulation on TfR-positive juxtanuclear recycling endosomes observed in the SNX18 KO cells, overexpression of the SNX18 dynamin-binding mutant could not.

Taken together, we propose a model where SNX18 is recruited to recycling endosomes to facilitate trafficking of ATG9 from recycling endosomes to sites of autophagosome formation. SNX18 stimulates tubulation of ATG9 positive membrane and recruits dynamin to induce scission of membrane vesicles containing ATG9 destined for the autophagosomes.

DISCUSSION

The major aim of this thesis has been to increase our knowledge about the two PX-domain containing proteins SNX18 and HS1BP3 and their role in autophagy. Both proteins were identified in an siRNA-based imaging screen performed in our lab, targeting all human PX-domain proteins to identify new regulators of autophagy. The PX-domain is a lipid-binding domain with a preference for PtdIns(3)P, but can also mediate binding to other phosphoinositides. SNX18 was found to have a binding preference for PtdIns(4,5)P_2, whereas HS1BP3 binds to PA and 3-phosphorylated phosphoinositides. Through our studies we have shown that SNX18 and HS1BP3 act as a positive and negative regulator of autophagy, respectively, and that they both localise to recycling endosome membranes. We propose a model were both proteins, through different membrane remodelling mechanisms regulate the formation of recycling endosome derived autophagosome precursor membranes, providing us with a wider understanding of the proteins and lipids involved in the regulation of autophagy.

Membrane input from recycling endosomes to forming autophagosomes

During starvation-induced autophagy, the general idea is that phagophore membrane emerge from omegasomes in the ER and thus expands and elongated by receiving input from several membrane sources. Such input has been suggested to originate from compartments as the Golgi, mitochondria, plasma membrane and recently also recycling endosomes. All three papers included in this thesis support the latter, that recycling endosomes provide input to growing phagophores.

Overexpression of the RAB11-binding protein TBC1D14 was shown to generate tubules from ATG9- and ULK1-positive recycling endosomes that had a negative effect on autophagy (Longatti et al., 2012). Similarly, we found that overexpression of SNX18 leads to formation of membrane tubules positive for recycling endosome markers (RAB11 and TfR) and ATG9, but in contrast to TBC1D14, the tubules generated by SNX18 seem to promote autophagosome formation. As we did not observe SNX18 on the TBC1D14-induced tubules (paper III), we conclude that although both proteins stimulate tubulation of recycling endosomes, the tubules are not the same. Moreover, whereas overexpression of GFP-TBC1D14 significantly inhibited transferrin recycling, overexpression of SNX18 only slightly reduced the transferrin recycling (paper III). siRNA-mediated depletion of SNX18 did not affect transferrin recycling, in line with previously published data (Willenborg et al., 2011),

indicating that SNX18 is not generally required for recycling endosome function. The slightly more retained transferrin seen in cells with SNX18 overexpression might be due to a shift in recycling endosome function from recycling of cargo back to the plasma membrane towards membrane contribution in autophagy. As it is important to regulate the contribution of membranes to the forming autophagosomes, we propose that TBC1D14 and SNX18 oppositely control the formation of recycling endosome-derived autophagosome precursor vesicles. Interestingly, although SNX18 did not localise to the tubules generated by TBC1D14, we found TBC1D14 to be recruited to the SNX18-induced membranes (unpublished observations). However, how they operate in relation to each other to regulate autophagy needs further investigation.

During cytokinesis, SNX18 was, together with its family members SNX9 and SNX33, shown to be required for recruiting RAB11-positive recycling endosomes to the intracellular bridge to complete the cell division (Ma and Chircop, 2012). Moreover, following division of epithelial cells, SNX18 and its interaction partner, FIP5, a RAB11-effector protein, promote formation of the apical lumen by formation and/or scission of vesicles from recycling endosomes (Willenborg et al., 2011). It was suggested that binding of FIP5 activates and enhances the membrane remodelling activity of SNX18. The role of FIP5 in autophagy has not been studied in this thesis and it would be important to do so to obtain a better understanding of the link between RAB11, FIP5 and SNX18 in this context.

We found that the SNX18-induced tubules were positive for autophagy proteins such as ATG16L1, ATG9 and GFP-LC3. This is in line with previous publications showing that ATG16L1 and ATG9 meet in recycling endosomes after their trafficking via the plasma membrane, from where they are internalized into different populations of clathrin-coated vesicles (Puri et al., 2013). Moreover, it was recently shown that trafficking of ATG9 from recycling endosomes is important for autophagy, as inhibiting this reduced autophagosome formation and closure (Imai et al., 2016, Corcelle-Termeau et al., 2016). In paper I, we found transport of ATG16L1 to a juxtanuclear region positive for SNX18 and to DFCP1 spots (omegasomes) to be SNX18-dependent. siRNA depletion of SNX18 also prevented recruitment of RAB11 to the juxtanuclear area. Interestingly, in contrast, we observed juxtanuclear clustering of TfR and ATG9, but not ATG16L1, in SNX18 KO cells (paper III). As ATG9 and TfR are trans-membrane proteins, while RAB11 and ATG16L1 are both membrane-associated proteins, our data indicate that recycling endosomes accumulate in the juxtanuclear region in the absence of SNX18 and that SNX18 is important for membrane-

recruitment of ATG16L1 and RAB11. It has been found that excess levels of sphingomyelin results in ATG9 accumulation in TfR-positive juxtanuclear recycling endosomes and defective ATG9 traffic to WIPI2-positive early autophagic structures (Corcelle-Termeau et al., 2016). ATG16L1-vesicles did not accumulate and could still traffic to the forming autophagosomes, and it was speculated that spingomyelin specifically alters the recycling pathway of ATG9 and not ATG16L1. As ATG16L1 is absent from the juxtanuclear area also in our SNX18 KO cells, one could speculate the same thing for SNX18-mediated trafficking from recycling endosomes. On the other hand, the absence of ATG16L1 could also be explained by the fact that ATG16L1 only associates with membranes and is not a transmembrane protein as ATG9. It might therefore depend on SNX18 for its membrane association to recycling endosomes. Accordingly, in paper I, co-immunoprecipitation experiments demonstrated that ATG16L1 interacts with the PX-BAR region of SNX18. We found that overexpression of SNX18 increases the number of ATG16L1 spots (paper I) and in our experiments in paper III we found that SNX18 affects the localisation of ATG16L1 to WIPI2-positive structures. Taken together, these findings indicate that SNX18 affects ATG16L1 membrane association and/or trafficking. However, more work is needed to reveal the exact relationship between ATG16L1 and SNX18. Regarding the SNX18-dependent localisation of RAB11 to the juxtanuclear region, we only used TfR as a marker for recycling endosomes in paper III and did not really test how RAB11 behaves in the SNX18 KO cells. This will be done in the near future.

In paper II we demonstrate that the other PX-protein investigated in this thesis, HS1BP3, mainly is a cytosolic protein, but also localises to structures positive for ATG9, ATG16L1 and TfR. Live-cell imaging revealed that these structures fused with LC3-positive vesicles, indicating that these are recycling endosome-derived structures possibly providing input to autophagosomes. Our results show that HS1BP3 and SNX18 oppositely regulate autophagy, which will be discussed in more detail below.

SNX18 promotes autophagosome formation

In paper I we identified SNX18 as a positive regulator of autophagy as siRNA mediated depletion of SNX18 inhibited formation of GFP-LC3 puncta, GFP-LC3 lipidation and degradation of long-lived proteins. In contrast, overexpression of SNX18 resulted in increased GFP-LC3 spot formation and LC3 lipidation. For further investigation of SNX18's role in

autophagy, we generated a SNX18 knock-out (KO) cell line in paper III and confirmed that autophagy was inhibited also in these cells.

SNX18 contains a N-terminal PX-BAR region which enables SNX18 to both sense and induce membrane curvature (Håberg et al., 2008) and we found that this part is responsible for generating the SNX18-induced membrane tubules from recycling endosomes. Introducing mutations in this region, corresponding to mutations known to abolish membrane binding of the related SNX9 (Pylypenko et al., 2007, Yarar et al., 2007), abolished membrane binding of SNX18, as well as its ability to generate membrane tubules upon overexpression. Another characteristic of SNX18 is the presence of an amphipatic helix just upstream of the PX-domain (Pylypenko et al., 2007). According to the PhosphoSitePlus database (http://www.phosphosite.org/), this helix contains a serine residue (S233) which is phosphorylated upon rapamycin treatment (Chen et al., 2009). Similarly, our experiments showed that phosphorylation of S233 increases upon starvation and induction of autophagy (paper I). We thus generated phospho-mimicking (S233D) and -abolishing (S233A) mutants of S233 and found that although they both efficiently bound membranes, they could not generate membrane tubules or induce GFP-LC3 spots as SNX18 WT. These results led us to believe that the phosphorylation and de-phosphorylation of S233 is important for regulating the function of SNX18 in autophagy and that it is tightly controlled in order to adjust the SNX18-dependent membrane contribution in autophagy. So far we have not been able to investigate the kinase or phosphatase involved in regulation of S233-phosphorylation, but one possible candidate could be ULK1, as it is activated upon rapamycin and starvation when mTOR is inhibited (Jung et al., 2010). Moreover, as mentioned above, ULK1 was recruited to the tubules generated from recycling endosomes upon overexpression of TBC1D14 (Longatti et al., 2012), showing that ULK1 is present at and/or recruited to recycling endosomes. Further studies into the regulation of this important serine-residue in SNX18 are required.

To our surprise, although SNX18 clearly affects autophagosome formation as shown by several assays, depletion of SNX18 did not change the endogenous level of lipidated LC3. This has been quite difficult to assess and further investigation is needed to explain why SNX18 would affect GFP-LC3 but not endogenous LC3. One possibility is that adding a tag to LC3 changes its conjugation-properties. It could be that GFP-LC3 and endogenous LC3 are lipidated on different membranes and that only the membranes where GFP-LC3 lipidation occurs are affected by SNX18. Alternatively, although LC3-conjugation to PE occurs on both the inner and outer phagophore membrane, it could be that altered properties of GFP-LC3

would result in GFP-LC3 lipidation in the outer membrane whereas endogenous LC3 is mainly in the inner membrane and that SNX18 would affect the proteins in the outer membrane, thus only inhibiting GFP-LC3 and not endogenous LC3. We have not investigated the effect of SNX18 depletion on lipidation of LC3 tagged with smaller tags (e.g. myc or HA), nor have we tested the effect on GABARAP lipidation. As will be mentioned below, in paper I we found SNX18 to interact with LC3 and even more with GABARAP. It could be that SNX18 is mainly important for lipidation of GABARAP and not LC3, but in a system where LC3 is overexpressed an effect would still be visible. These are questions that need to be further studied.

SNX18 binds to PtdIns(4,5)P_2

Of the seven different PIs, PtdIns(3)P is best studied in the context of autophagy, where it is known to be important for induction of autophagy by recruiting PtdIns(3)P effector proteins as e.g. WIPIs to the phagophore. However, emerging evidence have implicated other PIs and PI modifying enzymes at several steps along the autophagic pathway (Jang and Lee, 2016). PtdIns(5)P was found to act as an alternative to PtdIns(3)P under glucose starvation, allowing binding of proteins that would normally bind PtdIns(3)P and affect autophagosome formation (Vicinanza et al., 2015). Moreover, PI(3,4,5)P_3 present in the plasma membrane was found to activate mTORC1-sinaling and thus regulate autophagy induction (Dall'Armi et al., 2013). PtdIns(4)P and PtdIns(4,5)P_2 as well as PI(3,5)P_2 have been implicated at the later steps of autophagy (Wang et al., 2015, Rong et al., 2012, Hasegawa et al., 2016).

siRNA-mediated depletion of SNX18 did not affect the number of omegasomes, marked by the PtdIns(3)P-binding protein DFCP1. However, depletion of ATG14L inhibited SNX18-mediated formation of GFP-LC3 puncta, indicating that SNX18 acts to stimulate autophagy downstream of omegasome formation. SNX18-depletion reduced ATG16L1 localisation to DFCP1 and WIPI2 puncta (paper I and III), indicating that SNX18 functions downstream of the PIK3C3-kinase complex and PtdIns(3)P. Instead of being a PtdIns(3)P-binding protein, SNX18 was rather found to bind PtdIns(4,5)P_2, which is present at a rich amount in the plasma membrane, but also to other compartments such as the Golgi and endosomes (Håberg et al., 2008, Watt et al., 2002). In paper I, we found that depletion of PtdIns(4,5)P_2 by treating cells with ionomycin inhibited the SNX18-mediated increase in GFP-LC3 spots. The same phenotype was observed when the rapalogue system was used to target a PtdIns(5)-phosphatase to the plasma membrane where it dephosphorylates PtdIns(4,5)P_2. This could

indicate that SNX18 facilitates delivery of membrane from the PtdIns(4,5)P_2-rich plasma membrane to growing phagophores. In line with such a model, it was indeed suggested that SNX18 has redundant functions with SNX9 and acts at the plasma membrane (Park et al., 2010). However, in our experiments, SNX18 mainly localises to cytoplasmic structures such as the Golgi network and recycling endosomes from where it generates membrane tubules and is therefore not likely to function at the plasma membrane.

The unstructured LC-domain of SNX18 mediates interaction with adaptor protein 1 (AP-1), involved in vesicle trafficking between the Golgi and endosomes (Håberg et al., 2008) and AP-1 and clathrin have been found to colocalise with LC3-positive structures during starvation and be important for autophagosome formation from the Golgi apparatus (Guo et al., 2012). One could therefore speculate that SNX18 is recruited to PtdIns(4,5)P_2 at the Golgi to promote AP-1 dependent trafficking of membrane input for autophagosomes in addition to its autophagic contribution from recycling endosomes.

Generation of PtdIns(4,5)P_2 from PI(4)P was found to be required for autophagic lysosome reformation (ALR), a membrane remodelling process generating lysosomes from autolysosomes, which is crucial for maintaining lysosome homeostasis (Rong et al., 2012). We proposed that the inhibition of PtdIns(4,5)P_2 affects SNX18-mediated formation of autophagosomes, but whether or not SNX18 is also involved in later steps of autophagy or during ALR remains to be investigated.

SNX18 interacts with LC3- and GABARAP-proteins

As SNX18 affects lipidation of GFP-LC3 and formation of GFP-LC3 spots we wanted to test if SNX18 interacts with the family of Atg8-homologues. Human Atg8-homologues consist of the LC3-family (containing LC3A, LC3B and LC3C) and GABARAP-family (including GABARAP, GABARAP-L1 and GABARAP-L2/GATE-16) (Shpilka et al., 2011).

Proteins interacting with LC3/GABARAPs contain a conserved motif called a LC3-interacting region (LIR), having the consensus sequence X_{-3} X_{-2} X_{-1} -W_0- X_1 X_2 -L-X_3, with an aromatic amino acid in the W-position, a hydrophobic amino acid in the L-position and several acidic amino acids in the X-positions (Johansen and Lamark, 2011). In paper I we found SNX18 to bind to LC3 and even more with GABARAP. Interestingly, the interaction was mediated through a WDDEW-motif in its unstructured LC-domain. The motif is similar to a canonical LIR due to the presence of an aromatic tryptophan followed by acidic residues,

but it lacks the hydrophobic residue in the L-position. Mutating this non-canonical LIR by changing one or both tryptophans abolished the interaction to LC3 and GABARAP. Additional experiments showed that SNX18 interacts even more with the non-lipidated form of LC3 (LC3-I; paper I) and that it co-migrates with both LC3-I and LC3-II in membrane fractions. Although LC3-I is generally believed to be a cytosolic protein, we show in paper I that it can also be membrane associated. Conjugation of LC3 to phosphatidylethanolamine (PE) in the autophagic membrane is mediated by the Atg12–5-16L1 complex that functions as an E3-ligase for LC3-conjugation (Fujita et al., 2008b). As ATG16L1 is recruited to the SNX18-induced membrane tubules we propose in paper I that SNX18 mediates recruitment of LC3-I and ATG16L1 to recycling endosome membranes to mediate LC3-lipidation.

SNX18-dynamin interaction is important during vesicle formation from recycling endosomes

The small GTPase dynamin, being recruited to clathrin-coated pits to mediate scission of vesicles, was previously found to interact with the SH3-domain of SNX18 through proline-rich regions (Håberg et al., 2008). As ATG9 accumulates in TfR-positive juxtanuclear recycling endosomes in the absence of SNX18 (paper III), it is likely that SNX18 can recruit dynamin to recycling endosomes to facilitate scission of ATG9-positive vesicles. Indeed, we found that dynamin was recruited to the SNX18-induced membrane tubules as mentioned earlier.

The observed phenotype of ATG9 accumulating on juxtanuclear recycling endosomes in SNX18 KO cells was rescued upon overexpression of wild-type (WT) SNX18, but not upon overexpression of a dynamin binding-deficient mutant of SNX18. This suggests that dynamin is recruited to the SNX18-induced tubules to mediate vesicle scission. Accordingly, when ATG9 accumulated in recycling endosomes there was a decrease in ATG9 colocalisation with ATG16L1-positive vesicles (paper III). A weakness using this readout is that SNX18 also probably affects ATG16L1 trafficking, and would thus give incorrect information about ATG9 trafficking to autophagosomes. It is therefore necessary to measure colocalisation of ATG9 with WIPI2-puncta in the SNX18 KO cells and to investigate the effect of the dynamin binding-deficient SNX18 mutant on autophagy.

The SNX18-related SNX9 mediates dynamin oligomerisation and assembly at the plasma membrane to perform clathrin-mediated endocytosis through AP-2 binding

(Lundmark and Carlsson, 2003, Soulet et al., 2005). As SNX18 binds dynamin and recruits dynamin to membrane tubules, it could be hypothesised that SNX18 performs the same function as SNX9, however at recycling endosomes instead of the plasma membrane. In line with this, the WDDEW motif in the LC-domain of SNX18 responsible for the LC3/GABARAP interaction (paper I) also facilitates interaction with AP-1 (Håberg et al., 2008). As mentioned above, mutating the SNX18 WDDEW-motif impaired the SNX18-mediated formation of GFP-LC3 puncta which could be due to inhibition of LC3/GABARAP binding, but also be due to lack of AP-1 interaction. Interestingly, in addition to its proposed role in autophagosome formation (Guo et al., 2012), AP-1 has also been demonstrated to mediate cargo sorting from recycling endosomes (Fields et al., 2010).

A binding motif for AP-2 was recently identified in the N-terminus of ATG9 (Imai et al., 2016, Zhou et al., 2017). Mutation of this motif resulted in accumulation of ATG9 in recycling endosomes and a subsequent inhibition of autophagy, indicating that AP-2 dependent ATG9 trafficking from recycling endosomes is important for autophagy (Imai et al., 2016). This could also be AP-1 dependent, as the same motif in ATG9 was found to bind AP-1 (Zhou et al., 2017). Combined with our studies, it is tempting to speculate that SNX18 functions together with coat-proteins and adaptor-proteins at recycling endosomes to recruit dynamin to mediate formation of ATG9 vesicles required for autophagosome biogenesis. Further studies are required to elucidate the relationship and the regulation of binding of AP-1/LC3 to the WDDEW-motif in SNX18.

A complex including TRAPPIII and TBC1D14 was recently shown to be important for ATG9 trafficking from recycling endosomes back to the Golgi apparatus, providing a cycling pool of ATG9 necessary for autophagy (Lamb et al., 2016b). It was found that this ATG9 traffic depends on the formation of a tubovesicular intermediate structure with a shift from RAB11 to RAB1. It remains to be investigated whether SNX18 and its membrane remodelling properties are involved in the formation of this compartment. Although our experiments indicate that SNX18 affects ATG9 traffic from recycling endosomes to the forming autophagosomes (paper III), further studies are required to find out if SNX18 also could also affect the cycling of ATG9 between other compartments.

HS1BP3 is a negative regulator of recycling endosome-derived autophagic precursors

The PX-domain containing protein HS1BP3 was characterised in paper II. It was found to act as a negative regulator of autophagy as depletion LC3-spot formation, LC3-lipidation and autophagic flux was increased upon HS1BP3-depletion and HS1BP3 overexpression resulted in decreased levels of lipidated LC3.

HS1BP3 only occasionally localises to WIPI2-structures, and we did not observe any localisation on structures positive for ATG14L or DFCP1. Nor did we find any changes in the number of WIPI2- or DFCP1-spots in cells lacking HS1BP3, thus we speculate that HS1BP3 acts at a step downstream or in parallel with autophagy initiation and nucleation. In contrast, HS1BP3 localised extensively to cytoplasmic structures positive for ATG9 and ATG16L1, but interestingly HS1BP3 depletion did not alter the formation of ATG16L1-puncta upon starvation. Instead it could rather be that HS1BP3 somehow changes the properties or the distribution of the ATG16L1-positive structures. We did not test the localisation of ATG16L1 or ATG9 to early autophagic structures such as WIPI2 or DFCP1 upon HS1BP3 depletion. In line with our findings in paper I and III, the HS1BP3-, ATG9- and ATG16L1-positive structures were positive for TfR. By live cell-imaging we observed that these vesicles fused with autophagosomes marked by LC3, and we therefore propose that they are recycling endosome-derived vesicles contributing to the forming autophagosomes.

The PX domain of HS1BP3 binds phosphatidic acid

We found that both full-length HS1BP3 and the PX-domain bind phosphatidic acid (PA) and other 3-phosphorylated phosphoinositides. Interestingly, siRNA-mediated depletion of HS1BP3 resulted in a 2-fold increase of the total PA content in HEK293 cells. Moreover, the activity of the PA-producing enzyme PLD1 was increased upon HS1BP3 knockdown. Additionally, we show that PLD1 localises to the same autophagic precursor membranes as HS1BP3 and PA generated by PLD1 is important for autophagy.

PA is a phospholipid that previously has been implicated in autophagy, although the function of PA in autophagy is somewhat contradictory. The interaction of PA with mTOR was found to activate mTOR signalling (Fang et al., 2001) and in line with this, inhibiting the PA-producing enzyme PLD1 promotes autophagy signalling (Jang et al., 2014). In contrast, our experiments showed induced autophagy and increased PA levels in cells lacking HS1BP3,

with no effect on mTOR activity, as analysed by immunoblotting for phosphorylated S6-kinase, a target of mTOR. Moreover, our results showed increased PLD1 activity (and thus elevated PA-content) in HS1BP3 depleted cells, contradictory to the above-mentioned studies. PA has multiple cellular roles as a lipid precursor and signalling molecule. The PA-producing enzymes generate PA form various substrates thereby creating several species of PA and we found that 9 out of 12 PA species were upregulated by HS1BP3 depletion. It could thus be that different pools of PA are regulated differently, involving HS1BP3 in affecting local PLD1 activity and PA-production for example in the autophagosomal membrane. In line with our studies, others have also demonstrated that PLD1 can be recruited to LC3-positive autophagosomes upon starvation in a PtdIns(3)P-dependent manner to promote autophagy (Dall'Armi et al., 2010). Furthermore, PLD1 can mediate autophagic degradation of α-synuclein protein aggregates and thus also be important for selective autophagy (Bae et al., 2014). Our results indicate that PLD1 and PA promote autophagy and that this is negatively regulated by binding of HS1BP3 to PA.

In addition to PLD1 generating PA from phosphatidylcholine (PC), PA can be produced by two other enzymes, lysophosphatidic acid acyltransferases (LPAATs) that generate PA from lysoPA and DAGK converting diacylglycerol DAG to PA (Coon et al., 2003, van Blitterswijk and Houssa, 2000). In paper II, we investigated the possible link between increased PA levels and increased autophagy observed in HS1BP3-depleted cells by chemically inhibiting PLD1, LPAATs and DAGK. Only by inhibiting the PLD1-pathway we were able to significantly block the HS1BP3-mediated induction of autophagy, suggesting that HS1BP3 acts on PA produced by PLD1. However, we did observe an inhibition in autophagy by blocking LPAATs although this was not HS1BP3-dependent indicating that the involvement of PA in autophagy is not restricted to only PLD1. As there is very little evidence of LPAATs being involved in autophagy, this would require further studies. In our hands, inhibiting DAGK did not affect autophagy, even though previous studies have demonstrated that treating neuronal cells with a DAGK-inhibitor, thus blocking PA-synthesis, stimulates autophagic degradation (Takita et al., 2011). This is more in line with the publications showing that PA activates mTOR-signalling and would probably not be regulated by HS1BP3.

There is evidence showing that simultaneous binding to PA and another phosphoinositide increases membrane binding of a protein. This was shown for the p47 subunit of NADPH oxidase, that binds both PA and PtdIns(3,4)P_2 in separate binding pockets

of the PX-domain (Karathanassis et al., 2002). The same increased membrane affinity was observed upon binding of the PLD1 PX-domain to PtdIns(3,4,5)P_3 and PtdIns(3)P in addition to PA, again in separate binding pockets (Stahelin et al., 2004). Our experiments from paper II show that HS1BP3 has similar phosphoinositide-binding properties as PLD1 and in line with this we observed that HS1BP3 and PLD1 compete for binding to ATG16L1 positive membranes. We did not investigate if the membrane affinity of HS1BP3 is affected by its binding to different PIs, nor did we characterise different PI-binding pockets in the HS1BP3 PX-domain. Further work is needed to elucidate the membrane binding properties of HS1BP3.

Not much is known about the lipid composition of the autophagosome or the involvement of lipid-binding and -modifying proteins in autophagy. Identifying PA in relation to HS1BP3 provides more knowledge and insight to the roles of phospholipids in autophagy. PA has several roles in the cell serving as a lipid precursor, signalling molecule and as a provider of membrane structure (Athenstaedt and Daum, 1999, Shin and Loewen, 2011, Kooijman et al., 2005). Moreover, it has been implicated in several membrane fusion processes, and although the exact function of PA in autophagy is not known, several of its properties make it interesting in the context of autophagy.

PA is an anionic lipid, which due to its cone-shape containing a small head group attached to a wide backbone generates negative membrane curvature when inserted into membranes (Zimmerberg and Kozlov, 2006, Kooijman et al., 2005). It could therefore contribute to generation of the highly curved phagophore membrane. Cone-shaped lipids such as PA and also PE generate less packaging of the surrounding lipid bilayer, which facilitates insertion of membrane proteins (van den Brink-van der Laan et al., 2004). The E2-like enzyme ATG3 was demonstrated to mediate lipidation of LC3/GABARAP by sensing local lipid-packing defects, and thus highly curved membranes, typically like the ones occurring in the presence of conical lipids (Nath et al., 2014). The membrane binding of ATG3 was found to require an N-terminal amphipatic helix, and it was thus proposed that ATG3 senses the highly curved ends of the growing phagophore where it facilitates lipidation of LC3/GABARAP (Nath et al., 2014). If PA is responsible for making such membrane stress, this could be the explanation for the increased levels of PA and LC3-lipidation observed in our HS1BP3-depleted cells (paper II).

During autophagosome biogenesis, the phagophore expands by receiving membrane input from other compartments, probably occurring by fusion of vesicles with the autophagic

membrane. Our experiments showed that PLD1 localises to autophagic precursor membranes deriving from recycling endosomes that fuse with LC3-positive autophagosomes. PA has been implicated in different vesicle fusion events, such as spore formation in yeast, mitochondrial fusion and exocytosis (Nakanishi et al., 2006, Choi et al., 2006). Furthermore, PLD1 was found to be important for fusion of VAMP7-vesicles during neurite formation in neurons (Ammar et al., 2013), further implicating PA in vesicle fusion events. It is thus possible that the increased autophagy observed in the absence of HS1BP3 is due to altered fusion ability of ATG16L1-positive precursor membranes with the phagophore because of elevated PA-levels. On its way from the plasma membrane, ATG16L1-vesicles undergo homotypic fusion mediated by the SNARE protein VAMP7, before they reach the recycling endosomes where they are united with ATG9 (Moreau et al., 2011, Puri et al., 2013). As HS1BP3 colocalised with vesicles positive for both ATG16L1 and ATG9 we believe that it acts at a step downstream of recycling endosomes, and not during homotypic fusion of ATG16L1 vesicles. More work is needed to further characterise the fusion of membrane input to the growing phagophores and the SNAREs and/or tethering factors involved.

Autophagy and the actin cytoskeleton

HS1BP3 has previously been identified as a binding partner of HS1 (Takemoto et al., 1999). HS1 is only expressed in hematopoietic cells and is homologous to cortactin, which is ubiquitously expressed in other cell types. They both recruit the actin related protein (Arp) 2/3-complex to promote actin branching (van Rossum et al., 2005). Indeed, our search for interaction partners of HS1BP3 identified cortactin to be specifically co-immunoprecipitated with HS1BP3 from cell lysate. We further established a direct interaction between the SH3-domain of cortactin and proline-rich regions of HS1BP3 and also showed that HS1BP3 interacts with the SH3 domain of HS1 (paper II). Cortactin was previously shown to be important for basal autophagy by interacting with HDAC6 to promote F-actin network that surrounds ubiquitinated substrates targeted to autophagosomes (Lee et al., 2010). Moreover, the cortactin-binding protein Alix, associated with the ESCRT machinery, was recently found to promote autophagosome maturation by interacting with ATG12-ATG3, also during basal autophagy (Murrow et al., 2015). We hypothesised that the effect of HS1BP3-depletion on autophagy could depend on its binding to cortactin. However, we did not see a difference in starvation-induced or basal autophagy in upon depletion of cortactin. As HS1BP3 was found to play a role both during basal and starvation-induced autophagy, we concluded that HS1BP3 affects autophagy independently of cortactin. We have not specifically investigated the role of

HS1BP3 in selective autophagy and cannot rule out that the HS1BP3-cortactin interaction may be important for selective autophagy of e.g. protein aggregates.

As for starvation-induced autophagy, actin filaments and the actin motor protein myosin II were found to be required for transport of ATG9-vesicles in mammalian cells (Tang et al., 2011). In addition, actin filaments support the structure of omegasomes and phagophore membranes upon autophagy induction (Mi et al., 2015). In our co-immunoprecipitation studies, other subunits of the Arp2/3 complex were also found to interact with HS1BP3, although we did not investigate if they directly interact. It is therefore possible that HS1BP3 is involved in some actin-related processes during autophagy and more studies are required to establish the relationship between HS1BP3, the actin cytoskeleton and autophagy.

Another protein that activates Arp2/3 and promotes actin polymerisation is N-WASP (Wiskott-Aldrich syndrome protein), which was found to interact with SNX18 and SNX9 (Park et al., 2010, Shin et al., 2007). SNX9 also interacts with Arp2/3 and this binding sequence is conserved in SNX18, linking SNX18 to the actin cytoskeleton. In our work of characterising the role of SNX18 in autophagy we did not investigate the relationship between SNX18 and actin, but in light of the findings demonstrating a role for actin filaments in providing mechanical support for autophagosomes, it would be interesting to look further into the role of actin in formation of the SNX18 tubules. It is thought that SNX9 operates together with actin filaments to narrow the neck of the budding vesicle, followed by the subsequent recruitment of dynamin to allow vesicle scission (Lundmark and Carlsson, 2008). One could speculate that since SNX9 and SNX18 are closely related, SNX18 could act together with actin in a similar manner. Furthermore, during endocytosis, following vesicle scission, actin filaments reorganise to generate an actin comet tail that promotes transport of the vesicle further into the cytoplasm (Mooren et al., 2012). It is possible that both SNX18 and HS1BP3 depend on actin recruitment to perform a similar function at recycling endosomes after budding of vesicles targeted to the forming autophagosome.

SNX18 and HS1BP3 regulate autophagosome formation

There are still many unanswered questions regarding the membrane sources that contribute to the growing phagophore during autophagy and the proteins and lipids involved. Moreover, the lipid composition of the autophagosomal membrane and the involvement of lipid-binding proteins and lipid-modifying enzymes are not well understood.

In this thesis, the focus has been to characterise the roles of the PX-domain containing proteins SNX18 (paper I and III) and HS1BP3 (paper II) in autophagy in order to provide more information about phospholipid-binding proteins in autophagy. We have established a role for both proteins at recycling endosomes, where they oppositely regulate membrane input from this compartment to the growing phagophore. Autophagosome formation is a process that needs to be tightly regulated and we found that whereas SNX18 promotes formation of autophagosomes, HS1BP3 acts to negatively regulate their biogenesis, summed up in Figure 6.

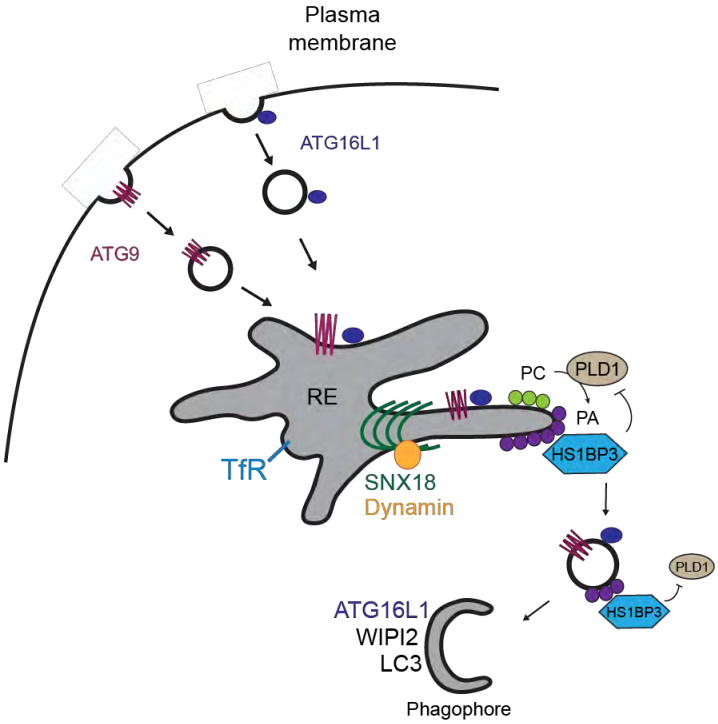

Figure 6: SNX18 and HS1BP3 regulate autophagosome formation. SNX18 generates tubules from recycling endosomes that promote autophagosome formation, contributing to the correct trafficking of ATG9 and ATG16L1. Oppositely, HS1BP3 provides negative feedback to control the formation of autophagosomes. By sensing local PA-levels in recycling endosome-derived membranes, it can regulate the activity of the PA-generating enzyme PLD1, thereby controlling the PA production necessary to induce autophagosome biogenesis.

During induction of autophagy, ATG9 and ATG16L1 traffic via the plasma membrane through recycling endosomes and this is important for autophagy. We found that SNX18 through its PX-BAR domain generates tubules from recycling endosomes containing both

ATG9 and ATG16L1 in addition to LC3. By recruiting dynamin, SNX18 generates vesicles from this compartment in a process important for proper trafficking of ATG9 and ATG16L1 to the autophagosomes. By inhibiting dynamin binding, ATG9 accumulates in the juxtanuclear recycling endosomes. Although we did not investigate ATG9 localisation or trafficking in the absence of HS1BP3, we found HS1BP3 to localise to recycling endosome-derived structures containing ATG9 and ATG16L1 that fuse with LC3-positive autophagosomes. Whereas PtdIns(4,5)P2 is important for the role of SNX18 in autophagy, HS1BP3 senses local PLD1-produced PA in recycling endosome-derived membranes to control the formation of autophagosomes. We found HS1BP3 and PLD1 to compete for binding to the ATG16L1 positive membranes, and thus propose that HS1BP3 provides a negative feedback by its binding to PA, controlling the activity and access of PLD1 to autophagic membranes. In the absence of HS1BP3, more PLD1 can bind autophagosome precursor membranes to produce PA that would stimulate formation of autophagosomes. A possible role for actin in SNX18 and HS1BP3 regulated vesicle formation from recycling endosomes remains to be investigated.

EXPERIMENTAL CONSIDERATIONS

Cell lines and transfections

The majority of the experiments performed in this thesis have been carried out using adherent human cell lines. In the lab, cell lines grow on plastic surfaces in media containing the necessary nutrients required for the cells to grow and divide, providing us with a simple model system to study human biology. The cells are usually immortalised and thus divide indefinitely, which is an advantage, but also a possible concern as the immortalisation process and several rounds of cell division make cell lines prone to developing certain genetic changes that could affect their normal functions and behaviour. Anyway, cell lines do not require much work and are easy to manipulate to perform lab experiments. As for autophagy, the process occurs in all cells and tissues, and observing the same autophagic phenotype in several cell lines thus indicates that the pathway is conserved. In this thesis, the cell lines used are mainly HeLa, HEK293A and U2OS. HeLa and U2OS are cancer-derived cells already having the ability of unlimited division whereas HEK293A cells are immortalised human embryonic kidney cells. Furthermore, in paper III, a HEK293A SNX18 knock-out (KO) cell line was generated together with the corresponding control/wild type. All these cell lines are valuable tools when it comes to studying autophagy as the pathway is readily induced upon stimulation and autophagic structures are easily visible by microscopy.

A common way of studying the function of a protein of interest is to analyse the effect of its depletion or transient expression in cell lines. Depletion of a protein is normally performed by transfecting in specific small interfering RNAs (siRNA) that leads to silencing of their respective target gene. To avoid toxicity leading to cell death, the siRNAs should be used at low concentrations. Furthermore, it is important to consider possible off-target effects when using siRNAs as it may cause misinterpretations of the result if the siRNA binds to other sequences than its target mRNA. This can be avoided by using more than one siRNA against a single mRNA to test if the same phenotype can be observed by several individual siRNAs. In paper I and III we employed rescue experiments, where SNX18 was reintroduced in siSNX18 and SNX18 KO cells to make sure that the observed phenotypes are due to the lack of SNX18 and not any off-target effects. In paper I, to avoid inhibition of SNX18-expression by the siRNA during the rescue experiment, we generated siRNA-resistant SNX18 constructs that would not be recognised by the siRNA.

If no antibody is available or to follow protein expression and localisation using live cell imaging, fluorescently tagged proteins can be transiently transfected into cells to investigate their localization and function. This method is also used when studying the effect of different mutants by imaging, and as it is both rapid and easy, it is widely used. However, there are certain challenges associated with transient transfections. Among these are the variation in transfection efficiency and the level of protein expression between cells and the fact that the expression level of transiently transfected proteins is often so much higher than the expression level of the endogenous protein. Very high levels of protein expression can in some cases cause formation of protein aggregates that could lead to misinterpretation of the protein's localisation and/or function. It is therefore important to analyse cells with low expression levels, or even better generate cell lines with stable (inducible) expression of the protein of interest. In paper I cells were transfected with different SNX18 mutants and as overexpression of SNX18 WT increased LC3 lipidation and the number of GFP-LC3 spots, formation of GFP-LC3 spots was used as readout. The overexpression of two proteins is clearly a disadvantage, but as depletion of different ATG proteins inhibited the SNX18-induced formation of GFP-LC3 puncta we concluded that this was dependent on the autophagic machinery and thus a physiologically relevant system to study the function of SNX18 in autophagy.

To overcome the problem of variable protein expression upon transient transfection, stably transfected cell lines can be used, that either continuously express the protein of interest, or can be induced to do so. In these cell lines all cells will express the protein of interest, in contrast to transiently transfected cells. This is beneficial in biochemical assays when all cells are analysed. The expression level in these cells would typically be lower than for transient transfected cells. In paper I and III we have used HEK 293A cells stably expressing GFP-LC3, whereas HeLa cells with inducible expression of GFP-LC3 were used in paper I. The HeLa GFP-LC3 cells were treated with tetracycline to induce expression of GFP-LC3, using a low concentration that did not affect cell growth or any intracellular processes. It is also important to include a control when using overexpressed proteins, to make sure that the observed phenotype is due to the protein of interest and not a side-effect of expressing the tag.

CRISPR-Cas9 technology

In paper III we used the CRISPR-Cas9 technology to generate a stable SNX18 KO cell line. This method involves gene editing and is based on the use of the bacterial CRISPR

(Clustered Regularly Interspaced Short Palindromic Repeats) and the CRISPR-associated protein-9 nuclease (Cas9). These genes are essential in the adaptive immune system of certain bacteria, allowing them to rapidly respond to and eliminate invading DNA (Horvath and Barrangou, 2010, Cong et al., 2013). The Cas9 is an endonuclease that with the help of a guide RNA is directed to cleave a specific target gene. There are several advantages regarding the CRISPR/Cas9-technology as it is relatively easy, cheap and an efficient method to produce cells depleted of a target gene. However, it is not possible to completely avoid the possibility of off-target effects, so a search for mutations within the genome at sites resembling the guide RNA target sequence should be performed. It is also possible that cells permanently lacking a gene could adapt to this situation and thus behave differently than cells transiently transfected with siRNA, so initial experiments should thus be performed under both conditions.

Confocal microscopy, electron microscopy and quantitative image analysis

The degree of localisation, colocalisation or trafficking of intracellular proteins can be studied and quantified by confocal immunofluorescence microscopy that has been used in all three studies in this thesis. Confocal microscopy provides images from a single plane mediated by exclusion of the background information above and below the plane, allowing high quality imaging. For quantification of the degree of colocalisation between two proteins, necessary precautions are needed to avoid false results and interpretations. It is important to avoid bleed-through of the fluorophores and it is necessary to scan all the fluorophores using the same optical slice thickness with the same laser settings to ensure that the detected signal comes from the same confocal plane. Moreover, for quantification, images should be obtained from a high number of randomly selected cells from independent experiments to increase the statistic strength of the results. In this thesis, a Zeiss LSM 710 confocal microscope was used and the quantification of colocalisation was measured using the Zeiss Zen software.

All three papers have used high-throughput imaging to quantify the number of GFP-LC3 spots in addition to other types of structures. This was performed using a fluorescent microscope, the Zeiss AxioVision Cell Observer followed by quantification of spots by the Zeiss Assay Builder software. The advantage of this system is that as it is fully automated, it can randomly analyse a large number of cells (thousands) and thus avoid errors due to small sample size. Moreover, this system was used in paper I to measure the number of GFP-LC3 spots in SNX18-transfected cells, using the Zeis Assay Builder software to identify

transfected cells. A challenge when it comes to the automated set-up to identify transfected cells is the identification of false positives. Occasionally, a non-transfected cell next to a transfected cell can be counted as transfected if there is overlap of the cytosol from both cells. To avoid this problem, we therefore inspected the cells manually and excluded the cells that were clearly not transfected. Another potential problem is that the cells are not always in focus, leading to the measurement of puncta that might not be the correct structures. However, as we normally would include images containing hundreds or thousands of cells in our analysis, this would not affect the final result.

To visualise the membrane tubules induced by SNX18-overexpression (paper I), we used electron microscopy (EM) in addition to confocal microscopy. EM is a technique that allows a better resolution of intracellular structures. However, it is a time consuming technique that requires experience both in sample preparation and quantitative imaging.

Autophagy monitoring assays

Several assays can be used to monitor autophagy and many of them are based on measuring the autophagic markers LC3 and p62 upon specific treatments. During autophagy, LC3 is conjugated to PE in the autophagic membrane and because the membrane bound form of LC3 (LC3-II) migrates slightly faster by SDS-PAGE than the non-membrane form (LC3-I), the conversion of LC3-I to LC3-II can be monitored by western blotting. As increased levels of LC3-II could indicate either increased formation of autophagosomes or a block in autophagosome maturation, including an inhibitor that blocks lysosomal degradation is necessary to measure the autophagic flux. Several inhibitors can be used and we have mainly used Bafilomycin A1, which inhibits the lysosomal proton pump, thereby blocking the degradation capacity of the lysosomes due to increased pH. Monitoring LC3 by western blotting has been used in all three papers. A recent study shows that differences in LC3-lipidation not always correlate with changes in autophagy (Engedal and Seglen, 2015) and it is thus important to include other autophagic flux assays to confirm the results. In paper III we observed that SNX18 depletion affects GFP-LC3, but not endogenous LC3 highlighting the importance of combining several assays to strengthen the results.

Another way of monitoring autophagic flux is to measure degradation of p62, which is a cargo receptor for autophagy, but also a substrate for autophagy as it gets degraded in the autolysosomes. In paper II we used a system where GFP-p62 expression was turned off upon

drug treatment allowing us to measure the degradation of GFP-p62 in HS1BP3-depleted cells by flow cytometry.

In this thesis, autophagic flux was also measured using the long-lived protein degradation assay. Long-lived proteins are mainly degraded by autophagy, and by labelling these with radioactive ^{14}C-Valine their degradation can be measured by quantifying the amount of soluble radioactive valine in the media (from degraded proteins) compared to the radioactivity left in the cells (intact protein). Following a 17 hours chase to get rid of short-lived radioactive proteins (in the presence of cold valine), autophagy is induced by treating the cells with EBSS. To analyse the specific degradation through autophagy, an autophagy-specific inhibitor is used, typically 3-methyladenine (3MA) that inhibits the PI3KC3-complex. One drawback of this method is that it is relatively expensive and time consuming. It is however considered to be a highly reliable method to study autophagic flux.

Interaction studies

Immunoprecipitation is a widely used method to study protein-protein interactions and involves pulldown of a protein from cell lysates using bead-coupled antibodies that either recognise the protein of interest or a tag attached to a transfected protein. This method is relatively easy, but it is important to include proper controls to make sure unspecific binding to the antibody or to a tag is avoided. This is especially important when doing proteomics to identify potential interaction partners of a protein as we did for HS1BP3 (paper II). We immunoprecipitated GFP-HS1BP3 and sent the whole sample for analysis of any interaction partners. This method is prone to contaminations and thus the identification of false positives. However, false positives could be excluded by comparison of the results between GFP-HS1BP3 and a GFP-control. During co-immunoprecipitation studies, there is also the risk of missing specific interaction partners, because of weak or transient interactions or too stringent experimental conditions.

Co-immunoprecipitations from cell lysates only confirm that the proteins are in complex with one another and do not necessarily mean that the proteins directly interact. Therefore, further validation of interactions using other assays is needed. Direct interactions can be investigated *in vitro* by combining recombinant proteins attached to different tags as we did in paper II using MBP-tagged HS1BP3 and a GST-tagged SH3 domain of cortactin. Additionally, in paper I we used a peptide array assay to verify the direct interaction between SNX18 and GST-tagged GABARAP. In this experiment, 18-mer peptides covering the SH3-

LC3 region of SNX18 was spotted on a membrane, where 17 amino acids from each peptide were overlapping. The membrane was incubated with purified GST-GABARAP allowing binding of the recombinant protein to the membrane. Using this assay we were able to determine the motif of SNX18 responsible for the interaction with GABARAP, but it is worth noticing that the peptides on the membrane are linear sequences so although we determined that GABARAP binds to this linear non-canonical LIR motif, additional experiments were done to confirm that the interaction is conserved when the domains are properly folded.

In paper II, we incubated recombinant HS1BP3 with membranes containing different phospholipids to investigate a possible protein-lipid interaction. As for the peptide array, these lipids are spotted on the membrane, which could affect their binding ability compared to the physiologically folded and intact lipids. We therefore repeated the experiment by incubating recombinant HS1BP3 with liposomes with different lipid compositions. These are small artificial vesicles containing a curved surface with different lipids. The main advantage is the resemblance of the lipids in their physiological conditions, and binding of a protein to liposomes would increase the probability of this interaction being correct. However, in our study to investigate if HS1BP3 binds PA on liposomes (paper II), we faced some challenges when it comes to the high PA-content resulting in increased membrane stress and thus higher membrane curvature that would lead to fusion of liposomes and generate highly curved structures. We therefore optimised the conditions and found the highest PA-content as possible without disrupting the liposomes.

Lipidomics analysis

To study the effect of depletion of HS1BP3 on the overall cellular lipid content, we analysed extracted lipids from these cells by lipidomics (paper II). This technique allows the large scale analysis of cellular lipids under certain conditions. Because lipids are highly dynamic and constantly changing with their environmental conditions, certain difficulties are associated with this technique and it is therefore important to be careful during sample preparation so that the samples are being prepared in a similar manner between the experiments and to include proper controls. The results are shown as the relative abundance of each lipid making to easier distinguish the differences of each condition on the lipid. There are several molecular species of each lipid and the use of lipidomics allows the analysis of each subtype.

The use of model organisms

The use of model organisms allows *in vivo* biological studies of genes in non-human systems. Many genes and gene functions are conserved between simpler organisms to humans, and to study the effect of a gene in a living organism provide a helpful tool to better understand a possible role for the gene or the protein in the human body.

In paper I we used *Drosophila melanogaster* as a model organism to study the effect of the SNX18 homologue, SH3PX1, on autophagy. Drosophila is a model organism with several benefits, including short generation time, large offspring and a variety of genetic tools are available. Most signaling pathways are conserved between Drosophila and humans and it is also a widely used model for studying autophagy (Jennings, 2011, Mauvezin et al., 2014). Moreover, there are generally very few restrictions regarding the use of Drosophila in the lab, as there are minimal associated ethical and safety issues.

In paper II we used another model organism, *Danio rerio* (zebrafish). Similarly to drosophila, zebrafish has a short generation time, produce large amounts of offspring and are relatively cheap to maintain compared to rodent model organisms. A great advantage of using zebrafish is that fertilisation and embryo development occurs outside the mother's body. Moreover, the embryos are nearly transparent, making it easy to investigate their development. In addition to being a good model for studying human diseases, zebrafish expressing GFP-Lc3 have been made, creating a nice tool to study autophagy (He and Klionsky, 2010, Varga et al., 2015). In paper II we took the advantage of the GFP-Lc3 line to investigate the effect of HS1BP3 depletion on autophagy in vivo.

The main drawback of drosophila and zebrafish is that they are not mammals and would thus not be completely identical to mammalian systems. However, both genomes have been fully sequenced and overall they share a high level of gene similarity to humans. More than 75 and 80 % of genes causing human diseases can be found in drosophila and zebrafish, respectively, thus making these model organisms valuable tools to study cellular pathways such as autophagy.

FUTURE PERSPECTIVES

By characterising the roles and functions of the two PX-domain proteins SNX18 and HS1BP3 in autophagy, the work in this thesis provides a better understanding of the contribution of recycling endosomes to the forming autophagosomes. We found both proteins to be present in recycling endosome-derived membrane structures, but whereas SNX18 promotes autophagy, HS1BP3 acts as a negative regulator of autophagosome formation. SNX18 generates tubular structures that pinches off and are required for proper trafficking of autophagy proteins to the early autophagic structures. On the other hand, HS1BP3 binds PA and thereby controls the activity of the PA-generating enzyme PLD1, important for the increased autophagy observed in the absence of HS1BP3.

It is widely accepted that starvation induced autophagy begins with the formation of a phagophore/isolation membrane from specific regions of the ER that expands by receiving membrane input from several other compartments. Our findings of SNX18 contributing with membrane input from recycling endosomes support this model. However, several aspects related to the role of SNX18 in autophagy are still unclear. We showed that the tubulation activity of SNX18 is dependent on phosphorylation of S233 and that this phosphorylation increases upon autophagy induction, but we did not investigate the kinase or phosphatase involved in the regulation of SNX18 membrane tubulation activity.

We found that ATG16L1 is recruited to the SNX18-induced tubules and that the two proteins interact. SNX18 also interacts with LC3 and GABARAPs and interestingly, SNX18 interacts with AP-1 through the same binding motif as LC3/GABARAP. We did not further explore how all these interactions are regulated in time and space, which would lead to a better understanding of the role of SNX18 in autophagy. Furthermore, we show that SNX18 interacts with dynamin and that this binding is important for trafficking of ATG9 from recycling endosomes to autophagosomes. As dynamin and AP-1 are associated with clathrin mediated vesicle formation, further investigation is needed to determine how the LC3/AP-1 binding mutant of SNX18 affects ATG9 trafficking and if SNX18 could be associated with clathrin coat-assembly at recycling endosomes.

Further studies are also needed to investigate the interaction between SNX18 and N-WASP and the link to actin assembly and whether or not this interaction is important for autophagy. Finally, as both TBC1D14 and SNX18 generate tubular structures from recycling

endosomes, but are found to oppositely affect autophagy, it is interesting to further explore a possible link between these proteins and the regulation of their functions.

HS1BP3 was found to bind PA and thus act to negatively regulate autophagy. However, we still do not know exactly when HS1BP3 operates during autophagosome biogenesis and further studies are needed to elucidate the regulation of HS1BP3. We still do not know if HS1BP3 acts on the phagophore membrane or on the precursor membranes so more experiments are needed to fully understand the role of HS1BP3, PA and PLD1 in autophagy. Since not much is known about the lipid composition of the autophagosomal membranes, the finding of PA on autophagic membranes is very interesting. The interesting fact that PA can mediate membrane fusion makes it a possible candidate to study how membrane input fuses with the growing phagophores and whether or not HS1BP3 would affect this and if the process involves any SNARE proteins. HS1BP3 also interacts with components of the actin polymerisation machinery, including cortactin, but so far we have not been able to find a link between HS1BP3, actin and autophagy. Moreover, further studies are required to investigate a possible role for HS1BP3 in actin and cortactin related processes, such as cell migration.

Obtaining a better understanding of the general aspects of autophagy and how the pathway is regulated is of great importance as autophagy has been implicated in a number of diseases such as neurodegeneration and different types of cancer. Thus, increasing our knowledge about the molecular mechanisms of the pathway could pave the way for development of drugs to treat such diseases.

REFERENCES

Abada, A. & Elazar, Z. 2014. Getting ready for building: signaling and autophagosome biogenesis. *EMBO Reports,* 15**,** 839-852.

Ammar, M.-R., Humeau, Y., Hanauer, A., Nieswandt, B., Bader, M.-F. & Vitale, N. 2013. The Coffin-Lowry Syndrome-Associated Protein RSK2 Regulates Neurite Outgrowth through Phosphorylation of Phospholipase D1 (PLD1) and Synthesis of Phosphatidic Acid. *The Journal of Neuroscience,* 33**,** 19470.

Arstila, A. U. & Trump, B. F. 1968. Studies on cellular autophagocytosis. The formation of autophagic vacuoles in the liver after glucagon administration. *The American Journal of Pathology,* 53**,** 687-733.

Athenstaedt, K. & Daum, G. 1999. Phosphatidic acid, a key intermediate in lipid metabolism. *European Journal of Biochemistry,* 266**,** 1-16.

Axe, E. L., Walker, S. A., Manifava, M., Chandra, P., Roderick, H. L., Habermann, A., Griffiths, G. & Ktistakis, N. T. 2008. Autophagosome formation from membrane compartments enriched in phosphatidylinositol 3-phosphate and dynamically connected to the endoplasmic reticulum. *J Cell Biol,* 182**,** 685-701.

Bae, E. J., Lee, H. J., Jang, Y. H., Michael, S., Masliah, E., Min, D. S. & Lee, S. J. 2014. Phospholipase D1 regulates autophagic flux and clearance of α-synuclein aggregates. *Cell Death and Differentiation,* 21**,** 1132-1141.

Barlowe, C., Orci, L., Yeung, T., Hosobuchi, M., Hamamoto, S., Salama, N., Rexach, M. F., Ravazzola, M., Amherdt, M. & Schekman, R. 1994. COPII: A membrane coat formed by Sec proteins that drive vesicle budding from the endoplasmic reticulum. *Cell,* 77**,** 895-907.

Barlowe, C. K. & Miller, E. A. 2013. Secretory Protein Biogenesis and Traffic in the Early Secretory Pathway. *Genetics,* 193**,** 383.

Blaskovich, M. A., Yendluri, V., Lawrence, H. R., Lawrence, N. J., Sebti, S. D. M. & Springett, G. M. 2013. Lysophosphatidic Acid Acyltransferase Beta Regulates mTOR Signaling. *PLOS ONE*.

Blommaart, E. F., Krause, U., Schellens, J. P., Vreeling-Sindelarova, H. & Meijer, A. J. 1997. The phosphatidylinositol 3-kinase inhibitors wortmannin and LY294002 inhibit autophagy in isolated rat hepatocytes. *Eur J Biochem,* 243**,** 240-6.

Bonifacino, J. S. & Lippincott-Schwartz, J. 2003. Coat proteins: shaping membrane transport. *Nat Rev Mol Cell Biol,* 4**,** 409-414.

Boya, P., Reggiori, F. & Codogno, P. 2013. Emerging regulation and functions of autophagy. *Nat Cell Biol,* 15**,** 713-20.

Burman, C. & Ktistakis, N. T. 2010. Regulation of autophagy by phosphatidylinositol 3-phosphate. *FEBS Letters,* 584**,** 1302-1312.

Chan, E. Y. W., Longatti, A., Mcknight, N. C. & Tooze, S. A. 2009. Kinase-Inactivated ULK Proteins Inhibit Autophagy via Their Conserved C-Terminal Domains Using an Atg13-Independent Mechanism. *Molecular and Cellular Biology,* 29**,** 157-171.

Chen, R.-Q., Yang, Q.-K., Lu, B.-W., Yi, W., Cantin, G., Chen, Y.-L., Fearns, C., Yates, J. R. & Lee, J.-D. 2009. CDC25B mediates rapamycin-induced oncogenic responses in cancer cells. *Cancer research,* 69**,** 2663-2668.

Choi, S.-Y., Huang, P., Jenkins, G. M., Chan, D. C., Schiller, J. & Frohman, M. A. 2006. A common lipid links Mfn-mediated mitochondrial fusion and SNARE-regulated exocytosis. *Nat Cell Biol,* 8**,** 1255-1262.

Cocucci, E., Gaudin, R. & Kirchhausen, T. 2014. Dynamin recruitment and membrane scission at the neck of a clathrin-coated pit. *Molecular Biology of the Cell,* 25**,** 3595-3609.

Cong, L., Ran, F. A., Cox, D., Lin, S., Barretto, R., Habib, N., Hsu, P. D., Wu, X., Jiang, W., Marraffini, L. A. & Zhang, F. 2013. Multiplex Genome Engineering Using CRISPR/Cas Systems. *Science,* 339**,** 819.

Cook, K. L., Soto-Pantoja, D. R., Abu-Asab, M., Clarke, P. a. G., Roberts, D. D. & Clarke, R. 2014. Mitochondria directly donate their membrane to form autophagosomes during a novel mechanism of parkin-associated mitophagy. *Cell & Bioscience,* 4**,** 16-16.

Coon, M., Ball, A., Pound, J., Ap, S., Hollenback, D., White, T., Tulinsky, J., Bonham, L., Morrison, D. K., Finney, R. & Singer, J. W. 2003. Inhibition of lysophosphatidic acid acyltransferase β disrupts proliferative and survival signals in normal cells and induces apoptosis of tumor cells. *Molecular Cancer Therapeutics,* 2**,** 1067-1078.

Corcelle-Termeau, E., Vindelov, S. D., Hamalisto, S., Mograbi, B., Keldsbo, A., Brasen, J. H., Favaro, E., Adam, D., Szyniarowski, P., Hofman, P., Krautwald, S., Farkas, T., Petersen, N. H., Rohde, M., Linkermann, A. & Jaattela, M. 2016. Excess sphingomyelin disturbs ATG9A trafficking and autophagosome closure. *Autophagy,* 12**,** 833-49.

Dall'armi, C., Devereaux, K. A. & Di Paolo, G. 2013. The role of lipids in the control of autophagy. *Curr Biol,* 23**,** R33-45.

Dall'armi, C., Hurtado-Lorenzo, A., Tian, H., Morel, E., Nezu, A., Chan, R. B., Yu, W. H., Robinson, K. S., Yeku, O., Small, S. A., Duff, K., Frohman, M. A., Wenk, M. R., Yamamoto, A. & Di Paolo, G. 2010. The Phospholipase D1 Pathway Modulates Macroautophagy. *Nature Communications,* 1**,** 142-142.

De Duve, C., Pressman, B. C., Gianetto, R., Wattiaux, R. & Appelmans, F. 1955. Tissue fractionation studies. 6. Intracellular distribution patterns of enzymes in rat-liver tissue. *Biochemical Journal,* 60**,** 604-617.

De Duve, C. & Wattiaux, R. 1966. Functions of Lysosomes. *Annual Review of Physiology,* 28**,** 435-492.

Devereaux, K., Dall'armi, C., Alcazar-Roman, A., Ogasawara, Y., Zhou, X., Wang, F., Yamamoto, A., De Camilli, P. & Di Paolo, G. 2013. Regulation of Mammalian Autophagy by Class II and III PI 3-Kinases through PI3P Synthesis. *PLOS ONE,* 8**,** e76405.

Di Paolo, G. & De Camilli, P. 2006. Phosphoinositides in cell regulation and membrane dynamics. *Nature,* 443**,** 651-657.

Doherty, G. J. & Mcmahon, H. T. 2009. Mechanisms of Endocytosis. *Annual Review of Biochemistry,* 78**,** 857-902.

Dooley, Hannah c., Razi, M., Polson, Hannah e., Girardin, Stephen e., Wilson, Michael i. & Tooze, Sharon a. 2014. WIPI2 Links LC3 Conjugation with PI3P, Autophagosome Formation, and Pathogen Clearance by Recruiting Atg12–5-16L1. *Molecular Cell,* 55**,** 238-252.

Engedal, N. & Seglen, P. O. 2015. Autophagy of cytoplasmic bulk cargo does not require LC3. *Autophagy,* 12**,** 439-441.

Eskelinen, E. L. 2005. Maturation of autophagic vacuoles in Mammalian cells. *Autophagy,* 1**,** 1-10.

Eskelinen, E. L., Prescott, A. R., Cooper, J., Brachmann, S. M., Wang, L., Tang, X., Backer, J. M. & Lucocq, J. M. 2002. Inhibition of autophagy in mitotic animal cells. *Traffic,* 3**,** 878-93.

Fang, Y., Vilella-Bach, M., Bachmann, R., Flanigan, A. & Chen, J. 2001. Phosphatidic Acid-Mediated Mitogenic Activation of mTOR Signaling. *Science,* 294**,** 1942.

Farhan, H. & Rabouille, C. 2010. Signalling to and from the secretory pathway. *Journal of Cell Science,* 124**,** 171.

Fasshauer, D., Sutton, R. B., Brunger, A. T. & Jahn, R. 1998. Conserved structural features of the synaptic fusion complex: SNARE proteins reclassified as Q- and R-SNAREs. *Proceedings of the National Academy of Sciences of the United States of America,* 95**,** 15781-15786.

Fields, I. C., King, S. M., Shteyn, E., Kang, R. S. & Fölsch, H. 2010. Phosphatidylinositol 3,4,5-trisphosphate Localization in Recycling Endosomes Is Necessary for AP-1B–dependent Sorting in Polarized Epithelial Cells. *Molecular Biology of the Cell,* 21**,** 95-105.

Filimonenko, M., Isakson, P., Finley, K. D., Anderson, M., Melia, T. J., Jeong, H., Bartlett, B. J., Myers, K. M., Birkeland, H. C. G., Lamark, T., Krainc, D., Brech, A., Stenmark, H., Simonsen, A. & Yamamoto, A. 2010. The selective macroautophagic degradation of aggregated proteins requires the phosphatidylinositol 3-phosphate binding protein Alfy. *Molecular cell,* 38**,** 265-279.

Fujita, N., Hayashi-Nishino, M., Fukumoto, H., Omori, H., Yamamoto, A., Noda, T. & Yoshimori, T. 2008a. An Atg4B Mutant Hampers the Lipidation of LC3 Paralogues and Causes Defects in Autophagosome Closure. *Molecular Biology of the Cell,* 19**,** 4651-4659.

Fujita, N., Itoh, T., Omori, H., Fukuda, M., Noda, T. & Yoshimori, T. 2008b. The Atg16L complex specifies the site of LC3 lipidation for membrane biogenesis in autophagy. *Mol Biol Cell,* 19**,** 2092-100.

Ganley, I. G., Lam, D. H., Wang, J., Ding, X., Chen, S. & Jiang, X. 2009. ULK1·ATG13·FIP200 Complex Mediates mTOR Signaling and Is Essential for Autophagy. *Journal of Biological Chemistry,* 284**,** 12297-12305.

Garofalo, T., Matarrese, P., Manganelli, V., Marconi, M., Tinari, A., Gambardella, L., Faggioni, A., Misasi, R., Sorice, M. & Malorni, W. 2016. Evidence for the involvement of lipid rafts localized at the ER-mitochondria associated membranes in autophagosome formation. *Autophagy,* 12**,** 917-35.

Gaugel, A., Bakula, D., Hoffmann, A. & Proikas-Cezanne, T. 2012. Defining regulatory and phosphoinositide-binding sites in the human WIPI-1 β-propeller responsible for autophagosomal membrane localization downstream of mTORC1 inhibition. *Journal of Molecular Signaling,* 7**,** 16-16.

Ge, L., Melville, D., Zhang, M. & Schekman, R. 2013. The ER–Golgi intermediate compartment is a key membrane source for the LC3 lipidation step of autophagosome biogenesis. *eLife,* 2**,** e00947.

Geng, J. & Klionsky, D. J. 2008. The Atg8 and Atg12 ubiquitin-like conjugation systems in macroautophagy. 'Protein Modifications: Beyond the Usual Suspects' Review Series. *EMBO Reports,* 9**,** 859-864.

Graef, M., Friedman, J. R., Graham, C., Babu, M. & Nunnari, J. 2013. ER exit sites are physical and functional core autophagosome biogenesis components. *Molecular Biology of the Cell,* 24**,** 2918-2931.

Griffiths, G., Hoflack, B., Simons, K., Mellman, I. & Kornfeld, S. 1988. The mannose 6-phosphate receptor and the biogenesis of lysosomes. *Cell,* 52**,** 329-341.

Guo, Y., Chang, C., Huang, R., Liu, B., Bao, L. & Liu, W. 2012. AP1 is essential for generation of autophagosomes from the trans-Golgi network. *Journal of Cell Science,* 125**,** 1706.

Hailey, D. W., Rambold, A. S., Satpute-Krishnan, P., Mitra, K., Sougrat, R., Kim, P. K. & Lippincott-Schwartz, J. 2010. Mitochondria supply membranes for autophagosome biogenesis during starvation. *Cell,* 141**,** 656-67.

Hamasaki, M., Furuta, N., Matsuda, A., Nezu, A., Yamamoto, A., Fujita, N., Oomori, H., Noda, T., Haraguchi, T., Hiraoka, Y., Amano, A. & Yoshimori, T. 2013. Autophagosomes form at ER-mitochondria contact sites. *Nature,* 495**,** 389-393.

Hanna Damke, T. B., Dale E. Warnock, and Sandra L. Schmid 1994. Induction of mutant dynamin specifically blocks endocytic coated vesicle formation. *The Journal of Cell Biology,* 127**,** 915-934.

Hao, F., Itoh, T., Morita, E., Shirahama‐Noda, K., Yoshimori, T. & Noda, T. 2016. The PtdIns3‐phosphatase MTMR3 interacts with mTORC1 and suppresses its activity. *Febs Letters,* 590**,** 161-173.

Haobam, B., Nozawa, T., Minowa-Nozawa, A., Tanaka, M., Oda, S., Watanabe, T., Aikawa, C., Maruyama, F. & Nakagawa, I. 2014. Rab17-mediated recycling endosomes contribute to autophagosome formation in response to Group A Streptococcus invasion. *Cellular Microbiology,* 16**,** 1806-1821.

Hara, T., Takamura, A., Kishi, C., Iemura, S.-I., Natsume, T., Guan, J.-L. & Mizushima, N. 2008. FIP200, a ULK-interacting protein, is required for autophagosome formation in mammalian cells. *The Journal of Cell Biology,* 181**,** 497.

Hasegawa, J., Iwamoto, R., Otomo, T., Nezu, A., Hamasaki, M. & Yoshimori, T. 2016. Autophagosome–lysosome fusion in neurons requires INPP5E, a protein associated with Joubert syndrome. *The EMBO Journal,* 35**,** 1853.

Hayashi-Nishino, M., Fujita, N., Noda, T., Yamaguchi, A., Yoshimori, T. & Yamamoto, A. 2009. A subdomain of the endoplasmic reticulum forms a cradle for autophagosome formation. *Nat Cell Biol,* 11**,** 1433-7.

He, C. & Klionsky, D. J. 2010. Analyzing autophagy in zebrafish. *Autophagy,* 6**,** 642-644.

Heiseke, A., Schöbel, S., Lichtenthaler, S. F., Vorberg, I., Groschup, M. H., Kretzschmar, H., Schätzl, H. M. & Nunziante, M. 2008. The Novel Sorting Nexin SNX33 Interferes with Cellular PrPSc Formation by Modulation of PrPc Shedding. *Traffic,* 9**,** 1116-1129.

Holen, I., Gordon, P. B. & Seglen, P. O. 1992. Protein kinase-dependent effects of okadaic acid on hepatocytic autophagy and cytoskeletal integrity. *Biochemical Journal,* 284**,** 633-636.

Horvath, P. & Barrangou, R. 2010. CRISPR/Cas, the Immune System of Bacteria and Archaea. *Science,* 327**,** 167.

Hosokawa, N., Hara, T., Kaizuka, T., Kishi, C., Takamura, A., Miura, Y., Iemura, S.-I., Natsume, T., Takehana, K., Yamada, N., Guan, J.-L., Oshiro, N. & Mizushima, N. 2009a. Nutrient-dependent mTORC1 Association with the ULK1–Atg13–FIP200 Complex Required for Autophagy. *Molecular Biology of the Cell,* 20**,** 1981-1991.

Hosokawa, N., Sasaki, T., Iemura, S., Natsume, T., Hara, T. & Mizushima, N. 2009b. Atg101, a novel mammalian autophagy protein interacting with Atg13. *Autophagy,* 5**,** 973-9.

Håberg, K., Lundmark, R. & Carlsson, S. R. 2008. SNX18 is an SNX9 paralog that acts as a membrane tubulator in AP-1-positive endosomal trafficking. *Journal of Cell Science,* 121**,** 1495.

Imai, K., Hao, F., Fujita, N., Tsuji, Y., Oe, Y., Araki, Y., Hamasaki, M., Noda, T. & Yoshimori, T. 2016. Atg9A trafficking through the recycling endosomes is required for autophagosome formation. *Journal of Cell Science,* 129**,** 3781.

Itoh, T. & De Camilli, P. 2006. BAR, F-BAR (EFC) and ENTH/ANTH domains in the regulation of membrane–cytosol interfaces and membrane curvature. *Biochimica et Biophysica Acta (BBA) - Molecular and Cell Biology of Lipids,* 1761**,** 897-912.

Jahn, R., Lang, T. & Südhof, T. C. 2003. Membrane Fusion. *Cell,* 112**,** 519-533.

Jang, D.-J. & Lee, J.-A. 2016. The roles of phosphoinositides in mammalian autophagy. *Archives of Pharmacal Research,* 39**,** 1129-1136.

Jang, Y. H., Choi, K. Y. & Min, D. S. 2014. Phospholipase D-mediated autophagic regulation is a potential target for cancer therapy. *Cell Death and Differentiation,* 21**,** 533-546.
Jennings, B. H. 2011. Drosophila – a versatile model in biology & medicine. *Materials Today,* 14**,** 190-195.
Johansen, T. & Lamark, T. 2011. Selective autophagy mediated by autophagic adapter proteins. *Autophagy,* 7**,** 279-296.
Juhász, G., Hill, J. H., Yan, Y., Sass, M., Baehrecke, E. H., Backer, J. M. & Neufeld, T. P. 2008. The class III PI(3)K Vps34 promotes autophagy and endocytosis but not TOR signaling in Drosophila. *The Journal of Cell Biology,* 181**,** 655-666.
Jung, C. H., Jun, C. B., Ro, S.-H., Kim, Y.-M., Otto, N. M., Cao, J., Kundu, M. & Kim, D.-H. 2009. ULK-Atg13-FIP200 Complexes Mediate mTOR Signaling to the Autophagy Machinery. *Molecular Biology of the Cell,* 20**,** 1992-2003.
Jung, C. H., Ro, S.-H., Cao, J., Otto, N. M. & Kim, D.-H. 2010. mTOR regulation of autophagy. *FEBS Letters,* 584**,** 1287-1295.
Kabeya, Y., Mizushima, N., Ueno, T., Yamamoto, A., Kirisako, T., Noda, T., Kominami, E., Ohsumi, Y. & Yoshimori, T. 2000. LC3, a mammalian homologue of yeast Apg8p, is localized in autophagosome membranes after processing. *The EMBO Journal,* 19**,** 5720-5728.
Kabeya, Y., Mizushima, N., Yamamoto, A., Oshitani-Okamoto, S., Ohsumi, Y. & Yoshimori, T. 2004. LC3, GABARAP and GATE16 localize to autophagosomal membrane depending on form-II formation. *Journal of Cell Science,* 117**,** 2805-2812.
Kakuta, S., Yamamoto, H., Negishi, L., Kondo-Kakuta, C., Hayashi, N. & Ohsumi, Y. 2012. Atg9 Vesicles Recruit Vesicle-tethering Proteins Trs85 and Ypt1 to the Autophagosome Formation Site. *Journal of Biological Chemistry,* 287**,** 44261-44269.
Kamal, A. & Goldstein, L. S. B. 2000. Connecting vesicle transport to the cytoskeleton. *Current Opinion in Cell Biology,* 12**,** 503-508.
Karathanassis, D., Stahelin, R. V., Bravo, J., Perisic, O., Pacold, C. M., Cho, W. & Williams, R. L. 2002. Binding of the PX domain of p47(phox) to phosphatidylinositol 3,4-bisphosphate and phosphatidic acid is masked by an intramolecular interaction. *The EMBO Journal,* 21**,** 5057-5068.
Kim, J., Kundu, M., Viollet, B. & Guan, K.-L. 2011. AMPK and mTOR regulate autophagy through direct phosphorylation of Ulk1. *Nat Cell Biol,* 13**,** 132-141.
Kirchhausen, T. 2000. Three ways to make a vesicle. *Nat Rev Mol Cell Biol,* 1**,** 187-198.
Klionsky, D. J. 2007. Autophagy: from phenomenology to molecular understanding in less than a decade. *Nat Rev Mol Cell Biol,* 8**,** 931-937.
Klionsky, D. J., Cregg, J. M., Dunn, W. A., Jr., Emr, S. D., Sakai, Y., Sandoval, I. V., Sibirny, A., Subramani, S., Thumm, M., Veenhuis, M. & Ohsumi, Y. 2003. A unified nomenclature for yeast autophagy-related genes. *Dev Cell,* 5**,** 539-45.
Klionsky, D. J., Cuervo, A. M., Dunn, J. W. A., Levine, B., Van Der Klei, I. J. & Seglen, P. O. 2007. How Shall I Eat Thee? *Autophagy,* 3**,** 413-416.
Kooijman, E. E., Carter, K. M., Van Laar, E. G., Chupin, V., Burger, K. N. J. & De Kruijff, B. 2005. What Makes the Bioactive Lipids Phosphatidic Acid and Lysophosphatidic Acid So Special? *Biochemistry,* 44**,** 17007-17015.
Lamb, C. A., Longatti, A. & Tooze, S. A. 2016a. Rabs and GAPs in starvation-induced autophagy. *Small GTPases,* 7**,** 265-269.
Lamb, C. A., Nühlen, S., Judith, D., Frith, D., Snijders, A. P., Behrends, C. & Tooze, S. A. 2016b. TBC1D14 regulates autophagy via the TRAPP complex and ATG9 traffic. *The EMBO Journal,* 35**,** 281-301.
Lamb, C. A., Yoshimori, T. & Tooze, S. A. 2013. The autophagosome: origins unknown, biogenesis complex. *Nat Rev Mol Cell Biol,* 14**,** 759-74.

Lang, T., Reiche, S., Straub, M., Bredschneider, M. & Thumm, M. 2000. Autophagy and the cvt Pathway Both Depend on AUT9. *Journal of Bacteriology,* 182**,** 2125-2133.

Lassègue, B., Alexander, R. W., Clark, M., Akers, M. & Griendling, K. K. 1993. Phosphatidylcholine is a major source of phosphatidic acid and diacylglycerol in angiotensin II-stimulated vascular smooth-muscle cells. *Biochemical Journal,* 292**,** 509-517.

Lawe, D. C., Patki, V., Heller-Harrison, R., Lambright, D. & Corvera, S. 2000. The FYVE Domain of Early Endosome Antigen 1 Is Required for Both Phosphatidylinositol 3-Phosphate and Rab5 Binding: CRITICAL ROLE OF THIS DUAL INTERACTION FOR ENDOSOMAL LOCALIZATION. *Journal of Biological Chemistry,* 275**,** 3699-3705.

Lee, E.-J. & Tournier, C. 2011. The requirement of uncoordinated 51-like kinase 1 (ULK1) and ULK2 in the regulation of autophagy. *Autophagy,* 7**,** 689-695.

Lee, J.-Y., Koga, H., Kawaguchi, Y., Tang, W., Wong, E., Gao, Y.-S., Pandey, U. B., Kaushik, S., Tresse, E., Lu, J., Taylor, J. P., Cuervo, A. M. & Yao, T.-P. 2010. HDAC6 controls autophagosome maturation essential for ubiquitin-selective quality-control autophagy. *The EMBO Journal,* 29**,** 969-980.

Letourneur, F., Gaynor, E. C., Hennecke, S., Démollière, C., Duden, R., Emr, S. D., Riezman, H. & Cosson, P. 1994. Coatomer is essential for retrieval of dilysine-tagged proteins to the endoplasmic reticulum. *Cell,* 79**,** 1199-1207.

Leung, D. W. 2001. THE STRUCTURE AND FUNCTIONS OF HUMAN LYSOPHOSPHATIDIC ACID ACYLTRANSFERASES. *Frontiers in Bioscience***,** d944-953.

Longatti, A., Lamb, C. A., Razi, M., Yoshimura, S., Barr, F. A. & Tooze, S. A. 2012. TBC1D14 regulates autophagosome formation via Rab11- and ULK1-positive recycling endosomes. *J Cell Biol,* 197**,** 659-75.

Lundmark, R. & Carlsson, S. R. 2002. The beta-appendages of the four adaptor-protein (AP) complexes: structure and binding properties, and identification of sorting nexin 9 as an accessory protein to AP-2. *Biochemical Journal,* 362**,** 597-607.

Lundmark, R. & Carlsson, S. R. 2003. Sorting Nexin 9 Participates in Clathrin-mediated Endocytosis through Interactions with the Core Components. *Journal of Biological Chemistry,* 278**,** 46772-46781.

Lundmark, R. & Carlsson, S. R. 2004. Regulated Membrane Recruitment of Dynamin-2 Mediated by Sorting Nexin 9. *Journal of Biological Chemistry,* 279**,** 42694-42702.

Lundmark, R. & Carlsson, S. R. 2008. SNX9 – a prelude to vesicle release. *Journal of Cell Science,* 122**,** 5.

Lystad, A. H., Ichimura, Y., Takagi, K., Yang, Y., Pankiv, S., Kanegae, Y., Kageyama, S., Suzuki, M., Saito, I., Mizushima, T., Komatsu, M. & Simonsen, A. 2014. Structural determinants in GABARAP required for the selective binding and recruitment of ALFY to LC3B-positive structures. *EMBO Reports,* 15**,** 557-565.

Ma, M. P. C. & Chircop, M. 2012. SNX9, SNX18 and SNX33 are required for progression through and completion of mitosis. *Journal of Cell Science*.

Mari, M., Griffith, J., Rieter, E., Krishnappa, L., Klionsky, D. J. & Reggiori, F. 2010. An Atg9-containing compartment that functions in the early steps of autophagosome biogenesis. *J Cell Biol,* 190**,** 1005-22.

Marsh, D. 2007. Lateral Pressure Profile, Spontaneous Curvature Frustration, and the Incorporation and Conformation of Proteins in Membranes. *Biophysical Journal,* 93**,** 3884-3899.

Martin, S., Harper, C. B., May, L. M., Coulson, E. J., Meunier, F. A. & Osborne, S. L. 2013. Inhibition of PIKfyve by YM-201636 Dysregulates Autophagy and Leads to Apoptosis-Independent Neuronal Cell Death. *PLOS ONE,* 8**,** e60152.

Matsunaga, K., Morita, E., Saitoh, T., Akira, S., Ktistakis, N. T., Izumi, T., Noda, T. & Yoshimori, T. 2010. Autophagy requires endoplasmic reticulum targeting of the PI3-kinase complex via Atg14L. *J Cell Biol,* 190**,** 511-21.

Mauvezin, C., Ayala, C., Braden, C. R., Kim, J. & Neufeld, T. P. 2014. Assays to monitor autophagy in Drosophila. *Methods (San Diego, Calif.),* 68**,** 134-139.

Mayor, S., Parton, R. G. & Donaldson, J. G. 2014. Clathrin-Independent Pathways of Endocytosis. *Cold Spring Harbor Perspectives in Biology,* 6**,** a016758.

Mercer, C. A., Kaliappan, A. & Dennis, P. B. 2009. A novel, human Atg13 binding protein, Atg101, interacts with ULK1 and is essential for macroautophagy. *Autophagy,* 5**,** 649-62.

Mi, N., Chen, Y., Wang, S., Chen, M., Zhao, M., Yang, G., Ma, M., Su, Q., Luo, S., Shi, J., Xu, J., Guo, Q., Gao, N., Sun, Y., Chen, Z. & Yu, L. 2015. CapZ regulates autophagosomal membrane shaping by promoting actin assembly inside the isolation membrane. *Nat Cell Biol,* 17**,** 1112-1123.

Mizushima, N., Sugita, H., Yoshimori, T. & Ohsumi, Y. 1998. A New Protein Conjugation System in Human: THE COUNTERPART OF THE YEAST Apg12p CONJUGATION SYSTEM ESSENTIAL FOR AUTOPHAGY. *Journal of Biological Chemistry,* 273**,** 33889-33892.

Mizushima, N., Yoshimori, T. & Ohsumi, Y. 2011. The Role of Atg Proteins in Autophagosome Formation. *Annual Review of Cell and Developmental Biology,* 27**,** 107-132.

Mooren, O. L., Galletta, B. J. & Cooper, J. A. 2012. Roles for Actin Assembly in Endocytosis. *Annual Review of Biochemistry,* 81**,** 661-686.

Moreau, K., Ravikumar, B., Renna, M., Puri, C. & Rubinsztein, David c. 2011. Autophagosome Precursor Maturation Requires Homotypic Fusion. *Cell,* 146**,** 303-317.

Mortimore, G. E., Hutson, N. J. & Surmacz, C. A. 1983. Quantitative correlation between proteolysis and macro- and microautophagy in mouse hepatocytes during starvation and refeeding. *Proceedings of the National Academy of Sciences of the United States of America,* 80**,** 2179-2183.

Murrow, L., Malhotra, R. & Debnath, J. 2015. ATG12-ATG3 Interacts with Alix to Promote Basal Autophagic Flux and Late Endosome Function. *Nature cell biology,* 17**,** 300-310.

Nakanishi, H., Morishita, M., Schwartz, C. L., Coluccio, A., Engebrecht, J. & Neiman, A. M. 2006. Phospholipase D and the SNARE Sso1p are necessary for vesicle fusion during sporulation in yeast. *Journal of Cell Science,* 119**,** 1406.

Nakatogawa, H., Ichimura, Y. & Ohsumi, Y. 2007. Atg8, a ubiquitin-like protein required for autophagosome formation, mediates membrane tethering and hemifusion. *Cell,* 130**,** 165-78.

Nakatogawa, H., Suzuki, K., Kamada, Y. & Ohsumi, Y. 2009. Dynamics and diversity in autophagy mechanisms: lessons from yeast. *Nat Rev Mol Cell Biol,* 10**,** 458-67.

Nath, S., Dancourt, J., Shteyn, V., Puente, G., Fong, W. M., Nag, S., Bewersdorf, J., Yamamoto, A., Antonny, B. & Melia, T. J. 2014. Lipidation of the LC3/GABARAP family of autophagy proteins relies on a membrane-curvature-sensing domain in Atg3. *Nat Cell Biol,* 16**,** 415-424.

Neufeld, T. P. 2010. TOR-dependent control of autophagy: biting the hand that feeds. *Current opinion in cell biology,* 22**,** 157-168.

Nguyen, T. N., Padman, B. S., Usher, J., Oorschot, V., Ramm, G. & Lazarou, M. 2016. Atg8 family LC3/GABARAP proteins are crucial for autophagosome–lysosome fusion but not autophagosome formation during PINK1/Parkin mitophagy and starvation. *The Journal of Cell Biology*.

Noda, T., Kim, J., Huang, W.-P., Baba, M., Tokunaga, C., Ohsumi, Y. & Klionsky, D. J. 2000. Apg9p/Cvt7p Is an Integral Membrane Protein Required for Transport Vesicle Formation in the Cvt and Autophagy Pathways. *The Journal of Cell Biology,* 148**,** 465-480.

Olsvik, H. L., Lamark, T., Takagi, K., Larsen, K. B., Evjen, G., Øvervatn, A., Mizushima, T. & Johansen, T. 2015. FYCO1 Contains a C-terminally Extended, LC3A/B-preferring LC3-interacting Region (LIR) Motif Required for Efficient Maturation of Autophagosomes during Basal Autophagy. *Journal of Biological Chemistry,* 290**,** 29361-29374.

Orsi, A., Razi, M., Dooley, H. C., Robinson, D., Weston, A. E., Collinson, L. M. & Tooze, S. A. 2012. Dynamic and transient interactions of Atg9 with autophagosomes, but not membrane integration, are required for autophagy. *Mol Biol Cell,* 23**,** 1860-73.

Pankiv, S., Alemu, E. A., Brech, A., Bruun, J.-A., Lamark, T., Øvervatn, A., Bjørkøy, G. & Johansen, T. 2010. FYCO1 is a Rab7 effector that binds to LC3 and PI3P to mediate microtubule plus end–directed vesicle transport. *The Journal of Cell Biology,* 188**,** 253-269.

Papinski, D., Schuschnig, M., Reiter, W., Wilhelm, L., Barnes, Christopher a., Maiolica, A., Hansmann, I., Pfaffenwimmer, T., Kijanska, M., Stoffel, I., Lee, Sung s., Brezovich, A., Lou, Jane h., Turk, Benjamin e., Aebersold, R., Ammerer, G., Peter, M. & Kraft, C. 2014. Early Steps in Autophagy Depend on Direct Phosphorylation of Atg9 by the Atg1 Kinase. *Molecular Cell,* 53**,** 471-483.

Park, J.-M., Jung, C. H., Seo, M., Otto, N. M., Grunwald, D., Kim, K. H., Moriarity, B., Kim, Y.-M., Starker, C., Nho, R. S., Voytas, D. & Kim, D.-H. 2016. The ULK1 complex mediates MTORC1 signaling to the autophagy initiation machinery via binding and phosphorylating ATG14. *Autophagy,* 12**,** 547-564.

Park, J., Kim, Y., Lee, S., Park, J. J., Park, Z. Y., Sun, W., Kim, H. & Chang, S. 2010. SNX18 shares a redundant role with SNX9 and modulates endocytic trafficking at the plasma membrane. *Journal of Cell Science,* 123**,** 1742.

Petiot, A., Ogier-Denis, E., Blommaart, E. F. C., Meijer, A. J. & Codogno, P. 2000. Distinct Classes of Phosphatidylinositol 3′ -Kinases Are Involved in Signaling Pathways That Control Macroautophagy in HT-29 Cells. *Journal of Biological Chemistry,* 275**,** 992-998.

Polson, H. E. J., De Lartigue, J., Rigden, D. J., Reedijk, M., Urbé, S., Clague, M. J. & Tooze, S. A. 2010. Mammalian Atg18 (WIPI2) localizes to omegasome-anchored phagophores and positively regulates LC3 lipidation. *Autophagy,* 6**,** 506-522.

Popovic, D. & Dikic, I. 2014. TBC1D5 and the AP2 complex regulate ATG9 trafficking and initiation of autophagy. *EMBO Reports,* 15**,** 392-401.

Proikas-Cezanne, T., Takacs, Z., Dönnes, P. & Kohlbacher, O. 2015. WIPI proteins: essential PtdIns3 effectors at the nascent autophagosome. *Journal of Cell Science,* 128**,** 207.

Proikas-Cezanne, T., Waddell, S., Gaugel, A., Frickey, T., Lupas, A. & Nordheim, A. 2004. WIPI-1[alpha] (WIPI49), a member of the novel 7-bladed WIPI protein family, is aberrantly expressed in human cancer and is linked to starvation-induced autophagy. *Oncogene,* 23**,** 9314-9325.

Puente, C., Hendrickson, R. C. & Jiang, X. 2016. Nutrient-Regulated Phosphorylation of ATG13 Inhibits Starvation-Induced Autophagy. *Journal of Biological Chemistry*.

Puri, C., Renna, M., Bento, C. F., Moreau, K. & Rubinsztein, D. C. 2013. Diverse autophagosome membrane sources coalesce in recycling endosomes. *Cell,* 154**,** 1285-99.

Pylypenko, O., Lundmark, R., Rasmuson, E., Carlsson, S. R. & Rak, A. 2007. The PX-BAR membrane-remodeling unit of sorting nexin 9. *The EMBO Journal,* 26**,** 4788-4800.

Ravikumar, B., Moreau, K., Jahreiss, L., Puri, C. & Rubinsztein, D. C. 2010. Plasma membrane contributes to the formation of pre-autophagosomal structures. *Nat Cell Biol,* 12**,** 747-757.

Razi, M., Chan, E. Y. W. & Tooze, S. A. 2009. Early endosomes and endosomal coatomer are required for autophagy. *The Journal of Cell Biology,* 185**,** 305-321.

Reggiori, F. & Tooze, S. A. 2012. Autophagy regulation through Atg9 traffic. *The Journal of Cell Biology,* 198**,** 151.

Rong, Y., Liu, M., Ma, L., Du, W., Zhang, H., Tian, Y., Cao, Z., Li, Y., Ren, H., Zhang, C., Li, L., Chen, S., Xi, J. & Yu, L. 2012. Clathrin and phosphatidylinositol-4,5-bisphosphate regulate autophagic lysosome reformation. *Nat Cell Biol,* 14**,** 924-934.

Rothman, J. E. 2002. The machinery and principles of vesicle transport in the cell. *Nat Med,* 8**,** 1059-1062.

Rowland, A. A. & Voeltz, G. K. 2012. Endoplasmic reticulum-mitochondria contacts: function of the junction. *Nat Rev Mol Cell Biol,* 13**,** 607-625.

Russell, R. C., Tian, Y., Yuan, H., Park, H. W., Chang, Y.-Y., Kim, J., Kim, H., Neufeld, T. P., Dillin, A. & Guan, K.-L. 2013. ULK1 induces autophagy by phosphorylating Beclin-1 and activating VPS34 lipid kinase. *Nat Cell Biol,* 15**,** 741-750.

Rusten, T. E., Vaccari, T., Lindmo, K., Rodahl, L. M. W., Nezis, I. P., Sem-Jacobsen, C., Wendler, F., Vincent, J.-P., Brech, A., Bilder, D. & Stenmark, H. 2007. ESCRTs and Fab1 Regulate Distinct Steps of Autophagy. *Current Biology,* 17**,** 1817-1825.

Saftig, P. & Klumperman, J. 2009. Lysosome biogenesis and lysosomal membrane proteins: trafficking meets function. *Nat Rev Mol Cell Biol,* 10**,** 623-635.

Scarlatti, F., Maffei, R., Beau, I., Codogno, P. & Ghidoni, R. 2008. Role of non-canonical Beclin 1-independent autophagy in cell death induced by resveratrol in human breast cancer cells. *Cell Death Differ,* 15**,** 1318-1329.

Schmid, S. L. 1997. CLATHRIN-COATED VESICLE FORMATION AND PROTEIN SORTING:An Integrated Process. *Annual Review of Biochemistry,* 66**,** 511-548.

Schöbel, S., Neumann, S., Hertweck, M., Dislich, B., Kuhn, P.-H., Kremmer, E., Seed, B., Baumeister, R., Haass, C. & Lichtenthaler, S. F. 2008. A Novel Sorting Nexin Modulates Endocytic Trafficking and α-Secretase Cleavage of the Amyloid Precursor Protein. *Journal of Biological Chemistry,* 283**,** 14257-14268.

Seet, L.-F. & Hong, W. 2006. The Phox (PX) domain proteins and membrane traffic. *Biochimica et Biophysica Acta (BBA) - Molecular and Cell Biology of Lipids,* 1761**,** 878-896.

Seglen, P. O. & Gordon, P. B. 1982. 3-Methyladenine: Specific inhibitor of autophagic/lysosomal protein degradation in isolated rat hepatocytes. *Proceedings of the National Academy of Sciences of the United States of America,* 79**,** 1889-1892.

Seglen, P. O., Gordon, P. B. & Poli, A. 1980. Amino acid inhibition of the autophagic/lysosomal pathway of protein degradation in isolated rat hepatocytes. *Biochimica et Biophysica Acta (BBA) - General Subjects,* 630**,** 103-118.

Shahnazari, S., Yen, W.-L., Birmingham, C. L., Shiu, J., Namolovan, A., Zheng, Y. T., Nakayama, K., Klionsky, D. J. & Brumell, J. H. 2010. A diacylglycerol-dependent signaling pathway contributes to regulation of anti-bacterial autophagy. *Cell host & microbe,* 8**,** 137-146.

Shewan, A., Eastburn, D. J. & Mostov, K. 2011. Phosphoinositides in Cell Architecture. *Cold Spring Harbor Perspectives in Biology,* 3**,** a004796.
Shin, J. J. H. & Loewen, C. J. R. 2011. Putting the pH into phosphatidic acid signaling. *BMC Biology,* 9**,** 85-85.
Shin, N., Ahn, N., Chang-Ileto, B., Park, J., Takei, K., Ahn, S.-G., Kim, S.-A., Di Paolo, G. & Chang, S. 2008. SNX9 regulates tubular invagination of the plasma membrane through interaction with actin cytoskeleton and dynamin 2. *Journal of Cell Science,* 121**,** 1252.
Shin, N., Lee, S., Ahn, N., Kim, S.-A., Ahn, S.-G., Yongpark, Z. & Chang, S. 2007. Sorting Nexin 9 Interacts with Dynamin 1 and N-WASP and Coordinates Synaptic Vesicle Endocytosis. *Journal of Biological Chemistry,* 282**,** 28939-28950.
Shirahama-Noda, K., Kira, S., Yoshimori, T. & Noda, T. 2013. TRAPPIII is responsible for vesicular transport from early endosomes to Golgi, facilitating Atg9 cycling in autophagy. *Journal of Cell Science,* 126**,** 4963.
Shpilka, T., Weidberg, H., Pietrokovski, S. & Elazar, Z. 2011. Atg8: an autophagy-related ubiquitin-like protein family. *Genome Biology,* 12**,** 226-226.
Simonsen, A., Birkeland, H. C. G., Gillooly, D. J., Mizushima, N., Kuma, A., Yoshimori, T., Slagsvold, T., Brech, A. & Stenmark, H. 2004. Alfy, a novel FYVE-domain-containing protein associated with protein granules and autophagic membranes. *Journal of Cell Science,* 117**,** 4239.
Simonsen, A., Lippe, R., Christoforidis, S., Gaullier, J.-M., Brech, A., Callaghan, J., Toh, B.-H., Murphy, C., Zerial, M. & Stenmark, H. 1998. EEA1 links PI(3)K function to Rab5 regulation of endosome fusion. *Nature,* 394**,** 494-498.
Simonsen, A. & Tooze, S. A. 2009. Coordination of membrane events during autophagy by multiple class III PI3-kinase complexes. *J Cell Biol,* 186**,** 773-82.
Soulet, F., Yarar, D., Leonard, M. & Schmid, S. L. 2005. SNX9 Regulates Dynamin Assembly and Is Required for Efficient Clathrin-mediated Endocytosis. *Molecular Biology of the Cell,* 16**,** 2058-2067.
Stahelin, R. V., Ananthanarayanan, B., Blatner, N. R., Singh, S., Bruzik, K. S., Murray, D. & Cho, W. 2004. Mechanism of Membrane Binding of the Phospholipase D1 PX Domain. *Journal of Biological Chemistry,* 279**,** 54918-54926.
Stenmark, H. 2009. Rab GTPases as coordinators of vesicle traffic. *Nat Rev Mol Cell Biol,* 10**,** 513-525.
Suzuki, K., Akioka, M., Kondo-Kakuta, C., Yamamoto, H. & Ohsumi, Y. 2013. Fine mapping of autophagy-related proteins during autophagosome formation in Saccharomyces cerevisiae

Journal of Cell Science, 126**,** 2534-2544.
Suzuki, K. & Ohsumi, Y. 2010. Current knowledge of the pre-autophagosomal structure (PAS). *FEBS Letters,* 584**,** 1280-1286.
Søreng, K., Neufeld, T. P. & Simonsen, A. Membrane trafficking in autophagy. *IRCMB*.
Taguchi-Atarashi, N., Hamasaki, M., Matsunaga, K., Omori, H., Ktistakis, N. T., Yoshimori, T. & Noda, T. 2010. Modulation of Local PtdIns3P Levels by the PI Phosphatase MTMR3 Regulates Constitutive Autophagy. *Traffic,* 11**,** 468-478.
Takai, Y., Sasaki, T. & Matozaki, T. 2001. Small GTP-Binding Proteins. *Physiological Reviews,* 81**,** 153.
Takemoto, Y., Furuta, M., Sato, M., Kubo, M. & Hashimoto, Y. 1999. Isolation and characterization of a novel HS1 SH3 domain binding protein, HS1BP3. *International Immunology,* 11**,** 1957-1964.

Takeshige, K., Baba, M., Tsuboi, S., Noda, T. & Ohsumi, Y. 1992. Autophagy in yeast demonstrated with proteinase-deficient mutants and conditions for its induction. *The Journal of Cell Biology,* 119**,** 301.

Takita, T., Konuma, T., Hanazato, M. & Inoue, H. 2011. Diacylglycerol kinase inhibitor R59022-induced autophagy and apoptosis in the neuronal cell line NG108-15. *Archives of Biochemistry and Biophysics,* 509**,** 197-201.

Tang, H.-W., Wang, Y.-B., Wang, S.-L., Wu, M.-H., Lin, S.-Y. & Chen, G.-C. 2011. Atg1-mediated myosin II activation regulates autophagosome formation during starvation-induced autophagy. *The EMBO Journal,* 30**,** 636-651.

Tanida, I., Ueno, T. & Kominami, E. 2004. LC3 conjugation system in mammalian autophagy. *The International Journal of Biochemistry & Cell Biology,* 36**,** 2503-2518.

Teasdale, Rohan d. & Collins, Brett m. 2012. Insights into the PX (phox-homology) domain and SNX (sorting nexin) protein families: structures, functions and roles in disease. *Biochemical Journal,* 441**,** 39.

Tsuboyama, K., Koyama-Honda, I., Sakamaki, Y., Koike, M., Morishita, H. & Mizushima, N. 2016. The ATG conjugation systems are important for degradation of the inner autophagosomal membrane. *Science*.

Tsukada, M. & Ohsumi, Y. 1993. Isolation and characterization of autophagy-defective mutants of Saccharomyces cerevisiae. *FEBS Letters,* 333**,** 169-174.

Ungermann, C. & Langosch, D. 2005. Functions of SNAREs in intracellular membrane fusion and lipid bilayer mixing. *Journal of Cell Science,* 118**,** 3819.

Van Blitterswijk, W. J. & Houssa, B. 2000. Properties and functions of diacylglycerol kinases. *Cellular Signalling,* 12**,** 595-605.

Van Den Brink-Van Der Laan, E., Antoinette Killian, J. & De Kruijff, B. 2004. Nonbilayer lipids affect peripheral and integral membrane proteins via changes in the lateral pressure profile. *Biochimica et Biophysica Acta (BBA) - Biomembranes,* 1666**,** 275-288.

Van Der Vaart, A., Griffith, J. & Reggiori, F. 2010. Exit from the Golgi Is Required for the Expansion of the Autophagosomal Phagophore in Yeast Saccharomyces cerevisiae. *Molecular Biology of the Cell,* 21**,** 2270-2284.

Van Rossum, A. G. S. H., Schuuring-Scholtes, E., Seggelen, V. V. B.-V., Kluin, P. M. & Schuuring, E. 2005. Comparative genome analysis of cortactin and HS1: the significance of the F-actin binding repeat domain. *BMC Genomics,* 6**,** 15-15.

Varga, M., Fodor, E. & Vellai, T. 2015. Autophagy in zebrafish. *Methods,* 75**,** 172-180.

Vergne, I., Roberts, E., Elmaoued, R. A., Tosch, V., Delgado, M. A., Proikas-Cezanne, T., Laporte, J. & Deretic, V. 2009. Control of autophagy initiation by phosphoinositide 3-phosphatase jumpy. *The EMBO Journal,* 28**,** 2244-2258.

Vicinanza, M., Korolchuk, Viktor i., Ashkenazi, A., Puri, C., Menzies, Fiona m., Clarke, Jonathan h. & Rubinsztein, David c. 2015. PI(5)P Regulates Autophagosome Biogenesis. *Molecular Cell,* 57**,** 219-234.

Wang, H., Sun, H.-Q., Zhu, X., Zhang, L., Albanesi, J., Levine, B. & Yin, H. 2015. GABARAPs regulate PI4P-dependent autophagosome:lysosome fusion. *Proceedings of the National Academy of Sciences,* 112**,** 7015-7020.

Wang, X., Devaiah, S. P., Zhang, W. & Welti, R. 2006. Signaling functions of phosphatidic acid. *Progress in Lipid Research,* 45**,** 250-278.

Watt, S. A., Kular, G., Fleming, I. N., Downes, C. P. & Lucocq, J. M. 2002. Subcellular localization of phosphatidylinositol 4,5-bisphosphate using the pleckstrin homology domain of phospholipase C delta1. *Biochemical Journal,* 363**,** 657-666.

Weidberg, H., Shvets, E., Shpilka, T., Shimron, F., Shinder, V. & Elazar, Z. 2010. LC3 and GATE-16/GABARAP subfamilies are both essential yet act differently in autophagosome biogenesis. *The EMBO Journal,* 29**,** 1792-1802.

Willenborg, C., Jing, J., Wu, C., Matern, H., Schaack, J., Burden, J. & Prekeris, R. 2011. Interaction between FIP5 and SNX18 regulates epithelial lumen formation. *The Journal of Cell Biology,* 195**,** 71-86.

Yamamoto, H., Kakuta, S., Watanabe, T. M., Kitamura, A., Sekito, T., Kondo-Kakuta, C., Ichikawa, R., Kinjo, M. & Ohsumi, Y. 2012. Atg9 vesicles are an important membrane source during early steps of autophagosome formation. *The Journal of Cell Biology,* 198**,** 219-233.

Yarar, D., Waterman-Storer, C. M. & Schmid, S. L. 2007. SNX9 Couples Actin Assembly to Phosphoinositide Signals and Is Required for Membrane Remodeling during Endocytosis. *Developmental Cell,* 13**,** 43-56.

Yla-Anttila, P., Vihinen, H., Jokitalo, E. & Eskelinen, E. L. 2009. 3D tomography reveals connections between the phagophore and endoplasmic reticulum. *Autophagy,* 5**,** 1180-5.

Young, A. R. J., Chan, E. Y. W., Hu, X. W., Köchl, R., Crawshaw, S. G., High, S., Hailey, D. W., Lippincott-Schwartz, J. & Tooze, S. A. 2006. Starvation and ULK1-dependent cycling of mammalian Atg9 between the TGN and endosomes. *Journal of Cell Science,* 119**,** 3888.

Zhou, C., Ma, K., Gao, R., Mu, C., Chen, L., Liu, Q., Luo, Q., Feng, D., Zhu, Y. & Chen, Q. 2017. Regulation of mATG9 trafficking by Src- and ULK1-mediated phosphorylation in basal and starvation-induced autophagy. *Cell Res,* 27**,** 184-201.

Zhou, X., Wang, L., Hasegawa, H., Amin, P., Han, B.-X., Kaneko, S., He, Y. & Wang, F. 2010. Deletion of PIK3C3/Vps34 in sensory neurons causes rapid neurodegeneration by disrupting the endosomal but not the autophagic pathway. *Proceedings of the National Academy of Sciences of the United States of America,* 107**,** 9424-9429.

Zhu, J.-H., Horbinski, C., Guo, F., Watkins, S., Uchiyama, Y. & Chu, C. T. 2007. Regulation of Autophagy by Extracellular Signal-Regulated Protein Kinases During 1-Methyl-4-Phenylpyridinium-Induced Cell Death. *The American Journal of Pathology,* 170**,** 75-86.

Zimmerberg, J. & Kozlov, M. M. 2006. How proteins produce cellular membrane curvature. *Nat Rev Mol Cell Biol,* 7**,** 9-19.

Zoppino, F. C., Militello, R. D., Slavin, I., Alvarez, C. & Colombo, M. I. 2010. Autophagosome formation depends on the small GTPase Rab1 and functional ER exit sites. *Traffic,* 11**,** 1246-61.

ORIGINAL PUBLICATIONS

I

Membrane remodeling by the PX-BAR protein SNX18 promotes autophagosome formation

Helene Knævelsrud,[1] Kristiane Søreng,[1] Camilla Raiborg,[2,3] Karin Håberg,[4] Fredrik Rasmuson,[4] Andreas Brech,[2,3] Knut Liestøl,[2] Tor Erik Rusten,[2,3] Harald Stenmark,[2,3] Thomas P. Neufeld,[5] Sven R. Carlsson,[4] and Anne Simonsen[1]

[1]Institute of Basic Medical Sciences and [2]Centre for Cancer Biomedicine, University of Oslo, 0316 Oslo, Norway
[3]Department of Biochemistry, Institute for Cancer Research, the Norwegian Radium Hospital, Oslo University Hospital, Montebello, 0310 Oslo, Norway
[4]Department of Medical Biochemistry and Biophysics, Umeå University, SE-901 87 Umeå, Sweden
[5]Department of Genetics, Cell Biology and Development, University of Minnesota, Minneapolis, MN 55455

The membrane remodeling events required for autophagosome biogenesis are still poorly understood. Because PX domain proteins mediate membrane remodeling and trafficking, we conducted an imaging-based siRNA screen for autophagosome formation targeting human PX proteins. The PX-BAR protein SNX18 was identified as a positive regulator of autophagosome formation, and its *Drosophila melanogaster* homologue SH3PX1 was found to be required for efficient autophagosome formation in the larval fat body. We show that SNX18 is required for recruitment of Atg16L1-positive recycling endosomes to a perinuclear area and for delivery of Atg16L1- and LC3-positive membranes to autophagosome precursors. We identify a direct interaction of SNX18 with LC3 and show that the pro-autophagic activity of SNX18 depends on its membrane binding and tubulation capacity. We also show that the function of SNX18 in membrane tubulation and autophagy is negatively regulated by phosphorylation of S233. We conclude that SNX18 promotes autophagosome formation by virtue of its ability to remodel membranes and provide membrane to forming autophagosomes.

Introduction

Autophagy is important for human health and development through protection against neurodegeneration and cancer, removal of invading pathogens, and promotion of life-span extension (Mizushima and Komatsu, 2011). Moreover, autophagy ensures cellular quality control at basal levels and recycles nutrients to permit cellular survival during stresses like starvation (Levine and Kroemer, 2008). Macroautophagy (here referred to as autophagy) is characterized by the sequestration of cytoplasmic material through expansion and closure of a phagophore membrane, forming double-membrane vesicles called autophagosomes. The autophagosomes mature by fusion with endosomes and finally fuse with lysosomes, where the contents are degraded and the products recycled to the cytosol for reuse.

The process of forming an autophagosome requires membrane remodeling and trafficking, and is still poorly understood. The origin of the autophagic membrane is a subject of debate, with the ER, Golgi, mitochondria, plasma membrane, and recycling endosomes as suggested sources (Axe et al., 2008; Hayashi-Nishino et al., 2009; Hailey et al., 2010; Ravikumar et al., 2010; Guo et al., 2012; Longatti et al., 2012). It is also unclear how the membrane curvature is generated. More than 30 proteins assisting this process have been described as Autophagy-related (Atg) proteins, which function in a hierarchical order to mediate autophagosome biogenesis (Xie and Klionsky, 2007; Itakura and Mizushima, 2010). Four multiprotein complexes have been found to be required for autophagosome formation, including the Atg1/ULK1 complex, the class III phosphatidylinositol 3-kinase (PI3K) complex with the associated subunit Atg14L, the Atg9 trafficking system, and finally, the two ubiquitin-like proteins Atg12 and Atg8/LC3 and their conjugation systems. In brief, Atg12 is conjugated to Atg5 through the activity of the

H. Knævelsrud and K. Søreng contributed equally to this paper.

Correspondence to Helene Knævelsrud: helene.knavelsrud@ibv.uio.no; Sven R. Carlsson, sven.carlsson@medchem.umu.se; or Anne Simonsen: anne.simonsen@medisin.uio.no

Abbreviations used in this paper: 5pase, phosphoinositide 5-phosphate; BafA1, Bafilomycin A1; BAR, Bin/Amphiphysin/Rvs homology; DFCP1, double FYVE containing protein 1; EBSS, Earls Balanced Salt Solution; LTR, LysoTracker red; PI3K, phosphatidylinositol 3-kinase; PI3P, phosphatidylinositol 3-phosphate; PI(4,5)P_2, phosphatidylinositol 4,5-bisphosphate; qPCR, quantitative real-time PCR; SNX, Sorting nexin; TfR, Transferrin receptor; WT, wild type.

The Rockefeller University Press $30.00
J. Cell Biol. Vol. 202 No. 2 331–349
www.jcb.org/cgi/doi/10.1083/jcb.201205129

Atg7 (E1-like) and Atg10 (E2-like) enzymes, followed by their interaction with membrane-bound Atg16L. Atg8/LC3 becomes conjugated to phosphatidylethanolamine in a reaction that requires Atg7 and the E2-like enzyme Atg3, and is facilitated by the Atg5–Atg12–Atg16L1 complex (Hanada et al., 2007).

PX domain proteins are known to mediate membrane remodeling and trafficking dependent on phosphoinositide binding (Seet and Hong, 2006). There are 47 human PX domain proteins, including the sorting nexins (SNXs), and many also contain Bin/Amphiphysin/Rvs homology (BAR) domains, which are sensors and inducers of membrane curvature (Itoh and De Camilli, 2006). To better understand the phosphoinositide signaling, membrane remodeling, and trafficking events in autophagy, we performed an siRNA screen targeting human PX domain proteins. Depletion of the PX-BAR protein SNX18 strongly inhibited the formation of GFP-LC3–positive autophagosomes, whereas overexpression of SNX18 promoted GFP-LC3 spot formation, dependent on its membrane binding and tubulating ability. SNX18 localizes to structures containing early autophagic markers and interacts with LC3 family members and Atg16L1. We propose a role for SNX18 in promoting LC3 lipidation on tubovesicular structures from recycling endosomes, thereby facilitating membrane delivery to the expanding phagophore. The role of SNX18 in autophagy is conserved, as the *Drosophila melanogaster* SNX18 homologue SH3PX1 is required for efficient autophagosome formation in larval fat body.

Results

siRNA screen reveals SNX18 as a positive regulator of autophagy

To uncover a role of PX domain proteins in autophagy, we performed an imaging-based siRNA-screen where HEK cells stably transfected with GFP-LC3 (HEK GFP-LC3; Chan et al., 2007) were transfected with pools of siRNA targeting PX domain proteins, using ULK1 and TSG101 as controls for reduced and increased autophagosome levels, respectively. The cells were starved or not starved before imaging and high-content image analysis where the total intensity (not depicted) and number of GFP-LC3 spots per cell (Fig. 1 A, Table S1, and Fig. S1 A) were quantified as a measure for autophagosome formation. SNX18 was a promising candidate because its silencing strongly inhibited GFP-LC3 spot formation in both fed and starved cells (Fig. 1 A).

The candidates that affected GFP-LC3 spot formation the most were further validated in a secondary screen where HEK GFP-LC3 cells were transfected with the four individual siRNA oligonucleotides from the pool used in the primary screen (Fig. 1 B and Table S2). To be selected for further analysis, three out of four individual siRNA oligos had to reproduce the effect from the primary screen and correlate with the level of knockdown, as measured by quantitative real-time PCR (qPCR; Fig. 1 B, spot size correlating to mRNA level). SNX18 and HS1BP3 passed our selection criteria, and in the present study we characterized the role of SNX18 in autophagy.

SNX18 is required for autophagosome formation

SNX18 is a member of the SNX9 family of PX-BAR proteins (Håberg et al., 2008). The membrane tubulation activity of these proteins made SNX18 an interesting candidate for a protein involved in autophagosome biogenesis. In line with the decreased number of GFP-LC3 spots seen in the secondary screen (Fig. 1, B and C: Fig. S1; and Table S2), SNX18 depletion also inhibited the conjugation of GFP-LC3 to phosphatidylethanolamine, as measured by quantification of lipidated LC3 (LC3-II) versus nonlipidated LC3 (LC3-I; Kabeya et al., 2000), in correlation with the level of SNX18 mRNA and protein knockdown (Fig. 2 A, Fig. S1 C, and Fig. S2 A). In the following experiments we used the best oligo from the pool (siSNX18-3) as well as another (siSNX18-5), which also efficiently depleted SNX18 protein and decreased GFP-LC3-II levels and GFP-LC3 spot formation upon starvation (Figs. 2 A and S2 B). SNX18 depletion did not decrease LC3 mRNA levels (Fig. S1 D). As a decrease in GFP-LC3 spots and GFP-LC3-II levels during starvation could result from inhibited formation or increased turnover of autophagosomes, we measured the autophagic flux in starved cells in the absence or presence of Bafilomycin A1 (BafA1), which inhibits lysosomal degradation. SNX18-depleted cells treated with BafA1 showed decreased accumulation of GFP-LC3-II compared with control cells (Fig. 2 A), confirming that depletion of SNX18 inhibits autophagosome formation. In line with this, depletion of SNX18 inhibited the starvation-induced degradation of long-lived proteins (Fig. 2 B). SNX18 levels did not change during starvation, nor accumulate upon BafA1 treatment (Fig. 2 A), which suggests that SNX18 itself is not an autophagic cargo. The inhibitory effect of siSNX18 on GFP-LC3 spot formation was rescued by siRNA-resistant myc-SNX18, confirming that the effect is specific (Fig. 2 C and Fig. S3 H). Interestingly, expression of myc-SNX18 in SNX18-depleted cells increased the number of GFP-LC3 spots compared with control cells (Fig. 2 C), which indicates that SNX18 overexpression may stimulate biogenesis of autophagosomal membranes. Indeed, expression of myc-SNX18 caused increased lipidation of endogenous LC3 (Fig. 2 D), as well as an increased number of GFP-LC3 spots, dependent on the core autophagy machinery (Fig. 2 E and Fig. S2 D). However, myc-SNX18 expression did not increase degradation of long-lived proteins (Fig. 2 F), indicating that although SNX18 overexpression stimulates LC3 lipidation and GFP-LC3 spot formation, it is insufficient for increased autophagic flux. Collectively, these results establish SNX18 as a positive regulator of autophagosome formation.

SNX18 functions downstream of the class III PI3K complex in autophagosome biogenesis

SNX18 has been reported to localize to the plasma membrane and endosomes, and is also called SNAG1 (SNX-associated Golgi protein 1; Håberg et al., 2008; Park et al., 2010; Willenborg et al., 2011). We detected SNX18 in both the cytosol and membrane fractions of HeLa cells (Fig. S2 E), and when the membrane fraction was further separated according to density by

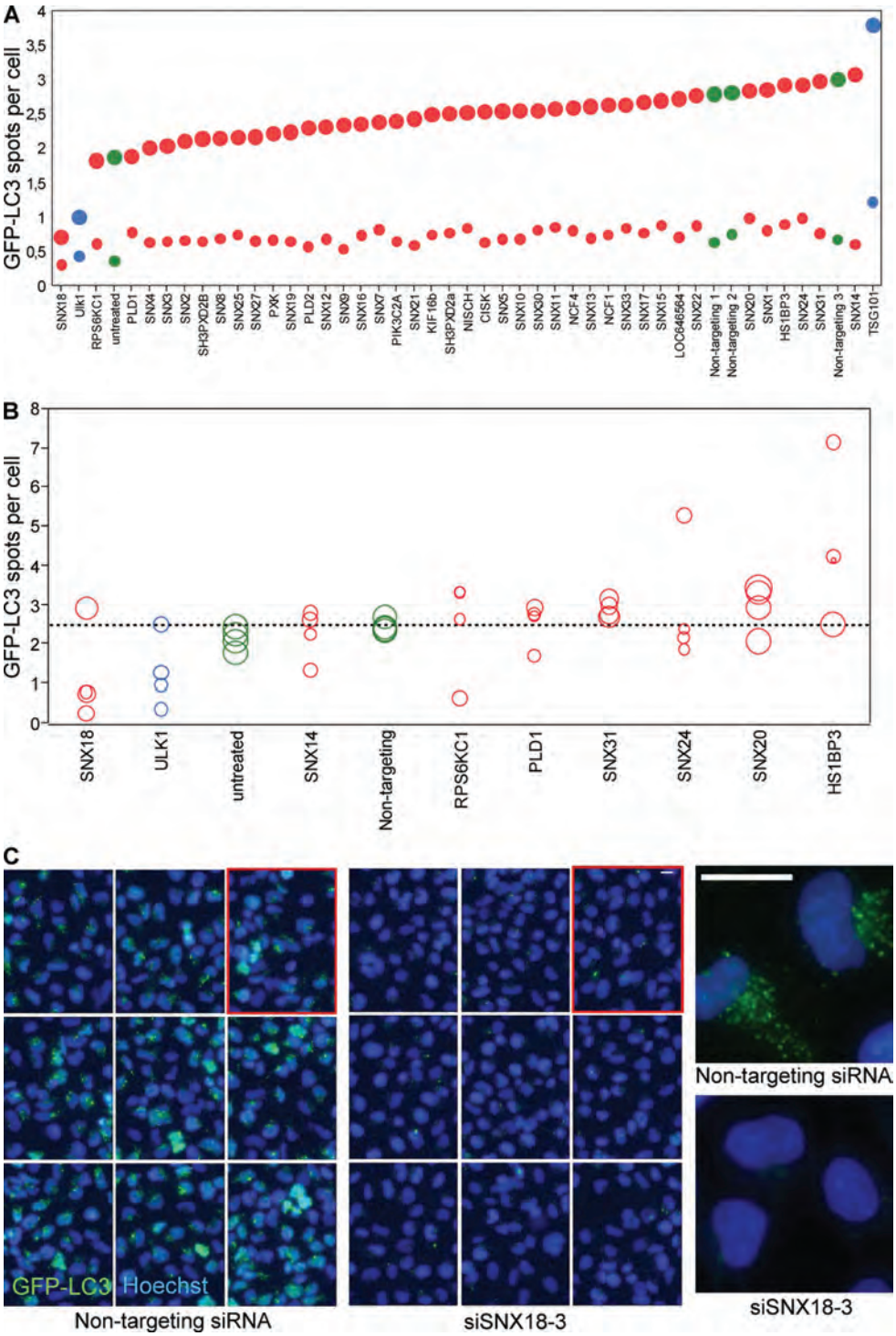

Figure 1. **siRNA screen for PX domain proteins in autophagy.** (A) HEK GFP-LC3 cells were transfected with siRNA pools targeting PX domain proteins and starved (large circles) or not starved (small circles) for 2 h, followed by fixation and counterstaining of the nuclei by Hoechst. The images were processed for high-content image analysis to quantify the number of GFP-LC3 spots per cell. The graph shows the average of three independent experiments in triplicate with a total of 30,000 cells. siRNA against ULK1 and TSG101 were used as controls (blue circles). Green, negative controls; red, PX domain proteins. (B) Selected PX domain proteins were depleted by transfection of HEK GFP-LC3 with the four individual siRNA oligos of the pools used in A. The cells were treated, imaged, and analyzed as in A. The area of each circle corresponds to the relative amount of target mRNA as measured by qPCR. The graph shows the average of two independent experiments in triplicate with a total number of 18,000 cells. Coloring is as in A. (C) Micrographs of starved HEK GFP-LC3 cells treated with nontargeting or siSNX18-3 siRNA. (left and middle) 3 × 3 fields of cells. (right) Close-up of a few cells from the respective population. The images in the right panels are shown again in Fig. S1 B alongside cells treated with other SNX18-targeting siRNAs. Bars, 10 µm. See also Table S1 and Table S2.

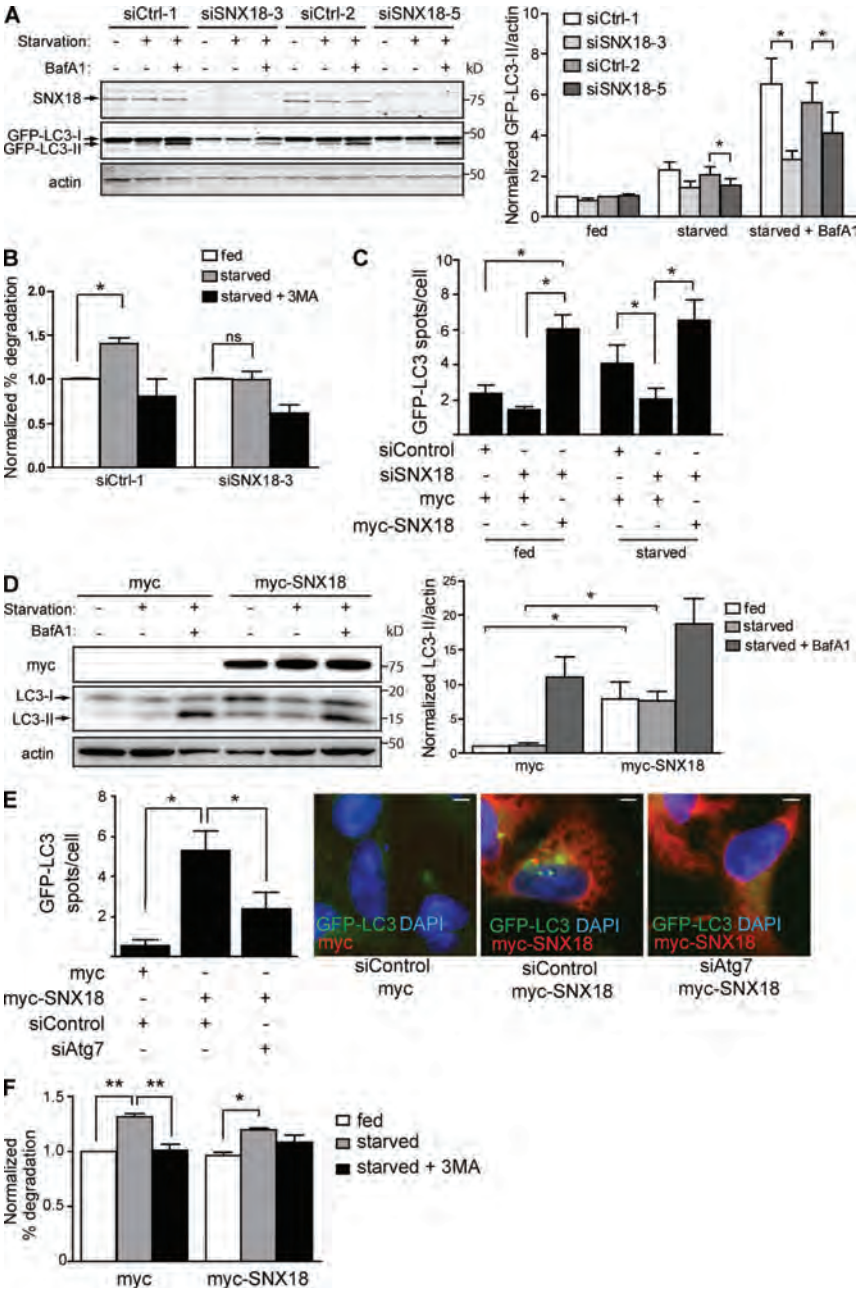

Figure 2. **SNX18 is a positive regulator of autophagy.** (A) HEK GFP-LC3 cells transfected with control (siCtrl) or two different SNX18 siRNA oligos (siSNX18-3 and siSNX18-5) were starved or not starved for 2 h in the presence or absence of BafA1. GFP-LC3 lipidation and SNX18 protein knockdown were monitored by immunoblotting. The graph shows the average GFP-LC3-II relative to actin normalized to siCtrl-1 fed ± SEM (error bars), $n = 4$. (B) The degradation of long-lived proteins in HeLa cells transfected with control or SNX18 siRNA was quantified after 4 h of starvation in the absence or presence of 3-MA and normalized to the degradation in fed cells (mean ± SEM [error bars], $n = 3$). (C) HEK GFP-LC3 cells were transfected with control or SNX18 siRNA and then with a myc control or siRNA-resistant myc-SNX18 plasmid. The number of GFP-LC3 spots per cell was quantified (graph shows mean ± SEM [error bars], $n = 3$). (D) HEK GFP-LC3 cells were transfected with myc-SNX18 or a myc control plasmid and treated as in A. The graph shows the average LC3-II levels relative to actin normalized to myc-transfected fed cells, ±SEM (error bars). $n = 3$. (E) HEK GFP-LC3 cells were transfected with control or Atg7 siRNA and then with myc-SNX18 or a myc control plasmid, followed by quantification of the number of GFP-LC3 spots per cell (graphs show mean ± SEM [error bars], $n = 3$). Representative images are shown. Bars, 5 µm. (F) The degradation of long-lived protein in HeLa cells transfected with myc-SNX18 or a myc control plasmid was quantified as in B (graph shows mean ± SEM [error bars], $n = 4$). *, $P < 0.05$; **, $P < 0.01$. See also Figs. S1 and S2.

gradient centrifugation (Lundmark and Carlsson, 2003, 2005), the majority of SNX18 banded at medium density in both fed and starved cells, partially co-migrating with markers of the ER (calnexin), Golgi (GM130), endosomes (Transferrin receptor [TfR], Rab11), and plasma membrane (SNX9; Fig. 3 A). SNX18 did not cofractionate with the majority of LC3-II–positive membranes, which supports the finding that it is not itself an autophagy cargo. Interestingly, a minor part of SNX18 was found on dense membranes together with the majority of membrane-associated LC3-I and GABARAP-I (Fig. 3 A). The identity of the LC3 and GABARAP bands were verified by siRNA and Western blotting (Fig. S2 F). A striking comigration was found between SNX18 and the core autophagy proteins Atg14L and Atg16L1 in the medium-density fractions, and with the latter also in the dense fractions, in both fed and starved cells (Fig. 3 A), which further suggests a role for SNX18 in autophagosome biogenesis. The SNX18-related protein SNX9 was heterogeneously distributed in heavier membrane fractions, and depletion of SNX9 did not inhibit autophagosome formation (Fig. 1 A and Fig. S2 C), which suggests that the role of SNX18 in autophagosome formation is not shared by SNX9.

To further investigate the cellular localization of SNX18 and its role in autophagy, cells costained for endogenous SNX18 and autophagy markers were analyzed by confocal microscopy. SNX18 was mainly present in a perinuclear area, colocalizing

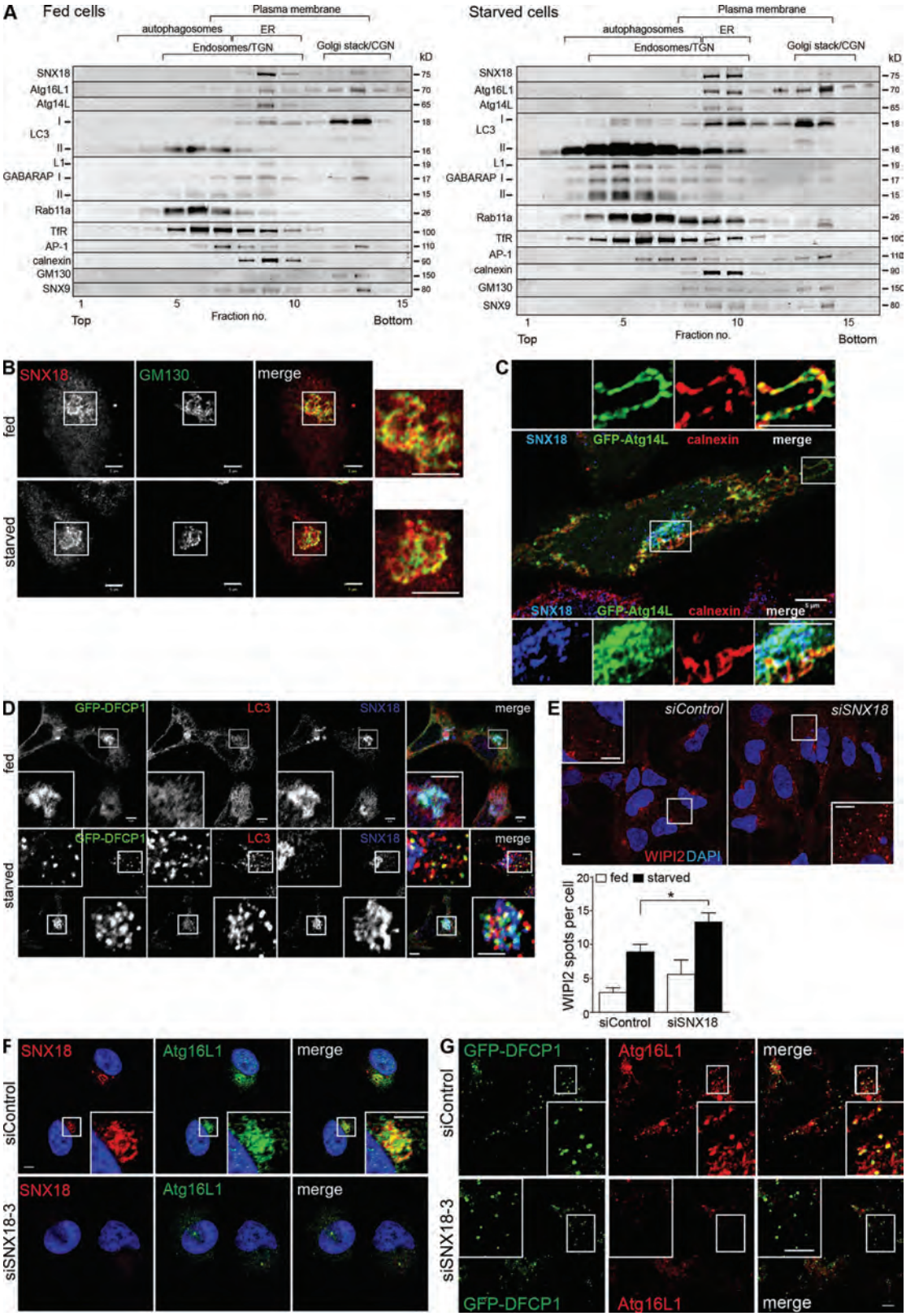

Figure 3. **SNX18 colocalizes with autophagic markers in the perinuclear area.** (A) The total membrane fractions from fed or starved HeLa cells were analyzed by density gradient centrifugation and probed for the indicated proteins by immunoblotting. Migration of different organelles is indicated, based on the positions in the gradient of calnexin (ER), GM130 (Golgi stack/CGN), SNX9 (plasma membrane), AP-1, TfR and Rab11a (Endosomes/TGN), and

with the Golgi marker GM130, in both fed and starved HeLa cells (Fig. 3 B). Moreover, we observed a partial colocalization of SNX18 and GFP-Atg14L in areas outside the ER, although Atg14L also colocalized with the ER marker calnexin (Fig. 3 C). Atg14L has been shown to recruit the class III PI3K complex to the ER for localized production of phosphatidylinositol 3-phosphate (PI3P) at sites of autophagosome formation (called omegasomes; Axe et al., 2008) and can also promote membrane curvature through its BATS domain (Fan et al., 2011). GFP–double FYVE containing protein 1 (DFCP1), a marker of omegasomes, was found together with SNX18 and LC3 in the perinuclear area in both fed and starved cells; however, SNX18 did not colocalize with peripheral GFP-DFCP1– and LC3-positive spots formed upon starvation (Fig. 3 D). Moreover, whereas omegasome formation was strongly inhibited by depletion of the class III PI3K complex subunit Beclin 1, it was not significantly affected by SNX18 depletion (Fig. S3 B), which suggests that SNX18 functions downstream of the class III PI3K complex. In line with this, depletion of Atg14L and ULK1 prevented myc-SNX18–induced GFP-LC3 spot formation (Fig. S2 D). Depletion of SNX18 caused puncta of the PI3P-binding protein WIPI2 to accumulate (Fig. 3 E), which suggests that aberrant intermediate structures accumulate in the absence of SNX18. Endogenous Atg16L1 (or flag-Atg16L1) also colocalized specifically with SNX18 in the perinuclear region (Fig. 3 F and Fig. S3, C–E), and depletion of SNX18 prevented recruitment of Atg16L1 to this region (Fig. 3 F) and to omegasomes (Fig. 3 G), without affecting Atg16L1 protein levels (not depicted). Together, our data indicate that SNX18 functions downstream of DFCP1, Atg14L, and WIPI2 through recruitment of Atg16L1 to a perinuclear region to facilitate remodeling of LC3-positive membranes as a membrane source for autophagosome formation from omegasomes.

Binding of SNX18 to phosphatidylinositol 4,5-bisphosphate (PI(4,5)P_2)-containing membranes is needed for Atg16L1 spot formation and for SNX18-induced GFP-LC3 spots

To further address the molecular mechanisms underlying the role of SNX18 in autophagy, we took advantage of the fact that SNX18 overexpression stimulates LC3 lipidation and GFP-LC3 spot formation in an autophagy-specific manner (Fig. 2, D and E), and induces formation of membrane tubules containing GFP-LC3 and flag-Atg16L1 (Fig. 4, A and B). Endogenous Atg16L1 was also associated with myc-SNX18–induced tubules (unpublished data). Membrane tubules induced by SNX9 were negative for GFP-LC3 (Fig. S4 C). To investigate whether the membrane binding and tubulation activity of SNX18 are important for its role in autophagosome formation, we introduced mutations in the SNX18 PX-BAR region (Fig. 4 C), based on the resolved structure of the SNX9 PX-BAR unit (Pylypenko et al., 2007). The positively charged concave surface of the BAR domain dimer allows SNX9 to sense membrane curvature and provides affinity to the negatively charged membrane surface, and the SNX9 K366E/R367E mutation or mutation of the phosphoinositide-binding pocket, R286Q/Y287A/K288A, was found to abolish membrane binding (Pylypenko et al., 2007; Yarar et al., 2008). The corresponding mutations were introduced in mCherry-SNX18 (mCh-SNX18 K394E/R395E and R312Q/Y313A/K314A, designated KR and RYK, respectively) and expressed in HEK GFP-LC3 cells at similar levels (Fig. S3 F). The SNX18 KR and RYK mutants were defective in membrane binding (Fig. 4 D) and unable to induce GFP-LC3 spots (Fig. 4 E and Fig. S3 H) and LC3 lipidation (Fig. 4 F and Fig. S3 G) as efficiently as wild-type (WT) SNX18, which indicates that SNX18 membrane binding is important for its function in autophagy. SNX18 was previously found to bind PI(4,5)P_2 (Håberg et al., 2008), and depletion of PI(4,5)P_2 by ionomycin (Várnai and Balla, 1998; Fig. 4 G) or by rapalog-induced recruitment of a phosphoinositide 5-phosphatase to the plasma membrane (Varnai et al., 2006; Zoncu et al., 2007; Fig. 4 H) strongly inhibited the induction of GFP-LC3 spots seen in myc-SNX18–transfected cells. Inhibition of GFP-LC3 spot formation by ionomycin was also observed after starvation without SNX18 overexpression (Fig. S3 I). Furthermore, SNX18 membrane binding was important for starvation-induced formation of Atg16L1 spots, and although the total intensity of endogenous Atg16L1 spots was increased by expression of myc-SNX18, it was strongly decreased by myc-SNX18 KR compared with control-transfected cells (Fig. 4 I). Moreover, Atg16L1 depletion prevented SNX18-induced GFP-LC3 spots (unpublished data). The close colocalization and interdependence of SNX18 and Atg16L1 prompted us to investigate if they interact, and we found myc-SNX18 full-length or the PX-BAR domain, but not the SH3-LC region, to coimmunoprecipitate with flag-Atg16L1 (Fig. 4 J). Thus, binding of SNX18 to PI(4,5)P_2-containing membranes is important for its role as a positive regulator of autophagy.

The tubulation activity of SNX18 is important for its role in autophagy and is regulated by phosphorylation

A short conserved sequence just upstream of the PX domain is suggested to form an amphipathic helix upon membrane contact (Pylypenko et al., 2007; referred to as helix 0), and is, together with the PX-BAR, required for efficient membrane tubulation by SNX9 (Lundmark and Carlsson, 2009).

LC3-II and GABARAP-II (autophagosomes). (B) HeLa cells were starved or not starved for 2 h and immunostained for SNX18 and GM130. Panels to the right show enlarged views of the boxed regions. (C) HeLa cells were transfected with GFP-Atg14L and immunostained for SNX18 and calnexin. The boxed regions are enlarged on the top and bottom. (D and E) HEK GFP-DFCP1 cells were starved or not starved for 50 min and immunostained for SNX18 and LC3 (D) or WIPI2 (E). Results shown are mean ± SEM (error bars), $n = 3$ with 30 cells in each experiment. *, $P < 0.05$. (F) HeLa cells were transfected with control or SNX18 siRNA, starved for 2 h, and immunostained against SNX18 and Atg16L1. (G) HEK GFP-DFCP1 cells were transfected with control or SNX18 siRNA, starved for 50 min, and immunostained for Atg16L1. All images are from confocal microscopy. Inset panels show enlarged views of the boxed regions. Bars, 5 µm. See also Fig. S3.

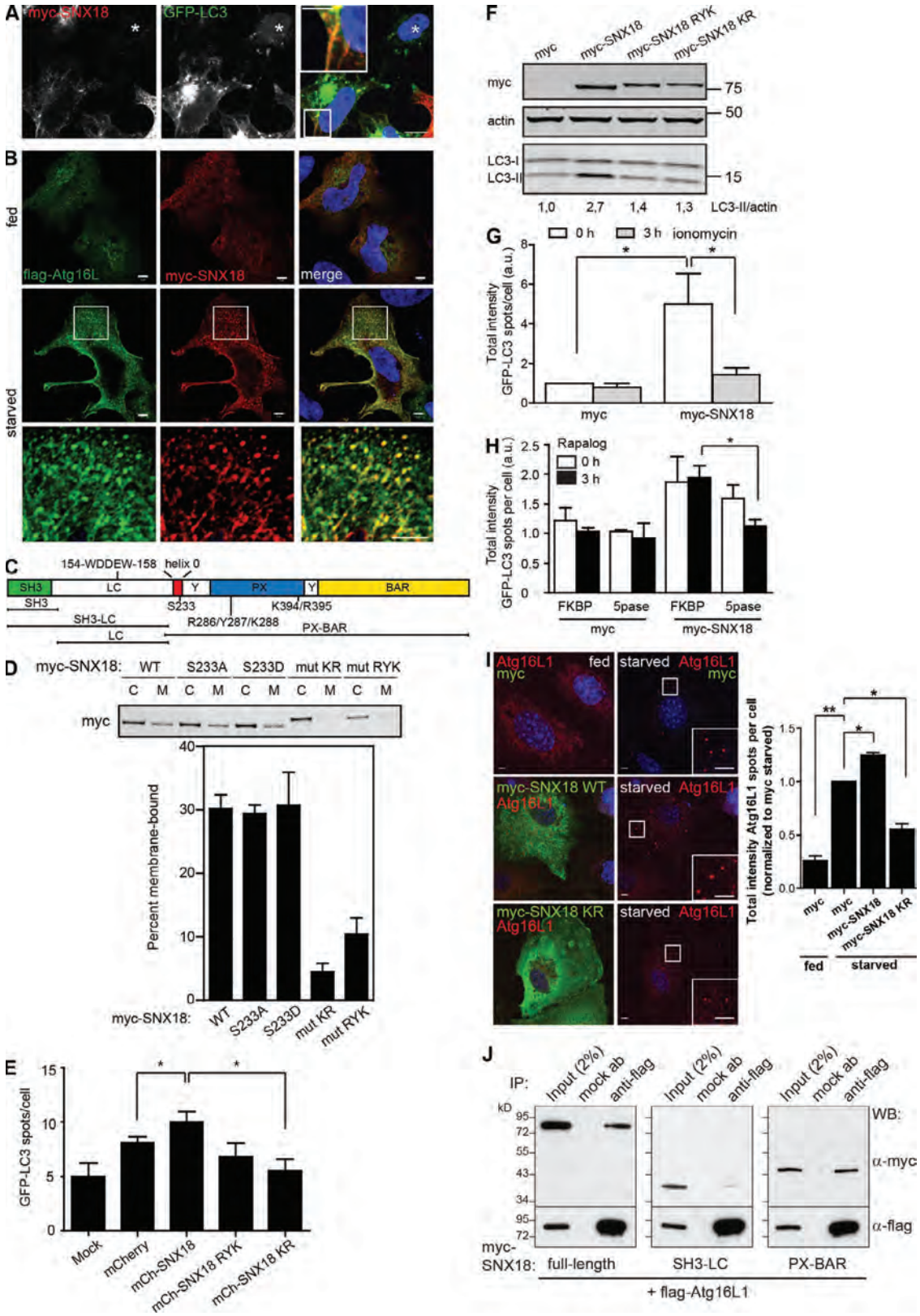

Figure 4. **SNX18 binding to PI(4,5)P_2 membranes is required for its function in autophagy.** (A) HeLa GFP-LC3 cells were transfected to express myc-SNX18, immunostained against myc, and analyzed by confocal imaging. Asterisks indicate a nontransfected cell. Bars: (main panels) 20 µm; (inset) 10 µm. (B) HeLa cells transfected with flag-Atg16L1 and myc-SNX18 were starved or not starved for 2 h before immunostaining with anti-myc and anti-flag antibodies and

The PhosphoSitePlus database (http://www.phosphosite.org/) reports a phosphorylation in the corresponding SNX18 helix 0 at serine-233, which increased in cells treated with the autophagy-inducing drug rapamycin (Chen et al., 2009). We raised a phosphospecific antibody against this site (Fig. S3, J and K) and found that GFP-SNX18 showed a time-dependent increase in SNX18 S233 phosphorylation during starvation, correlating with increased levels of LC3-II, that was reversed by re-feeding of starved cells (Fig. 5 A). To elucidate the role of SNX18 S233 phosphorylation in autophagy, we made myc-SNX18 S233 nonphosphorylatable (S233A) or phosphomimicking (S233D) mutants. The S233A or S233D mutants bound as efficiently to membranes as WT myc-SNX18 (Fig. 4 D). However, the PX-BAR S233A mutant was less efficient at, and the S233D mutant completely incapable of, inducing membrane tubulation as compared with WT PX-BAR (Fig. 5 B). The two phospho mutants were also much less efficient at inducing GFP-LC3 spots (Fig. 5 C and Fig. S3 H) when expressed at similar levels to SNX18 WT (Fig. S3 L). Moreover, neither the membrane binding (KR and RYK)– nor the membrane tubulation (S233D)–deficient mutants were able to induce formation of GFP-LC3–positive tubules as efficiently as myc-SNX18 WT (Fig. 5 D). Interestingly, although expression of SNX18 PX-BAR did induce extensive membrane tubulation, these tubules were devoid of GFP-LC3 (Fig. 5 D), and the number of GFP-LC3 spots in these cells was reduced (Fig. 5 E), which indicates that the N-terminal part of SNX18 is required for recruitment of LC3 onto SNX18-induced tubules and for autophagosome formation. We further noticed that SNX18 overexpression induced a strong perinuclear localization of GFP-LC3 (Figs. 4 A and 5 D) that was neither seen in cells expressing the membrane-binding deficient SNX18 mutants (Fig. 5 D), nor upon depletion of Atg16L1 (Fig. 5 F), which suggests that SNX18 facilitates membrane recruitment of LC3 dependent on Atg16L1. Together these results indicate that the membrane-remodeling capability of SNX18 is required for autophagosome formation, and that this activity is negatively regulated by a phosphorylation in the amphipathic helix 0.

SNX18 interacts with LC3/GABARAP

Our findings that SNX18 cofractionates with LC3 (Fig. 3 A), and recruits GFP-LC3 to the perinuclear area and onto SNX18-induced membrane tubules (Fig. 5 D), indicated that SNX18 might interact with LC3. Indeed, endogenous SNX18 coimmunoprecipitated with GFP-LC3, and even more so with the lipidation-defective GFP-LC3 G120A mutant (Kabeya et al., 2000; Fig. 6 A), which suggests that SNX18 preferentially interacts with the nonlipidated form of LC3 (LC3-I). LC3-I is generally considered to be cytosolic, but cell fractionation (Fig. S2 E) and density gradient separation of the membrane fraction (Fig. 3 A) clearly show that LC3-I and GABARAP-I can associate with membranes. Interestingly, we observed a shift in the LC3-I/GABARAP-I distribution from heavier fractions to the medium-density LC3-II– and SNX18-positive membranes upon starvation, which might suggest that LC3 lipidation occurs on SNX18-positive membranes (Fig. 3 A). GFP-GABARAP was also detected on SNX18-induced membrane tubules (Fig. S4 B). Endogenous SNX18 from both fed and starved MDBK cell lysates bound strongly to recombinant GST-GABARAP and GST-LC3 (Fig. 6 B), further indicating that SNX18 interacts with nonlipidated Atg8 homologues.

SNX18, like p62, an autophagy receptor known to interact with Atg8 proteins (Pankiv et al., 2007), was found to interact with all Atg8 family members, although little interaction was observed with GABARAPL2 (Fig. 6 C). The interaction site was mapped to the SNX18 SH3-LC region (Fig. 7 A) and the exact sequence was determined by a peptide array covering the entire SNX18 SH3-LC sequence, where GST-GABARAP bound to all peptides containing 154-WDDEW-158 (Fig. 7 B), the same motif previously found to mediate binding of SNX18 to AP-1 (Håberg et al., 2008). Mutation of one or both of the tryptophan residues (W154S and/or W158S) abolished the interaction with LC3/GABARAP (Fig. 7, C and D). Furthermore, although tubules were still formed in cells expressing the myc-SNX18 W154S/W158S mutant, these were negative for GFP-LC3 (Fig. 7 E), and the number of GFP-LC3 spots was also significantly reduced compared with SNX18 WT (Fig. 7 F). In summary, SNX18 interacts with Atg8 proteins through a WDDEW sequence in its SH3-LC region, and this interaction is required for localization of GFP-LC3 to SNX18-induced tubules and for GFP-LC3 spot formation.

Recycling endosomes provide membrane for SNX18-mediated autophagosome biogenesis

Our results thus far indicate that SNX18 is involved in membrane remodeling and recruitment of Atg16L1 and LC3 to membranes contributing to autophagosome biogenesis. We asked whether these were endosomal membranes, and found TfR and the small GTPase Rab11, involved in trafficking from recycling

confocal microscopy. Bars, 5 µm. (C) SNX18 domain structure. An N-terminal SH3 domain is followed by a low-complexity region (LC). The membrane-remodeling part consists of an amphipathic helix (helix 0), a PX domain that is flanked by sequences forming a Yoke domain (Y), and a BAR half-domain. The functional BAR domain is formed by dimerization. Truncated constructs and point mutations used are indicated. (D) HeLa cells were transfected with the indicated myc-SNX18 plasmids for 6 h and starved for an additional 2 h before harvest. Equal parts of cytosol (C) and membrane (M) fractions were analyzed by Western blotting. The graph shows the average membrane-bound myc-SNX18 ± SEM (error bars), $n = 3$. (E and F) HEK GFP-LC3 cells were transfected with the indicated mCherry-SNX18 (E) or mycSNX18 (F) constructs for 16 h. The number of GFP-LC3 spots per transfected cell (E; graph shows mean ± SEM [error bars], $n = 5$) or ratio of LC3-II to actin determined by Western blotting (F) was quantified. (G and H) HEK GFP-LC3 cells transfected with myc-SNX18 or a myc control plasmid alone (G) or together with CFP-FRB and mRFP-FKBP or mRFP-FKBP 5pase (H) for 6 h were treated or not treated with 5 µM ionomycin (G) or 2.5 µM A/C heterodimerizer (rapalog; H) for the last 3 h before analysis of the total intensity of GFP-LC3 spots per transfected cell (graph shows mean ± SEM [error bars], $n = 3$). (I) MEFs were transfected with myc, myc-SNX18 WT, or KR for 16 h, starved or not starved for 2 h, and immunostained for endogenous Atg16L1. Insets show enlarged views of the boxed regions. Bars, 5 µm. (J) HeLa cells were transfected for 12 h with the indicated constructs and starved for 90 min. Cells were solubilized and immunoprecipitated with anti-flag or an unrelated antibody of the same isotype (mock ab). Immunoprecipitates and 2% of the lysates were analyzed by immunoblotting against myc and flag. *, $P < 0.05$; **, $P < 0.01$. See also Fig. S3.

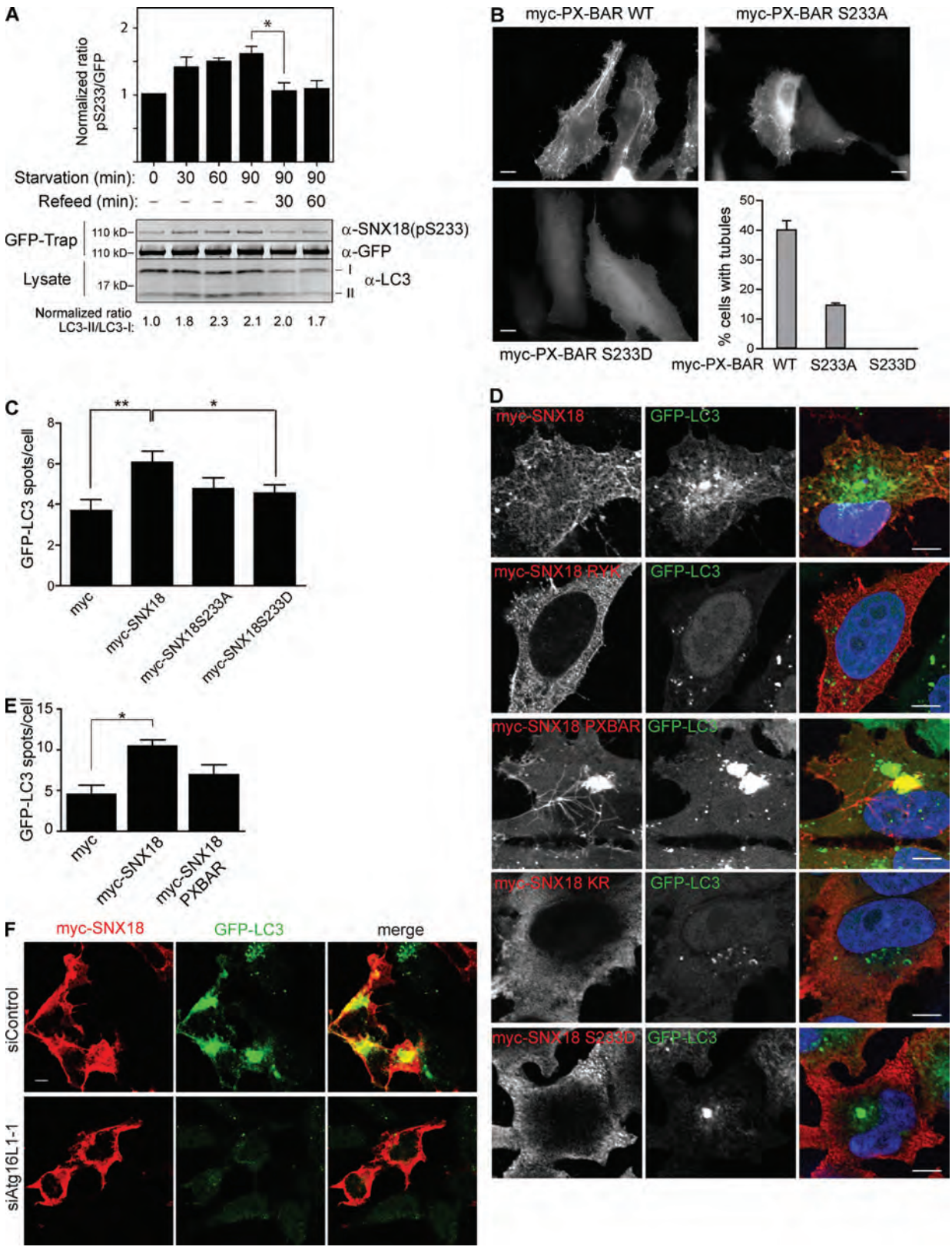

Figure 5. **The tubulation activity of SNX18 is important for its role in autophagy and is regulated by phosphorylation.** (A) HeLa GFP-SNX18 cells were starved for the indicated time, followed by incubation in full medium (Refeed) where indicated. Cell lysates were analyzed for LC3 by immunoblotting, or immunoprecipitated with GFP-Trap before immunoblotting against SNX18(pS233) and GFP. The ratio of pS233 to GFP, and the ratio of LC3-II to LC3-I,

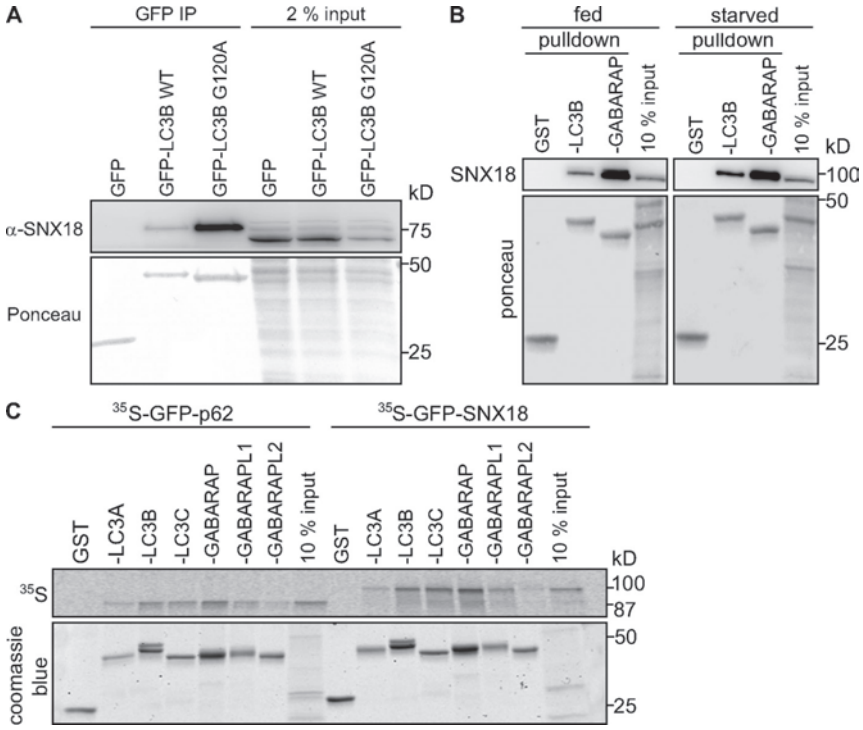

Figure 6. **SNX18 interacts with LC3 family members.** (A) GFP, GFP-LC3, or GFP-LC3 G120A were immunoprecipitated from transfected HeLa cells. The immunoprecipitates and 2% of the lysate were analyzed by immunoblotting against SNX18. The GFP proteins were detected by Ponceau staining. (B) Lysates from fed or starved MDBK cells were incubated with the indicated glutathione-Sepharose–bound GST-tagged proteins. SNX18 was detected by immunoblotting. Ponceau staining shows the GST proteins. (C) In vitro translated GFP-p62 or GFP-SNX18 were incubated with the indicated GST-tagged Atg8 family proteins. Bound proteins were detected by autoradiography and GST proteins by Coomassie blue staining.

endosomes, to colocalize with perinuclear GFP-LC3 in myc-SNX18–expressing cells (Fig. 8, A and B), whereas no colocalization with early endosomal antigen 1 (EEA1), LAMP-1, or lyso-bisphosphatidic acid (LBPA) was detected (Fig. S4 D). Interestingly, TfR (Fig. 8 A), but not Rab11 (Fig. 8 B), was detected on the GFP-LC3–positive SNX18-induced tubules. SNX18-induced membrane tubules were also apparent at the ultrastructural level, and clusters of tubulo-vesicular structures together with small multivesicular body–like vesicles were typically seen (Fig. 8 C, i). By immuno-EM these tubules were found to be positive for myc-SNX18, GFP-LC3, and TfR (Fig. 8 C). GFP-LC3–labeled structures that resembled more typical autophagosomal vesicles were also found (Fig. 8 C, iv), although at similar levels in myc-SNX18– and myc-transfected cells. Also in nontransfected cells, Rab11 was strongly recruited to the SNX18-positive perinuclear area upon starvation, where it partially colocalized with TfR (Fig. 9 A), but not with EEA1 (Fig. S3 A). SNX18 also partially cofractionated with Rab11 and TfR (Fig. 3 A).

Interestingly, Atg16L1 colocalized extensively with Rab11 and TfR, both in peripheral spots (Fig. 9 B) and in the SNX18-positive perinuclear area (Fig. 9 C). To delineate the mechanistic relationship among these proteins, we depleted each one and observed the localization of the others. Depletion of SNX18 inhibited the perinuclear localization of Rab11 during starvation (Fig. 9 D) and depletion of Rab11 inhibited the perinuclear localization of Atg16L1, but not SNX18 (Fig. 9 E). We previously showed that SNX18 depletion prevents the perinuclear localization of Atg16L1 (Fig. 3 F) and that Atg16L1 depletion prevents the SNX18-induced perinuclear localization of GFP-LC3 (Fig. 5 F). Collectively, our results indicate that upon induction of autophagy, Atg16L1-positive recycling endosomes redistribute in a Rab11- and SNX18-dependent manner to a perinuclear SNX18-positive region where Atg16L1 facilitates recruitment of LC3, followed by SNX18-mediated membrane remodeling that provides membranes for autophagosome biogenesis (Fig. 10 A).

The *D. melanogaster* SNX18 homologue SH3PX1 is also required for autophagy

Whereas the vertebrate SNX9 family consists of three proteins, insects and nematodes have only one. To test if the *D. melanogaster* SNX18 homologue SH3PX1 is also involved in autophagy, we used mosaic analysis of SH3PX1 RNAi

was quantified, and normalized to 1 for the zero-time sample in both cases (graph shows mean ± SEM [error bars], $n = 4$; *, $P < 0.05$). (B) The indicated myc-SNX18 PX-BAR constructs were transfected into HeLa cells, and their tubulation efficiency was measured by scoring the percentage of cells displaying more than three elongated structures longer than 5 µm ($n = 300$). The graph shows the mean of two independent experiments ± range (error bars). Bars, 10 µm. (C) The indicated myc-tagged SNX18 constructs were transfected into HEK GFP-LC3 cells, and the number of GFP-LC3 spots per cell was quantified. The graph shows mean ± SEM (error bars), $n = 5$. (D) HeLa GFP-LC3 cells were transfected with the indicated myc-tagged SNX18 constructs for 16 h, starved for 2 h, and analyzed by confocal imaging. Bars, 10 µm. (E) HEK GFP-LC3 cells were transfected with myc-SNX18 WT or myc-SNX18 PX-BAR constructs, and the number of GFP-LC3 spots per cell was quantified. The graph shows mean ± SEM (error bars), $n = 3$. (F) HeLa GFP-LC3 cells were transfected with siRNA against Atg16L1 and later with myc-SNX18 constructs before immunostaining and confocal imaging. Bar, 5 µm.

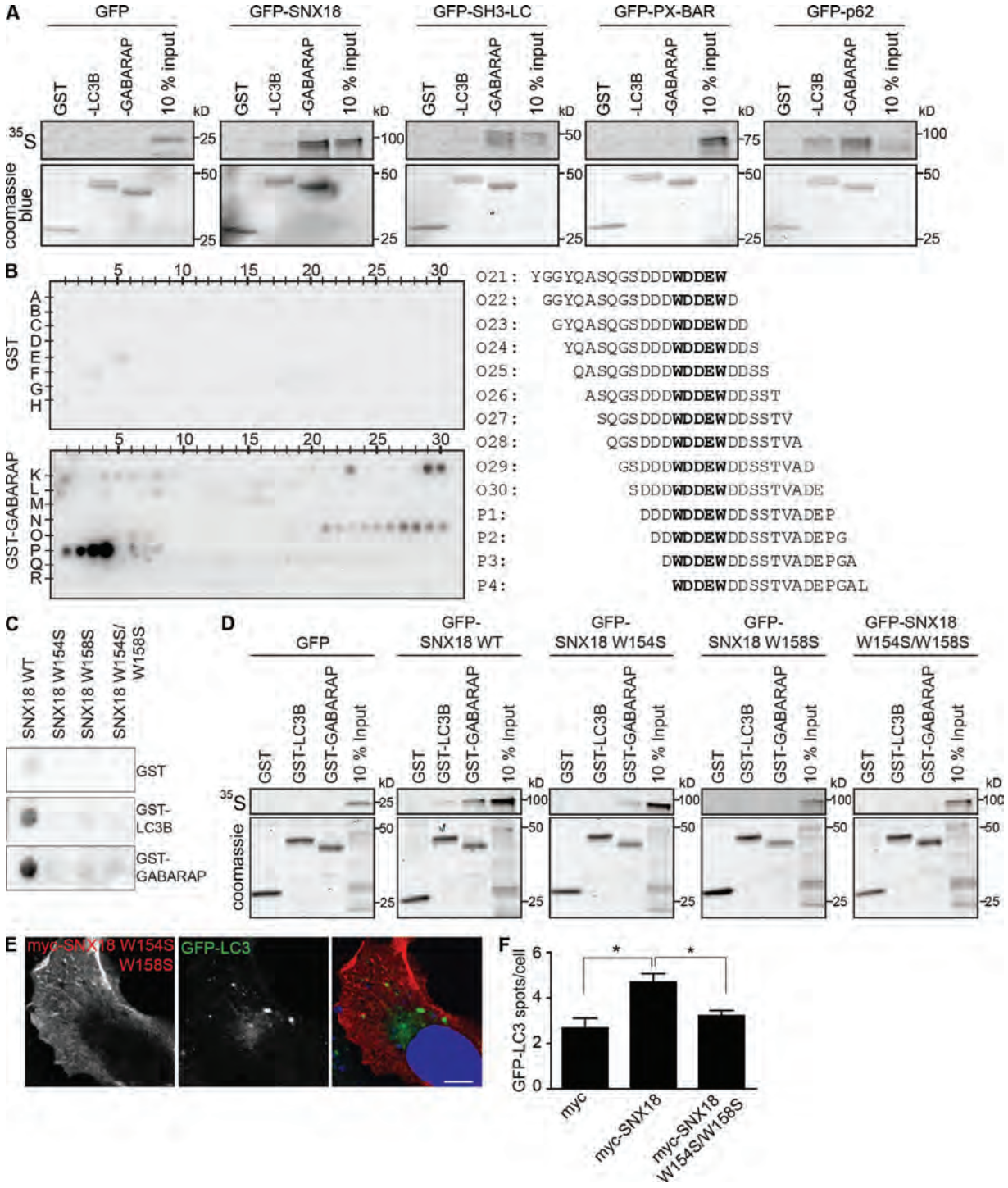

Figure 7. **A WDDEW sequence in the SNX18 LC region mediates the interaction with LC3/GABARAP.** (A) GFP-p62 or -SNX18 full-length, SH3-LC, or PX-BAR regions were in vitro translated and incubated with GST-LC3B or -GABARAP. The resulting pulldowns were separated by SDS-PAGE. Bound proteins were detected by autoradiography and GST proteins by Coomassie blue staining. (B) 18-mer peptides covering the entire sequence of the SNX18 SH3-LC region were spotted on a membrane that was incubated with GST or GST-GABARAP, which were detected by immunoblotting against GST. The peptide sequences that specifically bound GST-GABARAP are shown with the common WDDEW motif in bold. (C) Peptides with the sequence YGGYQASQGS-DDDWDDEWDDSSTVADEPGAL (SNX18 WT) or with the first (SNX18 W154S), the second (SNX18 W158S), or both (SNX18 W154S/W158S) W mutated to S were spotted on membranes that were incubated with GST, GST-LC3B, or GST-GABARAP. Binding was analyzed as in B. (D) GFP-SNX18 WT and the indicated mutants were in vitro translated and incubated with GST-LC3B or -GABARAP, and their binding was analyzed as in A. (E) HeLa GFP-LC3 cells were transfected with myc-SNX18 W154S/W158S mutant, starved for 2 h, immunostained against myc, and analyzed by confocal imaging. Bar, 10 µm. (F) Indicated myc-SNX18 constructs were transfected into HEK GFP-LC3 cells, and the number of GFP-LC3 spots per cell was quantified. The graph shows mean ± SEM (error bars), $n = 3$. *, $P < 0.05$.

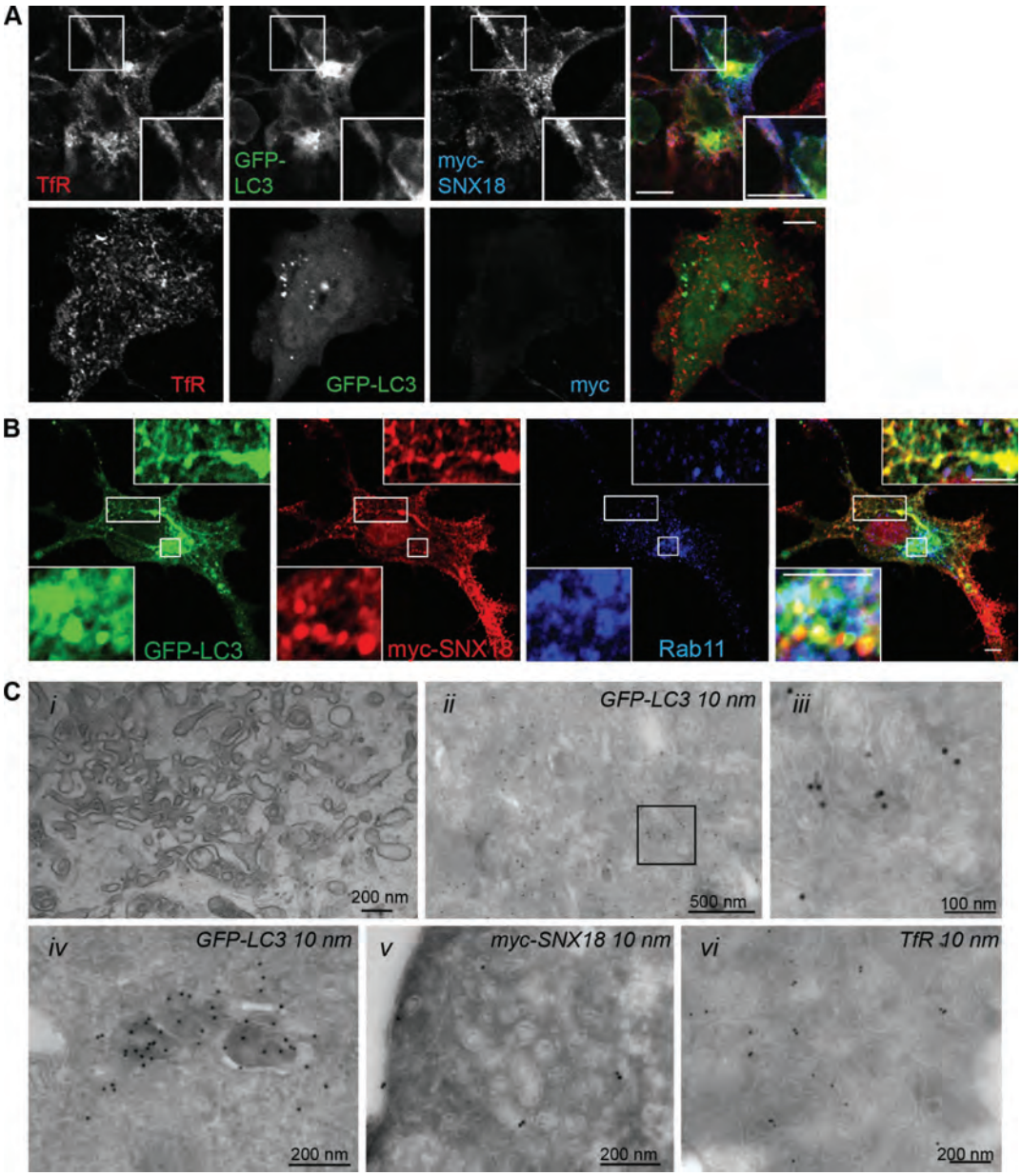

Figure 8. **SNX18 tubules are positive for TfR.** HeLa GFP-LC3 cells were transfected with myc-SNX18 or a control myc plasmid and then immunostained for myc and TfR (A) or Rab11 (B). Bars: (A) 10 µm; (B) 5 µm. Insets show enlarged views of the boxed regions. (C, i) Clusters of tubulo-vesicular structures together with small multivesicular body–like vesicles were observed upon plastic embedding of HeLa GFP-LC3 cells overexpressing myc-SNX18. (ii–vi) Immuno-EM showed that similar clusters labeled strongly for GFP-LC3 (ii, and enlarged in iii from the boxed region), myc-SNX18 (v), and TfR (vi). Strong GFP-LC3 labeling in structures resembling more typical autophagosomal vesicles was also detected (iv). See also Fig. S4.

cells (GFP positive) surrounded by WT cells (GFP negative) in the larval fat body, where autophagy is robustly induced in response to nutrient limitation or at late larval stages as part of the developmental program (Rusten et al., 2004; Scott et al., 2004; Neufeld, 2008). Immunostaining of SH3PX1 confirmed that SH3PX1 levels were decreased by SH3PX1 RNAi (Fig. S5 A). Autophagic compartments were virtually absent from well-fed third instar larvae fat body cells as visualized by LysoTracker red (LTR; not depicted) or mCherry-Atg8a (Fig. S5 B); they were, however, readily observed in WT fat body cells, but not in cells depleted of SH3PX1 after larval starvation (Fig. 10, B and C). After longer starvation, fewer and smaller autophagosomes were observed in SH3PX1-depleted cells compared with the larger autophagosomes in WT cells (Fig. S5 C). Moreover, LTR (Fig. 10 D)- or mCherry-Atg8a (Fig. 10 E)–positive compartments were easily detected in WT fat body cells from 110-h-old well-fed larvae undergoing developmental autophagy, whereas very few were visible in the SH3PX1 RNAi–expressing cells. These compartments were larger in the WT fat body cells from older larvae (113 h),

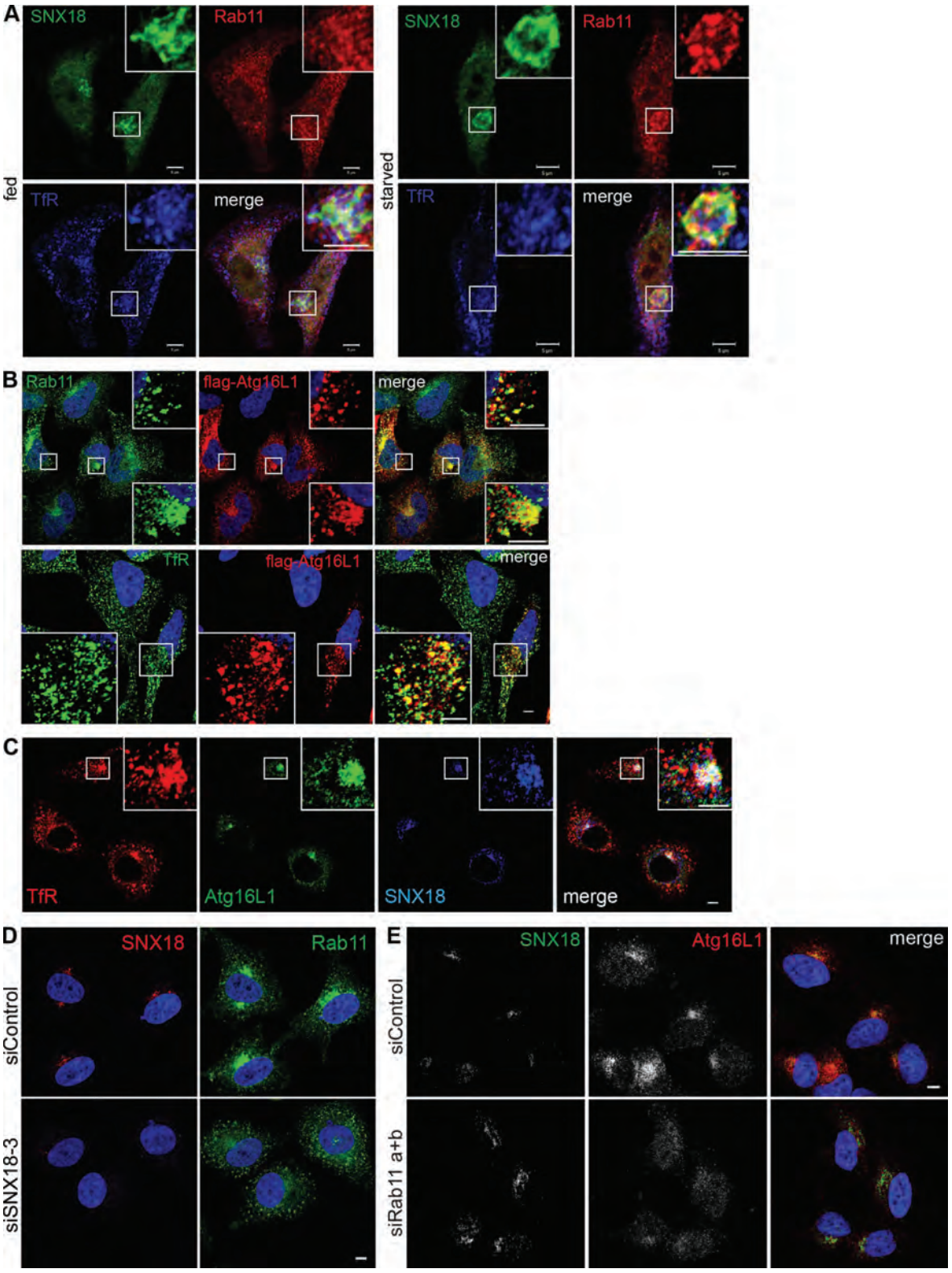

Figure 9. **Recycling endosomes provide membranes for SNX18-mediated GFP-LC3 membrane trafficking and remodeling.** (A) HeLa cells were starved or not starved for 2 h before fixation and immunostaining against endogenous SNX18, Rab11, and TfR. (B) Cells were transfected to express flag-Atg16L1, starved, and immunostained against Rab11 or TfR and flag. (C) Cells were starved and immunostained against TfR, Atg16L1, and SNX18. (D) Cells were transfected with control or SNX18 siRNA, starved, and immunostained against SNX18 and Rab11. Inset panels show enlarged views of the boxed regions. (E) Cells were transfected with control or Rab11 a+b siRNA, starved, and immunostained against SNX18 and Atg16L1. Cells were imaged by confocal microscopy. Bars, 5 μm.

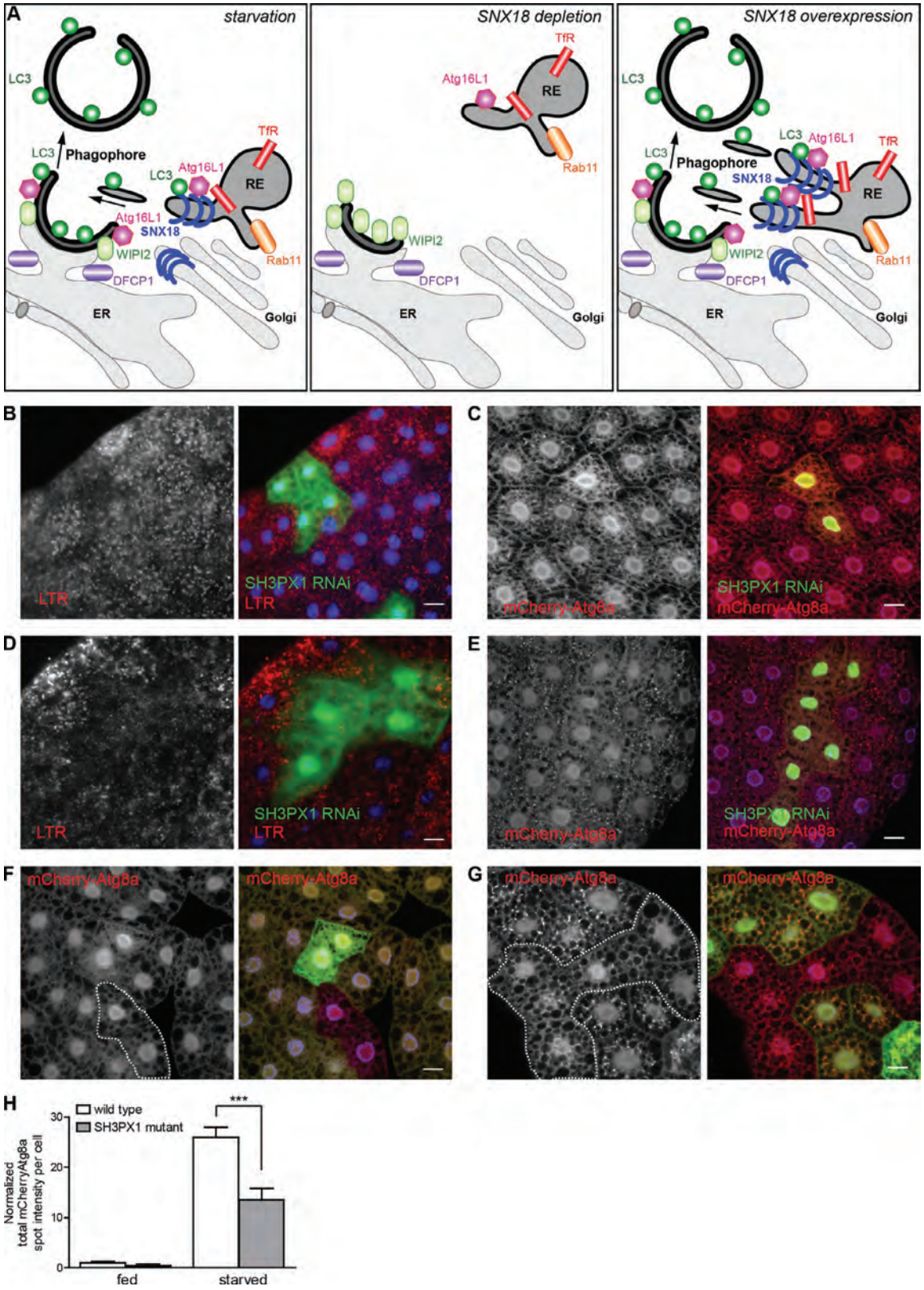

Figure 10. **SNX18 is a positive regulator of autophagy and its function is conserved in *D. melanogaster* fat body cells.** (A) During starvation, Rab11-positive recycling endosomes are recruited to the SNX18-positive perinuclear area dependent on SNX18 itself. SNX18 and Rab11 are required for the perinuclear localization of Atg16L1 to omegasomes marked by DFCP1. LC3 lipidation and autophagosome formation proceeds. In the absence of SNX18, recruitment of recycling endosomes to the perinuclear site is inhibited, Atg16L1 fails to localize to DFCP1-positive omegasomes, and WIPI2 accumulates.

and were fewer and smaller in SH3PX1 RNAi cells (Fig. S5, D and E). Collectively, this indicates that the *D. melanogaster* SNX18 homologue SH3PX1 is also required for efficient autophagosome formation, both during starvation-induced and developmental autophagy.

To verify the results obtained with the SH3PX1 RNAi line, we generated a fly strain lacking the first exon and start codon of SH3PX1 ($SH3PX1^{HK62b}$), which expressed no detectable SH3PX1 protein (Fig. S5, I–K) and was viable, which is consistent with the viability of other Atg mutants (Scott et al., 2004; Juhász et al., 2007). No autophagosomes were observed in fat bodies from well-fed 96-h-old larvae (Fig. 10, F and H), whereas mCherry-Atg8a–positive structures were abundant in cells heterozygous for the SH3PX1 deletion (GFP positive) after starvation, but fewer and smaller in cells homozygous for the SH3PX1 deletion (GFP negative; Fig. 10, G and H), which supports the finding that SH3PX1 is necessary for normal autophagosome formation.

Finally, although SH3PX1 was efficiently overexpressed (Fig. S5 F), and able to interact with DmAtg8a (Fig. S5 L), autophagosome formation was not induced by overexpression of SH3PX1 in the fat body of well-fed third instar larvae (Fig. S5 G), nor did SH3PX1 overexpression affect the formation of autophagosomes during starvation (Fig. S5 H). Collectively, these results show that SH3PX1 is necessary, but not sufficient, for normal formation of autophagosomes in vivo.

Discussion

We identified SNX18 as a PX domain protein involved in autophagy by a siRNA-mediated screen and validated SNX18 as a positive regulator of autophagy dependent on its membrane remodeling activity and binding to $PI(4,5)P_2$-containing membranes. SNX18 interacts with Atg16L1 and is required for recruitment of Atg16L1-positive recycling endosomes to a perinuclear region in a Rab11-dependent manner. Importantly, SNX18 interacts directly with LC3 family proteins, and its overexpression was shown to induce perinuclear recruitment of GFP-LC3 in an Atg16L1-dependent manner. The membrane binding and tubulation activity of SNX18, as well as its binding to LC3, is required for formation of GFP-LC3–, Atg16L1-, and TfR-positive tubules that we propose contribute to the formation of transport vesicles that provide membrane to the forming autophagosome (Fig. 10 A).

Because autophagy depends on the generation of PI3P, it was surprising to find a protein with specificity for $PI(4,5)P_2$ (Håberg et al., 2008) as a prime candidate in a screen for autophagy-related PX-domain proteins. Indeed, the observed inhibitory effect on SNX18-induced GFP-LC3 spot formation by rapalog-induced recruitment of a phosphoinositide 5-phosphatase to the plasma membrane (known to deplete $PI(4,5)P_2$), as well as the use of PX domain mutants, indicate that binding of SNX18 to $PI(4,5)P_2$-containing membranes is essential for its function in autophagy. $PI(4,5)P_2$ has previously been shown to be important for autophagy through the formation of Atg16L1-positive autophagosome precursors from the plasma membrane (Ravikumar et al., 2010; Moreau et al., 2012). Interestingly, we find that Atg16L1 extensively colocalizes with markers of recycling endosomes (Rab11 and TfR) and localizes to an SNX18-positive perinuclear area in a Rab11- and SNX18-dependent manner, and that Atg16L1 and SNX18 PX-BAR interact, which suggests that the SNX18-dependent perinuclear recruitment of Atg16L1-positive recycling endosomes could depend on SNX18 binding to $PI(4,5)P_2$.

We found membrane tubulation by SNX18 to be regulated by phosphorylation at S233, a residue located within the proposed amphipathic helix 0 just upstream of the PX domain. Interestingly, increased phosphorylation of this residue was previously reported upon rapamycin treatment (Chen et al., 2009), and we found a similar increase upon starvation. However, S233 mutations inhibited formation of GFP-LC3 spots, which suggests that SNX18 S233 phosphorylation negatively regulates its function in autophagy. It is possible that the membrane tubulation activity of SNX18 is regulated through cycles of phosphorylation and dephosphorylation to prevent excessive delivery of membranes to forming autophagosomes, and we speculate that S233 dephosphorylation might stimulate dissociation of SNX18 from the forming LC3-positive tubules.

Interaction partners of LC3 family members have been found to bind through a conserved $X_{-3}X_{-2}X_{-1}W_0X_1X_2LX$ motif, requiring an aromatic residue in the W and a hydrophobic residue in the L position, and with acidic amino acids often found in the X positions (Noda et al., 2008; Johansen and Lamark, 2011). The SNX18 WDDEW motif found to interact with LC3/GABARAP is a noncanonical motif because of the presence of the W and several acidic residues, and the lack of the hydrophobic residue in the L position. Interestingly, this motif is also required for the SNX18 interaction with AP-1, an adaptor protein implicated in autophagosome biogenesis from the trans-Golgi network (Guo et al., 2012). The dynamic interplay of the SNX18 interaction with LC3/GABARAP and AP-1 in relation to autophagy remains to be studied. Furthermore, our

LC3 lipidation and autophagosome formation is inhibited. Upon SNX18 overexpression, Rab11-, TfR-, and LC3-positive membranes accumulate at a perinuclear site, and extensive membrane tubules with SNX18, Atg16L1, LC3, and TfR form from perinuclear recycling endosomes. LC3 lipidation and autophagosome formation is increased. Based on the experimental observations summarized in this model, we propose that SNX18 facilitates LC3 lipidation via Atg16L1 and provides membrane from recycling endosomes to forming autophagosomes. (B and C) RNAi against SH3PX1 (GFP-positive clones) decreases formation of LTR punctae in response to 4 h of starvation in 20% sucrose (B) and inhibits formation of mCherry-Atg8a-positive autophagosomes in response to 2 h starvation (C). (D and E) RNAi against SH3PX1 inhibits formation of LTR (D) and mCherry-Atg8a–positive structures (E) at early stages of developmental autophagy in fat bodies of 110-h-old larvae. (F) There was no change in mCherry-Atg8a in SH3PX1 mutant clones (GFP negative, outlined) in well-fed larvae. (G) Decreased formation of mCherry-Atg8a–positive autophagosomes in SH3PX1 mutant clones (GFP negative, outlined) in fat bodies from larvae starved in 20% sucrose for 3 h. Bars, 20 µm. (H) The graph shows quantification of total mCherry-Atg8a spot intensity per cell for WT and SH3PX1 mutant cells. The graph shows mean ± SEM (error bars); ***, $P < 0.001$. Genotypes: (B and D) *hs-flp; UAS-dicer/+; Act>CD2>GAL4 UAS-GFPnls/UAS-SH3PX1 RNAi*; (C and E) *hs-flp; UAS-dicer/+; r4:mCherry-Atg8a Act>CD2>GAL4 UAS-GFPnls/UAS-SH3PX1 RNAi*; (F and G) *hs-flp; Cg-GAL4 UAS-mChAtg8a/+; FRT80B UAS-2XeGFP/FRT80B* $SH3PX1^{HK62b}$. See also Fig. S5.

results suggest that SNX18 interacts mainly with the nonlipidated LC3-I. Although LC3-I is generally considered to be cytosolic, we clearly show that SNX18 is found in membrane fractions containing both LC3-I and –II, as well as Atg16L. Membrane-associated LC3-I has previously been largely ignored, but can be detected if physiological buffers are used in cell fractionations (see, e.g., Polson et al., 2010).

SNX18 affects the localization of Atg16L1, which can stimulate LC3 lipidation (Hanada et al., 2007; Fujita et al., 2008). We propose that the SNX18 interaction with Atg16L1 and LC3 facilitates LC3 lipidation on membranes to allow their subsequent fusion with the growing phagophore. Because Rab11 relocalized to the perinuclear region during starvation in a SNX18-dependent manner and SNX18-induced membrane tubules were positive for TfR, we propose that SNX18 provides membrane input from recycling endosomes to forming autophagosomes (Fig. 10 A). This is in line with recent findings showing that vesicular transport from recycling endosomes contributes to starvation-induced autophagy (Longatti et al., 2012). Overexpression of the Rab11-binding protein TBC1D14 was found to cause tubulation of recycling endosomes and inhibit autophagosome formation (Longatti et al., 2012). Furthermore, it was shown that TBC1D14 relocates to the Golgi upon starvation and that Rab11 is required for formation of autophagosomes. These results are complementary to ours and indicate that tubulation of recycling endosome by TBC1D14 and SNX18 has opposite effects on autophagosome formation.

Materials and methods

Antibodies

The antibodies were from the following providers: rabbit anti-Atg16L1 (for Western blotting), rabbit anti-LC3 and rabbit anti-myc (Cell Signaling Technology), rabbit anti-Atg16L1 (for immunofluorescence), rabbit anti-Atg14L, rabbit anti-GABARAP and rabbit anti-LC3 (MBL), mouse anti–γ-adaptin (AP-1), mouse anti-flag M2, mouse anti–β-actin and mouse anti-GFP (Sigma-Aldrich), guinea pig anti-p62 (Progen), mouse anti-p62 (BD), mouse anti-tubulin, rabbit anti-GM130 (Abcam), rabbit anti-Rab11 (Invitrogen), mouse anti-TfR (Boehringer Mannheim clone B3/25), mouse anti-GM130 (BD), anti-calnexin (Santa Cruz Biotechnology, Inc.), mouse anti-LAMP1 (Developmental Studies Hybridoma Bank), rabbit anti-Atg16L1 (for Western blotting; Cosmo Bio Co.), HRP- or Cy2/3/5-conjugated secondary antibodies (Jackson ImmunoResearch Laboratories), and Alexa Fluor–conjugated secondary antibodies (Invitrogen). The rabbit anti-SH3PX1 antibody (Worby et al., 2001) was a gift from J.E. Dickson (University of Michigan Medical School, Ann Arbor, MI). The mouse anti-WIPI2 antibody was a gift from S. Tooze (Cancer Research UK, London, England, UK). Mouse monoclonal anti–lyso-bisphosphatidic acid (LBPA) was provided by J. Gruenberg (University of Geneva, Geneva, Switzerland) and human anti-EEA1 antiserum was from B.-H. Toh (Monash University, Melbourne, Australia). Affinity-purified rabbit antibodies against SNX9 (Lundmark and Carlsson, 2003) and SNX18 (Håberg et al., 2008) were produced by immunizing with recombinant full-length proteins fused to GST, and subsequently affinity purified using the respective antigen without GST. Chicken anti-SNX18 (used for immunofluorescence) was produced by immunizing with recombinant SH3 domain of SNX18, and affinity purified from egg yolk using the same antigen. In some experiments, rabbit anti-SNX18 from a commercial source was also used (Prestige Antibodies; Sigma-Aldrich). The phosphospecific SNX18 pS233 antibody was raised in rabbits against a phospho-peptide corresponding to the helix 0 sequence in SNX18 (CRNLNRFpSTFVKSGG; pS233; Genscript USA Inc.).

Constructs

See Table S3.

Cell lines, media, and inhibitors

Cells were maintained in DMEM (Gibco) supplemented with 10% fetal bovine serum, 5 U/ml penicillin, and 50 µg/ml streptomycin. The HEK 293A GFP-LC3 cell line (Chan et al., 2007) was a gift from S. Tooze. The HEK GFP-DFCP1 cell line (Axe et al., 2008) was a gift from N. Ktistakis (Babraham Institute, Cambridge, England, UK). HeLa cells inducibly expressing GFP, GFP-SNX18, GFP-LC3, or GFP-GABARAP (see Fig. S4 A) were made with the TRex FlpIN system (Invitrogen) with the TRex HeLa FlpIn cell line (Tighe et al., 2008), which was obtained as a gift from A. Thige and S.S. Taylor (University of Manchester, Manchester, England, UK). Expression was induced by addition of 10–500 ng/ml Tetracycline or Doxycycline (Sigma-Aldrich). Mouse embryonic fibroblasts (MEFs) were a gift from M. Komatsu (Tokyo Metropolitan Institute of Medical Science, Tokyo, Japan). Glass support was coated by 20 µg/ml fibronectin (Sigma-Aldrich) before plating HEK cell lines. For starvation in nutrient-deplete medium, the cells were incubated in Earls Balanced Salt Solution (EBSS; Invitrogen), with the exception of the HEK GFP-DFCP1 cells, which were starved as described previously (Axe et al., 2008) in 140 mM NaCl, 1 mM $CaCl_2$, 1 mM $MgCl_2$, 5 mM glucose, and 20 mM Hepes, pH 7.4. BafA1 (AH Diagnostics) was used at 100–200 nM and ionomycin at 5 µM (Sigma-Aldrich).

Transfection of plasmids or siRNA oligonucleotides and Western blotting

Plasmids were transfected using FuGene (Roche) or Lipofectamine 2000 (Invitrogen). The siRNAs used in the primary screen were Dharmacon SMARTpool ON-TARGET plus (Thermo Fischer Scientific). In the secondary screen, the corresponding individual Dharmacon ON-TARGET plus oligonucleotides were used. See Tables S1 and S2 for Dharmacon siRNA numbers and siRNA sequences. siSNX18-1, -2, -3, and -4 correspond to Dharmacon J-013438-09, -10, -11, and -12. The following siRNA oligonucleotides were obtained from Invitrogen (Stealth): siSNX18-5, 5′-CAGGAUCGCUGUAACACUAUUUCUU-3′; siSNX9-1, 5′-AAGAGAGUCAGCAAUCAUGUCU-3′; and siSNX9-2, 5′-AACCUACUAACACUAAUCGAU-3′. Other siRNA sequences used were from Thermo Fisher Scientific: siAtg14L, 5′-GCAAAUCUUCGACGAUCCCAUAUUU-3′; siAtg7, 5′-GCCCACAGAUGGAGUAGCA-3′; siULK1, 5′-UCACUGACCUGCUCCUUAA-3′; siAtg16L1-1, 5′-UGUGGAUGAUUAUCGAUUA-3′; siAtg16L1-2, 5′-GUUAUUGAUCUCCGAACAA-3′; siRab11a, 5′-GUAGGUGCCUUAUUGGUUU-3′; and siRab11b, 5′-CAAGAGCGAUAUCGAGCUA-3′. SMARTpools (Thermo Fisher Scientific) were used against: siLC3A, M-013579-00; siLC3B, M-012846-01; siGAB, M-012368-01; and siGAB L1, M-014715-01. The siRNA was delivered to cells by Lipofectamine RNAi max (Invitrogen). For rescue experiments, siRNA-resistant plasmids were delivered to cells by transfection with Extremegene (Roche) the day after siRNA transfection. For SDS-PAGE, the cells were lysed in 25 mM Hepes, pH 7.5, 125 mM K-Acetate, 2.5 mM Mg-Acetate, 5 mM EGTA, 1 mM DTT, and 0.5% NP-40 supplemented with Complete protease inhibitor (Roche). Protein concentration was measured by a protein assay (Bio-Rad Laboratories) to run equal amounts of cell lysate on SDS-PAGE, followed by Western blotting using specified primary antibodies and HRP-conjugated secondary antibodies detected by the Supersignal West Dura Extended Duration Substrate kit (Pierce). Imaging and quantification of protein levels were performed using the Syngene gel documentation unit, GeneSnap acquisition, and GeneTools analysis software (all from Syngene). In some cases, Western blotting was performed with far red fluorophore-conjugated secondary antibodies, and detection and analysis were performed with the Odyssey imaging system (LI-COR).

High-content immunofluorescence microscopy and confocal microscopy

For the screen, siRNA-treated HEK GFP-LC3 cells growing in glass-bottom 96-well plates were starved or not starved for 2 h and pre-permeabilized on ice with 0.05% saponin in 80 mM K-Pipes, pH 6.8, 5 mM EGTA, and 1 mM $MgCl_2$ before fixation in 3% PFA. The nuclei were counterstained with 1 µg/ml Hoechst in PBS. The number of GFP-LC3 spots was quantified from a total of ∼30,000 cells from three independent experiments in triplicate using the automated ScanR microscope (Olympus) equipped with a ULS-Apochromat 40× objective lens (NA 0.95) and the corresponding analysis program. For other experiments, cells were grown on glass coverslips and after the described treatments, fixed in 3% PFA for 15 min on ice or in methanol for 10 min at −20°C before immunostaining with indicated antibodies and mounting in Mowiol or Prolong Gold mounting media (Life technologies) containing 1 µg/ml Hoechst or DAPI. The cells were imaged on an automated Cell Observer equipped with a 40× EC Plan Neofluar objective (NA 0.75) and a camera (AxioCam MRm) using Axiovision software (all from Carl Zeiss). The number of GFP-DFCP1,

WIPI2, Atg16L1, or GFP-LC3 spots was quantified from ∼300 cells using the Physiology module of the Assaybuilder software (Carl Zeiss). Confocal images were acquired with a confocal microscope (LSM780; Carl Zeiss) equipped with an Ar laser multiline (458/488/514 nm), a DPSS-561 10 (561 nm), a laser diode 405-30 CW (405 nm), and a HeNe laser (633 nm). The objective used was a Plan-Apochromat 63×/1.4 NA oil DIC III objective lens (Carl Zeiss). Image processing was performed with basic software (zen 2010; Carl Zeiss) and Photoshop CS4 (Adobe). Some confocal images were acquired on a laser scanning confocal microscope (FluoView 1000; Olympus) based on an inverted microscope (IX81; Olympus) fitted with a Super Apochromat 60×/1.35 NA oil objective lens and the following laser lines: UV laser diode (405 nm, 6 mW), multiline Ar laser (457 nm, 488 nm, 515 nm, and 30 mW), green helium-neon laser (561 nm, 10 mW), and a red helium-neon laser (633 nm, 10 mW). Images were acquired using the dedicated FV1000 software (Olympus).

EM

Cells for conventional plastic embedding were fixed with 2% glutaraldehyde in 0.1 M Cacodylate buffer, followed by postfixation in 2% OsO_4 and 1.5% KFeCN, dehydration in graded ethanol series, and epon embedding. Ultrathin sections were poststained with Uranyl acetate followed by Pb-citrate. Samples for immuno-EM were fixed in 4% formaldehyde and 0.1% glutaraldehyde, scraped and embedded in 10% gelatin, infused with 2.3 M sucrose, and mounted and frozen in liquid nitrogen. Sectioning was performed at −110°C, and 70–100 nm sections were collected with a 50:50 mixture of 2.3 M sucrose and 2% methyl cellulose. Labeling was performed with the following antibodies: rabbit anti-GFP (T. Johansen, University of Tromsø, Tromsø, Norway), mouse anti-myc (Sigma-Aldrich), and mouse anti-TfR (Boehringer Mannheim). Monoclonal antibodies were followed by secondary rabbit anti–mouse (Dako) antibodies and finally protein A gold 10 nm (University Medical Center, Utrecht, Netherlands). Sections were observed in a transmission electron microscope (JEM 1230; JEOL) at 80 kV and images were recorded with a Morada camera (SIS; Olympus), using iTEM software (Olympus). Further image processing was done with Photoshop CS5 (Adobe).

Rapalog-induced depletion of PI(4,5)P_2

Experiments were performed as described previously (Zoncu et al., 2007), with some modifications: In brief, HEK GFP-LC3 cells were triple transfected with plasmids encoding plasma membrane–targeted FRB domain of human mTOR (CFP-FRB), FKBP alone (mRFP-FKBP), or the phosphoinositide 5-phosphate (5pase) fused to FKBP (mRFP-FKBP-5pase; (provided by P. Di Camilli, Yale University School of Medicine, New Haven, CT; and T. Balla, National Institutes of Health, Bethesda, MD) and myc or myc-SNX18. Addition of 2.5 µM rapalog (A/C heterodimerizer; Takara Bio Inc.) results in the heterodimerization of FRB and FKBP, leading to the recruitment of 5pase to the plasma membrane and depletion of PI(4,5)P_2. The cells were fixed before immunostaining against myc and analysis of GFP-LC3 spots per cell.

qPCR

siRNA-transfected cells grown in 96-well plates were frozen dry at −80°C, RNA was isolated with an RNeasy plus kit (QIAGEN), cDNA was synthesized by reverse transcription (iScript; Bio-Rad Laboratories), and qPCR was performed using SYBR green (QIAGEN) and primer sets for the described targets relative to SDHA as a housekeeping gene on a Lightcycler 480 (Roche). All primer sets were predesigned and bought from QIAGEN (Quantitect), with the exception of SNX18, where a primer set was designed separately: 5′-GGACCTATTAGCGCTGTATCAG-3′ and 5′-CACGTGTCGCCTACTCTC-3′.

In vitro translation and GST pulldown

Indicated GFP fusion proteins were in vitro translated in TNT T7–coupled reticulocyte lysate (L4610; Promega) in the presence of [^{35}S]methionine (PerkinElmer) and precleared on glutathione-Sepharose before incubation in NETN buffer (50 mM Tris, pH 8, 100 mM NaCl, 6 mM EDTA, 6 mM EGTA, 0.5% NP-40, 1 mM DTT, and Roche Complete protease inhibitor) together with glutathione-Sepharose–bound recombinant GST-tagged Atg8 proteins expressed in and purified from *Escherichia coli* according to manufacturer's instructions. The resulting pulldowns were separated by SDS-PAGE. The gels were Coomassie blue stained, and the in vitro translated copurified proteins were detected by autoradiography on a Typhoon phosphorimaging scanner (GE Healthcare). For GST pulldown from cell lysate, cells were lysed in 10 mM Tris-HCl, pH 7.5, 150 mM NaCl, 0.5 mM EDTA, 0.5% NP-40, protease inhibitor (Roche), and phosphatase inhibitor (Sigma-Aldrich), and the cell lysate was incubated with recombinant glutathione-Sepharose–bound GST proteins. The resulting pulldowns were analyzed by immunoblotting.

Long-lived protein degradation

To measure the degradation of long-lived proteins by autophagy, proteins were first labeled with 0.25 µCi/ml L-[^{14}C]valine (PerkinElmer) for 24 h in GIBCO-RPMI 1640 medium (Invitrogen) containing 10% FBS. The cells were washed and then chased for 3 h in nonradioactive DMEM (Invitrogen) containing 10% FBS and 10 mM valine (Sigma-Aldrich) to allow degradation of short-lived proteins. The cells were washed twice with EBSS (Invitrogen), and starved or not starved for 4 h in the presence or absence of 10 mM 3-methyladenine (3MA; Sigma-Aldrich). 10% TCA was added to the cells before incubation at 4°C to precipitate radioactive proteins. Ultima Gold LSC cocktail (PerkinElmer) was added to the samples and protein degradation was determined by measuring the ratio of TCA-soluble radioactivity relative to the total radioactivity detected by a liquid scintillation analyzer (Tri-Carb 3100TR; PerkinElmer), counting 3 min per sample.

Immunoprecipitation

GFP, GFP-LC3 WT, GFP-LC3 G120A, and GFP-SNX18 were immunoprecipitated by GFP trap (ChromoTek) according to the manufacturer's instructions. To determine the specificity of the phosphospecific SNX18 pS233 antibody, a sample of GFP-Trap–enriched GFP-SNX18 was either mock-treated or treated with Lambda phosphatase (LPP; New England Biolabs, Inc.) for 30 min at 30°C, and analyzed by immunoblotting. For immunoprecipitation of GFP-SNX18, the HeLa GFP-SNX18 cells were harvested and lysed in 1% NP-40 in PBS containing PhosSTOP (Roche) and protease inhibitors (EMD Millipore). After centrifugation at 70,000 *g* for 30 min, the supernatants were immunoprecipitated with GFP-Trap. For flag-Atg16L1 immunoprecipitations, HeLa cells were transfected to express flag-Atg16L1 and myc-SNX18 variants followed by solubilization of the cells, and were immunoprecipitated with anti-flag or an unrelated antibody of the same isotype.

Cell fractionation and density-gradient centrifugation

The cells were harvested by trypsinization and resuspended in 2–5 volumes of KSHM buffer (100 mM potassium acetate, 85 mM sucrose, 20 mM HEPES-KOH, pH 7.4, and 1 mM magnesium acetate) containing 1 mM PMSF and protease inhibitor cocktail (EMD Millipore) before a quick freeze/thaw cycle to open up the plasma membrane (Lundmark and Carlsson, 2003). Cells were centrifuged at 1,500 *g* for 5 min, and the supernatant was centrifuged at 70,000 *g* for 30 min, then collected (cytosol). The pellets from the high- and low-speed centrifugations were combined and solubilized in KSHM containing 1% NP-40 and protease inhibitors, and centrifuged at 70,000 *g* for 30 min to obtain a supernatant (membranes). Equal proportions of cytosol and membrane were analyzed by immunoblotting.

For density gradient separation of total membranes, HeLa cells grown in full medium or in nutrient-deficient medium in the presence of BafA1 for 2 h were trypsinized and washed in PBS. After resuspension in 10 vol of 15 mM Hepes-KOH, pH 7.4, 1 mM EDTA, and 0.25 M sucrose (HES buffer) containing protease and phosphatase inhibitors, the cells were gently homogenized by passage through a ball-bearing device (Lundmark and Carlsson, 2002). Nuclei were pelleted by centrifugation at 800 *g* for 10 min, and organelles and membranes in the supernatant were collected by centrifugation at 70,000 *g* for 30 min. The organelle/membrane pellet was resuspended in 200 µl HES buffer and layered on top of a 4-ml 0–50% continuous Nycodenz gradient prepared in HES buffer. Centrifugation was performed at 70,000 *g* for 16 h after which 250-µl fractions were collected from the top. Equal volumes of each fraction were analyzed by SDS-PAGE followed by immunoblotting.

Peptide array

Peptide arrays were synthesized at the Biotechnology Centre of Oslo, University of Oslo, on cellulose membranes using a MultiPep automated synthesizer (INTAVIS Bioanalytical Instruments AB) as described previously (Frank, 1992).

Drosophila genetics

The *SH3PX1*^{EY08084} and *SH3PX1 RNAi* (TRiP.JF02730) lines were obtained from the Bloomington Drosophila Stock Center at Indiana University. Clonal analysis was performed using the methods and fly stocks described in Arsham and Neufeld (2009). In brief, *SH3PX1* was depleted

in fat body clones by crossing *SH3PX1*^{JF02730} to *y,w,hs-flp; UAS-dicer; act>CD2>GAL4, UAS-GFPnls/TM6B, Hu, Tb* or *y,w,hs-flp; UAS-dicer; r4:mCherryAtg8a, act>CD2>GAL4, UAS-GFPnls/TM6B, Hu, Tb*. Clones of fat body cells overexpressing SH3PX1 were generated in crosses of *SH3PX1*^{EY08084} to *y,w,hs-flp; r4:mCherryAtg8a, act>CD2>GAL4, UAS-GFPnls/TM6B, Hu, Tb* or *y,w,hs-flp; act>CD2>GAL4, UAS-GFPnls/TM6B, Hu, Tb*. Clones of homozygous *SH3PX1* mutant cells were generated from the cross *SH3PX1*^{HK62b} *FRT80B/TM6B, Hu, Tb* χ *y,w,hs-flp; Cg-GAL4, UAS-mChAtg8a; UAS-2XeGFP, FRT80B*. The resulting progeny were subjected to a 1-h heat shock (37°C) at 0–6 h after egg deposition.

Fat body autophagy assays

72-h-old larvae were moved to fresh food with yeast paste. 24 h later, the larvae were starved or not starved for the indicated times in 20% sucrose. The larvae were bisected, inverted, and fixed in 3.7% formaldehyde. After washing in PBS with 0.1% Triton X-100 (PBS-T) and counterstaining with 1 µg/ml DAPI, the fat bodies were dissected out and mounted in Fluoroguard. Fat bodies for antibody staining were blocked in 5% goat serum in PBS-T before staining with the indicated antibodies. For LTR (Invitrogen) staining, freshly dissected fat bodies were incubated in 100 nM LTR and 1 µg/ml DAPI for 3 min and imaged immediately. All larval samples were imaged on a confocal microscope equipped (LSM510) with a 40× objective lens (both from Carl Zeiss). Total mCherryAtg8a spot intensity was quantified by the Carl Zeiss AssayBuilder Physiology module.

Generation of SH3PX1 deletion mutant

The P element SH3PX1^{EY08084} located in the 5′ UTR of the SH3PX1 gene was remobilized, and lines where part of the gene region was deleted were screened by PCR using primers 5′-ACGAAAACAAAGCGCAGCGC-3′ and 5′-ACGCCTCGCATTTGGTGCAA-3′. One such line missing 1,198 bp of the gene region was identified (SH3PX1^{HK62b}), and sequencing showed that the first exon of SH3PX1 including the start codon was deleted (1,198 nucleotides removed from the EY08084 insertion site (3L:9,706,877; FlyBase release FB2012_02).

Lysate of larval fat bodies

Fat bodies were dissected out of 96-h-old larvae and immediately boiled for 5 min at 95°C in SDS sample buffer before SDS-PAGE and immunoblotting.

Statistics

For the primary siRNA screen, data were collected from three experiments with three repetitions each. In a quality control process, plates were inspected with respect to the number of cells in the wells and the consistency of results in wells with equal siRNA. Based on this, some plates were excluded, leaving 6–8 plates of each type. The estimated GFP-LC3 count for each siRNA was then computed as a weighted mean over all experiments and repetitions to eliminate systematic differences in the level of GFP-LC3 spots between plates. The weights were adjusted in such a way that plates with equal siRNA layout had an equal mean count over all wells, and plates with different layout had equal mean count over the control wells. A similar procedure was used for the secondary screen. The P-values of other analysis were derived from statistical tests using a two-sided *t* test from Excel (Microsoft), and considered statistically significant at $P < 0.05$.

Online supplemental material

Fig. S1 shows how the Olympus ScanR software detects the GFP-LC3 spots as well as images showing GFP-LC3 spots for all SNX18 siRNAs and the corresponding relative expression of SNX18 and LC3 mRNA upon SNX18 knockdown. Fig. S2 shows the effect of siSNX18 compared with siSNX9 and includes controls relating to membrane fractionation and induction of GFP-LC3 spots. Fig. S3 complements the characterization of endogenous SNX18 localization and provides further controls for the perinuclear recruitment of Atg16L1 and induction of GFP-LC3 spots. Fig. S4 is a characterization of the TRex FlpIN HeLa GFP-LC3 and -GABARAP cells including data on myc-SNX18 and endocytic markers. Fig. S5 shows that SH3PX1 RNAi results in formation of smaller mCherry-Atg8a–marked autophagosomes, whereas SH3PX1 overexpression does not induce or change formation of mCherry-positive autophagosomes in larval fat bodies. It also describes how the SH3PX1 deletion mutant was generated by remobilization of the P element SH3PX1^{EY08084} located in the 5′ UTR of the SH3PX1 gene, and that SH3PX1 binds to DmAtg8a. Table S1 is a comprehensive list of the gene targets, siRNA numbers, number of cells analyzed, and GFP-LC3 spots per cell from the primary screen. Table S2 lists the gene targets, siRNA numbers and sequences, percent knockdown of mRNA for the specified target, number of cells analyzed, and GFP-LC3 spots per cell from the secondary screen. Table S3 lists the plasmids used in this study. Online supplemental material is available at http://www.jcb.org/cgi/content/full/jcb.201205129/DC1.

We thank S. Tooze, N. Ktistakis, I. Dikic, P. de Camilli, T. Balla, T. Johansen, M. Komatsu, and J.E. Dickson for generously sharing reagents, A. Engen for assistance with cell culture, C. Knudsen for help with Fig. 10 A, and the confocal microscopy core facility at the Institute for Cancer Research, Oslo, for providing access to confocal microscopes. We received materials through the Drosophila Genomics Resource Center.

This work was supported by grants from the Molecular Life Science program of the University of Oslo, the Swedish Research Council, and the Kempe Foundation.

Submitted: 21 May 2012
Accepted: 6 June 2013

References

Arsham, A.M., and T.P. Neufeld. 2009. A genetic screen in *Drosophila* reveals novel cytoprotective functions of the autophagy-lysosome pathway. *PLoS ONE*. 4:e6068. http://dx.doi.org/10.1371/journal.pone.0006068

Axe, E.L., S.A. Walker, M. Manifava, P. Chandra, H.L. Roderick, A. Habermann, G. Griffiths, and N.T. Ktistakis. 2008. Autophagosome formation from membrane compartments enriched in phosphatidylinositol 3-phosphate and dynamically connected to the endoplasmic reticulum. *J. Cell Biol.* 182:685–701. http://dx.doi.org/10.1083/jcb.200803137

Chan, E.Y., S. Kir, and S.A. Tooze. 2007. siRNA screening of the kinome identifies ULK1 as a multidomain modulator of autophagy. *J. Biol. Chem.* 282:25464–25474. http://dx.doi.org/10.1074/jbc.M703663200

Chen, R.Q., Q.K. Yang, B.W. Lu, W. Yi, G. Cantin, Y.L. Chen, C. Fearns, J.R. Yates III, and J.D. Lee. 2009. CDC25B mediates rapamycin-induced oncogenic responses in cancer cells. *Cancer Res.* 69:2663–2668. http://dx.doi.org/10.1158/0008-5472.CAN-08-3222

Fan, W., A. Nassiri, and Q. Zhong. 2011. Autophagosome targeting and membrane curvature sensing by Barkor/Atg14(L). *Proc. Natl. Acad. Sci. USA*. 108:7769–7774. http://dx.doi.org/10.1073/pnas.1016472108

Frank, R. 1992. Spot-synthesis: an easy technique for the positionally addressable, parallel chemical synthesis on a membrane support. *Tetrahedron*. 48:9217–9232. http://dx.doi.org/10.1016/S0040-4020(01)85612-X

Fujita, N., T. Itoh, H. Omori, M. Fukuda, T. Noda, and T. Yoshimori. 2008. The Atg16L complex specifies the site of LC3 lipidation for membrane biogenesis in autophagy. *Mol. Biol. Cell*. 19:2092–2100. http://dx.doi.org/10.1091/mbc.E07-12-1257

Guo, Y., C. Chang, R. Huang, B. Liu, L. Bao, and W. Liu. 2012. AP1 is essential for generation of autophagosomes from the trans-Golgi network. *J. Cell Sci.* 125:1706–1715. http://dx.doi.org/10.1242/jcs.093203

Håberg, K., R. Lundmark, and S.R. Carlsson. 2008. SNX18 is an SNX9 paralog that acts as a membrane tubulator in AP-1-positive endosomal trafficking. *J. Cell Sci.* 121:1495–1505. http://dx.doi.org/10.1242/jcs.028530

Hailey, D.W., A.S. Rambold, P. Satpute-Krishnan, K. Mitra, R. Sougrat, P.K. Kim, and J. Lippincott-Schwartz. 2010. Mitochondria supply membranes for autophagosome biogenesis during starvation. *Cell*. 141:656–667. http://dx.doi.org/10.1016/j.cell.2010.04.009

Hanada, T., N.N. Noda, Y. Satomi, Y. Ichimura, Y. Fujioka, T. Takao, F. Inagaki, and Y. Ohsumi. 2007. The Atg12-Atg5 conjugate has a novel E3-like activity for protein lipidation in autophagy. *J. Biol. Chem.* 282:37298–37302. http://dx.doi.org/10.1074/jbc.C700195200

Hayashi-Nishino, M., N. Fujita, T. Noda, A. Yamaguchi, T. Yoshimori, and A. Yamamoto. 2009. A subdomain of the endoplasmic reticulum forms a cradle for autophagosome formation. *Nat. Cell Biol.* 11:1433–1437. http://dx.doi.org/10.1038/ncb1991

Itakura, E., and N. Mizushima. 2010. Characterization of autophagosome formation site by a hierarchical analysis of mammalian Atg proteins. *Autophagy*. 6:764–776. http://dx.doi.org/10.4161/auto.6.6.12709

Itoh, T., and P. De Camilli. 2006. BAR, F-BAR (EFC) and ENTH/ANTH domains in the regulation of membrane-cytosol interfaces and membrane curvature. *Biochim. Biophys. Acta*. 1761:897–912. http://dx.doi.org/10.1016/j.bbalip.2006.06.015

Johansen, T., and T. Lamark. 2011. Selective autophagy mediated by autophagic adapter proteins. *Autophagy*. 7:279–296. http://dx.doi.org/10.4161/auto.7.3.14487

Juhász, G., B. Erdi, M. Sass, and T.P. Neufeld. 2007. Atg7-dependent autophagy promotes neuronal health, stress tolerance, and longevity but is dispensable for metamorphosis in Drosophila. *Genes Dev.* 21:3061–3066. http://dx.doi.org/10.1101/gad.1600707

Kabeya, Y., N. Mizushima, T. Ueno, A. Yamamoto, T. Kirisako, T. Noda, E. Kominami, Y. Ohsumi, and T. Yoshimori. 2000. LC3, a mammalian homologue of yeast Apg8p, is localized in autophagosome membranes after processing. *EMBO J.* 19:5720–5728. http://dx.doi.org/10.1093/emboj/19.21.5720

Levine, B., and G. Kroemer. 2008. Autophagy in the pathogenesis of disease. *Cell*. 132:27–42. http://dx.doi.org/10.1016/j.cell.2007.12.018

Longatti, A., C.A. Lamb, M. Razi, S. Yoshimura, F.A. Barr, and S.A. Tooze. 2012. TBC1D14 regulates autophagosome formation via Rab11- and ULK1-positive recycling endosomes. *J. Cell Biol.* 197:659–675. http://dx.doi.org/10.1083/jcb.201111079

Lundmark, R., and S.R. Carlsson. 2002. The beta-appendages of the four adaptor-protein (AP) complexes: structure and binding properties, and identification of sorting nexin 9 as an accessory protein to AP-2. *Biochem. J.* 362:597–607. http://dx.doi.org/10.1042/0264-6021:3620597

Lundmark, R., and S.R. Carlsson. 2003. Sorting nexin 9 participates in clathrin-mediated endocytosis through interactions with the core components. *J. Biol. Chem.* 278:46772–46781. http://dx.doi.org/10.1074/jbc.M307334200

Lundmark, R., and S.R. Carlsson. 2005. Expression and properties of sorting nexin 9 in dynamin-mediated endocytosis. *Methods Enzymol.* 404:545–556. http://dx.doi.org/10.1016/S0076-6879(05)04048-6

Lundmark, R., and S.R. Carlsson. 2009. SNX9 - a prelude to vesicle release. *J. Cell Sci.* 122:5–11. http://dx.doi.org/10.1242/jcs.037135

Mizushima, N., and M. Komatsu. 2011. Autophagy: renovation of cells and tissues. *Cell*. 147:728–741. http://dx.doi.org/10.1016/j.cell.2011.10.026

Moreau, K., B. Ravikumar, C. Puri, and D.C. Rubinsztein. 2012. Arf6 promotes autophagosome formation via effects on phosphatidylinositol 4,5-bisphosphate and phospholipase D. *J. Cell Biol.* 196:483–496. http://dx.doi.org/10.1083/jcb.201110114

Neufeld, T.P. 2008. Genetic manipulation and monitoring of autophagy in *Drosophila*. *Methods Enzymol.* 451:653–667. http://dx.doi.org/10.1016/S0076-6879(08)03236-9

Noda, N.N., H. Kumeta, H. Nakatogawa, K. Satoo, W. Adachi, J. Ishii, Y. Fujioka, Y. Ohsumi, and F. Inagaki. 2008. Structural basis of target recognition by Atg8/LC3 during selective autophagy. *Genes Cells*. 13:1211–1218. http://dx.doi.org/10.1111/j.1365-2443.2008.01238.x

Pankiv, S., T.H. Clausen, T. Lamark, A. Brech, J.A. Bruun, H. Outzen, A. Øvervatn, G. Bjørkøy, and T. Johansen. 2007. p62/SQSTM1 binds directly to Atg8/LC3 to facilitate degradation of ubiquitinated protein aggregates by autophagy. *J. Biol. Chem.* 282:24131–24145. http://dx.doi.org/10.1074/jbc.M702824200

Park, J., Y. Kim, S. Lee, J.J. Park, Z.Y. Park, W. Sun, H. Kim, and S. Chang. 2010. SNX18 shares a redundant role with SNX9 and modulates endocytic trafficking at the plasma membrane. *J. Cell Sci.* 123:1742–1750. http://dx.doi.org/10.1242/jcs.064170

Polson, H.E., J. de Lartigue, D.J. Rigden, M. Reedijk, S. Urbé, M.J. Clague, and S.A. Tooze. 2010. Mammalian Atg18 (WIPI2) localizes to omegasome-anchored phagophores and positively regulates LC3 lipidation. *Autophagy*. 6:506–522. http://dx.doi.org/10.4161/auto.6.4.11863

Pylypenko, O., R. Lundmark, E. Rasmuson, S.R. Carlsson, and A. Rak. 2007. The PX-BAR membrane-remodeling unit of sorting nexin 9. *EMBO J.* 26:4788–4800. http://dx.doi.org/10.1038/sj.emboj.7601889

Ravikumar, B., K. Moreau, L. Jahreiss, C. Puri, and D.C. Rubinsztein. 2010. Plasma membrane contributes to the formation of pre-autophagosomal structures. *Nat. Cell Biol.* 12:747–757. http://dx.doi.org/10.1038/ncb2078

Rusten, T.E., K. Lindmo, G. Juhász, M. Sass, P.O. Seglen, A. Brech, and H. Stenmark. 2004. Programmed autophagy in the *Drosophila* fat body is induced by ecdysone through regulation of the PI3K pathway. *Dev. Cell*. 7:179–192. http://dx.doi.org/10.1016/j.devcel.2004.07.005

Scott, R.C., O. Schuldiner, and T.P. Neufeld. 2004. Role and regulation of starvation-induced autophagy in the *Drosophila* fat body. *Dev. Cell*. 7:167–178. http://dx.doi.org/10.1016/j.devcel.2004.07.009

Seet, L.F., and W. Hong. 2006. The Phox (PX) domain proteins and membrane traffic. *Biochim. Biophys. Acta*. 1761:878–896. http://dx.doi.org/10.1016/j.bbalip.2006.04.011

Tighe, A., O. Staples, and S. Taylor. 2008. Mps1 kinase activity restrains anaphase during an unperturbed mitosis and targets Mad2 to kinetochores. *J. Cell Biol.* 181:893–901. http://dx.doi.org/10.1083/jcb.200712028

Várnai, P., and T. Balla. 1998. Visualization of phosphoinositides that bind pleckstrin homology domains: calcium- and agonist-induced dynamic changes and relationship to myo-[3H]inositol-labeled phosphoinositide pools. *J. Cell Biol.* 143:501–510. http://dx.doi.org/10.1083/jcb.143.2.501

Varnai, P., B. Thyagarajan, T. Rohacs, and T. Balla. 2006. Rapidly inducible changes in phosphatidylinositol 4,5-bisphosphate levels influence multiple regulatory functions of the lipid in intact living cells. *J. Cell Biol.* 175:377–382. http://dx.doi.org/10.1083/jcb.200607116

Willenborg, C., J. Jing, C. Wu, H. Matern, J. Schaack, J. Burden, and R. Prekeris. 2011. Interaction between FIP5 and SNX18 regulates epithelial lumen formation. *J. Cell Biol.* 195:71–86. http://dx.doi.org/10.1083/jcb.201011112

Worby, C.A., N. Simonson-Leff, J.C. Clemens, R.P. Kruger, M. Muda, and J.E. Dixon. 2001. The sorting nexin, DSH3PX1, connects the axonal guidance receptor, Dscam, to the actin cytoskeleton. *J. Biol. Chem.* 276:41782–41789. http://dx.doi.org/10.1074/jbc.M107080200

Xie, Z., and D.J. Klionsky. 2007. Autophagosome formation: core machinery and adaptations. *Nat. Cell Biol.* 9:1102–1109. http://dx.doi.org/10.1038/ncb1007-1102

Yarar, D., M.C. Surka, M.C. Leonard, and S.L. Schmid. 2008. SNX9 activities are regulated by multiple phosphoinositides through both PX and BAR domains. *Traffic*. 9:133–146. http://dx.doi.org/10.1111/j.1600-0854.2007.00675.x

Zoncu, R., R.M. Perera, R. Sebastian, F. Nakatsu, H. Chen, T. Balla, G. Ayala, D. Toomre, and P.V. De Camilli. 2007. Loss of endocytic clathrin-coated pits upon acute depletion of phosphatidylinositol 4,5-bisphosphate. *Proc. Natl. Acad. Sci. USA*. 104:3793–3798. http://dx.doi.org/10.1073/pnas.0611733104

Supplemental material JCB

Knævelsrud et al., http://www.jcb.org/cgi/content/full/jcb.201205129/DC1

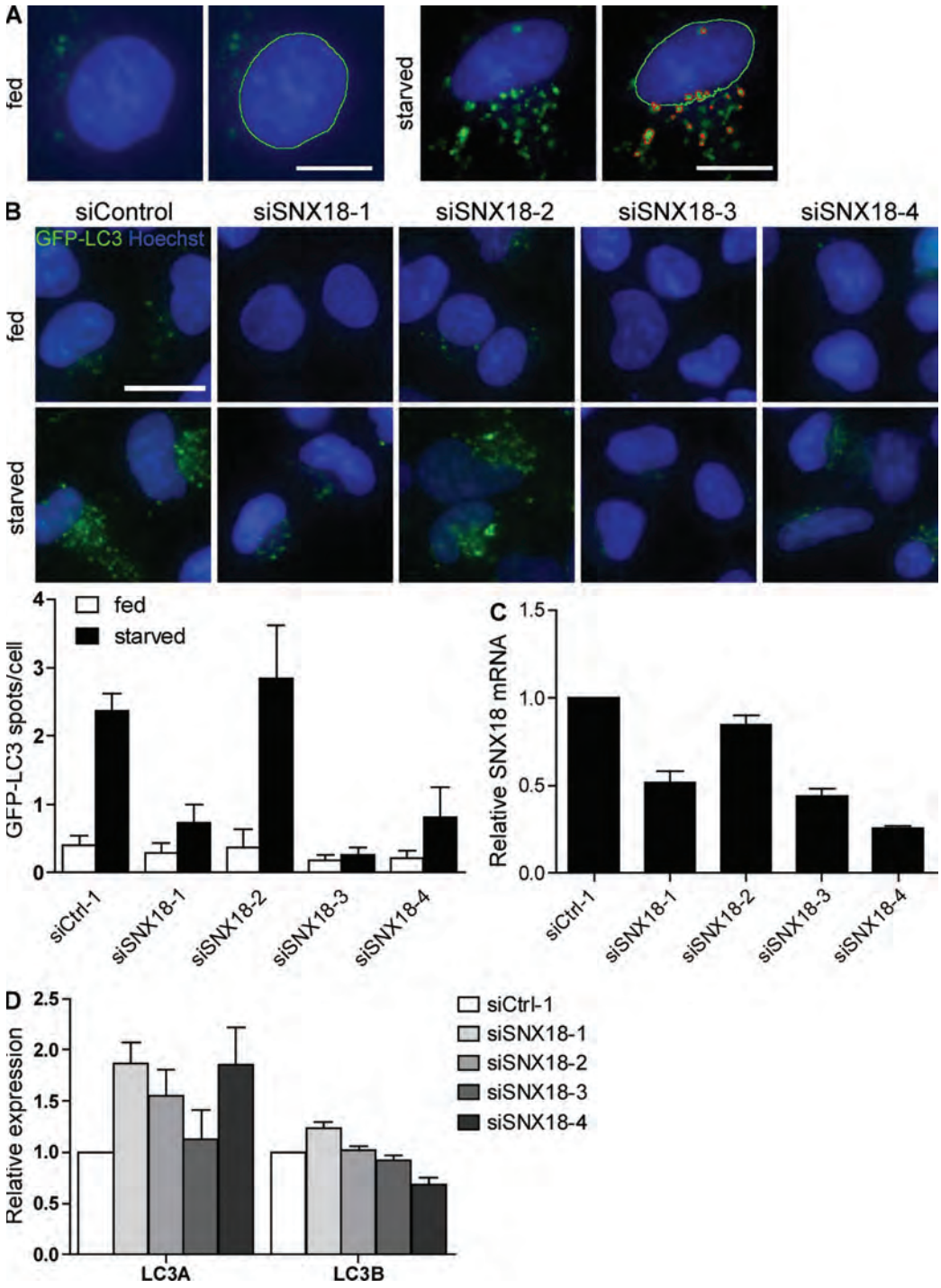

Figure S1. **The effect of SNX18 siRNA on GFP-LC3 spots correlates with SNX18 mRNA levels.** (A) Detection of GFP-LC3 spots by the Olympus ScanR software (detected nuclei delineated in green, detected spots in red). Note that only the strongest and most defined spots were detected. Bars, 5 µm. (B) HEK GFP-LC3 cells were separately transfected with the four different siRNA oligonucleotides of the SMARTpool against SNX18, and the number of GFP-LC3 spots/cell was quantified. The images for starved cells treated with siControl and siSNX18-3 are also shown in Fig. 1 C. Bars, 10 µm. The graphs show mean ± SEM (error bars), $n = 3$. (C) Relative expression of SNX18 mRNA corresponding to the images in B. The graph shows mean relative expression from two experiments performed in triplicate ± range (error bars). (D) Relative expression of LC3A and LC3B mRNA upon SNX18 knockdown, corresponding to B. The graph shows mean relative expression from two experiments performed in triplicate ± range (error bars).

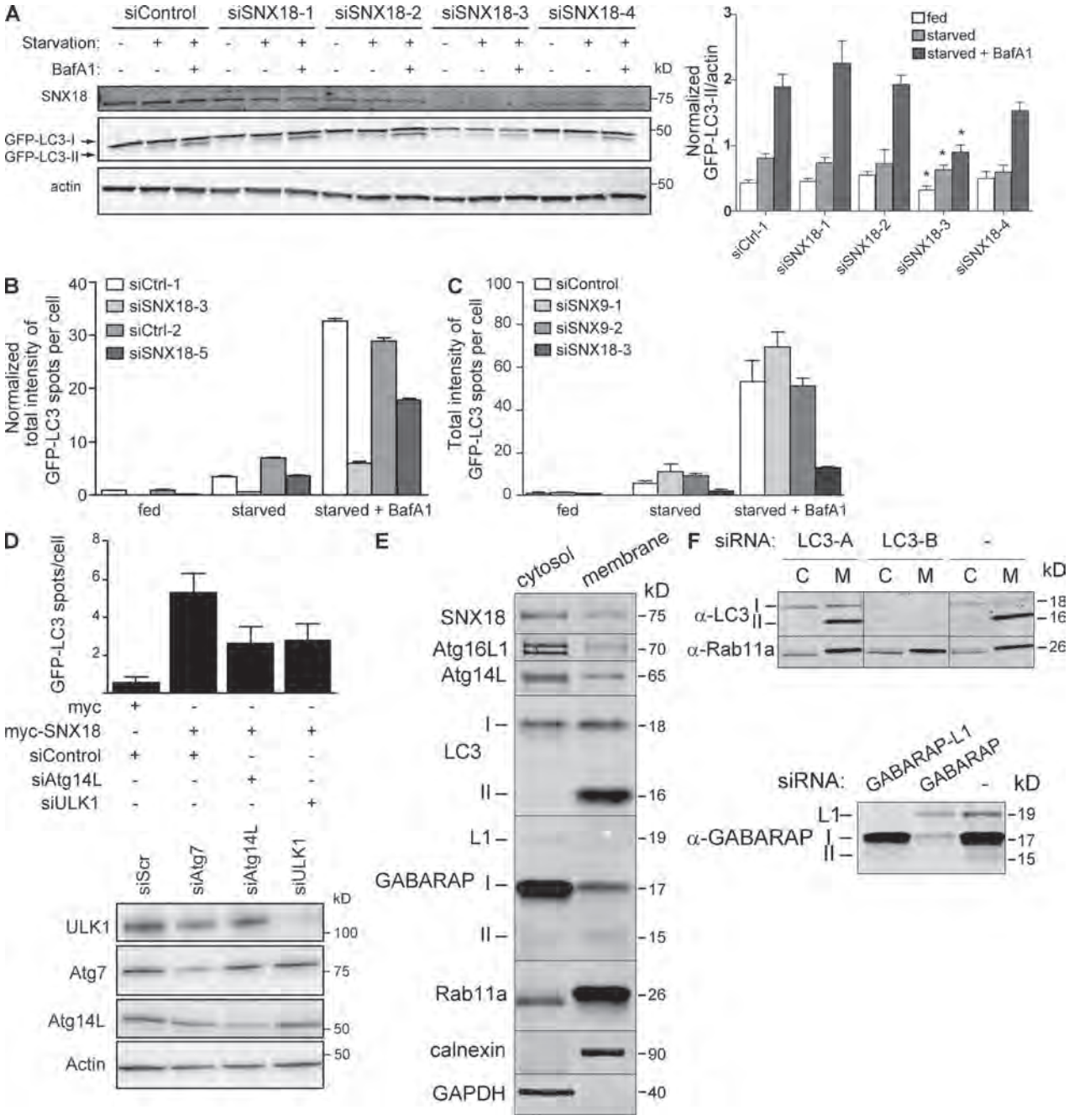

Figure S2. **SNX18, but not SNX9, is required for autophagosome formation.** (A) HEK GFP-LC3 cells were separately transfected with the four different siRNA oligonucleotides of the SMARTpool against SNX18 or the corresponding control and starved or not starved for 2 h in the presence or absence of BafA1. After lysis and separation by SDS-PAGE, Western blotting was performed to monitor GFP-LC3 lipidation and to confirm SNX18 protein knockdown. The graph shows quantification of the levels of GFP-LC3-II/actin (graph shows mean ± SEM [error bars], $n = 3$; *, $P < 0.05$ between siSNX18 and the corresponding siControl sample). (B) HEK GFP-LC3 cells were transfected with the indicated siRNA oligonucleotides and starved or not starved for 2 h in the presence or absence of BafA1. The total intensity of GFP-LC3 spots per cell for each condition was determined. The graph shows mean ± SEM (error bars), $n = 3$. (C) HEK GFP-LC3 cells were transfected with the indicated siRNA oligonucleotides against SNX9 or SNX18 and treated as in B. The graph shows mean ± SEM (error bars), $n = 3$, with a total of 1,500 cells. (D) HEK GFP-LC3 cells were transfected with the indicated siRNA oligonucleotides and then with myc-SNX18 or a myc control vector, followed by automated imaging and analysis of the number of GFP-LC3 spots per cell. The graph shows mean ± SEM (error bars), $n = 3$. Immunoblot analysis of knockdown is shown below. (E) Equal proportions of cytosol and membrane fractions from HeLa cells grown in full medium were analyzed by immunoblotting using antibodies against the indicated proteins. Analysis of calnexin and GAPDH validated the fractionation method and showed no cross-contamination between the fractions. Atg16L appeared as a doublet, which corresponds to two different splice forms present in HeLa cells as previously shown (Mizushima et al., 2003). (F) HeLa cells were transfected with siRNA against LC3-A, LC3-B, GABARAP, or GABARAP-L1, or left untreated (−), and after 72 h, membrane (M) and cytosol (C) were prepared (for LC3 analysis) or lysed (for GABARAP analysis), and analyzed by immunoblotting using the indicated antibodies. Black lines indicate that intervening lanes have been spliced out.

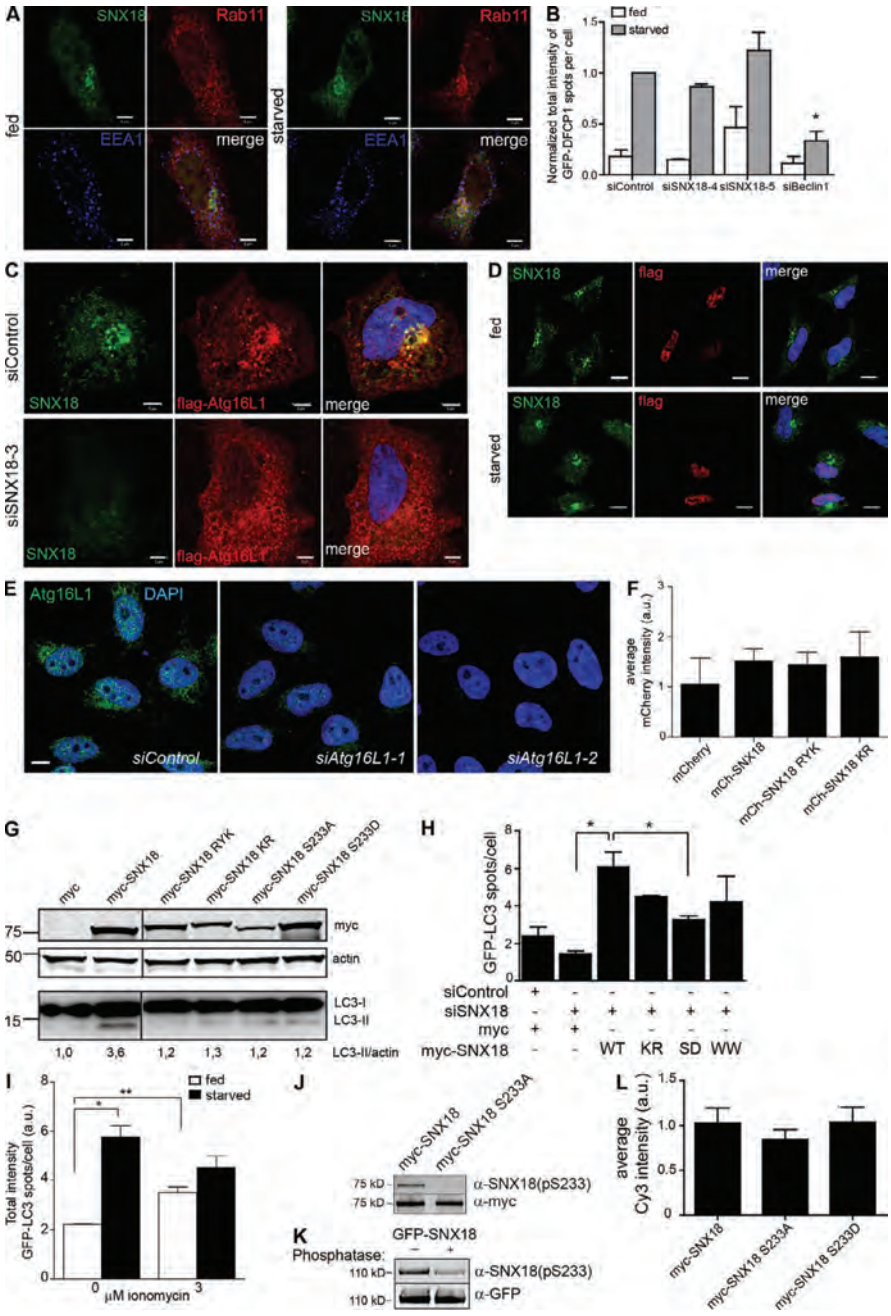

Figure S3. **SNX18 membrane binding and phosphorylation mutants.** (A) HeLa cells were grown in nutrient-rich medium (fed) or starved for 2 h before fixation and immunostaining against endogenous SNX18, Rab11, and EEA1. Bars, 5 µm. (B) HEK GFP-DFCP1 cells transfected with the indicated siRNAs were starved or not starved for 50 min. After fixation, the total intensity of GFP-DFCP1 spots per cell was quantified from 500 cells (graph shows mean ± SEM [error bars], $n = 3$). *, $P < 0.05$. (C) HeLa cells were transfected with control or SNX18 siRNA and later with flag-Atg16L1, followed by a 2-h incubation in nutrient-rich (fed) or starvation medium before immunostaining and confocal imaging. Bars, 5 µm. (D) HeLa cells were transfected with myc-SNX18 and a 3×flag control vector and then starved or not starved for 2 h before immunostaining with anti-myc and anti-flag antibodies and confocal microscopy analysis (control for Fig. 4 B). Bars, 10 µm. (E) HeLa cells were transfected with two different siRNA oligos against Atg16L1 or the corresponding control and immunostained with anti-Atg16L1 antibodies and analyzed by confocal microscopy. Bar, 5 µm. (F) HEK GFP-LC3 cells were transfected to overexpress the indicated mCherry-tagged SNX18 constructs for 16 h. The mean mCherry intensity was quantified as a control for equal expression levels (control for corresponding Fig. 4 D). (G) HEK GFP-LC3 cells were transfected to overexpress the indicated myc-tagged SNX18 constructs for 16 h. The ratio of LC3-II to actin, as determined by Western blotting, was quantified. Black lines indicate that intervening lanes have been spliced out. (H) HEK GFP-LC3 cells were transfected with control siRNA or siRNA against SNX18. The next day, they were transfected with siRNA-resistant plasmids encoding myc-SNX18 WT, or with mutations KR, S233D (SD) or W154S/W158S (WW). 1 d later, the number of GFP-LC3 spots per cell was quantified (mean ± SEM [error bars], $n = 3$; *, $P < 0.05$.) (I) HEK GFP-LC3 cells were starved or not starved for 2 h in the absence of presence of 3 µM ionomycin followed by automated imaging and analysis of the total intensity of GFP-LC3 spots per cell. The graph shows mean ± SEM (error bars), $n = 3$. *, $P < 0.05$; **, 0.01. (J) HeLa cells were transfected to overexpress myc-tagged full-length WT SNX18 (myc-SNX18) or mutant S233A (myc-SNX18 S233A) for 16 h, after which the cells were starved in EBSS for 90 min. Proteins were immunoprecipitated from lysates with anti-myc antibodies and analyzed by immunoblotting using phosphospecific SNX18 pS233 and myc antibodies. (K) GFP-Trap–enriched GFP-SNX18, obtained from cells starved for 90 min, was either mock-treated or treated with Lambda phosphatase and analyzed by immunoblotting using the phosphospecific SNX18 pS233 antibody. Anti-GFP shows equal amount of GFP-SNX18. (L) HEK GFP-LC3 cells were transfected to overexpress the indicated myc-tagged SNX18 constructs for 16 h, followed by immunostaining with an anti-myc antibody and a Cy3-labeled secondary antibody. The mean Cy3 intensity of was quantified as a control for equal expression levels in cells used to quantify the number of GFP-LC3 spots per cell (Fig. 5 C). The graph shows mean ± SEM (error bars).

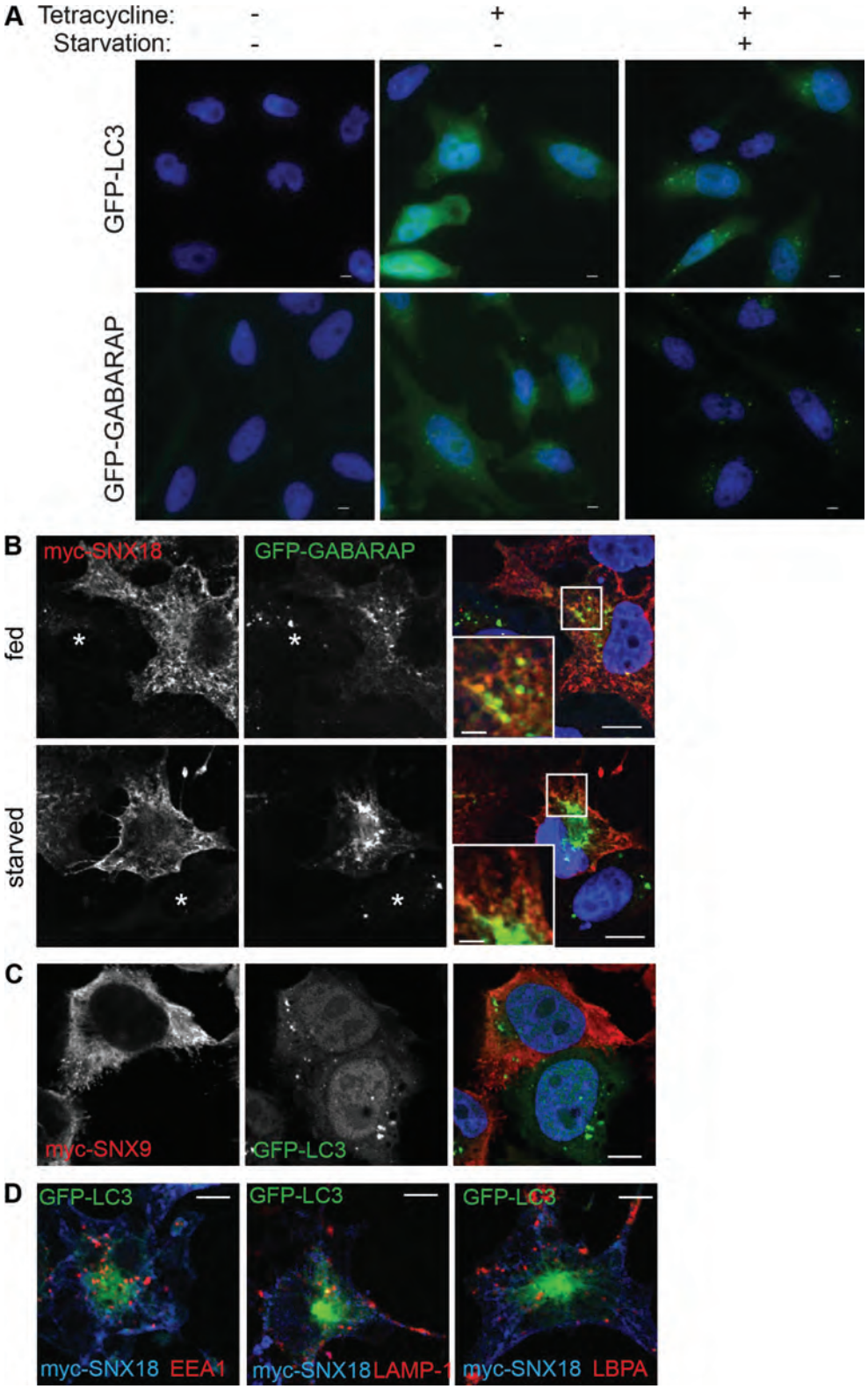

Figure S4. **myc-SNX18 induced GFP-LC3–positive membrane tubules.** (A) TRex FlpIN HeLa cells were stably transfected to express GFP-LC3 or -GABARAP under the control of a tetracycline-inducible promoter. (B) HeLa cells inducibly expressing GFP-GABARAP were transfected with a plasmid encoding myc-SNX18. The asterisks denote cells not expressing myc-SNX18. Insets show enlarged views of the boxed regions. (C) HeLa cells inducibly expressing GFP-LC3 were transfected with a plasmid encoding myc-SNX9. (D) HeLa cells inducibly expressing GFP-LC3 were transfected with a plasmid encoding myc-SNX18 and immunostained for the indicated proteins. Bars: (A) 5 µm; (B, main panels) 20 µm; (B, insets) 5 µm; (C and D) 10 µm.

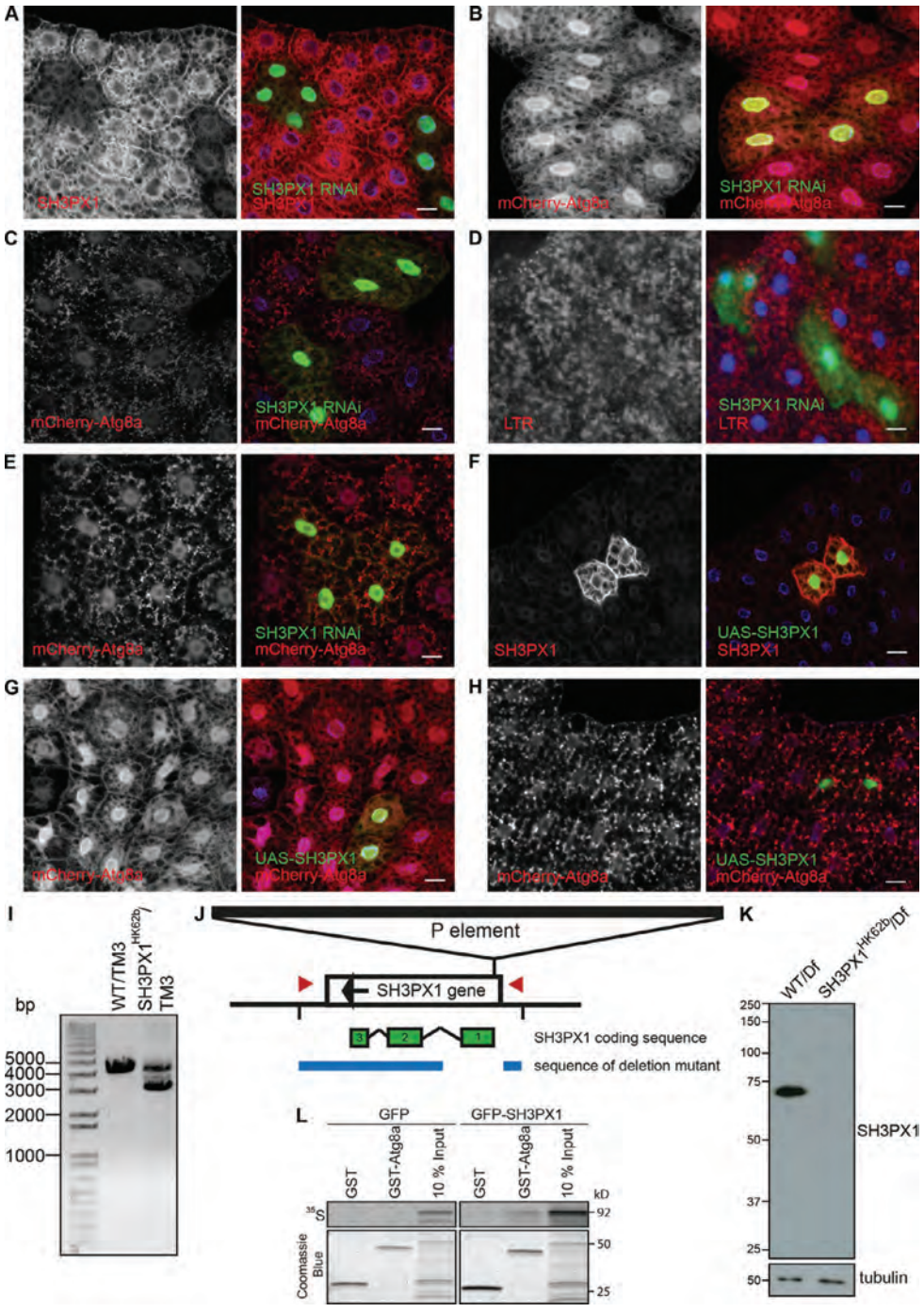

Figure S5. **SH3PX1 is necessary, but not sufficient for autophagosome formation.** (A) SH3PX1 protein levels are decreased by SH3PX1 RNAi. Fat bodies from third instar larvae expressing SH3PX1 RNAi (GFP-positive cells) were stained for endogenous SH3PX1. (B) Fat bodies from mCherry-Atg8a–expressing fed larvae with SH3PX1 RNAi clones (GFP positive). (C) SH3PX1 RNAi (GFP-positive cells) results in formation of smaller mCherry-Atg8a–marked autophagosomes after 3 h of starvation compared with WT cells. (D and E) LTR punctae (D) and mCherry-Atg8a–positive autophagosomes (E) are smaller in SH3PX1 RNAi clones (GFP-positive) compared with WT cells during developmental autophagy in 113-h-old larvae. (F) Fat body overexpressing SH3PX1 (GFP-positive cells) by actin-GAL4 through the UAS in the $SH3PX1^{EY08084}$ P element in the 5′ UTR of the SH3PX1 gene was stained for endogenous SH3PX1. (G and H) SH3PX1 overexpression does not induce or change formation of mCherry-positive autophagosomes in fat bodies from fed (G) or 3-h starved (H) larvae. Bars, 20 µm. Genotypes: (A and D) hsflp; UAS-dicer/+; Act>CD2>GAL4 UAS-GFPnls/UAS-SH3PX1 RNAi; (B, C, and E) hsflp; UAS-dicer/+; r4:mCherry-Atg8a Act>CD2>GAL4 UAS-GFPnls/UAS-SH3PX1 RNAi; (F) hsflp; +; Act>CD2>GAL4 UAS-GFPnls/UAS-SH3PX1; (G and H) hsflp; +; r4:mCherry-Atg8a Act>CD2>GAL4 UAS-GFPnls/UAS-SH3PX1. (I–K) The P element $SH3PX1^{EY08084}$ located in the 5′ UTR of the SH3PX1 gene was remobilized and lines where part of the gene region was deleted were screened by PCR. One such line missing 1,198 bp of the gene region was identified (I; $SH3PX1^{HK62b}$), and sequencing showed that the first exon of SH3PX1 including the start codon, was deleted (1,198 nucleotides removed from the EY08084 insertion site [3L:9,706,877; FlyBase release FB2012_02]). This is depicted in J as an overview of the SH3PX1 gene region with the inserted P element, the coding sequence, and the sequence still present in the deletion mutant. Primers for PCR amplification are indicated by red arrowheads. (K) Fat bodies from third instar larvae with indicated genotypes were dissected out and lysed in SDS sample buffer. Lysates were analyzed by Western blotting using the indicated antibodies. (L) GFP and GFP-tagged SH3PX1 were in vitro translated in reticulocyte lysate in the presence of [^{35}S]methionine and incubated with GST or GST-tagged DrAtg8a. The resulting pulldowns were separated by SDS-PAGE. Coomassie blue staining shows the presence of the GST proteins and the in vitro translated copurified proteins were detected by autoradiography.

Table S1. **Reagents and results for the primary screen**

Gene	Gene ID	Accession no.	GI no.	Dharmacon SMARTpool	No. of cells analyzed	GFP-LC3 spots per cell			
						Fed		Starved	
						Average	SD	Average	SD
SNX18	112574	NM_052870	16418370	L-013438-01	37,513	0.30	0.11	0.70	0.29
ULK1	8408	NM_003565	225637564	L-005049-01	393,570	0.43	0.17	1.00	0.28
RPS6KC1	26750	NM_012424	19923722	L-005371-00	52,785	0.61	0.12	1.82	0.46
PLD1	5337	NM_002662	46276864	L-009413-00	46,270	0.78	0.18	1.88	0.68
SNX4	8723	NM_003794	23111044	L-011520-00	48,435	0.63	0.11	2.01	0.87
SNX3	8724	NM_152827	23111040	L-011521-01	40,693	0.65	0.23	2.04	0.56
SNX2	6643	NM_003100	23111037	L-017520-00	53,688	0.74	0.14	2.16	0.77
SH3PXD2B	285590	NM_001017995	63055058	L-032834-01	39,858	0.66	0.11	2.11	0.11
SNX8	29886	NM_013321	23943857	L-014196-01	42,526	0.64	0.15	2.14	0.25
SNX25	83891	NM_031953	38708168	L-014761-01	44,557	0.68	0.14	2.15	0.34
SNX27	81609	NM_030918	73695940	L-017346-01	52,888	0.65	0.13	2.17	0.91
PXK	54899	NM_017771	31543451	L-005367-00	49,517	0.66	0.12	2.22	0.32
SNX19	399979	NM_014758	7662025	L-029832-01	32,791	0.65	0.23	2.23	0.26
PLD2	5338	NM_002663	20070140	L-005064-00	53,258	0.57	0.20	2.30	0.75
SNX12	29934	NM_013346	23111029	L-013648-00	38,114	0.68	0.05	2.31	0.35
SNX9	51429	NM_016224	23111056	L-017335-00	43,436	0.53	0.10	2.34	0.44
SNX16	64089	NM_152837	23238247	L-013044-01	46,089	0.74	0.28	2.36	0.60
SNX7	51375	NM_152238	23111054	L-013216-01	54,382	0.82	0.32	2.38	0.80
PIK3C2A	5286	NM_002645	4505798	L-006771-00	37,354	0.65	0.11	2.40	0.55
SNX21	90203	NM_152897	23510349	L-013643-01	32,791	0.58	0.20	2.43	0.33
KIF16b	55614	NM_024704	41327690	L-009495-00	55,651	0.74	0.22	2.49	0.95
SH3PXD2a	9644	NM_014631	55749543	L-006657-00	39,858	0.77	0.15	2.51	0.16
NISCH	11188	NM_007184	66472381	L-019677-00	52,259	0.84	0.24	2.52	0.55
CISK	23678	NM_170709	25168266	L-004162-00	70,157	0.63	0.27	2.53	0.46
SNX5	27131	NM_014426	23111045	L-012524-00	48,111	0.68	0.13	2.54	0.84
SNX10	29887	NM_013322	23111022	L-017559-01	47,895	0.68	0.13	2.55	0.63
LOC64654/ SNX30	401548	XM_945049	89030537	L-029584-01	50,950	0.81	0.20	2.55	0.16
SNX11	29916	NM_013323	23111025	L-013673-01	42,716	0.85	0.19	2.57	0.63
NCF4	4689	NM_000631	47519797	L-011128-01	48,168	0.80	0.16	2.59	0.53
SNX13	23161	NM_015132	87196349	L-009381-01	43,526	0.69	0.27	2.61	0.85
NCF1	4687	NM_000265	4557784	L-009958-00	33,652	0.74	0.05	2.62	0.52
SNX33	257364	NM_153271	23397573	L-015876-00	31,301	0.84	0.21	2.63	0.47
SNX17	9784	NM_014748	23238249	L-013427-01	49,559	0.76	0.36	2.67	0.64
SNX15	29907	NM_147777	46370088	L-017488-01	33,420	0.88	0.20	2.69	0.39
LOC646564	646564	XM_929500	89040212	L-037482-00	50,634	0.71	0.14	2.72	0.60
SNX22	79856	NM_024798	71772837	L-014452-01	49,639	0.87	0.50	2.77	0.37
SNX20	124460	NM_182854	33504570	L-016514-01	33,349	0.98	0.17	2.84	0.40
SNX1	6642	NM_148955	71772739	L-017518-00	34,301	0.80	0.23	2.85	0.25
HS1BP3	64342	NM_022460	68800429	L-013029-01	36,266	0.89	0.20	2.92	0.27
SNX24	28966	NM_014035	7662654	L-020568-01	48,714	0.98	0.26	2.92	0.81
SNX31	169166	NM_152628	24432084	L-016021-01	33,547	0.76	0.27	2.98	0.54
SNX14	57231	NM_020468	39777615	L-013190-01	33,568	0.60	0.20	3.07	0.37
TSG101	7251	NM_006292	18765712	L-003549-00	67,115	1.22	0.43	3.79	0.96
Non-targeting 1[a]					92,798	0.63	0.13	2.79	0.46
Non-targeting 2[b]					81,587	0.75	0.14	2.81	0.54
Non-targeting 3[c]					82,485	0.81	0.81	0.81	0.81

A comprehensive list of the gene targets, siRNA numbers, number of cells analyzed, and GFP-LC3 spots per cell (average and SD for fed and starved cells) from the primary screen. The siRNA treatments did not significantly affect cell proliferation as judged by limited variation in the total number of cells detected on the 100 images analyzed from each siRNA treatment.
[a]ON-TARGET plus Non-targeting Pool.
[b]siGENOME Non-targeting Pool.
[c]siGENOME Non-targeting Pool #2.

Table S2. **Reagents and results for the secondary screen**

Gene	Dharmacon ON target plus	siRNA sequence (5′–3′)	Percent knockdown of mRNA	No. of cells analyzed	GFP-LC3 spots			
					Fed		Starved	
					Average	SD	Average	SD
SNX18	J-013438-09[a]	AGAGCAAGAUAGACGGCUU	50	35,495	0.29	0.15	0.73	0.28
	J-013438-10[b]	GAGCAUACCCGGACCUCGA	0	61,436	0.38	0.26	2.85	0.77
	J-013438-11[c]	GCGGAGAAGUUCCCGGUCA	60	51,626	0.18	0.08	0.26	0.12
	J-013438-12[d]	CGGACAUCAUCCACGUUCA	70	37,378	0.22	0.11	0.82	0.44
ULK1	J-005049-05	CAGCAUCACUGCCGAGAGG	65	98,195	0.37	0.13	1.46	0.22
	J-005049-06	CCACGCAGGUGCAGAACUA	65	81,939	0.26	0.15	0.39	0.12
	J-005049-07	GCACAGAGACCGUGGGCAA	50	89,098	0.45	0.09	2.47	0.50
	J-005049-08	UCACUGACCUGCUCCUUAA	70	87,029	0.27	0.13	0.91	0.30
SNX14	J-013190-09	UGAAAUUUCUGCUGUGCGA	63	52,135	0.52	0.35	2.82	1.09
	J-013190-10	AGAUACUACCAGAUGUAAA	61	53,533	0.45	0.28	2.66	1.15
	J-013190-11	GUUAGGACUUCAGGAAUUA	77	49,324	0.36	0.19	2.28	0.92
	J-013190-12	CAUUAAUUCUUGUGAGUCU	65	44,819	0.43	0.27	1.28	0.32
RPS6KC1	J-005371-06	GGAAUUGUGUGCCGCGAUU	83	43,775	0.47	0.05	3.36	0.50
	J-005371-07	CAGCUCAGAUCCUAAGUUU	77	49,744	0.45	0.09	3.23	0.44
	J-005371-08	GGAGAUAUGUCUUUGUUAC	77	52,173	0.37	0.07	2.58	0.30
	J-005371-09	GGAAUAAAUACUCACACUA	64	35,236	0.24	0.06	0.64	0.12
PLD1	J-009413-05	CAACAGAGUUUCUUGAUAU	83	44,274	0.35	0.05	2.74	0.32
	J-009413-06	GGUAAUCAGUGGAUAAAUU	73	46,204	0.53	0.07	2.70	0.44
	J-009413-07	CCAUGGAGGUUUGGACUUA	73	45,901	0.31	0.07	1.62	0.34
	J-009413-08	CCGGGUAUAUGUCGUGAUA	53	50,080	0.46	0.08	2.94	0.30
SNX31	J-016021-09	ACAGAGUAUUAGAAUCGAA	30	47,529	0.34	0.05	2.80	0.33
	J-016021-10	GCAGAUUGAAGUUCCGGAA	51	47,439	0.46	0.06	3.05	0.53
	J-016021-11	GUCGAGAGCUCUUGGGCUA	34	34,578	0.52	0.06	3.34	0.62
	J-016021-12	AGGUACGGCACUAUGGAUA	46	48,243	0.43	0.05	2.77	0.58
SNX24	J-020568-09	GAAAAGAGAUACAGCGAAU	81	54,686	0.43	0.34	2.39	0.94
	J-020568-10	CUUGGAACAGCGACGACAA	64	46,423	0.97	0.73	5.24	1.98
	J-020568-11	GCCAAGUGUUUAAGAAGUA	80	45,944	0.34	0.26	2.05	1.58
	J-020568-12	GCGUAGAAACCCAUGAAAA	76	51,801	0.32	0.25	2.15	1.29
SNX20	J-016514-09	CGUUCAGGGAGGAGAUCGA	0	41,356	0.42	0.09	2.07	0.38
	J-016514-10	GCAAGGACUUCGUGACUCU	0	34,956	0.71	0.20	3.34	0.89
	J-016514-11	GCUGGAAGCACGUCAAACU	3	27,247	0.87	0.23	2.92	0.61
	J-016514-12	UCUCUAAGUUUGUGGUGUA	3	48,282	0.46	0.09	3.27	0.48
HS1BP3	J-013029-09	AAGAAGGAGUGACCGGUAU	67	51,365	0.60	0.40	4.14	1.05
	J-013029-10	UGAAGAGGCUUUCGACUUU	97	50,411	0.69	0.47	4.08	1.13
	J-013029-11	GAGCCUGAAGGGCGAGGAU	65	48,866	0.94	0.67	7.07	1.54
	J-013029-12	UCCCAAAGUGGCCGUGAAA	0	56,401	0.46	0.41	2.47	0.89
Non-targeting	D-001810-01[e]		0	199,315	0.41	0.13	2.37	0.26

Listing the gene targets, siRNA numbers and sequences, percent knockdown of mRNA for the specified target, number of cells analyzed, and GFP-LC3 spots per cell (average and SD for fed and starved cells) from the secondary screen. Names used in figures are defined by footnotes.
[a]siSNX18-1.
[b]siSNX18-2.
[c]siSNX18-3.
[d]siSNX18-4.
[e]siCtrl-1.

Table S3. **Plasmids used in this study**

Plasmid	Primer sequences	Reference
pCMVmycSNX18		Håberg et al., 2008
pCMVmycSNX18 RYK constructed by mutagenesis using the primers listed in the next column	5′-GCAGGTGCCGGTGCATCGGCAGGCCGCGCACTTCGACTGGCTGTACG-3′ and 5′-CGTACAGCCAGTCGAAGTGCGCGGCCTGCCGATGCACCGGCACCTGC-3′	This study
pCMVmycSNX18 KR constructed by mutagenesis using the primers listed in the next column	5′-GCCTGGAAGCAGGGCGAGGAGAAGGCCGAGAAGGA-3′ and 5′-TCCTTCTCGGCCTTCTCCTCGCCCTGCTTCCAGGC-3′	This study
pCMVmycPX-BAR		Håberg et al., 2008
pCMVmycPX-BAR S233A constructed by mutagenesis using the primers listed in the next column	5′-CAATCGCTTCGCCACCTTCGTCAAG-3′and 5′-CTTGACGAAGGTGGCGAAGCGATTG-3′	This study
pCMVmycPX-BAR S233D constructed by mutagenesis using the primers listed in the next column	5′-CCTCAATCGCTTCGACACCTTCGTCAAG-3′ and 5′-CTTGACGAAGGTGTCGAAGCGATTGAGG-3′	This study
pCMVmycSNX18 S233A constructed by mutagenesis using the primers listed in the next column	5′-CAATCGCTTCGCCACCTTCGTCAAG-3′and 5′-CTTGACGAAGGTGGCGAAGCGATTG-3′	This study
pCMVmycSNX18 S233D constructed by mutagenesis using the primers listed in the next column	5′-CCTCAATCGCTTCGACACCTTCGTCAAG-3′ and 5′-CTTGACGAAGGTGTCGAAGCGATTGAGG-3′	This study
pCMVmycSNX18 W154S/W158S constructed by mutagenesis using the primers listed in the next column	5′-GCAGCGATGATGACTCGGACGACGAGTGGGA-3′ and 5′-TCCCACTCGTCGTCCGAGTCATCATCGCTCC-3′ then 5′-ACTCGGACGACGAGTCGGACGACAGCTCCAC-3′ and 5′-GTGGAGCTGTCGTCCGACTCGTCGTCCGAGT-3′	This study
pDESTmyc SNX18 WT siSNX18 3 resistant constructed by mutagenesis of pENTR SNX18 using the primers listed in the next column	5′-GCGCGCCTGGCGGAAAAATTTCCTGTCATCTCCGTGCCC-3′ and 5′-GGGCACGGAGATGACAGGAAATTTTTCCGCCAGGCGCGC-3′	This study
pDESTmyc SNX18 KR siSNX18 3 resistant constructed by mutagenesis of pENTR SNX18 KR using the primers listed in the next column	5′-GCGCGCCTGGCGGAAAAATTTCCTGTCATCTCCGTGCCC-3′ and 5′-GGGCACGGAGATGACAGGAAATTTTTCCGCCAGGCGCGC-3′	This study
pDESTmyc SNX18 S233D siSNX18 3 resistent constructed by mutagenesis of pENTR SNX18 S233D using the primers listed in the next column	5′-GCGCGCCTGGCGGAAAAATTTCCTGTCATCTCCGTGCCC-3′ and 5′-GGGCACGGAGATGACAGGAAATTTTTCCGCCAGGCGCGC-3′	This study
pDESTmyc SNX18 W154S/W158S siSNX18 3 resistent constructed by mutagenesis of pENTR SNX18 W154S/W158S using the primers listed in the next column	5′-GCGCGCCTGGCGGAAAAATTTCCTGTCATCTCCGTGCCC-3′ and 5′-GGGCACGGAGATGACAGGAAATTTTTCCGCCAGGCGCGC-3′	This study
pEGFPAtg14L		Addgene plasmid 21635 Matsunaga et al., 2009
pDEST53-p62		Pankiv et al., 2007
pDEST53-SNX18 Constructed by subcloning from pCMVmycSNX18 (Håberg et al., 2008) into pENTR and subsequent Gateway cloning into pDEST53 (Invitrogen)		This study
pDEST53-SNX18 SH3-LC Constructed by restriction digest of pENTR SNX18 and subsequent Gateway cloning into pDEST53		This study
pDEST53-SNX18 PX-BAR Constructed by subcloning from pCMVmycSNX18 (Håberg et al., 2008) into pENTR and subsequent Gateway cloning into pDEST53		This study
pDEST15-LC3A		Pankiv et al., 2007
pDEST15-LC3B		Pankiv et al., 2007
pDEST15-LC3C Constructed by subcloning from pGEX-4T-1-LC3C (Kirkin et al., 2009), provided by I. Dikic (Goethe University Medical School, Frankfurt Am Main, Germany), into pENTR and subsequent Gateway cloning into pDEST15 (Invitrogen)		This study
pDEST15-GABARAP		Pankiv et al., 2007
pDEST15-GABARAPL1		Pankiv et al., 2007

Table S3. **Plasmids used in this study** *(Continued)*

Plasmid	Primer sequences	Reference
pDEST15-GABARAPL2		Pankiv et al., 2007
pDEST EGFP LC3 G120A Constructed by Gateway cloning from pENTR LC3 G120A (constructed by A. Jain and obtained as a gift from T. Johansen) into pDEST EGFP		This study
mCFP-FRB		Varnai et al., 2006
mRFP-FKBP		Varnai et al., 2006
mRFP-FKBP-5pase		Varnai et al., 2006
pDEST15-Atg8a Constructed by Gateway cloning from pENTR DmAtg8a, provided by T. Johansen, into pDEST15		
pDEST53-SH3PX1 Constructed by subcloning from pOT2 SH3PX1, received through the Drosophila Genomics Resource Center (Stapleton et al., 2002), into pENTR and subsequent Gateway cloning into pDEST15 (Invitrogen)		This study

References

Håberg, K., R. Lundmark, and S.R. Carlsson. 2008. SNX18 is an SNX9 paralog that acts as a membrane tubulator in AP-1-positive endosomal trafficking. *J. Cell Sci.* 121:1495–1505. http://dx.doi.org/10.1242/jcs.028530

Kirkin, V., T. Lamark, Y.S. Sou, G. Bjørkøy, J.L. Nunn, J.A. Bruun, E. Shvets, D.G. McEwan, T.H. Clausen, P. Wild, et al. 2009. A role for NBR1 in autophagosomal degradation of ubiquitinated substrates. *Mol. Cell.* 33:505–516. http://dx.doi.org/10.1016/j.molcel.2009.01.020

Matsunaga, K., T. Saitoh, K. Tabata, H. Omori, T. Satoh, N. Kurotori, I. Maejima, K. Shirahama-Noda, T. Ichimura, T. Isobe, et al. 2009. Two Beclin 1-binding proteins, Atg14L and Rubicon, reciprocally regulate autophagy at different stages. *Nat. Cell Biol.* 11:385–396. http://dx.doi.org/10.1038/ncb1846

Mizushima, N., A. Kuma, Y. Kobayashi, A. Yamamoto, M. Matsubae, T. Takao, T. Natsume, Y. Ohsumi, and T. Yoshimori. 2003. Mouse Apg16L, a novel WD-repeat protein, targets to the autophagic isolation membrane with the Apg12-Apg5 conjugate. *J. Cell Sci.* 116:1679–1688. http://dx.doi.org/10.1242/jcs.00381

Pankiv, S., T.H. Clausen, T. Lamark, A. Brech, J.A. Bruun, H. Outzen, A. Øvervatn, G. Bjørkøy, and T. Johansen. 2007. p62/SQSTM1 binds directly to Atg8/LC3 to facilitate degradation of ubiquitinated protein aggregates by autophagy. *J. Biol. Chem.* 282:24131–24145. http://dx.doi.org/10.1074/jbc.M702824200

Stapleton, M., J. Carlson, P. Brokstein, C. Yu, M. Champe, R. George, H. Guarin, B. Kronmiller, J. Pacleb, S. Park, et al. 2002. A *Drosophila* full-length cDNA resource. *Genome Biol.* 3:RESEARCHH0080. http://dx.doi.org/10.1186/gb-2002-3-12-research0080

Varnai, P., B. Thyagarajan, T. Rohacs, and T. Balla. 2006. Rapidly inducible changes in phosphatidylinositol 4,5-bisphosphate levels influence multiple regulatory functions of the lipid in intact living cells. *J. Cell Biol.* 175:377–382. http://dx.doi.org/10.1083/jcb.200607116

II

nature COMMUNICATIONS

ARTICLE

Received 14 Jun 2016 | Accepted 9 Nov 2016 | Published 22 Dec 2016

DOI: 10.1038/ncomms13889 OPEN

HS1BP3 negatively regulates autophagy by modulation of phosphatidic acid levels

Petter Holland[1,*], Helene Knævelsrud[1,*], Kristiane Søreng[1], Benan J. Mathai[1], Alf Håkon Lystad[1], Serhiy Pankiv[1], Gunnveig T. Bjørndal[1], Sebastian W. Schultz[2], Viola H. Lobert[2], Robin B. Chan[3], Bowen Zhou[3], Knut Liestøl[4], Sven R. Carlsson[5], Thomas J. Melia[6], Gilbert Di Paolo[3] & Anne Simonsen[1]

A fundamental question is how autophagosome formation is regulated. Here we show that the PX domain protein HS1BP3 is a negative regulator of autophagosome formation. HS1BP3 depletion increased the formation of LC3-positive autophagosomes and degradation of cargo both in human cell culture and in zebrafish. HS1BP3 is localized to ATG16L1- and ATG9-positive autophagosome precursors and we show that HS1BP3 binds phosphatidic acid (PA) through its PX domain. Furthermore, we find the total PA content of cells to be significantly upregulated in the absence of HS1BP3, as a result of increased activity of the PA-producing enzyme phospholipase D (PLD) and increased localization of PLD1 to ATG16L1-positive membranes. We propose that HS1BP3 regulates autophagy by modulating the PA content of the ATG16L1-positive autophagosome precursor membranes through PLD1 activity and localization. Our findings provide key insights into how autophagosome formation is regulated by a novel negative-feedback mechanism on membrane lipids.

[1] Department of Molecular Medicine, Institute of Basic Medical Sciences, University of Oslo, PO Box 1112, 0317 Oslo, Norway. [2] Centre for Cancer Biomedicine, Faculty of Medicine and Department of Molecular Cell Biology, Institute for Cancer Research, Oslo University Hospital, 0379 Oslo, Norway. [3] Department of Pathology and Cell Biology, Taub Institute for Research on Alzheimer's Disease and the Aging Brain, Columbia University Medical Center, 630 West 168th Street, New York, New York 10032, USA. [4] Centre for Cancer Biomedicine, Faculty of Medicine, University of Oslo, 0379 Oslo, Norway. [5] Department of Medical Biochemistry and Biophysics, Umeå University, SE-901 87 Umeå, Sweden. [6] Department of Cell Biology, Yale University School of Medicine, PO Box 208002, 333 Cedar Street, New Haven, Connecticut 06520-800210032, USA. * These authors contributed equally to this work. Correspondence and requests for materials should be addressed to A.S. (email: anne.simonsen@medisin.uio.no).

Autophagy targets intracellular components for lysosomal degradation to promote cellular and organismal health and homoeostasis, and has been shown to protect against neurodegeneration and cancer, help remove invading pathogens and promote longevity[1]. Macroautophagy (here referred to as autophagy) is characterized by the formation of double-membrane autophagosomes from an expanding cargo-enwrapping phagophore and the subsequent fusion of autophagosomes with lysosomes. Autophagy is induced by stresses like starvation and also provides cellular quality control under basal conditions[2]. Autophagy must be tightly controlled at each step of the process; autophagosome formation without proper turnover is linked to neurodegenerative disorders such as Alzheimer's disease[3], defective as well as excessive autophagy is detrimental for muscle health[4] and uncontrolled autophagy could potentially harm or even kill an otherwise healthy cell.

Nucleation of a phagophore and biogenesis of a functional autophagosome is regulated by several multi-subunit complexes, including the ULK1 complex, the integral membrane protein mATG9 and its associated proteins, the class III phosphatidylinositol (PI) 3-kinase (PI3K) complex and two ubiquitin-like conjugation systems, resulting in the conjugation of ATG12 to ATG5 and ATG8/LC3 family members to phosphatidylethanolamine (PE)[5]. ATG5–ATG12 further associates with ATG16L1 and the resulting complex is recruited to endoplasmatic reticulum-associated PI(3)P-rich sites of phagophore nucleation (called omegasomes)[6] by the PI(3)P-binding protein WIPI2 (ref. 7). Further expansion of the phagophore to generate an autophagosome requires input from several membrane sources, including the endoplasmatic reticulum[8–10], mitochondria[9,11], plasma membrane[12] and recycling endosomes[13–16]. Recycling endosome-derived membranes are positive for ATG9 and ATG16L1, and essential for autophagosome formation[13–16].

The autophagic pathway involves lipids as signalling molecules, constituents and cargo of autophagosomes. However, the role of different lipids in autophagy is not clear[17,18]. PA was initially found to activate mammalian target of rapamycin (mTOR)[19], a well-known inhibitor of autophagy, in a PLD1-specific manner[20]. Recent studies have also implicated PLD1-generated PA in autophagosome formation[21,22] and in autophagosome–lysosome fusion[23]. PI(3)P, the lipid product of the class III PI3K complex, has a central role in autophagy and several PI(3)P-binding proteins in autophagy have been identified[17,24], including the FYVE domain proteins DFCP1, a marker for omegasomes[6], the scaffold protein ALFY that links cargo to the autophagic machinery for selective autophagy[25,26] and FYCO1, which is involved in trafficking of autophagosomes on microtubuli[27]. Furthermore, the WD-repeat protein WIPI2 also binds PI(3)P and is found at omegasomes[28].

Another group of phosphoinositide-binding proteins are the PX domain-containing proteins, but little is known about their involvement in autophagy. Here we show that the PX domain protein HS1BP3 negatively regulates autophagosome formation, PA levels and PLD activity. HS1BP3 binds PA through its PX domain, which leads to the recruitment of HS1BP3 to PLD1- and ATG16L1-positive autophagosome precursor membranes. We propose that HS1BP3, through its binding to PA and inhibition of PLD1 activity, provides a novel negative-feedback mechanism to ensure the proper regulation of autophagosome biogenesis.

Results

HS1BP3 is a negative regulator of autophagy. To identify PX domain proteins involved in autophagy, we recently performed an imaging-based short interfering RNA (siRNA) screen in HEK GFP-LC3 cells[13] and one of the candidate proteins was HS1BP3. Using the individual siRNA oligos from the screen, we find that depletion of HS1BP3 results in increased amounts of GFP-LC3 spots (autophagosomes) both in complete (fed) and nutrient-deplete (starved) medium in correlation with knockdown levels (Fig. 1a–c). Depletion of HS1BP3 also increases the total intensity of endogenous LC3 spots in starved cells (Supplementary Fig. 1a).

Since depletion of HS1BP3 increased the number of autophagosomes, we next investigated whether this is due to the increased formation or inhibited maturation and turnover of autophagosomes. To this end, cells were starved in the presence or absence of the lysosomal proton pump inhibitor Bafilomycin A1 (BafA1; which inhibits autophagosome maturation and lysosomal degradation) and autophagic flux monitored by quantification of the level of PE-conjugated LC3 (LC3-II)[29]. We find that LC3-II levels are significantly increased in HS1BP3-depleted cells both in complete medium and after starvation (Fig. 1d,e), and increase further in the presence of BafA1, indicating that autophagosome formation is increased on HS1BP3 depletion. As expected, LC3 lipidation is strongly inhibited in ULK1-depleted cells. We verified that LC3 messenger RNA (mRNA) levels are not significantly affected by HS1BP3 depletion (Supplementary Fig. 1b).

To further determine if depletion of HS1BP3 activates autophagy, we studied the degradation of the cargo receptor protein p62 (also known as Sequestosome-1), which is itself an autophagy substrate[30,31]. GFP-p62 expression was shut off in a stable cell line[32] and the amount of GFP-p62 remaining after starvation was measured by flow cytometry. Whereas about half of the initial GFP-p62 is degraded in control cells, GFP-p62 strongly accumulates in ULK1-depleted cells, as well as in cells treated with BafA1 (Fig. 1f). Consistent with an increase in GFP-LC3 spots and LC3 lipidation, GFP-p62 degradation increases by 20% in cells depleted of HS1BP3 (Fig. 1f), indicating increased autophagic flux. This was further confirmed by assessing the degradation of long-lived proteins, which preferentially happens through autophagy and is inhibited by the PI3K inhibitor 3-methyladenine. As shown in Fig. 1g, the release of free ^{14}C-valine from the degradation of previously radiolabelled long-lived proteins is increased in HS1BP3-depleted cells compared with control cells both in fed and starved conditions, further indicating that HS1BP3 is a negative regulator of autophagy.

To analyse a possible role of HS1BP3 in regulation of autophagy *in vivo*, we employed transient silencing of *Hs1bp3* in the zebrafish line Tg*(CMV:EGFP-map1lc3b)*[33], using a translational-blocking morpholino targeting the start site of the *Hs1bp3* mRNA. The overall homology between human and zebrafish Hs1bp3 is 36%, with the PX domain being highly conserved (67% homology; Supplementary Fig. 1c). At 2 days post fertilization (dpf), abundant GFP-LC3 puncta are present in the trunk region of the morphant compared with the control embryos (Fig. 2a–d) and this difference is even more pronounced after chloroquine treatment, known to block autophagosome degradation in zebrafish[34,35]. On injection of *in vitro*-transcribed-capped human *Hs1bp3* mRNA alongside the *Hs1bp3* morpholino, we observe a partial rescue of the phenotype at 2 dpf both with and without chloroquine treatment (Fig. 2a–d; Supplementary Fig. 1d). These results suggest that autophagy is significantly elevated in *Hs1bp3* morphant zebrafish at 2 dpf and that *Hs1bp3* also regulates autophagy *in vivo*.

HS1BP3 interacts with cortactin. HS1BP3 was originally identified as an interaction partner of the actin cross-linking protein HS1 (ref. 36). HS1 is exclusively expressed in cells of hematopoietic lineage, whereas other cells express the homologous protein cortactin[37]. We therefore asked whether

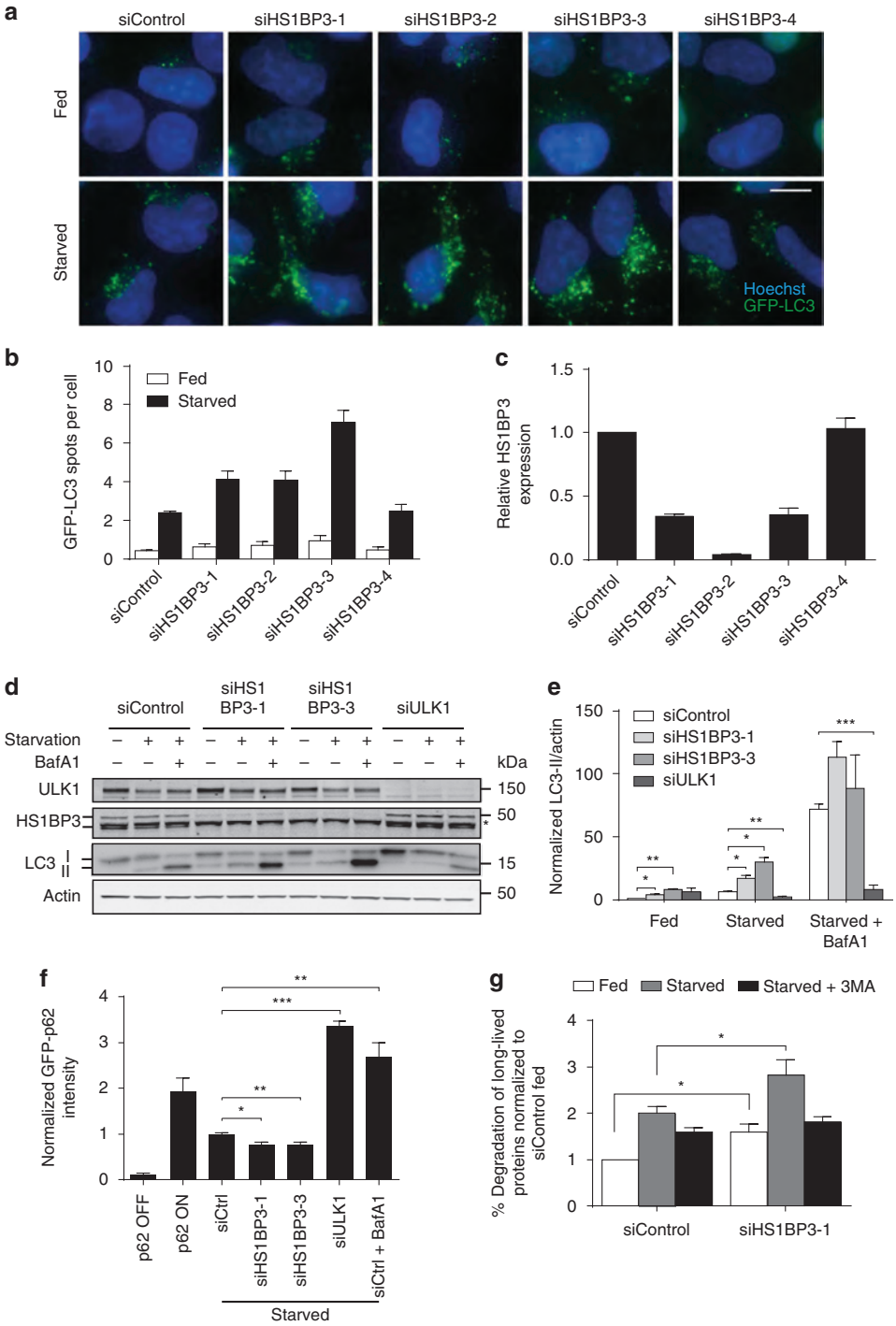

Figure 1 | HS1BP3 is a negative regulator of autophagy. (**a**) HEK GFP-LC3 cells were transfected with four individual siRNA oligonucleotides against HS1BP3. 72 h post transfection the cells were starved or not for 2 h in EBSS, followed by fixation and fluorescence microscopy. Scale bar, 10 μm. (**b**) The number of GFP-LC3 spots per cell in **a** was quantified by high-content analysis (mean ± s.d. from two independent experiments in triplicates, ~50,000 cells analysed per condition). (**c**) Relative expression of HS1BP3 after siRNA knockdown was measured by quantitative PCR with reverse transcription (mean ± s.d.). (**d**) HEK GFP-LC3 cells were transfected with the indicated siRNA oligos and starved or not for 2 h in EBSS in the presence or absence of BafA1. * Indicates an unspecific band in the HS1BP3 immunoblot. (**e**) The level of LC3-II/actin was quantified from immunoblots and normalized to siControl fed (mean ± s.e.m., $n=5$). (**f**) HEK GFP-p62 cells were transfected with siRNA against HS1BP3 or ULK1. Expression of GFP-p62 was induced by addition of tetracycline (compare ON versus OFF) for 48 h before expression was shut off and the cells were incubated in EBSS (starved) for 2.5 h to induce autophagic degradation of GFP-p62. GFP-p62 intensity was monitored by flow cytometry and normalized to starved siControl (siCtrl; mean ± s.e.m., $n=4$). (**g**) The degradation of long-lived proteins in HeLa cells transfected with control siRNA or siRNA against HS1BP3 was quantified as the release of ^{14}C-valine after 4 h starvation in the absence or presence of 3-methyladenine (3MA) and normalized to the degradation in fed control cells (mean ± s.e.m., $n=3$). *$P<0.05$, **$P<0.01$, ***$P<0.001$, by Student's *t*-test.

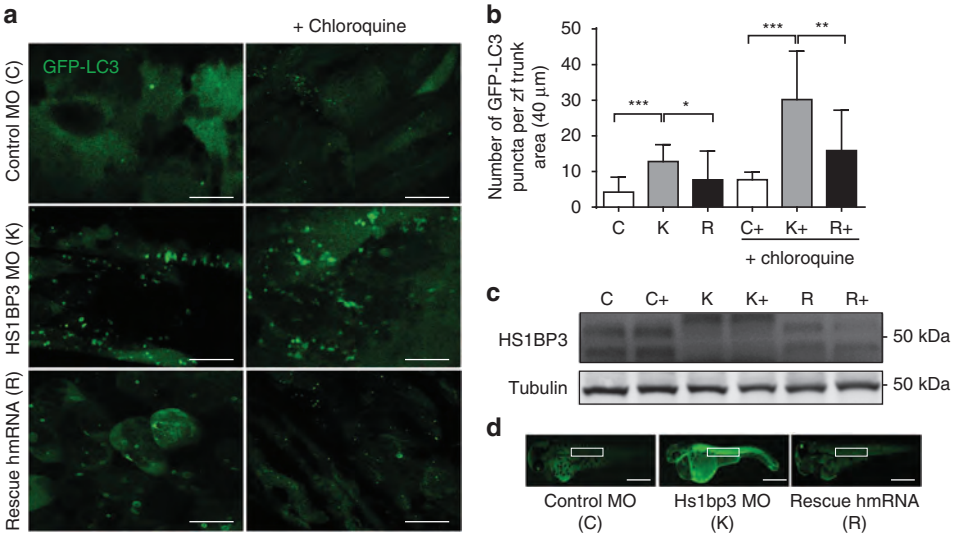

Figure 2 | HS1BP3 regulates autophagy in zebrafish. (**a**) Representative confocal images of GFP-LC3 puncta (autophagosomes) in the trunk area of GFP-LC3 transgenic zebrafish embryos injected with control morpholino (C), Hs1bp3 translational-blocking morpholino (K), and the human Hs1bp3 mRNA coinjected with the morpholino (R) and imaged at 2 dpf with or without pre-treatment with chloroquine (10 µM) for 6 h. Scale bars, 10 µm. (**b**) GFP-LC3 puncta were counted in the trunk region (marked in **d**) of the transgenic zebrafish embryos at 2 dpf (mean ± s.e.m., $n = 3$). Total of 7–13 embryos were used for each condition per experiment. $^{*}P < 0.05$, $^{**}P < 0.01$, $^{***}P < 0.001$, by Student's *t*-test. (**c**) Representative immunoblotting of Hs1bp3 and Tubulin in whole lysates of zebrafish embryos at 2 dpf, treated with or without chloroquine for 6 h before harvest. (**d**) Representative light fluorescent microscopy images of whole embryos at 2 dpf. Scale bars, 300 µm.

HS1BP3 also binds to cortactin and whether this interaction is involved in HS1BP3-mediated inhibition of autophagy. We find that endogenous cortactin co-immunoprecipitates with GFP-HS1BP3 (Supplementary Fig. 3a). The interaction is mediated by the SH3 domains of cortactin and HS1 (Supplementary Fig. 3b, lane 9 and 11), and is lost when a critical SH3 domain tryptophan is mutated to tyrosine (Supplementary Fig. 3b, lane 10 and 12). The HS1 and cortactin SH3 domains interact exclusively with the C-terminal part of HS1BP3 (HS1BP3-ΔPX, Supplementary Fig. 3c) containing four proline-rich regions (Fig. 4a). We can however not detect a role for cortactin in basal or starvation-induced autophagy (Supplementary Fig. 3d–e), indicating that binding of HS1BP3 to cortactin is not essential for its inhibitory function in autophagy.

HS1BP3 localizes to ATG9–ATG16L1-positive membranes. To identify the mechanisms underlying the role of HS1BP3 as a negative regulator of autophagy, the localization of HS1BP3 to autophagy-related membranes in HEK293 and U2OS cells was investigated. Cells were transfected with GFP- or mCherry-tagged HS1BP3 and their co-localization with WIPI2, ATG9, ATG16L1 or LC3 analysed by confocal imaging. While HS1BP3 is only occasionally detected on WIPI2-positive structures (Fig. 3a, white arrows), it co-localizes well with ATG9 and ATG16L1-positive membranes (Fig. 3a,b). Endogenous HS1BP3 also clearly co-localizes with endogenous ATG9 (Fig. 3c) and with GFP-ATG16L1-positive vesicles (Fig. 3d), and the co-localization is lost after HS1BP3 depletion (Fig. 3d, white arrowheads), demonstrating the specificity of the HS1BP3 antibody. In contrast, HS1BP3 does not show much co-localization with LC3-positive structures (Fig. 3e; Supplementary Fig. 2a) and does not interact with LC3 or GABARAP proteins (Supplementary Fig. 2b). Moreover, no co-localization of endogenous HS1BP3 with GFP-p62, -DFCP1 or -ATG14 is detected (Supplementary Fig. 2a).

Trafficking of ATG16L1 and ATG9 through recycling endosomes is important for autophagosome biogenesis[13–16]. Using confocal and live cell imaging, we find that the HS1BP3-, ATG9- and ATG16L1-positive membranes contain transferrin and transferrin receptor (TfR; Fig. 3b; Supplementary Fig. 5c) and seem to fuse with LC3-positive structures (Supplementary Movies 1–3), indicating they are recycling endosome-derived membranes. Depletion of HS1BP3 does not cause any quantitative changes in the early phagophore/omegasome markers GFP-DFCP1, WIPI2 and ATG16L1. Neither the total intensity of GFP-DFCP1 spots (Supplementary Fig. 2c) nor the number of endogenous WIPI2 or ATG16L1 spots (Supplementary Fig. 2d–e) are affected by HS1BP3 depletion. Taken together, we find that HS1BP3 localizes to ATG9 and ATG16L1-positive recycling endosome-derived membranes that contribute membrane to the forming autophagosome at a stage after omegasome formation, indicating that HS1BP3 regulates autophagy downstream or in parallel of the initial phagophore nucleation step.

HS1BP3 binds PA and regulates cellular PA levels. To investigate a possible role for HS1BP3 in regulation of membrane trafficking and/or biogenesis at the expanding phagophore, we first set out to characterize the lipid-binding specificity of the HS1BP3 N-terminal PX domain (Fig. 4a). PX domain proteins are known to mainly bind PI3P, but also other phosphoinositide-binding preferences have been described[38,39]. Using lipid-coated membrane strips, we find the HS1BP3 PX domain to bind strongly to PA, whereas full-length HS1BP3 binds PA, as well as monophosphorylated phosphoinositides (Fig. 4b; Supplementary Fig. 4a). The lipid specificities of purified HS1BP3 proteins (full length or PX domain) was further explored using liposome floatation experiments. We find that the binding of both HS1BP3 and the PX domain to PA increase with increasing concentrations of liposome PA (Fig. 4c).

Using liposomes containing various phosphoinositide species, we could confirm that the PX domain of HS1BP3 also has

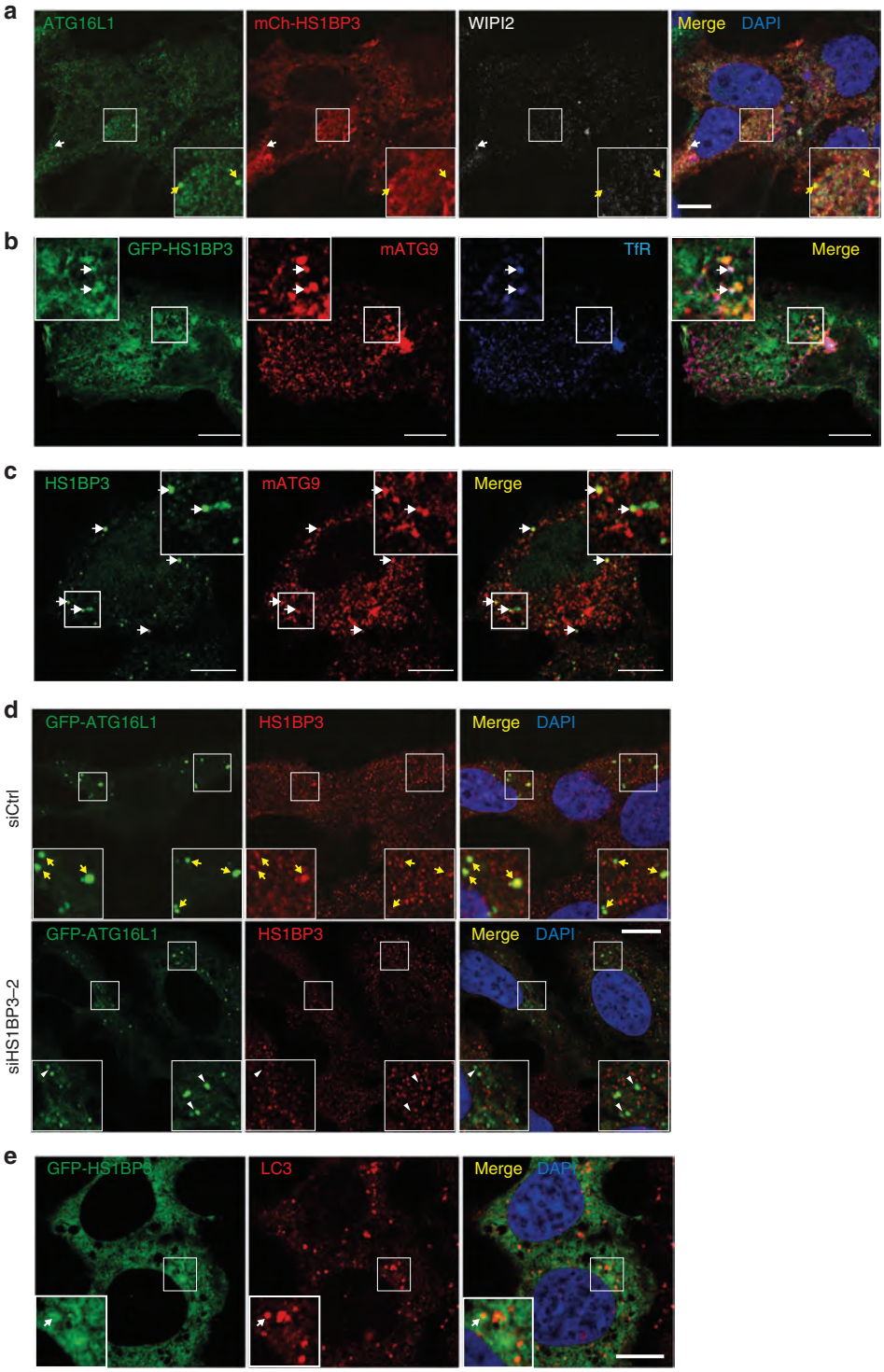

Figure 3 | HS1BP3 localizes to ATG16L1- and ATG9-positive vesicles. HEK293 and U2OS cells expressing the indicated proteins were starved for 2 h before fixation and immunostaining with the indicated antibodies. Confocal micrographs show: (**a**) HEK cells expressing mCherry-HS1BP3 stained for endogenous ATG16L1 and WIPI2. Yellow arrows mark HS1BP3- and ATG16L1-positive structures. White arrow marks HS1BP3-, ATG16L1- and WIPI2-positive structure. (**b**) Co-localization of GFP-HS1BP3 with endogenous ATG9 and TfR (white arrows show triple co-localization) in U2OS cells. (**c**) Co-localization of endogenous HS1BP3 with endogenous ATG9 in HEK cells. (**d**) Control or HS1BP3-depleted U2OS cells expressing GFP-ATG16L1 stained for endogenous HS1BP3. Yellow arrows indicate ATG16L1-positive structures that are positive for HS1PB3, while white arrow heads indicate ATG16L1-positive structures that are not positive for HS1BP3. Note that in addition to the specific staining (co-localization with ATG16L1), the HS1BP3 antibody also recognizes other proteins non-specifically both on immunofluorescence and western blotting (Fig. 1d). (**e**) HEK cells expressing GFP-HS1BP3 stained for endogenous LC3. Scale bars, 10 μm.

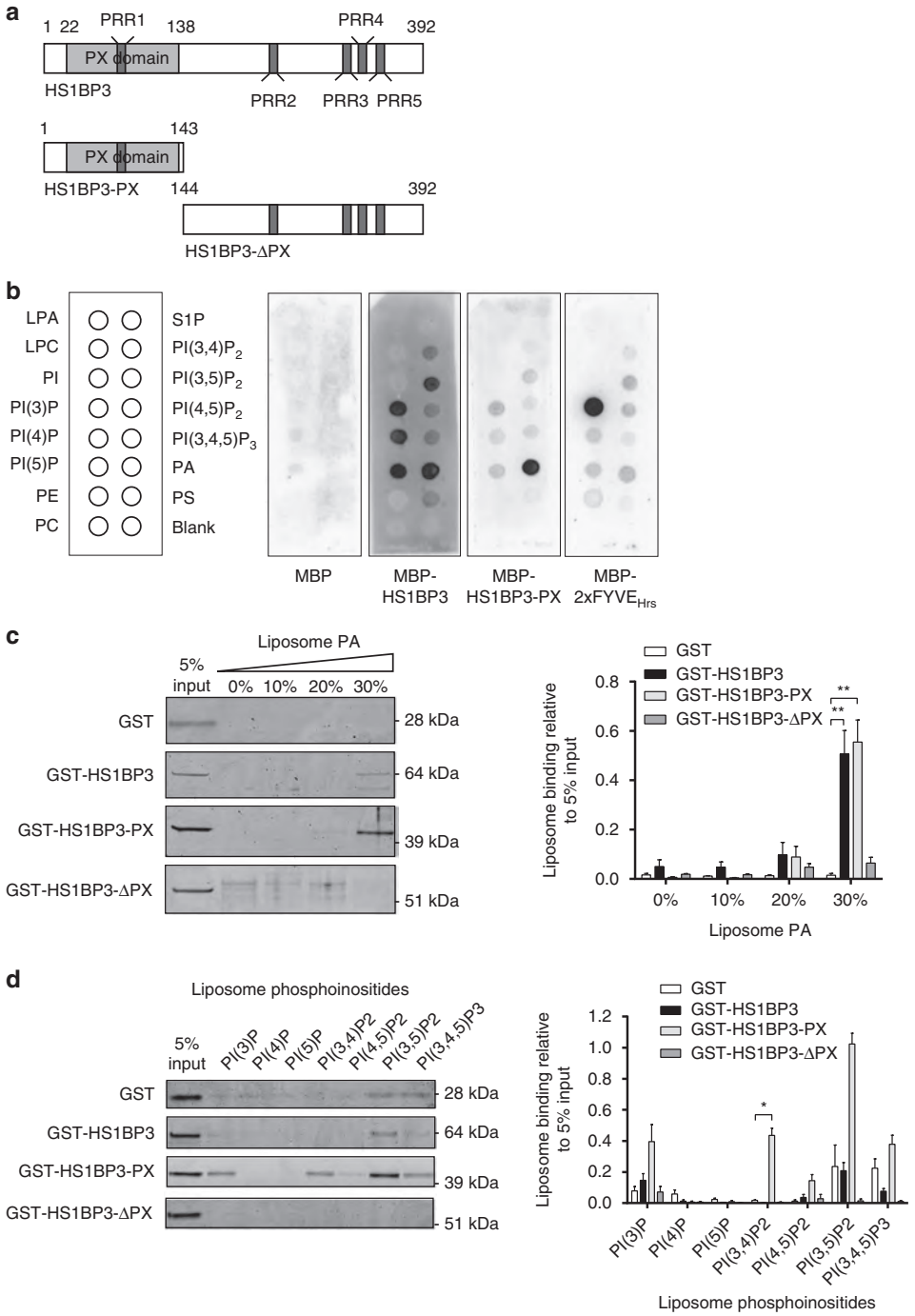

Figure 4 | HS1BP3 binds PA through its PX domain. (**a**) Domain structure of HS1BP3: an N-terminal PX domain followed by an unstructured C terminus. The positions of five proline-rich regions (PRRs) are indicated. HS1BP3 truncations lacking the C-terminal (HS1BP3-PX) or the PX domain (HS1BP3-ΔPX) are shown. (**b**) Membranes spotted with the indicated lipids were incubated with 1 μg ml^{-1} of the indicated recombinant MBP-tagged proteins in a lipid protein overlay assay and bound proteins were detected with anti-MBP immunoblotting. (**c**,**d**) Liposomes with the indicated molar ratios of dioleyoyl-phosphatidic acid (DOPA) (**c**) or the indicated phosphoinositides (**d**) were incubated with GST or GST-tagged HS1BP3 protein constructs. Protein binding to liposomes was analysed by a lipid floatation assay. Representative coomassie-stained gels are shown and quantified from three independent experiments (mean ± s.e.m.). Significance is calculated as compared with GST control. If significance is calculated as compared to GST-HS1BP3-ΔPX, then GST-HS1BP3-PX shows significantly increased binding to PI(3)P, PI(3,4)P2, PI(4,5)P2, PI(3,5)P2 and PI(3,4,5)P3. *$P<0.05$, **$P<0.01$, by Student's *t*-test.

increased affinity for PI(3)P, PI(3,4)P2 and PI(3,5)P2 as compared with the GST control (Fig. 4d). The full-length HS1BP3 protein also shows affinity for phosphoinositides and if compared with GST-HS1BP3-ΔPX it binds several of the same phosphoinositides as the PX domain alone, most notably PI(3)P and PI(3,5)P2 (Fig. 4d). The discrepancy between the data obtained using lipid strips and liposomes is most likely due to differences in the context that the lipids are presented,

where the liposomes more closely resemble the context proteins bind to membranes in cells. We conclude that HS1BP3 binds to PA and several phosphoinositides and we speculate that HS1BP3 has phosphoinositide affinity *in vivo* for PI(3,5)P2 and PI(3)P. Interestingly, the HS1BP3 PX domain co-localizes with ATG16L1 (Supplementary Fig. 4b), suggesting that the lipid affinity of the PX domain contributes to its specific recruitment to ATG16L1-positive membranes.

To get an unbiased quantification of a wide range of lipids in HS1BP3-depleted cells compared with control cells under starvation conditions, the total cellular lipid content was measured by lipidomics (Fig. 5a). Interestingly, whereas the quantities of several lipids are significantly altered (Fig. 5a; Supplementary Fig. 4c); the quantitatively biggest effect is on PA levels, as depletion of HS1BP3 causes a twofold increase in the total abundance of the lipid (Fig. 5a). In total, the levels of 9 out of

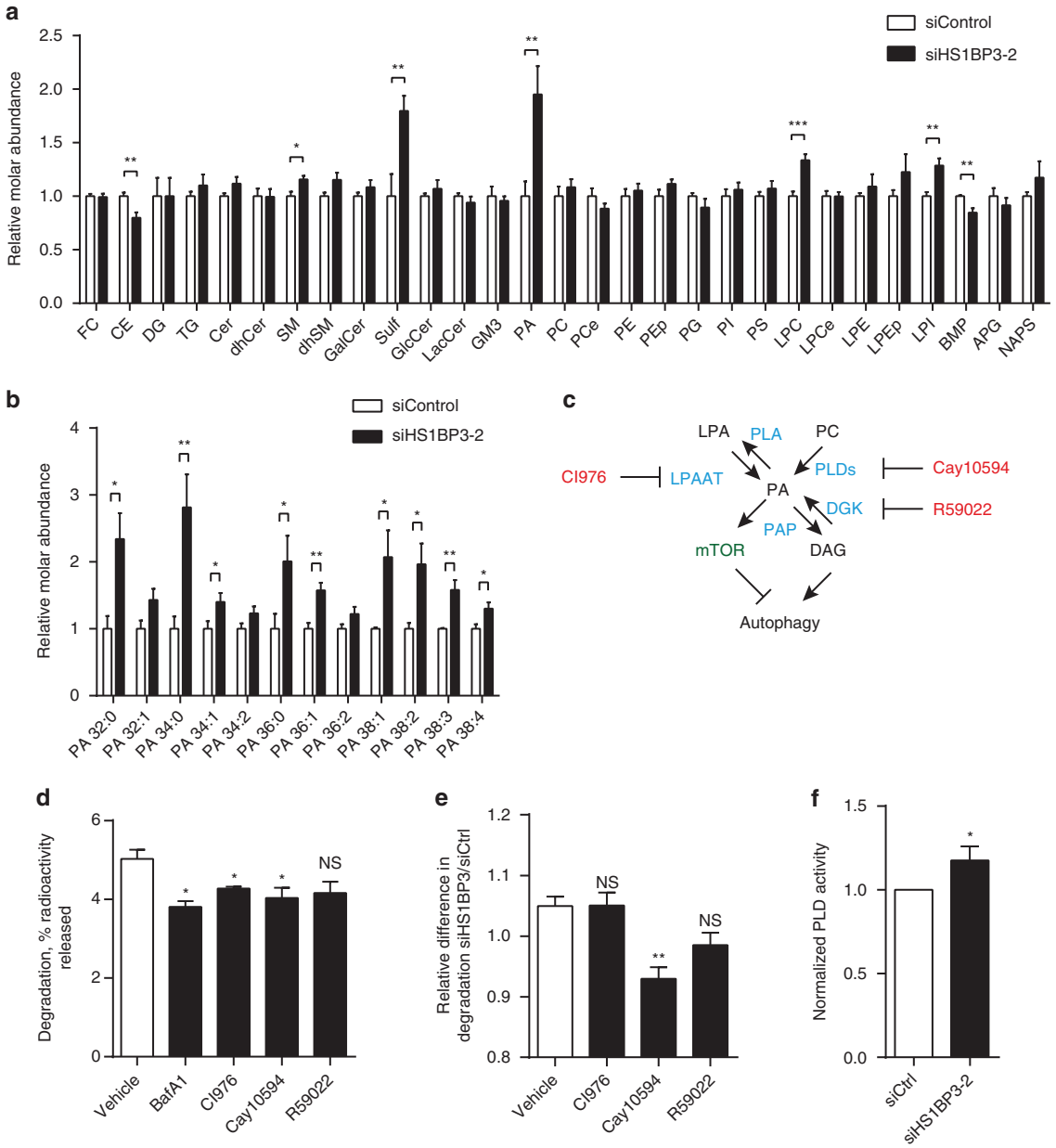

Figure 5 | Autophagy is dependent on PA synthesis and HS1BP3 affects PLD activity. (**a**) HEK cells were treated with non-targeting or HS1BP3 siRNA and starved for 2 h. The total lipid content was extracted and analysed by mass spectrometry. Only lipid species that were present in all experimental runs were included. The measured lipid concentrations were first normalized to total lipid per sample to determine molar percentages for each lipid subclass and species, before normalizing to the average molar percentage of controls (mean ± s.e.m., $n=6$). For a full list of all lipids with abbreviations, see Supplementary Table 1. The lipidomics data sets have been deposited in the Dryad Digital Repository (doi:10.5061/dryad.gq3fk). (**b**) The relative molar abundance of all 12 PA species is shown. (mean ± s.e.m., $n=6$). (**c**) Schematic overview of the enzymes (blue) governing the generation and turnover of PA from other lipid species (black) and the drugs (red) used to inhibit these pathways. (**d**) Degradation of long-lived proteins in HEK cells was quantified as the release of ^{14}C-valine after 4 h starvation in the presence of the indicated inhibitors (mean ± s.e.m., $n=3$). (**e**) The relative difference in long-lived protein degradation between HEK cells with siCtrl and siHS1BP3 was measured for the indicated inhibitors (mean ± s.e.m., $n=3$). (**f**) PLD activity was measured in HEK lysates of cells transfected with non-targeting or HS1BP3 siRNA (mean ± s.e.m., $n=3$). $^{*}P<0.05$, $^{**}P<0.01$, by Student's *t*-test.

12 PA species are increased by HS1BP3 depletion (Fig. 5b). Interestingly, many of these PA species have been shown to be products of PLD activity[40,41].

PA is a cone-shaped lipid that has been found to stimulate both autophagosome biogenesis[21,22] and autophagosome–lysosome fusion[23]. On the other hand, PA has been shown to activate mTOR signalling[19], which inhibits autophagy. We therefore asked whether depletion of HS1BP3 might stimulate autophagy through changes in mTOR activity. Phosphorylation of the mTORC1 substrate S6 Kinase (pS6K) is however not affected by HS1BP3 depletion (Supplementary Fig. 4d), indicating that the increased PA levels seen on HS1BP3 depletion is not inducing autophagy through decreased mTORC1 signalling.

HS1BP3 regulates PA levels and autophagy through PLD1. Several metabolic pathways lead to PA formation (Fig. 5c)[42]. To first determine which of these contribute to increased autophagic flux, cells were treated with inhibitors specific for each pathway followed by quantification of autophagic degradation of long-lived proteins (Fig. 5d). We find that inhibitors of PLD activity (Cay10594, inhibits both PLD1 and PLD2) and lysophosphatidic acid acyltransferases (LPAATs; CI-976) inhibit autophagic flux, whereas an inhibitor of diacylglycerol kinase (R50922) has no significant effect (Fig. 5d). These observations taken together with the increased levels of PA and autophagy on HS1BP3 depletion suggested that HS1BP3 may be inhibiting autophagy as a negative regulator of one of these PA-generating pathways. We reasoned that if HS1BP3 depletion increased the activity of one of the pathways, then chemical inhibition of this pathway should abolish the increased autophagy seen in HS1BP3-depleted cells. Indeed, the relative inhibition of autophagy by the PLD inhibitor Cay10594 is significantly larger in cells depleted of HS1BP3, compared with control cells and cells treated with inhibitors of LPAATs or diacylglycerol kinase (Fig. 5e), suggesting that HS1BP3 may regulate PA levels through PLDs. In line with this, we find that the total activity of PLD enzymes is increased in cell lysates of HS1BP3-depleted cells compared with control cells (Fig. 5f), in line with our data showing that HS1BP3 depletion leads to increased PA levels (Fig. 5a).

To determine which of the PLD enzymes are contributing to the HS1BP3 phenotype, we analysed the localization of GFP-PLD1 and -PLD2 in relation to the autophagy markers LC3 and ATG16L1. GFP-PLD2 staining is concentrated at the plasma membrane with no co-localization with either ATG16L1 (Fig. 6a) or LC3 (Supplementary Fig. 5a). In contrast, GFP-PLD1 shows extensive co-localization with ATG16L1-positive puncta (Fig. 6a), and is often seen in close proximity to LC3-positive puncta (Supplementary Fig. 5a,c). The majority of the vesicles stained by GFP-PLD1 and ATG16L1 contain transferrin and TfR (Fig. 6b), and seem to fuse with Cherry-LC3B-positive structures (Supplementary Fig. 5c; Supplementary Movies 1 and 2), indicating that they are recycling endosome-derived vesicles destined for autophagosome biogenesis. HS1BP3 is also detected at the TfR- and PLD1-positive structures (Supplementary Fig. 5b). Because PLD1, and not PLD2, localize to ATG16L1-positive membranes (Fig. 6a), we conclude that the effect of HS1BP3 on PLD activity is most likely through the regulation of PLD1 on recycling endosomes or vesicles derived thereof.

To get some mechanistic insight into how HS1BP3 regulates PLD1 activity at the Atg16L1-positive membranes, we investigated the localization of PLD1 to ATG16L1-positive structures in the absence or presence of HS1BP3. Interestingly, there is a significant increase in the amount of ATG16L1-positive vesicles with GFP-PLD1 staining in HS1BP3-depleted cells compared with control cells (Fig. 6c), indicating that HS1BP3 may regulate PLD1's access to these vesicles.

As both HS1BP3 and PLD1 have a PX domain with similar lipid-binding specificities (Fig. 4; ref. 43), we hypothesized that they might compete for binding to lipids in ATG16L1-positive membranes. In line with this notion, the co-localization between HA-PLD1 and endogenous ATG16L1 is significantly decreased in cells expressing the full length or PX domain of GFP-HS1BP3 compared with control cells expressing GFP only, but not in cells expressing HS1BP3 lacking the PX domain (GFP-HS1BP3 ΔPX; Fig. 6d,e).

We further looked for protein–protein interactions between these proteins that could explain their apparent co-localization and functional relationship, but were unable to detect any interactions between over-expressed or endogenous PLD1, HS1BP3 and ATG16L1 under the conditions tested (Supplementary Fig. 6a). Taken together, our data indicate that HS1BP3 prevents access of PLD1 to ATG16L1-positive vesicles and we speculate that the two proteins compete for binding to lipids in the ATG16L1-positive membranes.

To further map the functional relationship between HS1BP3 and PLD1 in regulation of autophagy, endogenous LC3 puncta were quantified in cells depleted of HS1BP3 and/or PLD1, and at the same time transfected with GFP, GFP-HS1BP3 or GFP-PLD1 (Fig. 7a). While depletion of HS1BP3 increases the number of LC3 spots and LC3-II levels (in line with data in Fig. 1), this effect is reversed in cells co-depleted of PLD1 (Fig. 7a; Supplementary Fig. 6b), indicating that the increase in autophagy seen with HS1BP3 depletion is dependent on PLD1, in line with our previous observation of the HS1BP3-mediated increase in autophagy being reverted by the use of PLD inhibitors (Fig. 5e). Moreover, overexpression of GFP-PLD1 causes a significant increase in the amount of LC3-positive spots (Fig. 7a), with no further increase on concurrent depletion of HS1BP3, further supporting that HS1BP3 and PLD1 are part of a common mechanism, where HS1BP3 acts on autophagy through regulation of PLD1.

Taken together, our observation that HS1BP3 inhibits the localization of PLD1 to ATG16L1-positive vesicles suggests that the effect of HS1BP3 on autophagy is through the regulation of PLD1-generated PA on ATG16L1-positive autophagosome precursors (Fig. 7b). In light of the binding of HS1BP3 to PA, we propose a mechanism by which HS1BP3 regulates PLD1 by providing negative feedback on PA production through regulating the access of PLD1 to target membranes.

Discussion

Autophagosome formation must be properly regulated to balance the need to ensure cellular quality control and nutrient availability during starvation, with the necessity to prevent excessive autophagosome formation and detrimental degradation of crucial cellular components. We here identify the PX domain protein HS1BP3, as an inhibitor of the autophagosome formation and autophagic degradation through a negative-feedback mechanism, involving the regulation of PLD1 activity, and hence PA levels, in ATG16L1-positive membranes. Depletion of HS1BP3 affects both PLD activity in lysates and PLD1 localization to ATG16L1-positive vesicles, suggesting that HS1BP3 acts as a sensor and regulator of local PA levels. On its recruitment, HS1BP3 will inhibit PLD1 activity on ATG16L1-positive autophagosome precursors, thereby reducing their PA content and autophagosome formation (Fig. 7b).

Many PX domains bind PI(3)P, but there are also other demonstrated lipid-binding specificities[38,39]. We found that both the full-length protein and the PX domain of HS1BP3 bind to

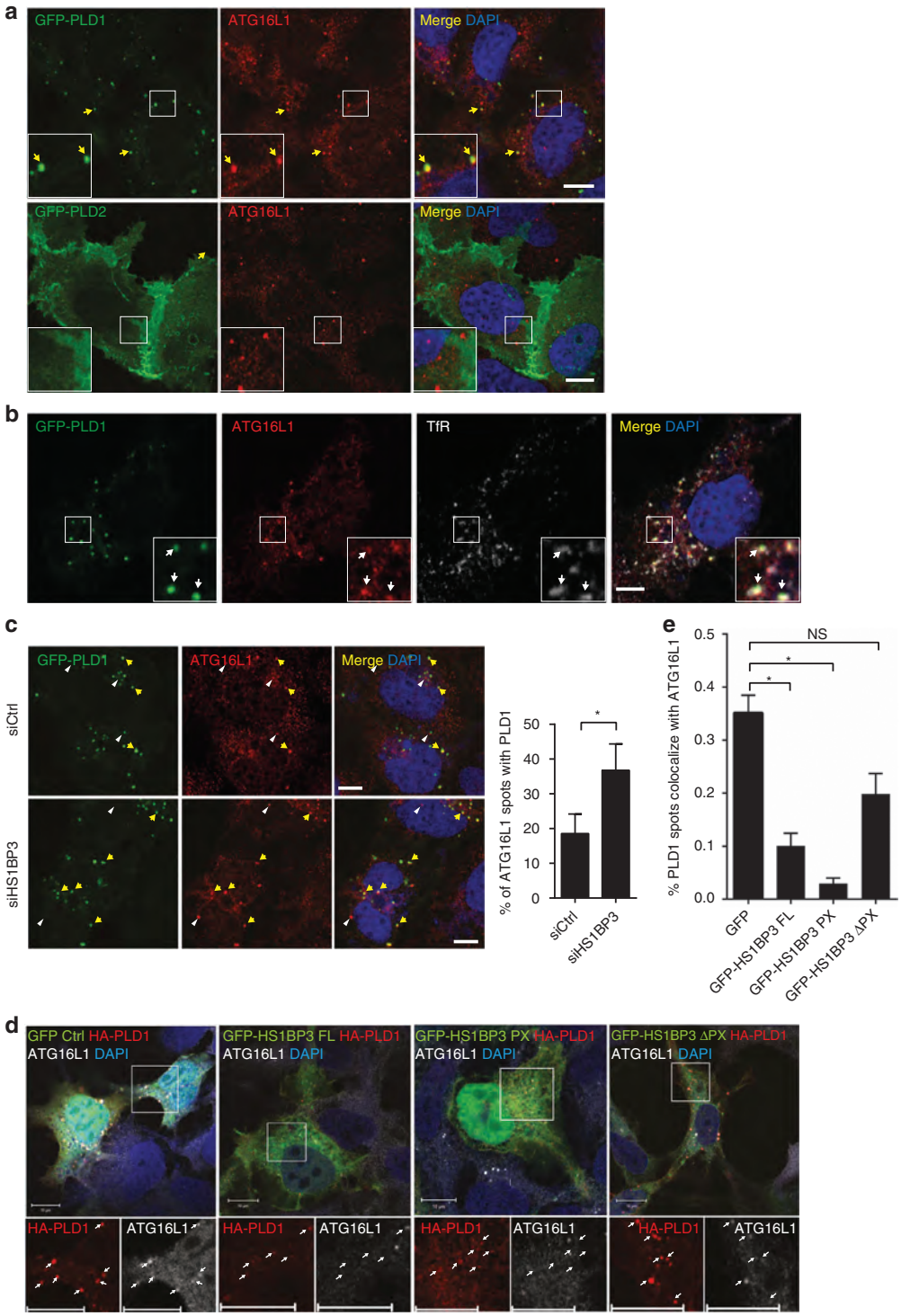

Figure 6 | PLD1 co-localization with ATG16L1 is affected by HS1BP3. (**a**) HEK cells were transfected with GFP-tagged PLD1 or PLD2. After starvation and fixation the cells were immunostained for ATG16L1 and analysed by confocal microscopy. (**b**) HEK cells were transfected with GFP-PLD1, starved, fixed and immunostained for ATG16L1 and TfR. (**c**) HEK cells were first treated with non-targeting or HS1BP3 siRNA, then transfected to express GFP-PLD1, starved, fixed and immunostained for ATG16L1. Yellow arrows indicate ATG16L1 vesicles positive for PLD1 and white arrow heads indicate ATG16L1 vesicles negative for PLD1. Co-localization of GFP-PLD1 to ATG16L1 vesicles was quantified in transfected cells using the ImageJ plugin Squassh, using 10 pictures of each condition from three independent experiments (mean ± s.e.m., $n=3$). (**d**) HEK cells were transfected with HA-PLD1 together with GFP, GFP-HS1BP3 full-length, -PX or ΔPX constructs, starved and stained for endogenous ATG16L1. Arrows indicate co-localization between ATG16L1 and HA-PLD1. (**e**) Co-localization of HA-PLD1 with endogenous ATG16L1 vesicles was quantified in transfected cells in **d** with the Zen software (Zeiss) using 10 pictures of each condition from three independent experiments (mean ± s.e.m., $n=3$). Scale bars, 10 μm. *$P<0.05$, by Student's *t*-test.

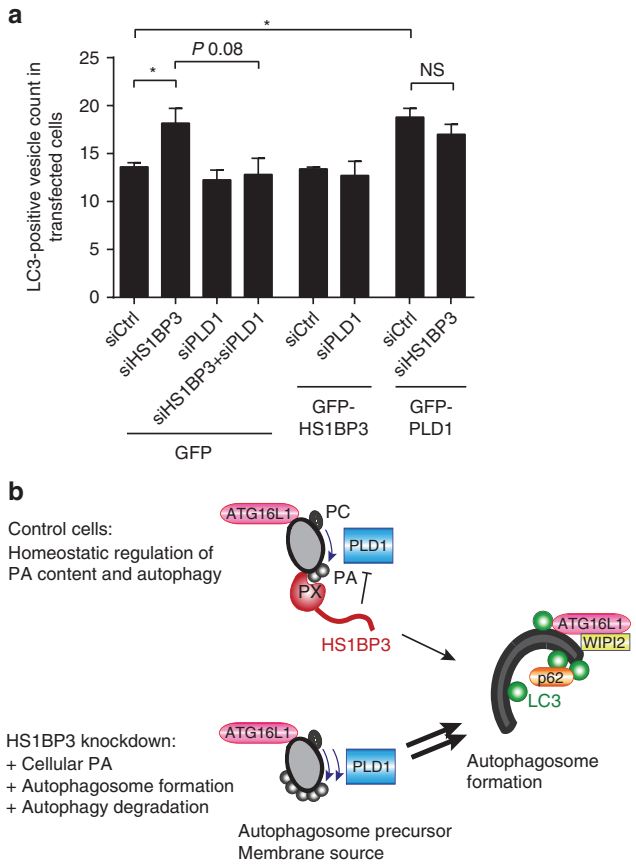

Figure 7 | HS1BP3 regulates autophagy through PLD1. (**a**) HEK cells were first treated with the indicated siRNA and then transfected with the indicated GFP-tagged construct. Cells were starved and fixed before immunostaining for endogenous LC3. LC3 spots were counted only in transfected cells, minimum 200 transfected cells per condition in three independent experiments (mean ± s.e.m., $n=3$). *$P<0.05$, by Student's *t*-test. (**b**) Model for the role of HS1BP3 in autophagy. PLD1 generates PA on ATG16L1-positive autophagosome precursor membranes. HS1BP3 is recruited to these membranes by the generated PA, inhibiting PLD1 activity and displacing it from the ATG16L1 vesicles. HS1BP3 thus provides a negative feedback on PA generation on these vesicles. If HS1BP3 is depleted from the cells, this negative feedback is lost, causing the PA concentrations of these membranes to increase and thereby drive increased autophagosome formation.

PA and phosphoinositides. PA binding by PX domains has previously been reported. A study of the PX domain of PLD1 demonstrated binding to PI(3,4,5)P3, PI(3)P, as well as other PI species and a moderate affinity for PA in a separate binding pocket on the PX domain[43]. Interestingly, the simultaneous binding of both sites was shown to increase the membrane affinity of the PX domain[43]. Similarly, the PX domain of the p47 subunit of NADPH oxidase was found to simultaneously bind PI(3,4)P2 and PA in separate binding pockets, increasing its membrane affinity[44]. Strikingly, we observed a competition between HS1BP3 and PLD1 for binding to ATG16L1-positive precursors. Having a similar lipid-binding specificity may be the basis of this competition between HS1BP3 and PLD1 for membrane binding, and this is something that will be interesting to explore further in future studies.

We also found that the LPAAT pathway of PA generation contributes to autophagy, demonstrating that the involvement of PA in autophagy is not limited to PLD1. The exact mechanism(s) underlying the role of PA in stimulation of autophagosome biogenesis is not clear and might be related to its role as a second messenger, but could also be associated with PA having a direct structural role in membrane curvature and/or fusion due to the unique characteristics of PA in a lipid bilayer. PA is the only anionic phospholipid that induces negative membrane curvature due to its cone shape under physiological conditions[45]. Cone-shaped lipids such as PA also facilitate penetration of proteins into the membrane, since the lipid head groups are more loosely packed[46], as shown to be important for insertion of ATG3 in the forming phagophore and subsequent lipidation of LC3/GABARAP[47].

Another relevant characteristic of PA is the demonstrated fusogenic properties of this lipid. PLD activity has been demonstrated as essential for various vesicle fusion events, such as sporulation in yeast[48], mitochondrial fusion[49] and exocytosis[50]. We speculate that the increased autophagy seen in HS1BP3-depleted cells might be facilitated by PA-mediated changes in the fusogenic properties of the ATG16L1-positive autophagosome precursors. Homotypic fusion of ATG16L1-positive vesicles has previously been found to facilitate their contribution to autophagosome formation and this was demonstrated to be dependent on the SNARE protein VAMP-7 (ref. 51). Intriguingly, VAMP-7 was recently described as an effector of PLD1 in neurite outgrowth[52], suggesting a possible mechanism by which PLD1-generated PA could affect autophagy. HS1BP3 is detected on ATG16L1 vesicles that also contain ATG9 and TfR, suggesting they are of recycling endosome origin. We recently identified the PX-BAR protein SNX18 as a positive regulator of autophagosome biogenesis by tubulation of recycling endosome membrane for the delivery to phagophore nucleation sites[13]. The RAB11-binding protein TBC1D14 is another negative regulator of autophagy found to regulate the recycling endosome membrane remodelling[15]. It will be interesting to explore how these membrane-associated proteins regulate the recycling endosome dynamics and how potential qualitative changes in these vesicles affect autophagy through homotypic and possibly heterotypic fusion processes.

In conclusion, we have identified HS1BP3 as a novel negative regulator of autophagy and cellular PA levels. We propose that PLD1 generates PA on ATG16L1-positive autophagosome precursor membranes and that HS1BP3 is recruited to these membranes by binding to PA (Fig. 7b). HS1BP3 affects the ability of PLD1 to generate PA, as well as regulating the access of PLD1 to ATG16L1-positive vesicles, changing the properties of these membranes and thereby providing a homoeostatic regulation of autophagy. HS1BP3 thus functions as a negative-feedback mediator of PA levels to regulate autophagosome formation.

Methods

Cell lines and inhibitors. HeLa, HEK and U2OS cells were from American Type Culture Collection and were maintained in Dulbecco's modified Eagle's medium (Gibco) supplemented with 10% fetal bovine serum (FBS), 5 U ml^{-1} penicillin and 50 μg ml^{-1} streptomycin. The HEK 293A GFP-LC3 cell line[53] was a kind gift from S. Tooze, Cancer Research UK, London, UK. The HEK GFP-DFCP1 cell line[6] was a kind gift from N. Ktistakis, Babraham Institute, Cambridge, UK. The HEK GFP-p62 cell line was a kind gift from G. Bjørkøy, HiST, Trondheim, Norway. All cell lines have been tested negative for mycoplasma. Bafilomycin A1 (Enzo Lifesciences) was used at 100 nM. CI 976 (Tocris Bioscience), Cay10594 (Cayman Chemical) and R59022 (Tocris Bioscience) were used at 20 μM. Glass support was coated by 20 μg ml^{-1} fibronectin (Sigma) before plating HEK cell lines to avoid the cells from detaching from the surface. For starvation in nutrient-deplete medium, the cells were incubated in Earls Balanced Salt Solution (EBSS; Invitrogen), with the exception of the HEK GFP-DFCP1 cells that were starved as described previously[6] in 140 mM NaCl, 1 mM $CaCl_2$, 1 mM $MgCl_2$, 5 mM glucose and 20 mM Hepes, pH 7.4.

Antibodies and dyes. The following primary antibodies were used: mouse anti-cortactin (Upstate, 05-180, 1:1,000), mouse anti-GFP (Clontech, 632381,

1:1,000), mouse anti-Flag (Sigma, F1804, 1:500), mouse anti-MBP (NEB, e8032S, 1:10,000), rabbit anti-ULK1 (Santa Cruz, sc-33182, 1:250), rabbit anti-HS1BP3 (GeneTex, GTX107715, 1:10,000 for WB and 1:500 for IF), rabbit anti-LC3 (Cell Signaling, 27755, 1:1,000 for WB), mouse anti-β-actin (Sigma, SAB1305567 1:20,000), mouse anti-myc (DSHB, 9E10, 1:20), mouse anti-alpha tubulin (Sigma, T5168, 1:20,000), rabbit anti-LC3 (MBL, PM036, 1:500 for IF), mouse anti-p62 (BD biosciences, 610833, 1:1,000 for WB), goat horseradish peroxidase (HRP)-conjugated anti-GST (Abcam, ab58626, 1:10,000 for phosphatidylinositol phosphate (PIP) strips), rabbit anti-phospho-AKT Ser473 (Cell Signaling, 4060, 1:2,000), rabbit anti-phospho-p70-S6K Thr389 (Cell Signaling, 9202, 1:1,000), rabbit anti-p70-S6K (Cell Signaling, 9205, 1:1,000), rabbit anti-ATG16L1 (MBL, PM040, 1:200), mouse anti-TfR CD71 (Santa Cruz, sc-65877, 1:200), mouse anti-WIPI2 (kind gift from Sharon Tooze, 1:2,000), rabbit anti-PLD1 (Cell Signaling, 3832S, 1:200), mouse anti-HA (Abcam, ab18181, 1:200), hamster anti-mAtg9 (kind gift from Sharon Tooze, 1:1,000). HRP- and Cy2/3/5-conjugated secondary antibodies were obtained from Jackson Immunolabs. Far-red fluorophore-conjugated secondary antibodies were from LI-COR. Transferrin–Alexa 647 was from Invitrogen.

Transfection of siRNA oligonucleotides and western blotting. siRNA oligonucleotides were Dharmacon ON-TARGET plus; HS1BP3-1J-013029-09 AAGAAGGAGUGACCGGUAU, HS1BP3-2J-013029-10 UGAAGAGGCUUUCG ACUUU, HS1BP3-3J-013029-11 GAGCCUGAAGGGCGAGGAU, HS1BP3-4J-013029-12 UCCCAAAGUGGCCGUGAAA, ULK1 J-005049-06 CCACGCAG-GUGCAGAACUA, cortactin CCCAGAAAGACUAUGUGAAAGGG[54] and PLD1 SmartPool consisting of four oligonucleotides pooled together. An amount of 20–100 nM siRNA was delivered to the cells by Lipofectamine RNAi max (Invitrogen). To demonstrate specific protein knockdown and monitor LC3 levels, the cells were lysed in 25 mM Hepes pH 7.5, 125 mM K-acetate, 2.5 mM Mg-acetate, 5 mM EGTA, 1 mM DTT and 0.5% NP-40 supplemented with Complete protease inhibitor (Roche). Protein concentration was measured by Biorad Protein Assay to run equal amounts of cell lysate on SDS–polyacrylamide gel electrophoresis (PAGE), followed by western blotting using specified primary antibodies and secondary antibodies for enhanced chemiluminescent (ECL) detection or far-red fluorescence. For ECL detection: membranes were incubated with HRP-conjugated secondary antibodies detected by the Supersignal West Dura Extended Duration Substrate kit (Pierce). Imaging and quantification of protein levels were performed using the Syngene gel documentation unit, Genesnap acquisition software and GeneTools analysis software. For far-red fluorophores: membranes were incubated with far-red fluorophore-conjugated secondary antibodies, and detection and analysis was performed by LI-COR Odyssey imaging. Uncropped scans of western blots are found in Supplementary Fig. 7.

Plasmids and transfection for ectopic expression. HS1BP3 complementary DNA (cDNA) was amplified by PCR using primers 5′-ATAGTCGA-CATGCAGTCCCCGGCGGTGCTC-3′ and 5′-ATAGCGGCCGCTCAGAAGA-GACTGGGGGCGG-3′ from a cDNA library made by reverse transcription (Biorad iScript) from mRNA isolated from HEK cells, TA cloned into pCR2.1-TOPO (Invitrogen) and subcloned into pENTR1A (Invitrogen) using *Sal*I and *Not*I restriction sites. From there, sequences coding for HS1BP3-PX and HS1BP3-ΔPX were amplified by PCR using primers 5′-ATAGTCGACATGCAGTCCCCGGCGG TGCTC-3′and 5′-ATAGCGGCCGCTCAGGATCTGGTACCTAAGAACTC-3′ or 5′-ATAGTCGACGCTGCAGGGCTCACCAGCAG-3′ and 5′-ATAGCGGCCGCT CAGAAGAGACTGGGGGCGG-3′, respectively, and cloned into pENTR1A (Invitrogen). Tagged variants were made by Gateway LR cloning (Invitrogen) into respective pDEST vectors (Invitrogen). See Supplementary Table 2 for a full list of plasmids used in this study. To transfect cells with plasmids encoding GFP- or mCherry-tagged HS1BP3 variants, the plasmids were delivered to the cells by forward transfection with FuGene (Roche) or Lipofectamine 2000 (Invitrogen) before further treatment as described.

Microscopy. siRNA-treated HEK GFP-LC3 cells grown on glass support, were starved or not for 2 h, pre-permeabilized on ice with 0.05% saponin in 80 mM K-Pipes pH 6.8, 5 mM EGTA and 1 mM $MgCl_2$ before fixation in 3% paraformaldehyde (PFA) or fixed directly in methanol for 10 min at −20 °C. The nuclei were counterstained with 1 μg ml^{-1} Hoechst in phosphate-buffered saline or mowiol. The number of GFP-LC3 spots was quantified using the automated Olympus ScanR microscope equipped with a ULSAPO 40× objective and the corresponding analysis program or by an automated Zeiss CellObserver equipped with a 40× EC Plan Neofluar objective, and using the physiology module of the Zeiss Assaybuilder software. For immunostaining and confocal analysis, cells were grown on glass cover slips and after the described treatments, fixed in 3% PFA for 15 min on ice or in methanol for 10 min at −20 °C and mounted in mowiol containing 1 μg ml^{-1} Hoechst or 4,6-diamidino-2-phenylindole to stain the nuclei. Confocal images were taken on an Olympus confocal microscope equipped with a UPlanSApo 60× objective. Co-localization of stainings of interest from confocal images was quantified using the ImageJ-based Squassh plugin[55]. The plugin subtracts background, segments the image into vesicles in each channel and co-localization is quantified as degree of signal intensity overlap in the segmented regions. Cell mask thresholding was used to include vesicles only in transfected cells.

For live cell imaging, HEK293A cells were plated in complete media in wells of Lab-Tek II chambered coverglass (2×10^4 cells per well), precoated with poly-D-lysine and transfected with indicated constructs. Complete media was removed 24 h after transfection, cells were washed 2× in phosphate-buffered saline, then starved for 1 h in EBSS containing 5 μg ml^{-1} of transferrin–Alexa Fluor 647 conjugate and imaged live with Zeiss LSM710 confocal microscope (63× 1.4 plan-apochromat objective, single plane).

Quantitative PCR. siRNA-transfected cells were frozen dry at −80 °C, RNA isolated by RNeasy plus kit (Qiagen), cDNA synthesized by reverse transcription (Biorad iScript) and quantitative real-time PCR performed using SYBRGreen (Qiagen), and pre-designed Quantitect (Qiagen) primer sets for the described targets relative to SDHA or TBP as housekeeping genes on a Lightcycler 480 (Roche Applied Science) or on a CFX96 (Bio-Rad).

GFP-p62 measured by flow cytometry. The GFP-p62 flow cytometry assay was described previously[32]. Briefly, HEK GFP-p62 cells in 24-well plates were transfected with siRNA and 24 h later induced with 1 ng ml^{-1} doxicyclin to express GFP-p62 for 48 h. GFP-p62 expression was shut off and the cells were starved in EBSS for 2.5 h or treated as indicated. The cells were then trypsinized and passed through cell strainer caps (BD Biosciences) to obtain single-cell suspensions. Cells were analysed on a FACSAria cell sorter running FACSDiva software version 5.0 (BD Biosciences) using the blue laser for excitation of GFP. GFP fluorescence was collected through a 530/30 nm band-pass filter in the E detector. Data were collected from a minimum of 10,000 singlet events per tube, and the median GFP-p62 value was used for quantification.

Long-lived protein degradation. To measure the degradation of long-lived proteins by autophagy, proteins were first labelled with 0.25 μCi ml^{-1} L-^{14}C-valine (Perkin Elmer) for 24 h in GIBCO-RPMI 1640 medium (Invitrogen) containing 10% FBS. The cells were washed and then chased for 3 h in nonradioactive Dulbecco's modified Eagle's medium (Invitrogen) containing 10% FBS and 10 mM valine (Sigma), to allow degradation of short-lived proteins. The cells were washed twice with EBSS (Invitrogen), and starved or not for 4 h in the presence or absence of 10 mM 3-methyladenine (Sigma). 10% Trichloroacetic acid was added to the cells before incubation at 4 °C to precipitate radioactive proteins. Ultima Gold LSC cocktail (Perkin Elmer) was added to the samples and protein degradation was determined by measuring the ratio of trichloroacetic acid-soluble radioactivity relative to the total radioactivity detected by a liquid scintillation analyser (Tri-Carb 3100TR, Perkin Elmer), counting 3 min per sample.

***In vitro* interaction pull-down assays and immunoprecipitation.** Recombinant GST- or MBP-tagged proteins were expressed and purified from *Escherichia coli*. 1 μg of proteins of interest were incubated together in NETN buffer (50 mM Tris pH 8, 100 mM NaCl, 6 mM EDTA, 6 mM EGTA, 0.5% NP-40, 1 mM DTT, Roche Complete protease inhibitor) followed by GST pulldown by glutathione sepharose (GE Healthcare). For GST pulldown from cell lysate, cells were lysed in 10 mM TrisHCl pH 7.5, 150 mM NaCl, 0,5 mM EDTA, 0,5% NP-40, protease inhibitor (Roche) and phosphatase inhibitor (Sigma), and the cell lysate incubated with recombinant glutathione sepharose-bound GST proteins. The resulting pulldowns were analysed by immunoblotting. For *in vitro* translation, indicated GFP fusion proteins were *in vitro* translated in TNT T7-coupled reticulocyte lysate (Promega L4610) in the presence of ^{35}S-methionine (PerkinElmer) and precleared on glutathione–sepharose before incubation in NETN buffer together with glutathione–sepharose-bound recombinant GST-tagged LC3B or GABARAP proteins expressed in and purified from *E. coli* according to manufacturer's instructions. The resulting pulldowns were separated by SDS–PAGE. The gels were Coomassie blue stained and the *in vitro*-translated co-purified proteins were detected by autoradiography on a Typhoon phosphorimaging scanner (GE Healthcare). For immunoprecipitation from lysates, GFP, GFP-HS1BP3 or GFP-PLD1 were immunoprecipitated by GFP trap (Chromotek) following the manufacturer's protocol. The resulting immunoprecipitates or pulldowns were separated by SDS–PAGE and analysed by western blotting.

Lipid-binding assays. PIP strips or membrane lipid strips (Echelon biosciences) were blocked in 3% fatty acid-free bovine serum albumin (Sigma) in TBS-T (50 mM Tris pH 7.4, 150 mM NaCl, 0.1% Tween) before incubation with 1 μg ml^{-1} recombinant MBP proteins in TBS-T. After repeated washing in TBS-T, bound protein was immunodetected with chemiluminescence. Liposomes were prepared by mixing different molar ratios of palmitoyl-oleyl-phosphatidylcholine, dioleyoyl-phosphatidic acid, dioleyoyl-PE–rhodamine and the PIPs in chloroform and drying the lipids to a thin film. Lipids were reconstituted in a buffer containing 20 mM Hepes, pH 7.4, 150 mM NaCl and 1 mM MgCl2 and exposed to seven cycles of flash-freezing in liquid nitrogen and thawing in a 37 °C water bath, before extruding the lipid mixtures through two polycarbonate filters with 200 nm pores a total of 21 times. Lipid binding to liposomes was

analysed by a floatation assay, where 5 μM of GST-tagged protein was incubated with 2 mM total lipid and 1 mM DTT in a buffer composed of 20 mM Hepes pH 7.4, 150 mM NaCl and 1 mM $MgCl_2$ for 20 min at 25 °C. To separate liposomes and bound protein from free protein, this mixture was subjected to a Nycodenz liposome flotation assay as described in ref. 47. Gradients were centrifuged at 48,000 r.p.m. (280,000*g*) in a SW55Ti rotor (Beckman) for 4 h at 4 °C, and the liposomes and bound protein were recovered from the top 80 μl of the gradient. The lipid recovery from the gradient was determined by measuring dioleyoyl-PE–rhodamine fluorescence using a SpectraMax fluorescence spectrometer. Floatation reactions were analysed on a 12% bis-Tris gel (Novex) by SDS–PAGE, where 10% of the total lipid from each floatation reaction was run together with a protein control containing 0.5% of the total protein. The proteins were visualized with Coomassie Blue stain per the manufacturer's instruction (Imperial Protein Stain, Thermo Scientific).

High-performance liquid chromatography–mass spectrometry. Lipid extracts were prepared from total cell lysates (after 2 h starvation) using a modified Bligh/Dyer extraction procedure as previously described[56]. Samples were analysed using an Agilent Technologies 6490 Ion Funnel LC/MS Triple Quadrupole system with front end 1260 Infinity HPLC. Phospholipids and sphingolipids were separated by normal-phase high-performance liquid chromatography (HPLC), while neutral lipids were separated using reverse-phase HPLC. For normal-phase analysis, lipids were separated on an Agilent Rx-Sil column (i.d. 2.1 × 100 mm) using a gradient consisting of A: chloroform/methanol/ammonium hydroxide (89.9:10:0.1) and B: chloroform/methanol/water/ammonium hydroxide (55:39:5.9:0.1), starting at 5% B and ramping to 70% B over a 20 min period before returning back to 5% B. Neutral lipids were separated on an Agilent Zorbax XDB-C18 column (i.d. 4.6 × 100 mm), using an isocratic mobile phase chloroform:methanol:0.1 M ammonium acetate (100:100:4) at a flow rate of 300 μl min^{-1}. Multiple reaction monitoring transitions were set up for quantitative analysis of different lipid species and their corresponding internal standards as described previously[56]. Lipid levels for each sample were calculated relative to the spiked internal standards and then normalized to the total amount of all lipid species measured and presented as relative mol %. Data are presented as mean mol % for three samples of each condition.

PLD activity assay. PLD activity was measured using the Amplex Red Phospholipase D Assay Kit (Invitrogen) according to the manufacturer's instructions. Cell lysates were made of six-well plates using the assay reaction buffer with 1% Triton X-100. For each replicate, 20 μg of lysate was diluted to 50 μl of lysis buffer and added to 50 μl of reaction mixture. Four technical replicates per sample were distributed in a black half-area 96-well plate (Corning). The plate was covered and the reaction proceeded for 30 min at 37 °C before fluorescence was measured.

Zebrafish work. Experimental procedures followed the recommendations of the Norwegian Regulation on Animal Experimentation. All experiments were conducted on GFP-LC3 transgenic larvae[57] under 5 dpf. Translation-blocking antisense morpholino oligonucleotides for *Hs1bp3* (5′-TTcTaATACcTC CcTCTcACATTGT-3′) or a scrambled-sequence morpholino (5′-TTGTTAT ACGTCCGTCTGACATTGT-3′) were designed according to the manufacturer's recommendations (Gene Tools, Philomath, OR, USA) and 16.86 ng of either was injected into embryos at the one-cell stage. Capped full-length human wild-type Hs1bp3 mRNA was transcribed from linearized pSP64 Poly (A) Vector (Promega; Supplementary Table 2) using mMessage mMachine (Ambion) and 50–150 pg was coinjected with the *Hs1bp3* morpholino as described[58]. Microscopic visualization, screening and imaging of the fish were performed on a stereomicroscope Leica DFC365FX with a 1.0 × planapo lens. Control morpholino, *Hs1bp3* morpholino and human *Hs1bp3* mRNA injected live embryos were anaesthetized with tricaine at 2 dpf and mounted in low-melting point agarose for imaging with Olympus FV1000 scanning confocal microscope (under a 60 × /1.00 numerical aperture water immersion objective). Injected embryos were treated or not with 10 μM chloroquine at 28 °C for 6 h and then followed by immunoblot analysis and imaging. Embryos at 2 dpf were deyolked and then homogenized in lysis buffer (50 mM Tris-HCl (pH 8), 150 mM NaCl, 5 mM EDTA, 1% NP-40, 0.5% sodium deoxycholate, 0.1% SDS, protease inhibitor cocktail (Roche)). All experiments were replicated at least three times with 7–13 embryos per condition. Embryos were randomly distributed to receive the described treatments. No blinding was used and no animals were excluded from the analysis.

Statistics. The *P* values were derived from two-tailed *t*-test from Excel (Microsoft) for paired samples, and considered statistically significant at $P \leq 0.05$. In some cases, values were log-transformed to obtain a normal distribution.

Data availability. The lipidomics datasets have been deposited in the Dryad Digital Respository (DOI: doi:10.5061/dryad.gq3fk).

References

1. Mizushima, N. & Komatsu, M. Autophagy: renovation of cells and tissues. *Cell* **147,** 728–741 (2011).
2. Kaur, J. & Debnath, J. Autophagy at the crossroads of catabolism and anabolism. *Nat. Rev. Mol. Cell. Biol.* **16,** 461–472 (2015).
3. Nixon, R. A. The role of autophagy in neurodegenerative disease. *Nat. Med.* **19,** 983–997 (2013).
4. Sandri, M., Coletto, L., Grumati, P. & Bonaldo, P. Misregulation of autophagy and protein degradation systems in myopathies and muscular dystrophies. *J. Cell Sci.* **126,** 5325–5333 (2013).
5. Mizushima, N., Yoshimori, T. & Ohsumi, Y. The role of Atg proteins in autophagosome formation. *Annu. Rev. Cell Dev. Biol.* **27,** 107–132 (2011).
6. Axe, E. L. *et al.* Autophagosome formation from membrane compartments enriched in phosphatidylinositol 3-phosphate and dynamically connected to the endoplasmic reticulum. *J. Cell Biol.* **182,** 685–701 (2008).
7. Dooley, H. C. *et al.* WIPI2 Links LC3 conjugation with PI3P, autophagosome formation, and pathogen clearance by recruiting Atg12-5-16L1. *Mol. Cell* **55,** 238–252 (2014).
8. Yla-Anttila, P., Vihinen, H., Jokitalo, E. & Eskelinen, E. L. 3D tomography reveals connections between the phagophore and endoplasmic reticulum. *Autophagy* **5,** 1180–1185 (2009).
9. Hamasaki, M. *et al.* Autophagosomes form at ER-mitochondria contact sites. *Nature* **495,** 389–393 (2013).
10. Hayashi-Nishino, M. *et al.* A subdomain of the endoplasmic reticulum forms a cradle for autophagosome formation. *Nat. Cell Biol.* **11,** 1433–1437 (2009).
11. Hailey, D. W. *et al.* Mitochondria Supply membranes for autophagosome biogenesis during starvation. *Cell* **141,** 656–667 (2010).
12. Ravikumar, B., Moreau, K., Jahreiss, L., Puri, C. & Rubinsztein, D. C. Plasma membrane contributes to the formation of pre-autophagosomal structures. *Nat. Cell Biol.* **12,** 747–757 (2010).
13. Knævelsrud, H. *et al.* Membrane remodeling by the PX-BAR protein SNX18 promotes autophagosome formation. *J. Cell Biol.* **202,** 331–349 (2013).
14. Puri, C., Renna, M., Bento, C. F., Moreau, K. & Rubinsztein, D. C. Diverse autophagosome membrane sources coalesce in recycling endosomes. *Cell* **154,** 1285–1299 (2013).
15. Longatti, A. *et al.* TBC1D14 regulates autophagosome formation via Rab11- and ULK1-positive recycling endosomes. *J. Cell Biol.* **197,** 659–675 (2012).
16. Imai, K. *et al.* Atg9A trafficking through the recycling endosomes is required for autophagosome formation. *J. Cell Sci.* **129,** 3781–3791 (2016).
17. Dall'Armi, C., Devereaux, K. A. & Di Paolo, G. The role of lipids in the control of autophagy. *Curr. Biol.* **23,** R33–R45 (2013).
18. Carlsson, S. R. & Simonsen, A. Membrane dynamics in autophagosome biogenesis. *J. Cell Sci.* **128,** 193–205 (2015).
19. Fang, Y., Vilella-Bach, M., Bachmann, R., Flanigan, A. & Chen, J. Phosphatidic acid-mediated mitogenic activation of mTOR signaling. *Science* **294,** 1942–1945 (2001).
20. Yoon, M. S., Du, G., Backer, J. M., Frohman, M. A. & Chen, J. Class III PI-3-kinase activates phospholipase D in an amino acid-sensing mTORC1 pathway. *J. Cell. Biol.* **195,** 435–447 (2011).
21. Dall'Armi, C. *et al.* The phospholipase D1 pathway modulates macroautophagy. *Nat. Commun.* **1,** 142 (2010).
22. Moreau, K., Ravikumar, B., Puri, C. & Rubinsztein, D. C. Arf6 promotes autophagosome formation via effects on phosphatidylinositol 4,5-bisphosphate and phospholipase D. *J. Cell Biol.* **196,** 483–496 (2012).
23. Bae, E. J. *et al.* Phospholipase D1 regulates autophagic flux and clearance of alpha-synuclein aggregates. *Cell Death Differ* **21,** 1132–1141 (2014).
24. Simonsen, A. & Tooze, S. A. Coordination of membrane events during autophagy by multiple class III PI3-kinase complexes. *J. Cell Biol.* **186,** 773–782 (2009).
25. Simonsen, A. *et al.* Alfy, a novel FYVE-domain-containing protein associated with protein granules and autophagic membranes. *J. Cell Sci.* **117,** 4239–4251 (2004).
26. Filimonenko, M. *et al.* The selective macroautophagic degradation of aggregated proteins requires the PI3P-binding protein Alfy. *Mol. Cell* **38,** 265–279 (2010).
27. Pankiv, S. *et al.* FYCO1 is a Rab7 effector that binds to LC3 and PI3P to mediate microtubule plus end-directed vesicle transport. *J. Cell Biol.* **188,** 253–269 (2010).
28. Polson, H. E. *et al.* Mammalian Atg18 (WIPI2) localizes to omegasome-anchored phagophores and positively regulates LC3 lipidation. *Autophagy* **6,** 506–522 (2010).
29. Kabeya, Y. *et al.* LC3, a mammalian homologue of yeast Apg8p, is localized in autophagosome membranes after processing. *EMBO J.* **19,** 5720–5728 (2000).
30. Bjorkoy, G. *et al.* p62/SQSTM1 forms protein aggregates degraded by autophagy and has a protective effect on huntingtin-induced cell death. *J. Cell Biol.* **171,** 603–614 (2005).

31. Pankiv, S. *et al.* p62/SQSTM1 binds directly to Atg8/LC3 to facilitate degradation of ubiquitinated protein aggregates by autophagy. *J. Biol. Chem.* **282,** 24131–24145 (2007).
32. Larsen, K. B. *et al.* A reporter cell system to monitor autophagy based on p62/SQSTM1. *Autophagy* **6,** 784–793 (2010).
33. He, C., Bartholomew, C. R., Zhou, W. & Klionsky, D. J. Assaying autophagic activity in transgenic GFP-Lc3 and GFP-Gabarap zebrafish embryos. *Autophagy* **5,** 520–526 (2009).
34. Boglev, Y. *et al.* Autophagy induction is a Tor- and Tp53-independent cell survival response in a zebrafish model of disrupted ribosome biogenesis. *PLoS Genet.* **9,** e1003279 (2013).
35. Ganesan, S., Moussavi Nik, S. H., Newman, M. & Lardelli, M. Identification and expression analysis of the zebrafish orthologues of the mammalian MAP1LC3 gene family. *Exp. Cell Res.* **328,** 228–237 (2014).
36. Takemoto, Y., Furuta, M., Sato, M., Kubo, M. & Hashimoto, Y. Isolation and characterization of a novel HS1 SH3 domain binding protein, HS1BP3. *Int. Immunol.* **11,** 1957–1964 (1999).
37. van Rossum, A. G., Schuuring-Scholtes, E., van Buuren-van, S. V., Kluin, P. M. & Schuuring, E. Comparative genome analysis of cortactin and HS1: the significance of the F-actin binding repeat domain. *BMC Genomics* **6,** 15 (2005).
38. Seet, L. F. & Hong, W. The Phox (PX) domain proteins and membrane traffic. *Biochim. Biophys. Acta* **1761,** 878–896 (2006).
39. Teasdale, R. D. & Collins, B. M. Insights into the PX (phox-homology) domain and SNX (sorting nexin) protein families: structures, functions and roles in disease. *Biochem. J.* **441,** 39–59 (2012).
40. Oliveira, T. G. *et al.* Phospholipase d2 ablation ameliorates Alzheimer's disease-linked synaptic dysfunction and cognitive deficits. *J. Neurosci.* **30,** 16419–16428 (2010).
41. Pettitt, T. R., McDermott, M., Saqib, K. M., Shimwell, N. & Wakelam, M. J. Phospholipase D1b and D2a generate structurally identical phosphatidic acid species in mammalian cells. *Biochem. J.* **360,** 707–715 (2001).
42. Bruntz, R. C., Lindsley, C. W. & Brown, H. A. Phospholipase D signaling pathways and phosphatidic acid as therapeutic targets in cancer. *Pharmacol. Rev.* **66,** 1033–1079 (2014).
43. Stahelin, R. V. *et al.* Mechanism of membrane binding of the phospholipase D1 PX domain. *J. Biol. Chem.* **279,** 54918–54926 (2004).
44. Karathanassis, D. *et al.* Binding of the PX domain of p47(phox) to phosphatidylinositol 3,4-bisphosphate and phosphatidic acid is masked by an intramolecular interaction. *EMBO J.* **21,** 5057–5068 (2002).
45. Zimmerberg, J. & Kozlov, M. M. How proteins produce cellular membrane curvature. *Nat. Rev. Mol. Cell Biol.* **7,** 9–19 (2006).
46. van den Brink-van der Laan, E., Killian, J. A. & de Kruijff, B. Nonbilayer lipids affect peripheral and integral membrane proteins via changes in the lateral pressure profile. *Biochim. Biophys. Acta* **1666,** 275–288 (2004).
47. Nath, S. *et al.* Lipidation of the LC3/GABARAP family of autophagy proteins relies on a membrane-curvature-sensing domain in Atg3. *Nat. Cell Biol.* **16,** 415–424 (2014).
48. Nakanishi, H. *et al.* Phospholipase D and the SNARE Sso1p are necessary for vesicle fusion during sporulation in yeast. *J. Cell Sci.* **119,** 1406–1415 (2006).
49. Choi, S. Y. *et al.* A common lipid links Mfn-mediated mitochondrial fusion and SNARE-regulated exocytosis. *Nat. Cell Biol.* **8,** 1255–1262 (2006).
50. Vitale, N. *et al.* Phospholipase D1: a key factor for the exocytotic machinery in neuroendocrine cells. *EMBO J.* **20,** 2424–2434 (2001).
51. Moreau, K., Ravikumar, B., Renna, M., Puri, C. & Rubinsztein, D. C. Autophagosome precursor maturation requires homotypic fusion. *Cell* **146,** 303–317 (2011).
52. Ammar, M. R. *et al.* The Coffin-Lowry syndrome-associated protein RSK2 regulates neurite outgrowth through phosphorylation of phospholipase D1 (PLD1) and synthesis of phosphatidic acid. *J. Neurosci.* **33,** 19470–19479 (2013).
53. Chan, E. Y., Kir, S. & Tooze, S. A. siRNA screening of the kinome identifies ULK1 as a multidomain modulator of autophagy. *J. Biol. Chem.* **282,** 25464–25474 (2007).
54. Jia, L., Uekita, T. & Sakai, R. Hyperphosphorylated cortactin in cancer cells plays an inhibitory role in cell motility. *Mol. Cancer Res.* **6,** 654–662 (2008).
55. Rizk, A. *et al.* Segmentation and quantification of subcellular structures in fluorescence microscopy images using Squassh. *Nat. Protoc.* **9,** 586–596 (2014).
56. Chan, R. B. *et al.* Comparative lipidomic analysis of mouse and human brain with Alzheimer disease. *J. Biol. Chem.* **287,** 2678–2688 (2012).
57. van der Vaart, M. *et al.* The DNA damage-regulated autophagy modulator DRAM1 links mycobacterial recognition via TLR-MYD88 to authophagic defense. *Cell Host Microbe* **15,** 753–767 (2014).
58. Chi, N. C. *et al.* Cardiac conduction is required to preserve cardiac chamber morphology. *Proc. Natl Acad. Sci. USA* **107,** 14662–14667 (2010).

Acknowledgements

We thank S. Tooze, N. Ktistakis, G. Bjørkøy, A. Thige, S.S. Taylor, W. Eskild, B.-H. Toh, M. Frohman and J.K. Burkhardt for sharing reagents. This research was supported by the Molecular Life Science program of the University of Oslo and the Norwegian Cancer Society. G.D.P. is supported by NIH grant R21 AG045020. T.J.M is supported by NIH grant R01 GM100930. The authors declare no competing financial interests.

Author contributions

H.K. and A.S. conceived the idea. H.K., P.H. and K.S. designed and conducted the experiments, analysed the data and generated figures. S.W.S. performed the ultra-structural studies, A.H.L. and T.J.M. performed the liposome interaction studies. S.P., S.R.C., V.H.L. and G.T.B. helped perform experiments. B.J.M. designed and performed the zebrafish experiments. R.B.C., B.Z. and G.D.P performed and analysed the lipidomics study. K.L. contributed to the statistical analysis. H.K., P.H. and A.S. wrote the manu-script with input from all co-authors.

Additional information

Supplementary Information accompanies this paper at http://www.nature.com/naturecommunications

Competing financial interests: The authors declare no competing financial interests.

Reprints and permission information is available online at http://npg.nature.com/reprintsandpermissions/

How to cite this article: Holland, P. *et al.* HS1BP3 negatively regulates autophagy by modulation of phosphatidic acid levels. *Nat. Commun.* **7,** 13889 doi: 10.1038/ncomms13889 (2016).

Publisher's note: Springer Nature remains neutral with regard to jurisdictional claims in published maps and institutional affiliations.

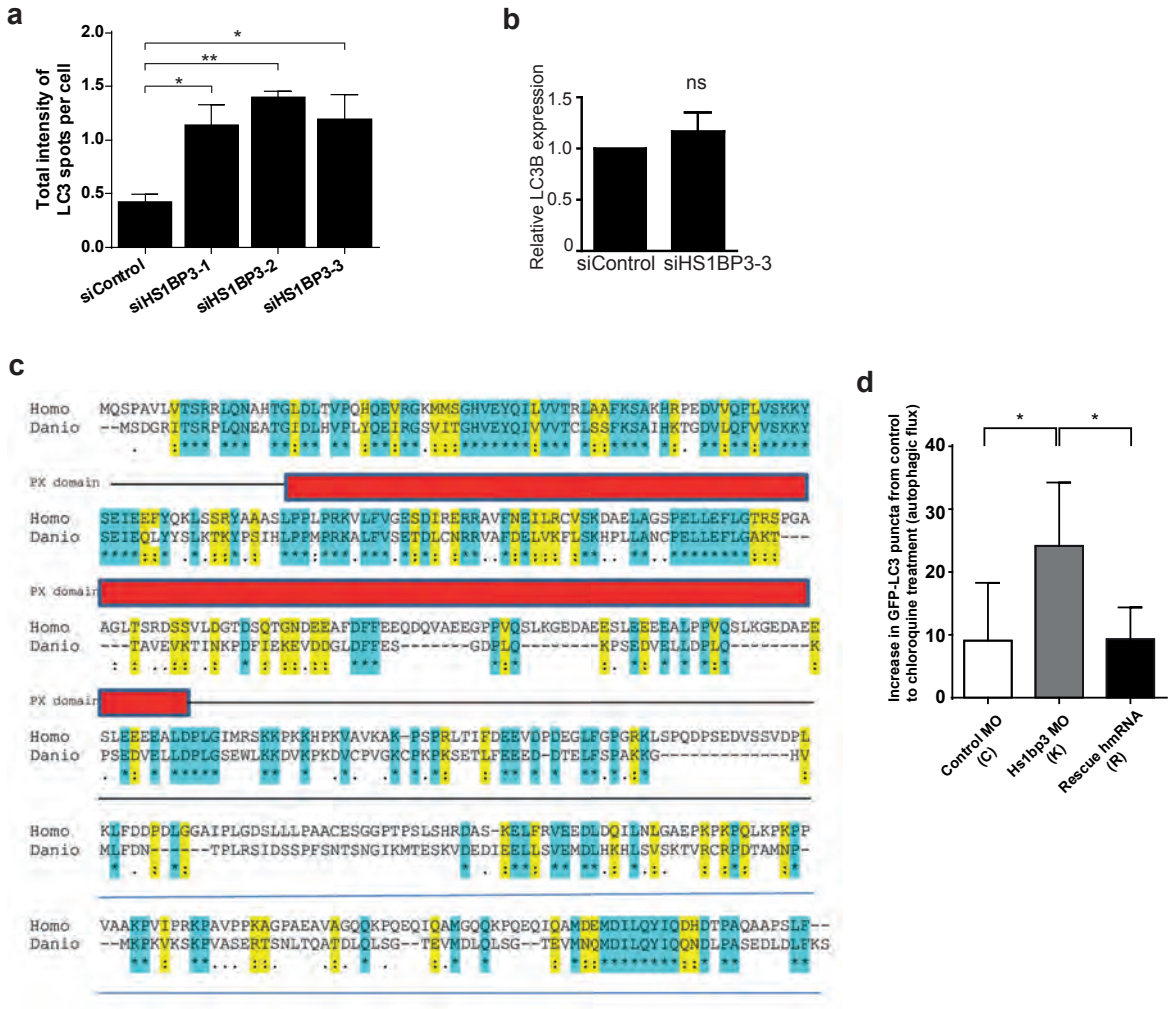

Supplementary Figure 1: HS1BP3 depletion increases autophagy in human cells and zebrafish
(**a**) HEK cells were transfected with siRNA against HS1BP3 and starved for 2 h before fixation, immunostaining against LC3 and imaging. The total intensity of endogenous LC3 spots per cell was quantified (mean +/- S.E.M., n = 3). 600 cells analyzed per condition. (**b**) LC3B mRNA levels were quantified by qPCR from siHS1BP3 or control transfected cells (mean +/- S.E.M., n = 3). (**c**) ClustalW alignment of Hs1bp3 amino acid sequences of human and Danio rerio. Identical and similar residues are boxed in cyan and yellow, respectively. The position of the conserved PX domain is indicated by a red box below the sequences. (**d**) Quantification of the difference in GFP-LC3 puncta count between the chloroquine treated and the untreated in embryos injected with control morpholino, Hs1bp3 translational blocking morpholino or Hs1bp3 translational blocking morpholino together with human Hs1bp3 mRNA (mean ± SEM, n = 3) . *: p< 0.05, **: p< 0.01, ns: non-significant.

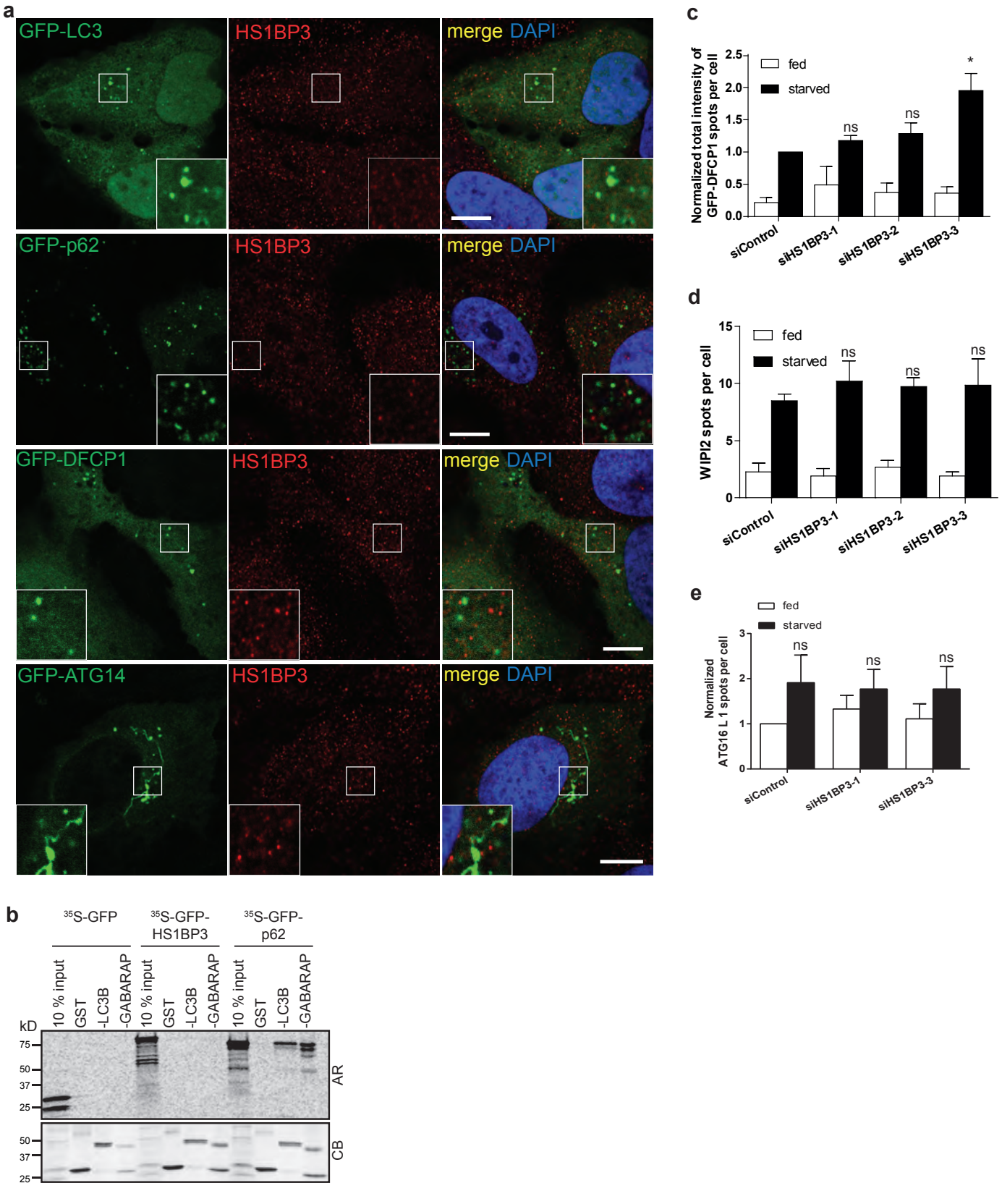

Supplementary Figure 2: Localization of endogenous HS1BP3 and its effects on early phagophore markers.
(**a**) HEK cells were transfected with the indicated GFP-tagged autophagy markers, starved, fixed and co-stained for endogenous HS1BP3. Scale bars 10 µm. (**b**) In vitro translated GFP, GFP-HS1BP3 or GFP-p62 was incubated with recombinant GST-tagged LC3B or GABARAP. Following GST pulldown, bound proteins were detected by autoradiography (AR) and GST proteins by Coomassie blue staining (CB). (**c**) HEK GFP-DFCP1 cells were transfected with siRNA against HS1BP3 and starved or not for 50 min before fixation and imaging. The total intensity of GFP-DFCP1 spots per cell was quantified and normalized to that of starved siControl cells (mean +/- S.E.M., n = 3). 1500 cells were analyzed per condition. (**d**) HEK GFP-DFCP1 cells were treated as in c, stained for endogenous WIPI2 and the number of WIPI2 spots per cell was quantified (mean +/- S.E.M., n = 3). (**e**) HeLa cells were transfected with either control or HS1BP3 siRNA, starved or not for 2 h before fixation and staining for endogenous ATG16L1. The number of ATG16L1 spots per cell was quantified (mean ± SEM, n = 3) *: p< 0.05, ns: non-significant.

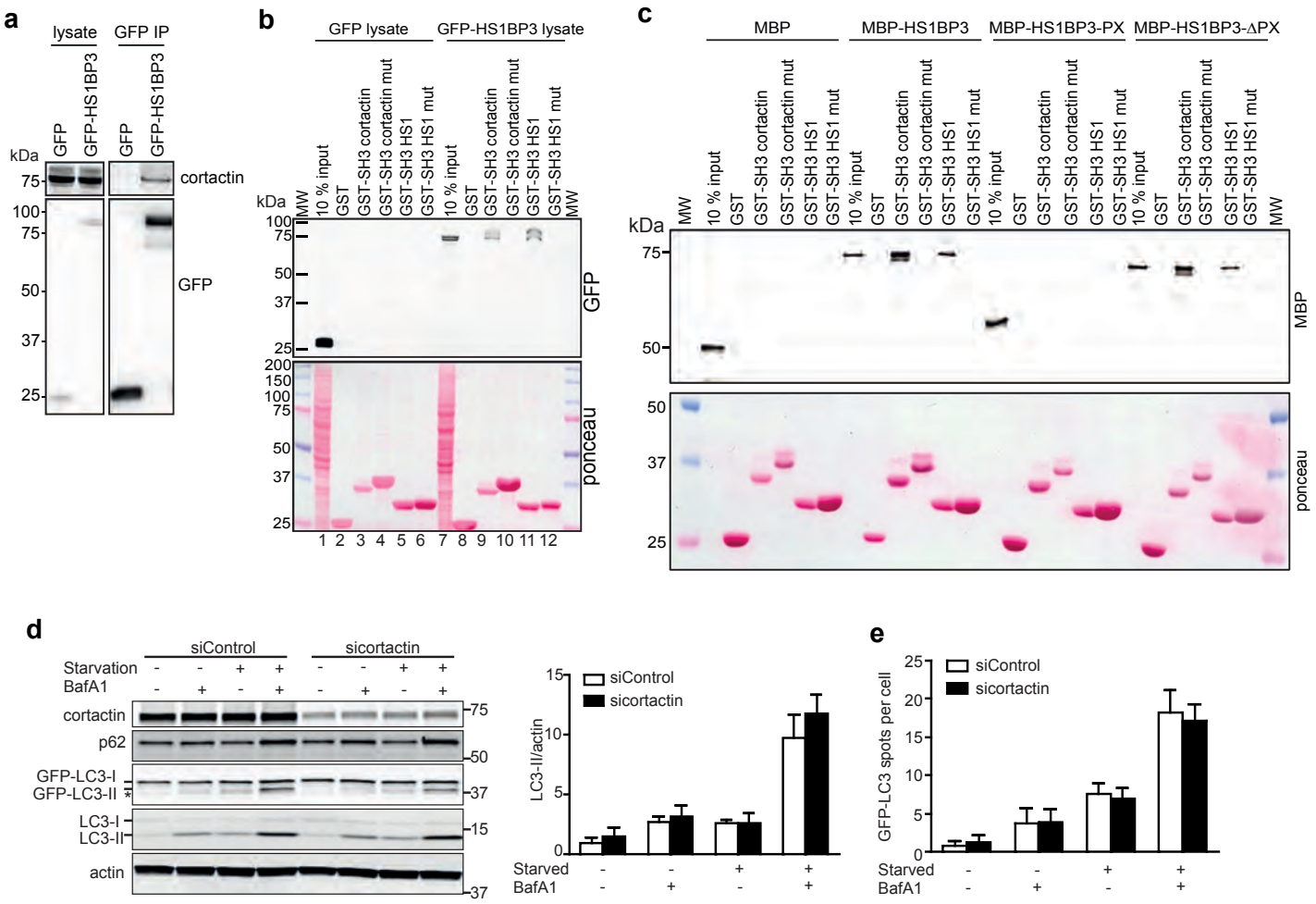

Supplementary Figure 3: HS1BP3 interacts with cortactin independently of its role in autophagy
(**a**) HeLa cell stably expressing tet-on GFP or GFP-HS1BP3 were induced by 50 ng/mL tetracycline for 16 h followed by immunoprecipitation using GFP trap. The resulting immunoprecipitates were separated by SDS-PAGE and analyzed by immunoblotting as indicated. (**b**) Lysates from HeLa GFP or GFP-HS1BP3 cells induced by 50 ng/mL tetracycline for 16 h were incubated with recombinant GST-tagged wild-type or mutated SH3 domain of cortactin or HS1, followed by pull-down using glutathione sepharose, separation by SDS-PAGE and immunoblotting against GFP. The membrane was stained with Ponceau S to visualize the GST-proteins and input lysate. (**c**) Recombinant MBP-tagged HS1BP3 full length or deletion mutants (HS1BP3-PX or HS1BP3-ΔPX) were incubated with recombinant GST-tagged wild-type or mutated SH3 domain of cortactin or HS1 followed by pull-down using glutathione beads, separation by SDS-PAGE and immunoblotting or Ponceau S staining as indicated. (**d**) HEK GFP-LC3 cells were transfected with siRNA against cortactin. 72 h later the cells were starved or not for 2 h in EBSS in the presence or absence of BafA1. Cell lysates were separated by SDS-PAGE and immunoblotted with the indicated antibodies. LC3-II/actin was quantified from immunoblots (mean +/- *S.E.M., n = 3).* (**e**) HEK GFP-LC3 cells treated as in d were fixed and analyzed by fluorescent microscopy and high-content image analysis. The number of GFP-LC3 spots per cell was quantified (mean +/- S.E.M., n = 3). Around 1500 cells were quantified per condition. Scale bars are 10 µm.

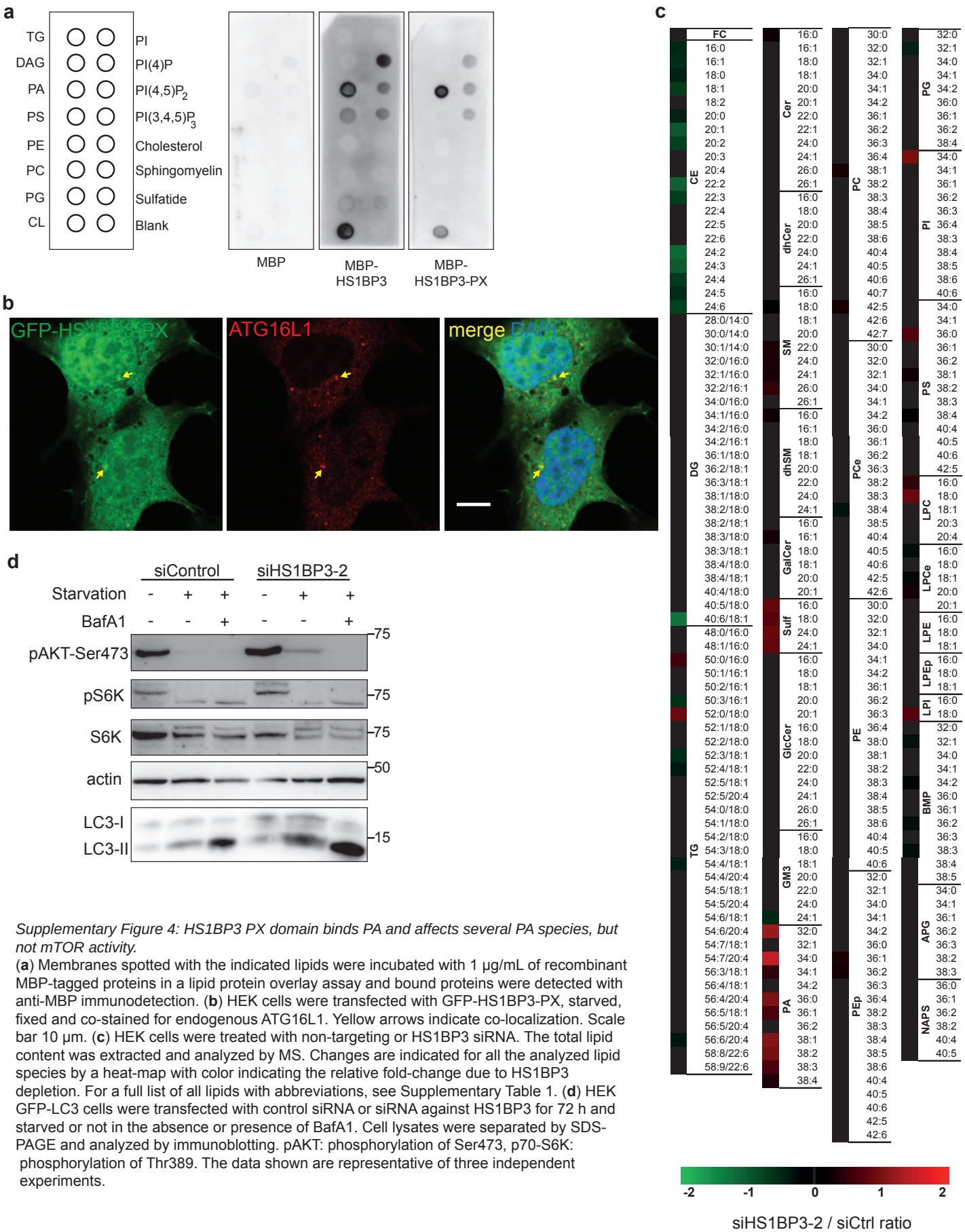

Supplementary Figure 4: HS1BP3 PX domain binds PA and affects several PA species, but not mTOR activity.

(**a**) Membranes spotted with the indicated lipids were incubated with 1 µg/mL of recombinant MBP-tagged proteins in a lipid protein overlay assay and bound proteins were detected with anti-MBP immunodetection. (**b**) HEK cells were transfected with GFP-HS1BP3-PX, starved, fixed and co-stained for endogenous ATG16L1. Yellow arrows indicate co-localization. Scale bar 10 µm. (**c**) HEK cells were treated with non-targeting or HS1BP3 siRNA. The total lipid content was extracted and analyzed by MS. Changes are indicated for all the analyzed lipid species by a heat-map with color indicating the relative fold-change due to HS1BP3 depletion. For a full list of all lipids with abbreviations, see Supplementary Table 1. (**d**) HEK GFP-LC3 cells were transfected with control siRNA or siRNA against HS1BP3 for 72 h and starved or not in the absence or presence of BafA1. Cell lysates were separated by SDS-PAGE and analyzed by immunoblotting. pAKT: phosphorylation of Ser473, p70-S6K: phosphorylation of Thr389. The data shown are representative of three independent experiments.

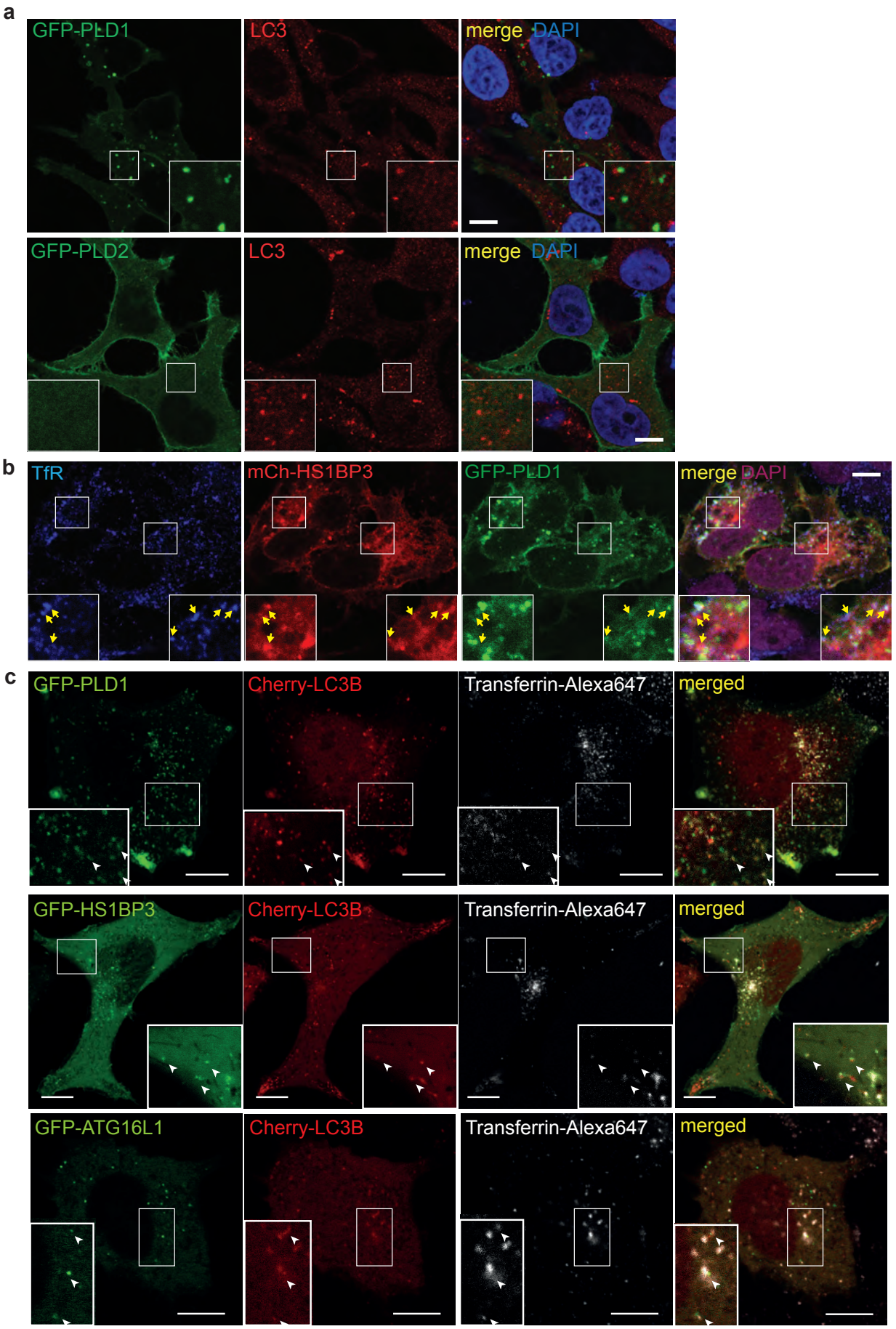

Supplementary Figure 5: HS1BP3 affects PLD1 on autophagy precursor membranes
(**a**) HEK cells were transfected to express GFP-tagged PLD1 or PLD2, starved and fixed then co-stained for endogenous LC3 and analyzed by confocal microscopy. (**b**) HEK cells were transfected to express GFP-tagged PLD1 and mCherry-HS1BP3, starved and fixed then co-stained for endogenous Transferrin receptor (TfR) and analyzed by confocal microscopy. All scale bars are 10 µm. (**c**) HEK293A cells expressing the indicated constructs were starved for 1h in EBSS containing 5µg/ml of transferrin-Alexa Fluor 647 conjugate and imaged live with Zeiss LSM710 confocal microscope. Shown are still image frames from live scan. Arrowheads point to structures positive for all three proteins. All scale bars are 10µm.

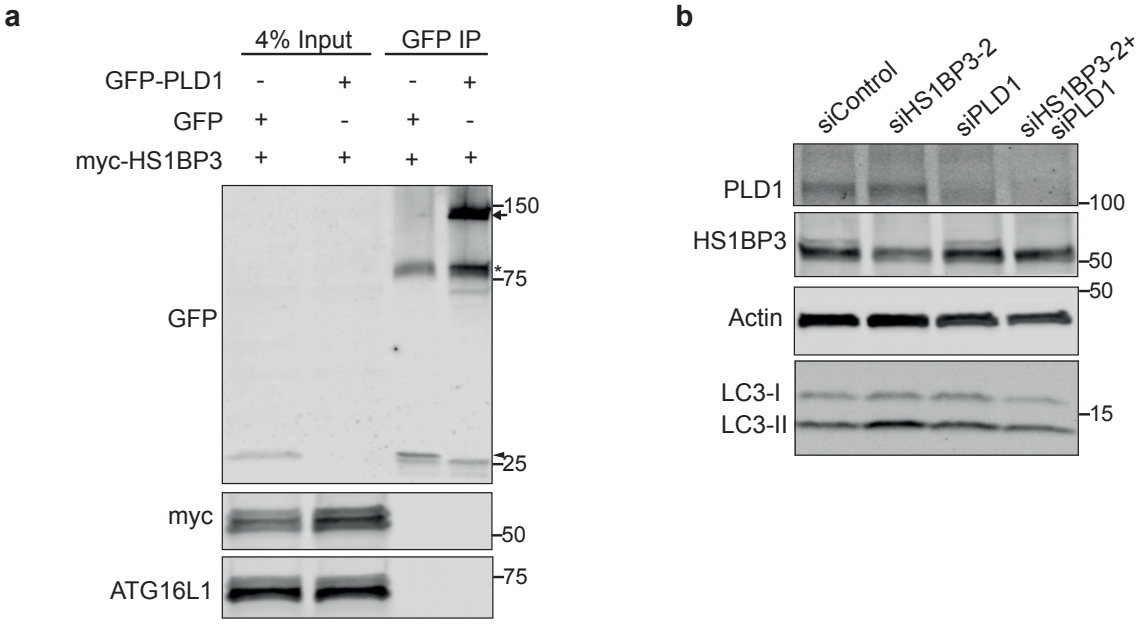

Supplementary Figure 6: HS1BP3 affects PLD1 on autophagy precursor membranes, but not through protein-protein interactions (**a**) Immunoprecipitation of GFP or GFP-PLD1 from HEK cells transfected with GFP and myc-HS1BP3 or GFP-PLD1 and myc-HS1BP3. An interaction between GFP-PLD1 and myc-HS1BP3 or ATG16L1 was investigated by western blotting. On the GFP blot the arrow indicates GFP-PLD1, arrowhead GFP and the star an unspecific band. (**b**) HEK cells transfected with the indicated siRNA were starved then lysed and analyzed by western blotting with the indicated antibodies. The cells were treated in parallel with the ones analyzed by microscopy in Figure 7a.

a

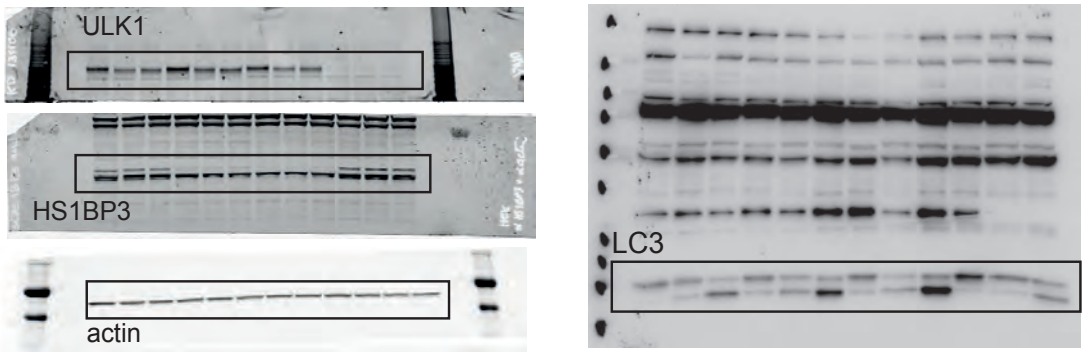

b

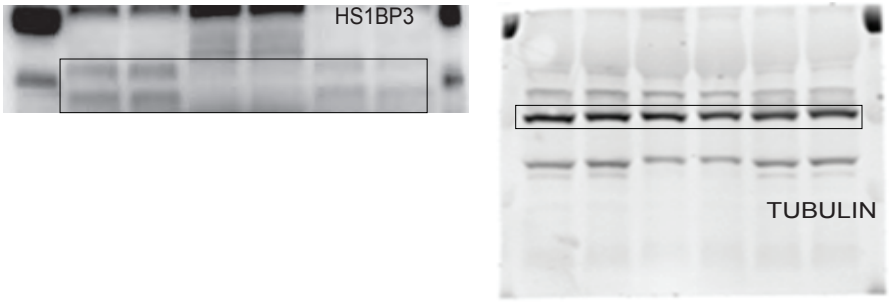

c

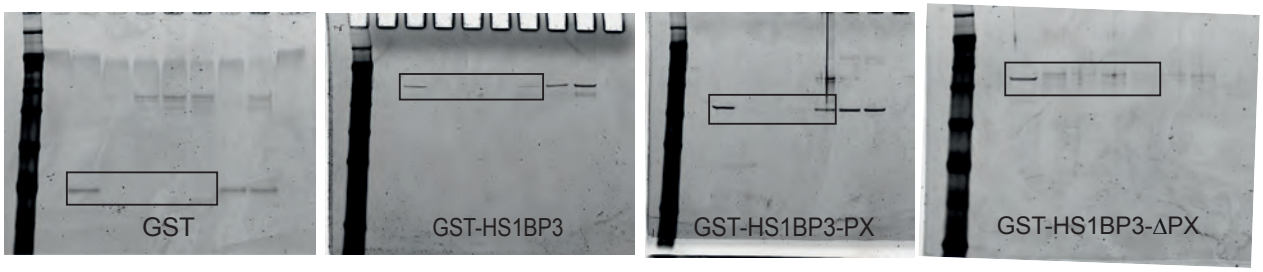

d

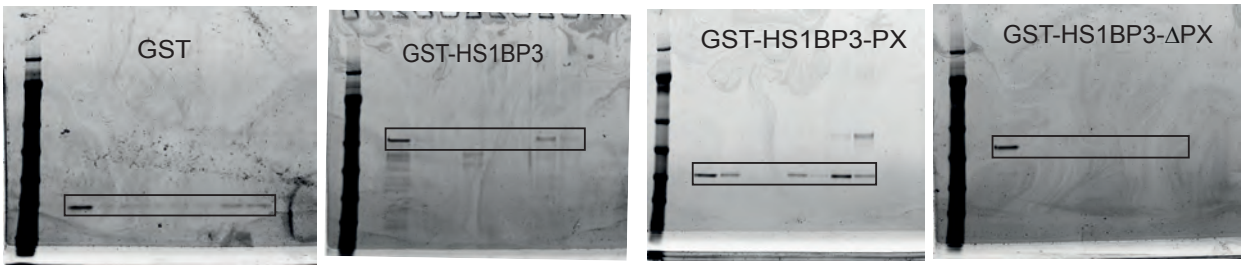

Supplementary Figure 7: Original scans used in the main text figures
(**a**) Blots from figure 1d
(**b**) Blots from figure 2c
(**c**) Gels from figure 4c
(**d**) Gels from figure 4d

Supplementary Table 1: Lipidomics data

Lipid species		**Average normalized mol %**		**SEM normalized mol %**		**t-test**
Abbrev.	**full name**	**siCtrl**	**siHS1 BP3-2**	**siCtrl**	**siHS1 BP3-2**	
FC	Free cholesterol	1	0.99	0.02	0.03	0.857
CE	Cholesteryl esters	1	0.80	0.03	0.05	0.007
DG	Diglycerides	1	1.00	0.17	0.17	0.995
TG	Triglycerides	1	1.10	0.04	0.10	0.391
Cer	Ceramide	1	1.12	0.03	0.06	0.112
dhCer	Dihydroceramide	1	1.00	0.07	0.07	0.967
SM	Sphingomyelin	1	1.16	0.04	0.03	0.017
dhSM	Dihydrosphingomyelin	1	1.15	0.03	0.07	0.069
GalCer	Galactosylceramide	1	1.08	0.03	0.07	0.287
Sulf	Sulfatide	1	1.80	0.21	0.14	0.010
GlcCer	Glucosylceramide	1	1.07	0.03	0.08	0.434
LacCer	Lactosylceramide	1	0.94	0.03	0.06	0.369
GM3	Monosialodihexosylganglioside	1	0.96	0.09	0.04	0.685
PA	Phosphatidic acid	1	1.95	0.14	0.26	0.010
PC	Phospatidylcholine	1	1.08	0.09	0.08	0.490
PCe	Phosphatidylcholine ether	1	0.88	0.07	0.05	0.219
PE	Phosphatidylethanolamine	1	1.05	0.07	0.07	0.583
PEp	Plasmalogen PE	1	1.11	0.06	0.04	0.154
PG	Phosphatidylglycerol	1	0.90	0.03	0.08	0.249
PI	Phosphatidylinositol	1	1.06	0.07	0.07	0.523
PS	Phosphatidylserine	1	1.07	0.04	0.07	0.401
LPC	Lysophosphatidylcholine	1	1.34	0.04	0.06	0.001
LPCe	Lysophosphatidylcholine ether	1	1.00	0.05	0.04	0.976
LPE	Lysophosphatidylethanolamine	1	1.09	0.03	0.11	0.456
LPEp	Plasmalogen LPE	1	1.23	0.06	0.17	0.225
LPI	Lysophosphatidylinositol	1	1.29	0.04	0.07	0.004
BMP	Bis(monoacylglycero)phosphates	1	0.85	0.01	0.04	0.005
APG	Acylphosphatidylglycerol	1	0.92	0.08	0.07	0.430
NAPS	N-acylphosphatidylserines	1	1.17	0.04	0.15	0.290

Supplementary Table 2: Plasmids used in this study.

Plasmid	**Primers**	**Cloning**
pEGFP-HS1BP3	5'-ATAGAATTCATGCAGTCCCCGGCGGTGCTC-3' 5'-ATAGTCGACTCAGAAGAGGCTGGGGGCGG-3'	Into pEGFP.C2 using EcoRI and SalI restriction sites
pENTR-HS1BP3	5'-ATAGTCGACATGCAGTCCCCGGCGGTGCTC-3' 5'-ATAGCGGCCGCTCAGAAGAGACTGGGGGCGG-3'	Amplification from cDNA library, into pENTR using SalI and NotI restriction sites
pENTR-HS1BP3-PX	5'-ATAGTCGACATGCAGTCCCCGGCGGTGCTC-3' 5'ATAGCGGCCGCTCAGGATCTGGTACCTAAGAACTC-3'	Amplification from pENTR-HS1BP3, into pENTR using SalI and NotI restriction sites
pENTR-HS1BP3-ΔPX	5'-ATAGTCGACGCTGCAGGGCTCACCAGCAG-3' 5'-ATAGCGGCCGCTCAGAAGAGACTGGGGGCGG-3',	Amplification from pENTR-HS1BP3, into pENTR using SalI and NotI restriction sites
pTH1-HS1BP3 (MBP tag)	-	Gateway LR cloning from pENTR-HS1BP3
pTH1-HS1BP3-PX (MBP tag)	-	Gateway LR cloning from pENTR HS1BP3-PX
pTH1-HS1BP3-ΔPX (MBP tag)	-	Gateway LR cloning from pENTR HS1BP3-ΔPX
pDEST-mCherry-HS1BP3	-	Gateway LR cloning from pENTR-HS1BP3
pTH1-2xFYVE-Hrs (MBP tag)	-	Gateway LR cloning from pENTR-2xFYVE-Hrs
pGEX-2xFYVE-Hrs	-	[1]
pCI2Flag Cortactin	-	Kindly provided by J. K. Burkhardt
pGEX kG hHS1 SH3	-	Kindly provided by J. K. Burkhardt
pGEX kG hHS1 SH3 W->Y	-	Kindly provided by J. K. Burkhardt
pGEX kG hcortactin SH3	-	Kindly provided by J. K. Burkhardt
pGEX kG h cortactin SH3 W->Y	-	Kindly provided by J. K. Burkhardt
pCGN-HA-hPLD1b	-	Kindly provided by M. Frohman [2]
pEGFP-C1-hPLD1b	-	Kindly provided by M. Frohman [2]
pEGFP-C1-mPLD2	-	Kindly provided by M. Frohman [2]
pDEST15-LC3B	-	[3]

(GST tag)		
pDEST15-GABARAP (GST tag)	-	[3]
pDEST15-HS1BP3-PX (GST tag)	-	Gateway LR cloning from pENTR HS1BP3-PX
pDEST53-p62 (in vitro translation)	-	[3]
pDEST53-HS1BP3 (in vitro translation)	-	Gateway LR cloning from pENTR-HS1BP3
pSP64 Poly (A)-Hs-Hs1bp3	5' taaaAAGCTTATGCAGTCCCCGGCGGTG 3' 5' taaaGAGCTCTCAGAAGAGGCTGGGGGC 3'	Expression of HS1BP3 in zebrafish
pEGFP-C2 DFCP1	-	Kindly provided by Nicholas Ktistakis
pEGFP – p62	-	-
pDEST-EGFP-LC3B	-	-
pEGFP(C1)-Atg16L	-	-
pEGFP-Atg14L	-	Kindly provided by Tamotsu Yoshimori

Supplementary references

1. Gillooly, D.J. *et al.* Localization of phosphatidylinositol 3-phosphate in yeast and mammalian cells. *The EMBO journal* **19**, 4577-4588 (2000).
2. Hammond, S.M. *et al.* Human ADP-ribosylation factor-activated phosphatidylcholine-specific phospholipase D defines a new and highly conserved gene family. *J Biol Chem* **270**, 29640-29643 (1995).
3. Pankiv, S. *et al.* p62/SQSTM1 binds directly to Atg8/LC3 to facilitate degradation of ubiquitinated protein aggregates by autophagy. *J.Biol.Chem.* **282**, 24131-24145 (2007).